Electrochemical and structural properties of some 1,2,3,5 and 1,3,2,4 dithiadiazolylium salts and related compounds

Aherne, Christine M.

Electrochemical and Structural Properties of Some 1,2,3,5 and 1,3,2,4 Dithiadiazolylium Salts and Related Compounds

Christine M. Aherne

Ph.D Thesis
University of Durham, England
Autumn 1995

To,

my mother, father and brother for all their support over the years

Acknowledgements

I would like to take time out to acknowledge the following people:

Dr Arthur J. Banister for his boundless enthusiasm for chemistry, for introducing me to sulphur nitrogen chemistry and most importantly for being a supervisor with a sense of humour.

Dr Zdenek 'Stan' Hauptman for making electrochemistry friendly.

To the Class of 1990-1994 for their friendship, loyalty and lots of laughter, albeit in the pub or the lab:-

Dr Anthony Luke
Dr Philip Coates
Dr Jeremy Rawson
Dr Ian Lavender
Tom Hibbert
Dr Simon Lawrence
Iain May
Colin Campbell
Dr Neil Bricklebank

An especial thanks to Ian Lavender and Jeremy Rawson for all their help in this field of chemistry.

The following list of crystallographers for structural determinations:- Prof's Clegg and Howard, Dr Christian Lehmann, project students Jackie Cole and Sarah Done, Dr Andrei Batsanov, Jason Cole, Dr Roy Copley and Dr Mark Elsegood.

I also express my thanks to the members of LAB 19, LAB 104, LAB 72 and Prof Bloor/Dr Graham Cross research group for a variety of collaborations.

A special mention to the following technical staff:- Ray and Gordon the kings of glass blowing, George for emergency nitrogen and solvent supplies, Jimmy in stores, Tom for holding the purse strings, all in the electrical and mechanical workshops, Brian for disposal of chemicals, mass spec department, Jaraka for elemental analysis and the char ladies (Maureen, Jean, Brenda and Hazel) for providing many welcome cups of coffee during a hard days work.

Finally it remains for me to show my appreciation to KOBE Steel and SERC for funding this project.

Publications:

1. "Solid state rearrangement of some 1,3,2,4 dithiadiazoles to their 1,2,3,5 analogues".
   C.M Aherne, A.J. Banister, A.W. Luke, J.M. Rawson and R.J. Whitehead.
   J. Chem. Soc., Dalton Trans., 1992, 1277-1282.

2. "Electrochemical studies of some dithiadiazolylium cations; evidence for the dithiadiazolide anion, $[PhCNSSN]^-$".
   C.M. Aherne, A.J. Banister, I.B. Gorrell, M.I. Hansford, Z.V. Hauptman, A.W. Luke and J.M. Rawson.
   J. Chem. Soc., Dalton Trans., 1993, 967-972.

3. "Redox chemistries of substituted aryl 1,2,3,5 dithiadiazolyls and 1,3,2,4 dithiadiazolylium cations".
   C.M. Aherne and A.J. Banister.
   Phosphorus, Sulphur and Silicon and the Related Elements, 1994, 93, 453-454.

4. "Reaction of $[SNS][AsF_6]$ with $Hg(CN)_2$ and PhHgCN - Preparation and crystal structures of $[Hg(CNSNS)_2][AsF_6]_2$ and $[PhS_4N_3Ph][AsF_6]$".
   C.M. Aherne, A.J. Banister, I. Lavender, S.E. Lawrence, J.M. Rawson and W. Clegg.
   Polyhedron, 1996, 15, No. 11, 1877-1886.

5. "Electrochemical investigation of some fluorinated dithiadiazolylium salts and related radicals".
   C.M. Aherne and A.J. Banister.
   Manuscript in preparation.

6. "Investigation into the ESR activity of fluorinated dithiadiazoles".
   C.M. Aherne, A.J. Banister and J.M. Rawson.
   Manuscript in preparation.

Abstract

This work centres around the electrochemical and structural studies of 1,2,3,5 and 1,3,2,4 dithiadiazolylium salts and associated radical derivatives.

Chapter one provides a brief history of sulphur nitrogen chemistry, in particular developments of 1,2,3,5 and 1,3,2,4 dithiadiazolylium/ heterocyclic species. Also a quick outline of the pathways my research took are discussed.

The following chapter is solely dedicated to the electrochemical investigations of (i) mono substituted aryl 1,2,3,4 and 1,3,2,4, (ii) di substituted aryl 1,2,3,4 and 1,3,2,4 and (iii) pyridyl 1,2,3,5 dithiadiazolylium salts and associated derivatives. This electrochemical process of interest involved the reduction of the 6π dithiadiazolylium cation going to the 7π radical. This was studied using a technique called Cyclic Voltammetry. Results from this survey revealed that all the derivatives studied were quasi-reversible to the same degree under these experimental conditions. The $E_{pc/2}$ potentials of *meta* and *para* derivatives were observed to increase with acceptor property of the substituent group attached. Using the relationship $E_{pc/2} = \sigma\rho$, when the potentials of these derivatives were plotted against corresponding Hammett σ values two excellent linear free energy relationships for both sets of derivatives were seen to exist. For the other systems this is not found to be so. Rationalisation of these responses are described by examination of electronic, solvent and steric factors of analogous benzoic acid and dithiadiazolylium/zolyl derivatives and how they compare with each other.

Chapter three concentrates on the structural properties of dithiadiazolyls and discusses the potential of these types of derivatives to form conducting, charge transfer or magnetically interesting materials. The X-ray structures of the following compounds were obtained and are described in detail: pMeS-C_6H_4-CNSSN$^\bullet$, pF-C_6H_4-CNSSN$^\bullet$, pCF_3-C_6H_4-CNSSN$^\bullet$, pNO_2-C_6H_4-CNSSN$^\bullet$, mBr-C_6H_4-CNSSN$^\bullet$, mClpMe-C_6H_4-CNSSN$^\bullet$, mC_5H_4N-CNSSN$^\bullet$ and pC_5F_4N-CNSSN$^\bullet$. Comparisons of how these and similar dithiadiazolyl compounds pack with a view to rationalising packing trends, in order to molecular tailor materials for applications, is tackled as well.

The forth chapter concerns the experimental details of this research and features information on technical procedures, synthetic routes and characterisation on the compounds examined.

Finally chapter five attempts to bridge the results of the previous chapters all together.

Contents:

Chapter 1

TABLE DES DIFFERENTS RAPPORTS
observes entre differentes substances

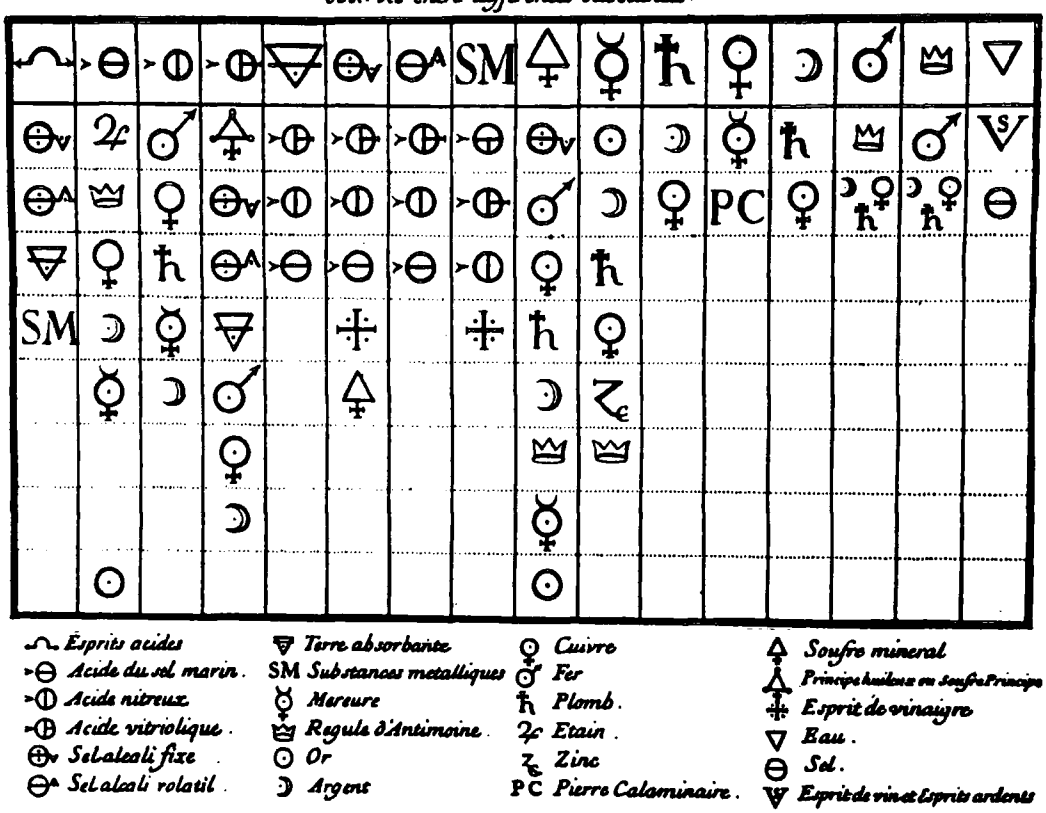

Esprits acides
Acide du sel marin.
Acide nitreux.
Acide vitriolique.
Sel alcali fixe.
Sel alcali volatil.
Terre absorbante.
SM Substances metalliques
Mercure.
Regule d'Antimoine.
Or.
Argent.
Cuivre.
Fer.
Plomb.
Etain.
Zinc.
PC Pierre Calaminaire.
Soufre mineral.
Principe huileux ou Soufre Principe
Esprit de vinaigre.
Eau.
Sel.
Esprit de vin et Esprits ardents

Fig. 10. Geoffroy's Table of Affinities. (From *Mémoires de l'académie royale des sciences*, 1718, p. 212.)

1. Introduction

1.1 History and development of Sulphur-Nitrogen chemistry

Sulphur nitrogen chemistry has been around for some 160 years. In 1835, W. Gregory first prepared S_4N_4 in an impure form[1]. It took 16 and 61 more years before the correct stoichiometry and its tetrameric nature were established respectively[2].

This material over the years, including the present day, has shown itself to be a very useful reagent for many other types of sulphur nitrogen systems[3]. In particular it is a useful source of S_2N_2. This is made by passing S_4N_4 vapour over silver wool at 250-300°C and 0.1-1.0mmHg[4]. Silver is used as it removes sulphur generated from the thermal decomposition of S_4N_4, with the added bonus that the silver sulphide formed catalyses the reaction.

$$S_4N_4 + 8Ag \longrightarrow 4Ag_2S + 2N_2$$

$$S_4N_4 \xrightarrow{Ag_2S \text{ catalyst}} 2S_2N_2$$

In 1910 F. B. Burt observed that this compound polymerised over several days to a metallic bronze coloured material, namely $(SN)_x$ [5]. It was not until 50 or so years later that the conducting properties of this material were realised. By 1973 it had been shown that this material was indeed a metal down to liquid helium temperatures.

Around the same time TTF-TCNQ charge transfer salt had been shown to have conducting properties equivalent to ordinary metals[6]. Therefore due to the unique properties of these sulphur containing systems an explosion in the field of S-N chemistry was seen with the aim of producing higher conducting non-metallic systems.

Around this time technology had developed sufficiently to allow synthesis and study of air sensitive systems which had been neglected before. This opened up a new field of sulphur nitrogen chemistry for academic research and industrial application.

By the late seventies and early eighties many new sulphur nitrogen cyclic systems had been reported, in particular the isomeric 1,2,3,5 and 1,3,2,4 dithiadiazolylium cationic species[7,8]

These ring systems are air sensitive five membered carbon/nitrogen/sulphur heterocycles. They exist only in two isomeric forms, see

figs 1a & b. The dithiadiazolylium cationic species possess 6π electrons which are delocalised in the ring.

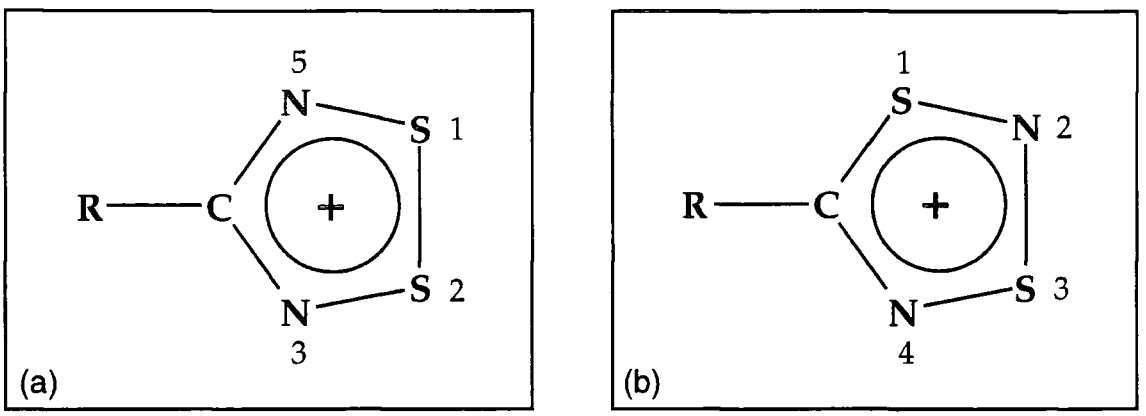

Fig 1. The isomeric (a) 1,2,3,5 and (b) 1,3,2,4 dithiadiazolylium species.

They can readily be reduced by common reducing agents such as zinc-copper couple or triphenyl antimony to 7π neutral dithiadiazolyl radicals[9]. These neutral species usually dimerise via one or two S···S interactions involving the π electrons in the solid state. The fact that each molecule has a half filled orbital or unpaired electron and shows the potential to stack through S···S interaction has lead to mainly investigating the conduction, magnetic and charge transfer properties of many derivatives of these compounds, (see section 3A.1.1 for solid state discussion).

This field of chemistry is still going strong today and this thesis describes electrochemical and structural properties of substituted aryl 1,2,3,5 and 1,3,2,4 dithiadiazolylium salts and related radicals.

Now a discussion on synthetic aspects of each compound will follow.

1.2 1,2,3,5 dithiadiazolylium salts

The first example of this ring system as a cation was reported in 1977 from the reaction of $(NSCl)_3$, sulphur and RCN, where R=CCl_3, Ph and Bu^t [10].

Further work in this field revealed that this system could be synthesised by a variety of routes as follows, running in chronological order[11,10,12]:

(1) $4(NSCl)_3 + 3RCH{=}N{-}N{=}CHR \text{ ----------> } 6RCNSSN^+Cl^- + 3N_2 + 6HCl$
where R=$C(CH_3)_3$ or Ph

(2) $[Ph{-}C(NH_2)_2]^+Cl^- + 2SCl_2 \text{ --------> } Ph{-}CNSSN^+Cl^- + 4HCl$

(3) $NH_4Cl + SCl_2$ ----------> $NSCl_{\text{in situ}} + S$ ----------> $RCNSSN^+Cl^-$
where R=CCl_3 and Ph

(4) $RCN + LiN(SiMe_3)_2$ ----> $R\text{-}C(NSiMe_3)_2^-Li^+ + 2SCl_2$ ----> $RCNSSN^+Cl^- + LiCl + 2SiMe_3Cl$
where R=aryl groups

Routes 1 to 3 are usually messy low-yielding reactions. However development of the amidine route in 2, using persilylated amidines made by the Sanger reaction[13], i.e, the addition of lithium bis trimethyl silyl amide to aryl nitrile, lead to the arrival of route 4, which is a more convenient way of preparing aryl 1,2,3,5 dithiadiazolylium chlorides.

1.3 1,3,2,4 dithiadiazolylium salts

The other isomer is made by reacting RCN with $S_2N^+AsF_6^-$ in liquid SO_2 at room temperature for 24 hours[14]. Percentage yields are typically between 80 to 98%.

$S_2N^+AsF_6^- + R\text{-}C{\equiv}N$ ----------> $RCNSNS^+AsF_6^-$

A discussion on the reagent $S_2N^+AsF_6^-$ will now follow with further details of the mechanism of this reaction

1.4 S_2N^+ reagent

The dithionitronium species, as the hexachloroantimonate salt, was first reported by Gillespie in 1978, and was produced from the oxidation of S_7NH, S_7NBCl_2 or 1,4-$S_6(NH)_2$ with $SbCl_3$ [15]. However other S-N side products were observed and yields were unspecified.

Soon after this discovery other workers reported the preparation and isolation of the hexafluoroarsenate salt from the following reactions[16]:

$S_8(AsF_6)_2 + NaN_3$ -----> $S_2NAsF_6 + NaAsF_6 + N_2 + 3/4S_8$

$1/2\ S_8 + S_4N_4 + 6AsF_5$ -----> $4S_2NAsF_6 + 2AsF_3$

These routes were shown to be a better method to obtaining a pure source of S_2N^+ species in high yields. A major draw back of the above two reactions is the starting materials involved are potentially hazardous, e.g, explosive S_4N_4 and azide, and toxic AsF_5. Hence a safer method of preparing this reagent was developed which involved dechlorinating $N(SCl)_2^+$ cation with tin (II) chloride as follows[17]:

$$N(SCl)_2^+X^- + SnCl_2 \xrightarrow[\text{solvent Y}]{} S_2N^+X^- + SnCl_4$$

where X= $SbCl_6$ and Y=SO_2 or X=$AlCl_4$ or Y=CH_2Cl_2

The dithionitronium hexafluoroarsenate salt is highly reactive and is a useful synthetic reagent as it is readily halogenated and undergoes concerted, symmetry allowed 4+2 cycloaddition reactions with unsaturated bonds, see fig 2.

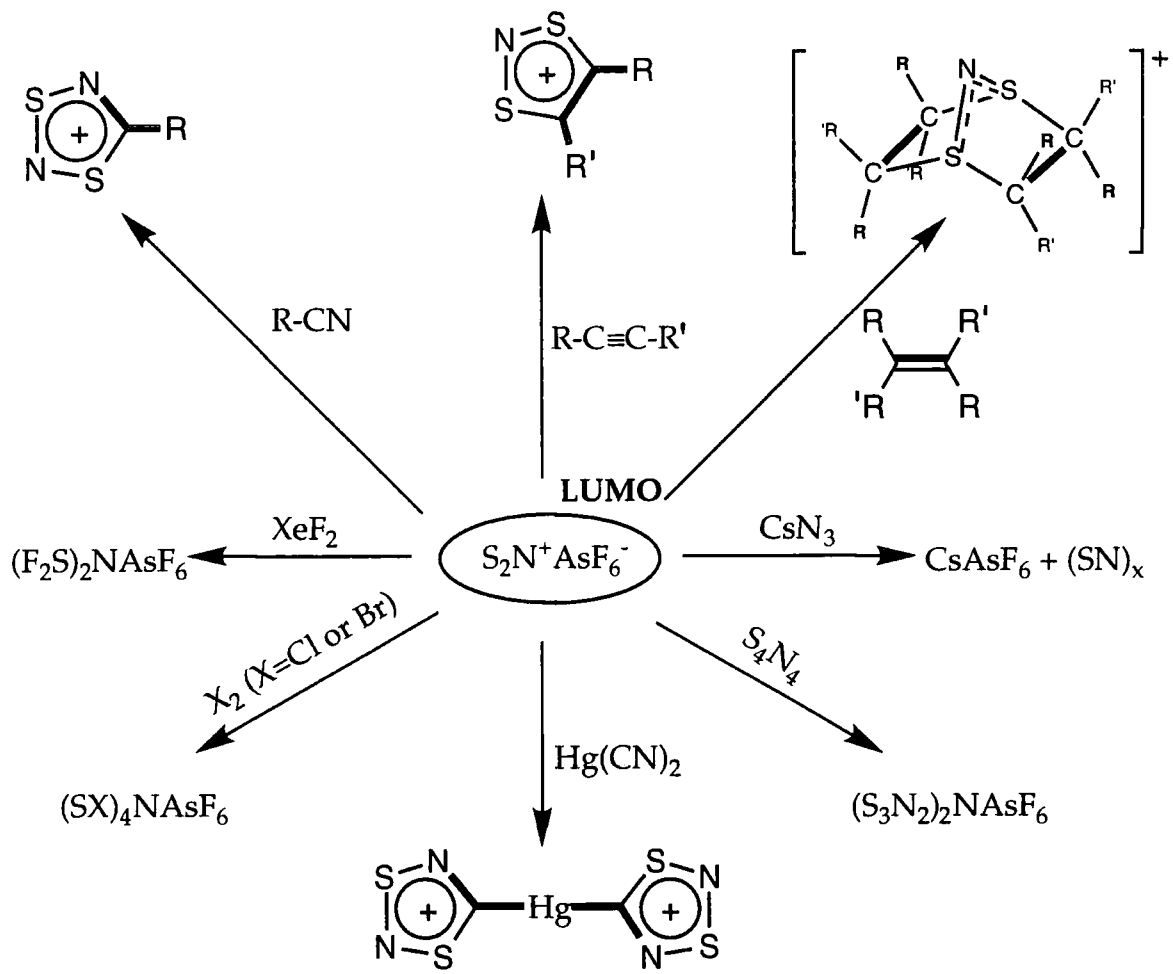

Fig 2. Reactions of $S_2N^+AsF_6^-$ [18].

Work by Oakley *et al* demonstrated that the cycloaddition reactions occur via a reverse electron demand process[19], i.e. primary interaction is donation from the HOMO of the unsaturated species to the LUMO of the S-N species, see fig 3

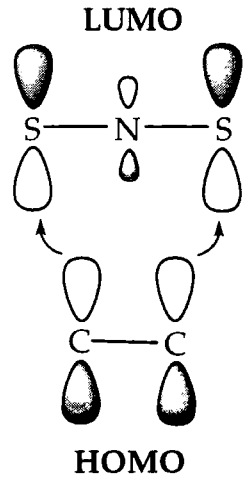

Fig 3. Reverse electron demand process for S_2N^+ species with an unsaturated hydrocarbon.

1.5 Rearrangement of 1,3,2,4 dithiadiazolyls to 1,2,3,5 analogues

The 1,3,2,4 radicals rearrange photochemically and thermally in solution to the 1,2,3,5 isomers. This has been proved by ESR, CV and DSC measurements[20].

MO calculations by Passmore et al show that the eigenvector coefficients for the SOMO orbital for this ring is π-type MO based primarily on the two sulphur atoms[20]. The proposed rearrangement mechanism relies on the fact that inherent dipole moment and the shape of the SOMO orbitals make the head to tail, face to face conformation the most favourable, see fig 4a.

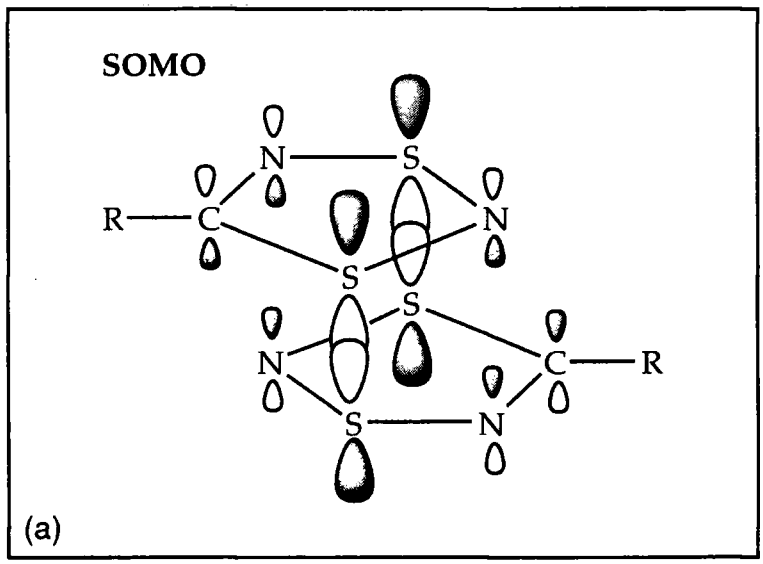

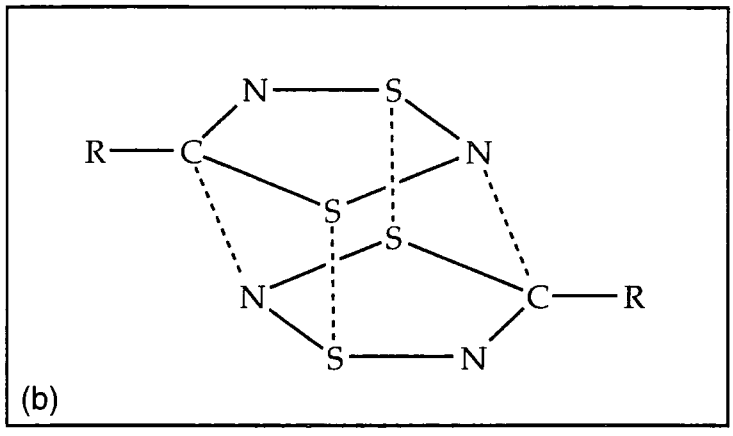

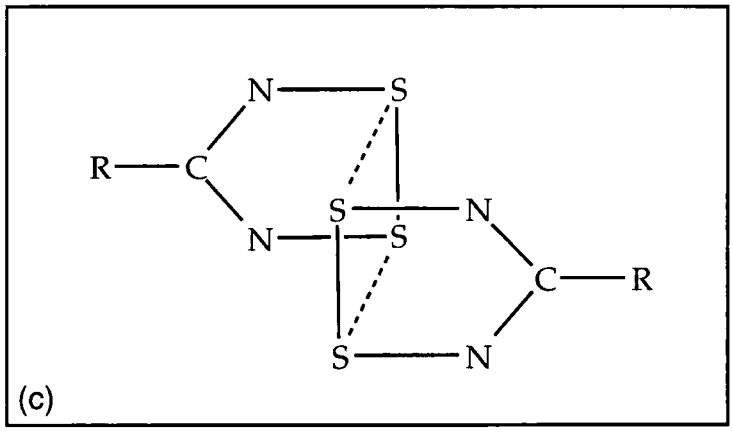

Fig 4a-c. Rearrangement process of the 1,3,2,4 dithiadiazolyl species to the corresponding 1,2,3,5 isomer

The effective overlap of the sulphurs and the additional interaction of the carbon and nitrogen atoms of opposite rings promotes formation of new C-N bonds. Hence, rearrangement from the 1,3,2,4 to the 1,2,3,5 can be achieved by minor spatial adjustment of the atoms, see fig 4b and 4c.

1.6 Research Aims of this Project

Introduction to research aims

The initial aim of this project was to investigate the non-linear optic (NLO) activity, in particular second order harmonic generation, of dithiadiazolyl species. These types of measurements had never been conducted on this family of compounds before. This project was a joint venture between the chemistry and physics departments of Durham University. I was mainly involved with the chemistry of these material, i.e. synthesising a selection of suitable dithiadiazolyl compounds, whose NLO activity would be tested by physicists in the applied physics group.

A brief background into NLO will now follow, which will assist in clarifying what this phenomenon is and the choice of compounds chosen for this investigation.

Non-linear Optics

NLO activity is basically a measure of a compounds ability to alter the frequency of light which passes through it[21]. A NLO response is observed because the oscillating electric field of the light which enters the medium creates a non linear polarisation in its molecules. This polarisation can be expressed as a power series of the field strength[22],

molecular $p= \alpha.E + \beta.EE + \gamma.EEE$

bulk $P= \chi^{(1)}.E + \chi^{(2)}.EE + \chi^{(3)}.EEE + \text{higher terms} = \chi_{eff}.E$

where
p = polarisation at the molecular level
P= polarisation in the bulk media
$\chi^{(2)}$ = second order susceptibility
β = second order hyperpolarisability term
$\chi^{(3)}$ = third order susceptibility
γ = third order hyperpolarisability term
E = electric field

If $E_{(z,t)} = E^{(0)}\cos(\omega t-kz)$, then the polarisation in the bulk media is given by,

$$P= \chi^{(1)}.E_0\cos(\omega t-kz) + 1/2\chi^{(2)}.E_0^2[1+\cos(2\omega t-2kz)] + \chi^{(3)}.E_0^3[3/4\cos(\omega t-kz) + 1/4\cos(3\omega t-3kz)] + \text{higher terms}$$

where
k = propagation constant in the material
z = direction ω = frequency

Naturally an analogous equation will exist for polarisation at the molecular level too.

$\chi^{(2)}$,$\chi^{(2)}$,β and γ NLO coefficients are subject to symmetry considerations of the medium. Second order NLO activity, $\chi^{(2)}$ and β components of the above equations, will only be observed for non-centrosymmetric media. However, third order NLO activity, terms $\chi^{(3)}$ and γ, will be observed regardless of symmetry. Therefore, any type of molecule is NLO active, but polarisation or the type and size of NLO observed differs between different materials.

The last equation can be used to show the effect on the frequency of light that occurs from particular types of NLO responses of materials. By looking at the terms which correspond to second and third order activity, it can be seen that a second order response results in the frequency of the light being doubled and for third order the frequency is tripled. Therefore, the type and size of NLO response can be detected by observing a ratio of the differences in the frequency of the light before and after it has passed through the NLO material. The light usually used to observe this phenomenon is laser light, as a laser can generate an intense coherent beam of light of one frequency.

Many photonic devices require light to be changed to a different frequency and therefore many of them have NLO materials incorporated into them, e.g. optical switches, optical storage and light modulators[23]. These types of devices are heavily used by the telecommunication industry. NLO materials used in these types of appliances are usually ones that can double the frequency of light, i.e second order NLO materials. In the first commercial appliances the materials used were inorganic[24]. However, as time progressed second order NLO active organic compounds with second order coefficients equivalent to or higher than the former compounds were discovered[25]. The organic materials were often easier and cheaper to produce than their inorganic counterparts. This sparked industrial interest to produce organic materials possessing high NLO activity. Many of these types of organic compounds can now be found in commercial photonic devices.

One of the main objectives of this project was to investigate novel NLO materials, with the possibility of developing them for industrial applications. As second order materials are of more interest commercially and this type of NLO activity is easier to detect accurately, only the second order NLO activity of these novel compounds was chosen to be investigated. If the materials investigated gave large β or $\chi^{(2)}$ coefficients, (i.e. high second order NLO responses), then the possibility of incorporating these materials into industrial photonic appliances would be considered.

As the main interest of the investigation was biased towards second order NLO response of novel materials, the following NLO discussions will not include any details on the corresponding third order processes.

The type and size of second order NLO activity that a material possesses is very dependent on the type and packing of its molecule[26]. Molecular specifications required for high second order activity are now assessed.

(1) As previously mentioned, the molecule or its bulk packing must be non-centrosymmetric for second order NLO response to occur (centrosymmetric for third harmonic generation).

(2) Secondly, the molecule must possess a dipole moment. The equation below shows how the incident field is related to the permanent and induced dipole moment. The even power terms cancel out if the medium is centrosymmetric, while the odd terms are non zero for media of any symmetry.

$$U(E) = U^0 - \sum_i n^0 E_i - \frac{1}{2}\sum_{ij} \alpha_{ij} E_i E_j - \frac{1}{3}\sum_{ijk} \beta_{ijk} E_i E_j E_k - \frac{1}{4}\sum_{ijkl} \gamma_{ijkl} E_i E_j E_k E_l$$

$$\mu_i(E) = \mu_i^0 + \sum_j \alpha_{ij} E_j + \sum_{jk} \beta_{ijk} E_j E_k + \sum_{jkl} \gamma_{ijkl} E_j E_k E_l$$

where U^0 = energy in absence of field $U(E)$ = energy in presence of field
μ_i^0 = permanent dipole moment μ_i = induced dipole moment

For a molecule to exhibit a high second order NLO response it must possess a large dipole moment.

(3) For a material to possess a high second order NLO response its molecule must also possess a polarisable delocalised system, e.g. vinyl or phenyl. Generally the NLO response increases with the length of the delocalised system up to a point and then begins to tail off. This is usually due to optical transparency of the material decreases as chain length increases.

(4) It is important that the frequency of the light used in the measurement is not in the region where the material can absorb it. If this is the case the absorbed light will heat the sample and probably begin to degrade it. Therefore, a weaker or no NLO response will be observed.

An example of a good basic second order NLO organic compound which possesses all the above features is *para* nitro phenyl aniline[27].

By referring to the previous molecular guidelines, it was considered that the best dithiadiazolyl radical compounds to start the NLO investigation off with were the *para* substituted 1,2,3,5 phenyl derivatives.

From experience of other NLO materials it is known that vinyl derivatives give better NLO values than phenyl analogues. However, substituted vinyl 1,2,3,5 dithiadiazolyl derivatives could not be made as the starting materials required to make the heterocyclic ring react with the unsaturated vinyl bond. The reverse is true for phenyl analogues, hence they were the next best derivatives for this type of NLO study[12].

Isomeric substituted phenyl 1,3,2,4 dithiadiazolyl analogues are possible to make too. These types of derivatives are known to rearrange in heat and light to analogous 1,2,3,5 derivatives[20]. Therefore, the NLO activity of isomeric 1,3,2,4 analogues was not investigated as it was assumed that they would be too unstable in the presence of laser light.

The last factor to be considered before the investigation could commence is how the NLO activity of these compounds was to be measured.

The NLO activity of a synthesised compound can be measured by several different methods: Solvatochromism[28], electric field induced second harmonic generation (EFISH) [29] and Kurtz powder technique[30]. These are now briefly described.

Solvatochromism This technique is used to evaluate the difference in dipole moment between ground and excited states of a material in order to determine its β value. It involves observing the effects that solvents of differing polarity have on the u.v. absorption of the material of interest. The mathematics involved in the determination of β from u.v. data can be found in reference 28.

EFISH With this second technique a solution of the sample of interest is placed into a cell with a quartz window of known dimensions. An electric field is then placed across the cell in order to orientate the molecules in one direction. Pulses of laser light are then allowed to enter the cell via the quartz window. Any light which exits the cell is picked up by a detector positioned directly behind it. The laser usually used in this experiment is a Nd^{+3} YAG laser which emits light with a frequency of 1.06μm. Therefore, light at twice this frequency will be observed if the material exhibits a second order NLO response. The equations and parameters required to calculate β of a sample from this experiment can be found in reference 29.

The above two methods involve investigating the second order NLO measurement of a sample while it is in solution. During the discussion of

molecular design of second order materials one of the criteria was that the bulk packing of the material must be non-centrosymmetric. Therefore, this factor can be ignored using the above methods. However symmetry of individual molecules is still an important factor in determining the NLO response of a material.

Kurtz powder technique As the name suggests, this method involves investigations of powders. In this case the NLO response is detected by observing changes in the frequency of light after it has passed through the powdered sample of interest, relative to that of a reference material. Again a Nd^{+3} YAG laser is usually used to generate light of 1.06μm frequency. In this experiment the single light beam from the laser is split into two such that one beam goes to the sample and the other to a reference compound which is a 2nd order NLO material. For these measurements it is critical that the molecules pack non-centrosymmetrically (asymmetrically) in order to observe a second order NLO response. The reference compound used is usually urea. During the measurements the powder needs to be confined. This is usually achieved beforehand by loading the compound of interest into the middle of a thin washer which has been stuck to a glass slide and gluing a cover slip on top such that the material of interest is sandwiched between two slides. When light is directed on to the reference and the sample, light which passes through them is picked up by detectors that are positioned behind the samples and then analysed. The NLO activity of the sample is then given as a ratio relative to the NLO activity of the reference. It is important to mention that this technique is very sensitive to particle size (typically 100μm or less). For more details see reference 30.

This method is often a very useful way of determining if a compound packs centrosymmetrically or asymmetrically, especially if its crystal structure is unknown.

The technique that was intended to be used for the NLO measurements on the dithiadiazolyl derivatives was EFISH. This was because these molecules would exist as monomers in solution rather than dimers as anticipated in the solid state, i.e. strong intradimer interactions that could effect the polarisation of these molecules in light could be ignored (see chapter 3). Also, as mentioned previously with this technique bulk packing of the samples can be ignored too. Finally, EFISH measurements could be conducted on these materials of interest as they were readily soluble in the desired solvents required to conduct the measurements.

Para NO_2, CN, CF_3, Br, Cl, F, H, MeS and MeO phenyl 1,2,3,5 dithiadiazolyl derivatives were made with the intent of studying the NLO activity among this group. Unfortunately, EFISH measurements were never conducted on these air sensitive materials due to problems the physicists encountered in designing a cell that was air tight and the laser rig used to conduct the measurements.

Nevertheless it was possible to measure the NLO activity of these compounds using the Kurtz powder method. This process introduces additional complications due to the requirement that the compounds must pack non-centrosymmetrically in order to observe a second order NLO response. At this stage of the proceeding the structures of the MeS, CN, CF_3 and H were known. Out of these compounds only the MeS and H packed asymmetrically. Therefore, even though a zero NLO response was expected for some samples, i.e. centrosymmetric ones, all the samples were run to see if this technique could be used as a method to screen if compounds packed centrosymmetrically or not.

When measurements on these compounds were conducted, zero reading were observed for all the derivatives, including the asymmetric packing pMeS and H derivatives which were expected to give a second order NLO response. Several reasons can be used to explain why zero readings were observed.

(1) Absorption. This is probably a small effect as prolonged exposure to the laser didn't result in any visible signs of degradation of the samples[21].

(2) Particle size does have an influence on the NLO response. When samples with finely crushed and course powders were examined a zero response was still observed.

(3) These compounds may just have a low NLO. This could be attributed to electron density preferring to stay in the dimer rather than polarise in light. Other inter and intramolecular contacts may place the same effect too.

These results clearly indicate the importance for EFISH measurements to be conducted on these materials in order to discover the NLO activity of these materials as monomers.

Electrochemistry

In conjunction to the NLO studies on the *para* substituted phenyl 1,2,3,5 dithiadiazolyl radicals an investigation of the electrochemical properties of these compounds and their associated hexafluoroarsenate salts was also conducted (see chapter 2). This involved studying the redox process between the dithiadiazolylium cation and dithiadiazolyl radical using CV. It was anticipated

that results from this survey would assist in assessing the electronic effects the substituent groups have on the environment of the ring. A very brief description of the electrochemical results achieved and the direction the research took will now follow.

The electrochemical survey on these materials revealed that they are all quasi-reversible to the same degree. The reduction potentials of these derivatives are seen to increase with increasing electron withdrawing capacity of the substituent group. The molecular bonding framework of these heterocyclic materials is very similar to that of analogous benzoic acids. Therefore, $E_{pc/2}$ reduction potentials of these dithiadiazolylium/zolyl derivatives were plotted against corresponding Hammett substituent values to see if a linear free energy relationship existed and an excellent relationship was indeed found. From these results it can be deduced that electron withdrawing groups make the reduction process more favourable and the opposite is observed for electron donating groups. This information can be used to deduce the relative effect a substituent would have on charge transfer within these derivatives.

A similar investigation involving analogous 1,3,2,4 dithiadiazolylium analogues was conducted in order to compare the electrochemistry of the *para* isomers. The results showed that both series of isomers are quasi-reversible to the same degree and that the range in potentials among the 1,3,2,4 series is the same as that observed among analogous 1,2,3,5 derivatives. A linear free energy relationship was also found to exist whose gradient was within experimental error of that observed for an analogous plot involving 1,2,3,5 analogues. Therefore, from these results it was deduced that solvents effects and the electronic influence a substituent places on the ring are comparable between these two series of isomers. One major difference between the isomeric analogues was found; the reduction potentials of the 1,3,2,4 derivatives were found to be lower than those of 1,2,3,5 analogues. This is attributed to the HOMO and the LUMO for the 1,2,3,5 derivatives being at lower energy and closer together than the corresponding MO's of a 1,3,2,4 analogue, i.e. a 1,2,3,5 derivative is easier to reduce than the corresponding 1,3,2,4 analogue.

The successful electrochemical studies of *para* derivatives prompted similar electrochemical investigation on other analogues, e.g. (i) *meta, ortho,* difluoro and disubstituted aryl dithiadiazolylium/zolyls and (ii) perfluoro and unsubstituted pyridyl dithiadiazolylium/zolyls derivatives. All these derivatives were found to be quasi-reversible to the same degree as the *para* derivatives. Also, for isomeric analogues, the potentials of the 1,2,3,5 derivatives was consistently found to be

higher than that of the corresponding 1,3,2,4 derivative. These trends occur for the same reason that were given to explain the similar *para* trends.

A larger difference in the range in potentials was observed among *para* derivatives, (possessing electron donating and withdrawing groups), relative to analogous *meta* derivatives. The main difference between *para* and *meta* substituents is that the *para* substituents possess a resonance contribution but the *meta* analogues can't. Therefore, differences in potentials are observed between these two groups because of the additional resonance contribution of the *para* substituents.

Simple linear free energy plots of derivatives possessing *ortho* substituents showed that simple linear plots couldn't be drawn. These discrepancies are attributed mainly to the presence of varying steric forces between series of *ortho* substituted phenyl dithiadiazolyls and analogous benzoic acids. For disubstituted derivatives further complications in these type of plots arose due to (i) possible competition of resonance contributions involving the substituents and the reaction centre and (ii) differing solvent effects. The effect of steric hindrance from *ortho* substituents was also encountered during the synthesis of many *ortho* 1,2,3,5 derivatives. As a result of this only 1,2,3,5 derivatives possessing small *ortho* groups, e.g. fluorine or hydrogen, could be successfully made.

This electrochemical survey revealed many interesting electrochemical trends among substituted phenyl and pyridyl dithiadiazolylium and associated radical derivatives. These results when compared with corresponding Hammett σ data, clearly showed the influence induction, resonance and steric contribution from a substituent group can place on the electronic environment of the reaction centre.

Due to the problems encountered with the NLO measurements involving *para* substituted phenyl 1,2,3,5 dithiadiazolyls, no attempt at investigating the NLO activity of the analogous materials prepared specially for the above electrochemical investigation was made.

Crystallography

Structural studies on many of the radical 1,2,3,5 derivatives and some *ortho* substituted phenyl 1,3,2,4 and a few pyridyl 1,2,3,5 dithiadiazolylium salts were also attempted (see chapter 3).

The *ortho* 1,3,2,4 derivatives were studied in order to get a better idea of the steric effects these types of substituents place on the geometry of the molecule and hence the influence this has on the electrochemistry or electronic environment of the reaction centre.

The other derivatives were studied as it was anticipated that results from these structural investigations would reveal packing trends among these derivatives and therefore this information would assist in predicting how other analogous derivatives would pack. Dithiadiazolyl derivatives have the potential to form materials which either have high NLO activity, possess interesting magnetic properties, form charge transfer salts or are highly conducting depending on their molecular packing. Therefore this type of structural information in packing trends is particularly useful in designing analogous materials for such applications.

The structures of the following substituted aryl 1,2,3,5 derivatives were obtained using x-ray crystallography methods: pMeS, pF, pCF_3, pNO_2, mBr and mClpMe. Also the structures of *meta* pyridyl and *para* perfluoropyridyl 1,2,3,5 dithiadiazolyl were obtained. The structural trends from these eight compounds and similar derivatives reported in the literature suggest that these types of derivatives will typically pack as dimers via S···S interaction and that the molecules of the dimers will usually be cis-oid for derivatives possessing small substituent groups. The dimers of derivatives possessing a strong electron withdrawing group tend to pack as ribbons. This is also observed for derivatives possessing many electron withdrawing groups too. However, herring-bone type packing is observed for derivatives possessing groups which are better electron donors or weak acceptors.

Conclusion

The following chapter is dedicated to the electrochemical research on these derivatives. This leads on to chapter 3 which deals with structural analysis for substituted aryl and pyridyl dithiadiazolyls. Finally, chapter 4 deals solely with the synthetic aspect of these materials.

Happy reading

References:

1 W. Gregory, *J. Pharm. Chim.*, 1835, 21, 315.

2 (a) C. Lu and J. Donohue, *J. Am. Chem. Soc.*, 1944, B18-27, 66.
(b) D. Clark, *J. Chem. Soc.*, 1952, 1615.

3 (a) H. W. Roesky, *Adv. Inorg. Chem. Radiochem.*, 1979, 22, 239.
(b) H. W. Roesky, *Angew. Chem., Int Edn.*, 1979, 18, 91.

4 N. N. Greenwood and A. Earnshaw, *Chemistry of the Elements*, Pergamon Press, 1984.

5 M. M. Labes, P. Love and L. F. Nichols, *Chem Rev.*,1979, 79, 1.

6 (a) L. R. Melby, R. J. Harder, W. R. Hertler, W. Mahler, R. E. Benson and M. E. Mochel, *J. Am. Chem. Soc.*, 1962, 84, 3374.
(b) D. S. Acker and D. C. Blomstrom, *U.S Patent* No. 3162641, 1962.
(c) J. B. Torrance, *Acc. Chem. Res.*, 1979, 12, No 3, 79.

7 O. Andreasen, A. C. Hazell, R. G. Hazell., *Acta. Crystallogr.*, 1977, B33, 1109.

8 (a) R. Neidlein, P. Leinberger, A. Gieren and B. Dederer, *Chem. Ber.*, 1978, 111, 698.
(b) R. Neiden and W. Lehr. *Chem. -Ztg.*, 1980, 104, 200.

9 (a) A. J. Banister, I. Lavender, J. M. Rawson and R. J. Whitehead, *J. Chem. Soc., Dalton Trans.*, 1992, 1449.
(b) A. J. Banister, M. I. Hansford, Z. V. Hauptman and S. T. Wait, *J. Chem. Soc., Dalton. Trans.*, 1989, 1705.
(c) A. J. Banister, N. R. M. Smith and R. G. Hey, *J. Chem. Soc., Perkin Trans.*, 1983, 1, 1181.

10 (a) G. G. Alange, A. J. Banister, B. Bell and P. W. Millen, *J. Chem. Soc., Perkin I*, 1979, 1192.
(b) G. G. Alange, A. J. Banister, B. Bell and P. W. Millen, *Inorg. Nucl. Chem. Letters*, 1977, 13, 143.

11 H. W. Roesky and T. Müller, *Chem Ber.*, 1978, 111, 2960.

12 (a) R. T. Boere, R. T. Oakley and R. W Reed, *J. Organomet. Chem.*, 1987, 331, 161.
(b) R. T. Boere, K. H. Moock, S. Derrick, W. Hoogerdijk, K. Preuss, J. Yip and M. Parvez, *Can. J. Chem*, 1993, 71, 473.

13 A. R. Sanger, *Inorg. Nucl. Chem. Lett.*, 1973, 9, 351.

14 G. K. MacLean, J. Passmore, M. J. Schriver, P. S. White, D. Bethell, R. S. Pilkington and L. H. Sutcliffe, *J. Chem. Soc., Chem. Commun.*, 1983, 807.

15 R. Faggini, R. J. Gillespie, C. J. L. Lock and J. D. Tyrer, *Inorg. Chem.*, 1978, 17, 2975.

16 A. J. Banister, R. G. Hey, G. K. MacLean, J. Passmore, *Inorg. Chem.*, 1982, 21, 1679.

17 (a) A. J. Banister and J. M. Rawson, *J. Chem. Soc., Dalton Trans.*, 1990, 1517.
(b) B. Ayres, A. J. Banister, P. D. Coates, M. I. Hansford, J. M. Rawson, C. E. F. Rickard, M. B. Hursthouse, K. M. Abdul Malik and M. Motevalli, *J. Chem. Soc., Dalton Trans.*, 1992, 3097.

18 (a) G. K. MacLean, J. Passmore, M. N. Sudheedra Rao, M. J. Schriver, P. S. White, D. Bethell, R. S. Pilkington and L. H. Sutcliffe, *J. Chem. Soc., Dalton Trans.*, 1985, 1405.
(b) N. Burford, J. P. Johnson, J. Passmore, M. J. Schriver and P. S. White, *J. Chem. Soc., Chem. Commun.*, 1986, 966.

(c) A. J. Banister, I. Lavender, S. E. Lawrence, J. M.Rawson and W. Clegg, *J. Chem. Soc., Chem. Commun.*, 1994, 29.

19 S. W. Liblong, R. T. Oakley, A. W. Cordes and M. C. Noble, *Can. J. Chem.*, 1983, 61, 2062.

20 (a) N. Burford, J. Passmore and M. J. Schriver, *J. Chem. Soc., Chem. Commun.*, 1986, 140.
(b) W. V. F. Brooks, N. Burford, J. Passmore, M. J. Schriver and L. H. Sutcliffe, *J. Chem. Soc., Chem. Commun.*, 1987, 69.
(c) C. Aherne, A. J. Banister, A. W. Luke, J. M. Rawson and R. J. Whitehead, *J. Chem. Soc., Dalton Trans.*, 1992, 1277.

21 (a) D. J. Williams, *Angew. Chem., Int. Edn. Engl.*, 1984, 23, 690
(b) P. N. Prasad and D. J. Williams, *Introduction to Non-linear Optical Effects in Molecules and Polymers*, Wiley, Chichester, 1991.

22 (a) P. N. Prasad and B. A. Reinhardt, *Chem. Mater.*, 1990, 2, 660.
(b) Y. R. Shen, *The Principles of Non-Linear Optics*, Wiley, N. Y., 1984.

23 (a) B. Clymer and S. A. Collins, *Opt. Eng.*, 1985, 24, 74.
(b) G. I. Stegeman, *Thin Solid Films*, 1987, 152, 231.

24 (a) D. A. Kleinman, A. Ashkin and G. D. Boyd, *Phys. Rev.*, 1966, 145, 338.
(b) J. Jerphagnon, S. K. Kurtz, *Phys. Rev. B.*, 1970, 1, 1739.
(c) P. D. Maker, R. W. Terhune, M. Nisenoff and C. M. Savage, *Phys. Rev. Letters*, 1962, 8, 21.
(d) R. F. Belt, G. Gashurov and U. S. Liu, *Laser Focus - Electro-Optics*, 1985, 21, No.10, 110.

25 (a) B. F. Levine, C. G. Bethea, C. D. Thurmond, R. T. Lynch and J. L. Bernstein, J. *Appl. Phys.*, 1979, 50, 2523.
(b) G. F. Lipscomb, A. F. Garito and R. S. Narang, *J. Chem. Phys.*, 1981, 75, 1509.
(c) A. F. Garito and K. D. Singer, *Laser Focus*, 1982, 18, 59.
(d) J. Zyss, D. S. Chemla and J. F. Nicoud, *J. Chem. Phys.*, 1981, 9, 74.
(e) S. R. Marder, J. E. Sohn and G. D. Stucky, *Materials for Non-linear: Chemical Perspectives*, ed. S. R. Marder, A. C. S. Symposium Series 455, A. C. S., Washington, DC, 1991.

26 (a) D. J. Williams, (Ed), *Non-linear Optical Properties of Organic and Polymeric Materials*, A. C. S Symposium Series 233, American Chemical Society ; Washington DC, 1983.
(b) D. S. Chemla and J. Zyss, *Non-Linear Optical Properties of Organic Molecules and Crystals*, Academic Press, Orlando Fl, 1987, Vol 1 and 2.
(c) S. Ghosal, M. Samoc, P. N. Prasad and J. J. Tufariello, *J. Phys. Chem.*, 1990, 94, 2847.
(d) M. Zhao, M. Samoc, P. N. Prasad, B. A. Reinhardt, M. R. Unroe, M. Prazak, R. C. Evers, J. J. Kane, C. Jarivala and M. Sinsky, *Chem. Mater.*, 1990, 2, 670.
(e) C. C. Frazier, M. A. Harvey, M. P. Cockerham, H. M. Hand, E. A. Chauchard and C. Lee, *J. Phys. Chem.*, 1986, 90, 5703.
(f) K. D. Singer, J. E. Sohn, L. A. King, H. M. Gordon, H. E. Katz and C. W. Dirk, *J. Opt. Soc. Am. B*, 1989, 6, No 7, 1339.
(g) J. L. Oudar, D. S. Chemla and E. Batifol, *J. Chem. Phys.*, 1977, 67, 1626.

27 C. C. Teng and A. F. Garito, *Phys. Rev. Letters*, 1983, 50, No 5, 350.

28 (a) M. S. Paley and J. M. Harris, *J. Org. Chem.*, 1989, 54, 3774

(b) W. Liptay, *Angew. Chem., Int. Edn. Engl.*, 1969, 8, No.3, 177.
29 (a) K. D. Singer and A. F. Garito, *J. Chem. Phys.*, 1981, 75, 3572.
(b) T. Thami, P. Bassoul, M. A. Petit, J. Simon, A. Fort, M. Barzoukas and A. Villaeys, *J. Am. Chem. Soc.*, 1992, 114, 915.
(c) V. Pushkara Rao, A. K. Y. Jen, K. Y. Wong and K. J. Drost, *J. Chem. Soc., Chem. Commun.*, 1993, 1118.
(d) B. F. Levine, *Chem. Phy. Letters*, 1976, 37, 516.
30 (a) S. K. Kurtz and T. T. Perry, *J. Appl. Phys.*, 1968, 89, 8798.
(b) A. G. Anderson, J. C. Calabrese, W. Tam and I. D. Williams, *Chem. Phys. Let*ters, 1987, 134, No. 4, 392.

Chapter 2

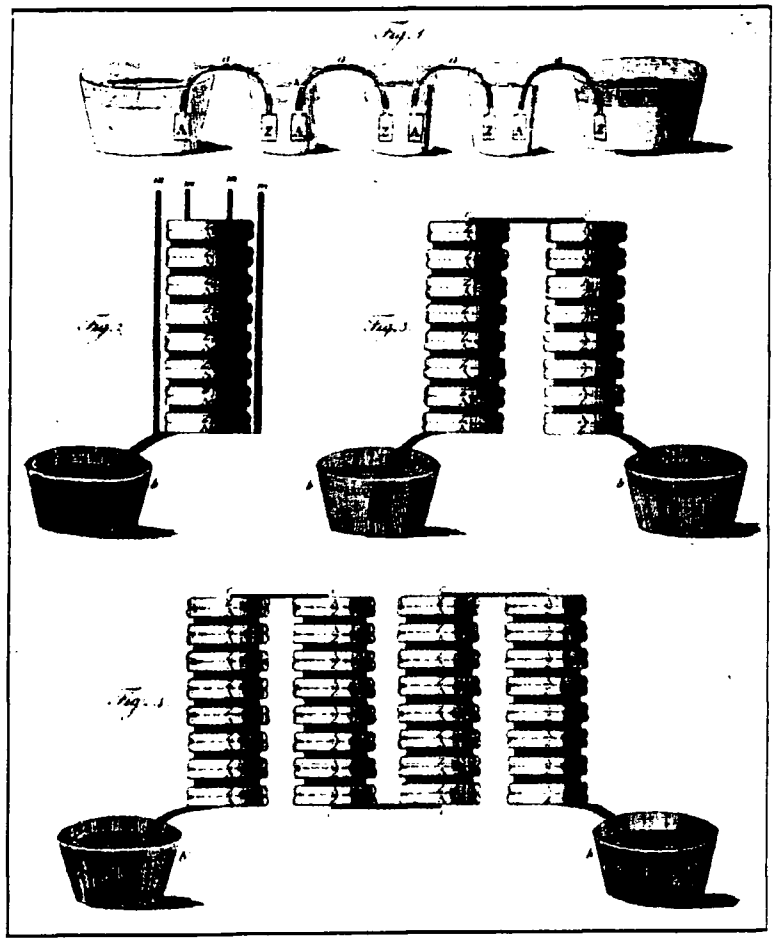

Fig. 14. Forms of the voltaic pile used by Volta. (From *Philosophical Transactions of the Royal Society*, 1800, p. 431.)

Section 2A

2A.1 Introduction

Dithiadiazolyl compounds are stable free radicals (under certain conditions) which often dimerise in the solid state via S···S interactions between the delocalised ring systems[1]. It is this unusual solid state property which makes this class of compounds attractive as potential (1) conducting, (2) charge transfer and (3) magnetic materials[2-6]

To date there is no report of a dithiadiazolylium salt or dithiadiazolyl showing an outstanding physical response of the aforementioned type, though more recently, semi-conducting and magnetically interesting examples have been reported. These are H-CNSSN$^{\bullet}$ and β*para* CN-C_6F_4-CNSSN$^{\bullet}$ respectively[6,7].

How molecular make up affects solid state properties of dithiadiazolyls is gradually beginning to be understood. But further work on the relationship between substituent groups and packing arrangements is needed before predictions of the structure and subsequent desirable properties can be made with any degree of confidence.

In order to gain further understanding of this system, the synthesis of several series of substituted aryl 1,2,3,5 and 1,3,2,4 dithiadiazolylium salts and related dithiadiazolyls was attempted. Once synthesised, structural and electrochemical properties of these materials were examined.

It was hoped that an electrochemical survey would reveal the extent that inductive, resonance and steric contributions of the substituent groups influence physico-chemical behaviour. This chapter will now deal solely with the electrochemistry of substituted aryl dithiadiazolylium salts and related compounds. Details on the crystallographic investigations can be found in Chapter 3.

The electrochemical technique which was employed for the analysis of these compounds was cyclic voltammetry (CV). This method was chosen since it is a quick, easy and convenient way of evaluating donor/acceptor properties of organic and inorganic compounds alike[8,9].

2A.2 Cyclic Voltammetry

2A.2.1 Reversible [10-12]

Cyclic voltammetry is a technique which involves sweeping from a potential where no electrode reaction occurs, through a potential where one or more electrochemical process of the solute occurs and traversing back through this potential region to the beginning, thus forming a circuit or cycle. As the potential range is scanned, variations of the concentration of the electroactive species at the surface of the electrode occur which are proportional to changes of the current. This phenomenon can be expressed by equations (1) and (2) [13],

$$i(t) = nFAD\left(\frac{\partial C(x,t)}{\partial x}\right)_{x=o} \qquad \text{Eqn (1)}$$

where i=current (A), n=number of electrons, F=Faraday constant ($Cmol^{-1}$), A=area of the electrode (cm^2), D=diffusion coefficient (cm^2s^{-1}), C=concentration at electrode surface ($molcm^{-3}$) and X=distance from electrode surface (cm).

$$i_p = 0.4463 \frac{n^{3/2}F^{3/2}}{R^{1/2}T^{1/2}} A\, D_o^{1/2} C_o^{\infty} \upsilon^{1/2} \qquad \text{Eqn (2)}$$

Equation (2) is known as the **Randles-Sevcik equation**. The terms are as defined above plus i_p=peak current (A), R=gas constant ($JK^{-1}mol^{-1}$), T=temperature (K), υ=scan rate (Vs^{-1}), C_o^{∞} concentration of bulk solution ($molcm^{-3}$).

From Eqn (2) it can be clearly seen that in addition to concentration, factors such as temperature, size of the diffusion coefficient of the sample and scan rate all affect the observed current or shape of the cyclic voltammogram. Thus, the peak height increases as concentration of electroactive species and scan rate increase, and decreases as temperature increases.

For these equations to be valid the predominant mode of mass transport must be diffusion rather than convection or migration. This is achieved in CV by not stirring the solution and making sure the solution is sufficiently conductive during measurements. The latter is usually achieved by adding an excess of an inert salt, called a supporting electrolyte and this will be discussed in more detail in part 2A.3.5.

During a CV scan the potential E is normally plotted against the current i. An example of a cyclic voltammogram for a typical reversible or Nernstian

couple is shown in Fig 1. Associated concentration profiles at the electrode surface during the scan have also been included. At the initial point, E_i, of the cyclic voltammogram of Fig 1., no reactant has been reduced and hence no increase in current is observed. As the potential is increased material starts to be progressively reduced at the surface of the working electrode and the current rises accordingly. When the concentration of the reactant is equal to that of the reduced product, (within the Nernst diffusion layer surrounding the electrode), the potential recorded is the standard potential E° for the system. Eventually there comes a point during the sweep when this diffusion layer becomes saturated with the reduced species and this is denoted by a maximum being seen on the voltammogram trace. After this point the current begins to drop as the material in the bulk solution starts to be reduced. The opposite happens on scan reversal. Therefore a cyclic voltammogram can be readily understood as being a concentration profile of electroactive species.

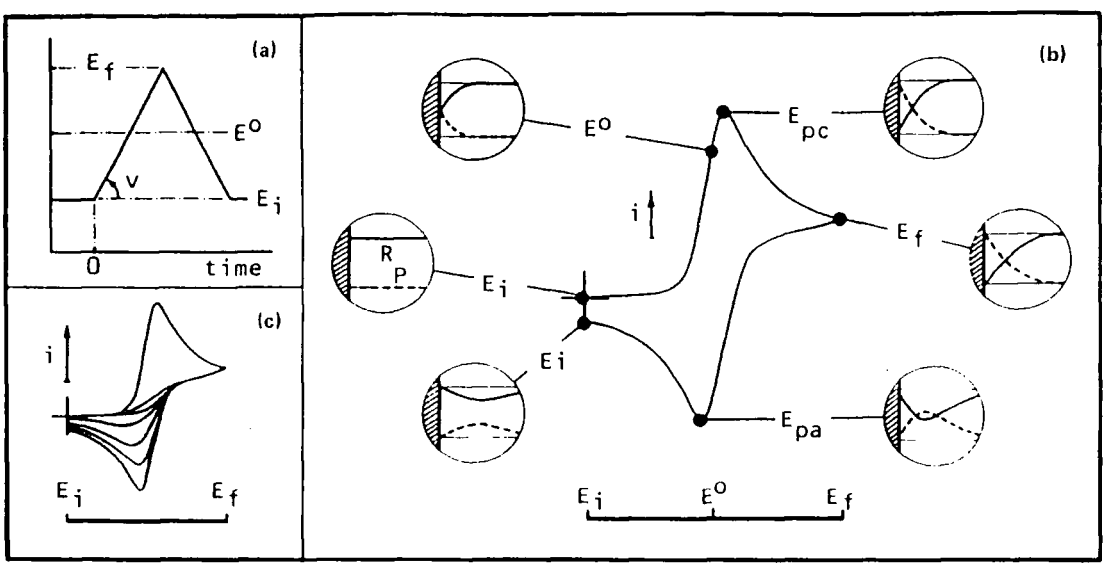

Cyclic voltammetry. (a) Imposed potential versus time variations. (b) Resulting transient current-potential curve for a simple electron transfer. The concentration profiles of the reactant R and product P are indicated at various characteristic potentials of the voltammogram. E_{pc} and E_{pa}, cathodic and anodic peak potentials. (c) Schematic change of the cyclic voltammogram as a function of the chemical stability of the product.

Fig 1. Cyclic voltammogram for a Nernstian reversible couple accompanied by several concentration profiles of electroactive species at the surface of the electrode.

Information that can be extracted from a cyclic voltammogram include the following[14] :

E_{px}	Peak potential
$E_{px/2}$	Half peak potential
$E_{1/2}$	Half wave potential
i_{px}	Peak current

where x=c for cathodic or x=a for anodic value.

Details of how these are measured is displayed in Fig 2 below.

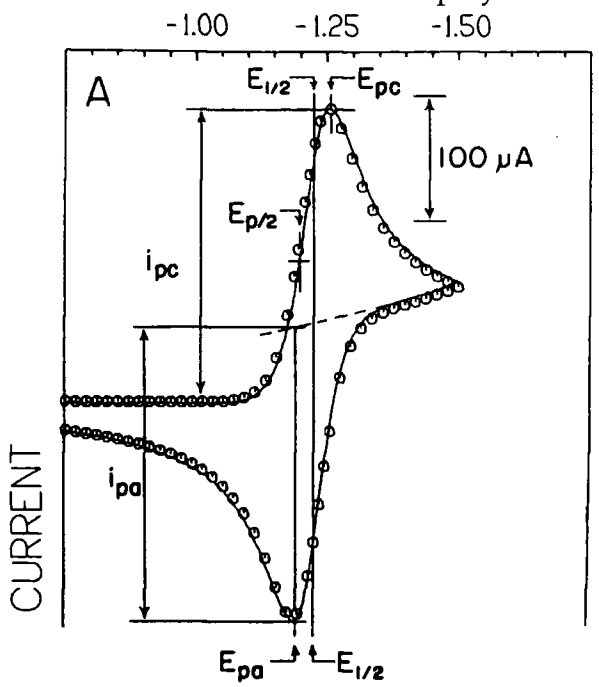

Fig 2. Cyclic voltammogram for a Nernstian reversible process.

From Fig 2, it is easy to see how the peak potentials (E_{px}) can be instantly determined from a cyclic voltammogram. Once these have been determined the middle point (known as $E_{1/2}$) between these peaks potentials can be calculated. In order to determine the other values the cathodic and anodic scan base lines must first be determined. Then the peak currents (i_{px}) and half peak potentials ($i_{px}/2$) can be measured.

For the following process to show a reversible cyclic voltammogram the rate of charge transfer is fast compared with the rate of mass transport.

$$O + ne^- \underset{k_b}{\overset{k_f}{\rightleftharpoons}} R$$

Where O=oxidized species, R=reduced species and k_f and k_b are the rate constants for the forward and backward electrochemical processes respectively.

A reversible cyclic voltammogram is readily identifiable as it will possess the following features:-

---

(1) Randles-Sevcik
Will obey equations (1) and (2), section 2A.2.1.

(2a) Half wave
If $E_{1/2}=E^\circ + (RT/nF)\ln(D_R/D_O)^{1/2}$ where $D_R=D_O$
and $E_p-E_{1/2}=E_p-E^\circ + (RT/nF)\ln(D_O/D_R)^{1/2}$
where O=oxidized species, R=reduced species, D=diffusion coefficient
Therefore,

$$|E_p-E_{1/2}|=-1.109(RT/nF) \text{ or } 29.5/n \text{ mV at } 25^\circ C$$

(2b) Standard reduction potential, E°
$(E_{pa}+E_{pc})/2 = E_{1/2} = E^\circ$

(3) Half peak
If $E_p=E_{1/2}+1.109(RT/nF)$
Therefore,

$$|E_p-E_{p/2}| = 2.2(RT/nF) \text{ or } 59/n \text{ mV at } 25^\circ C$$

(4) Peak separation
$E_{pa}-E_{pc}=2.2(RT/nF)$ or $59/n$ mV at $25^\circ C$

(5) Scan rate
$i_p \propto \upsilon^{1/2}$

(6) Peak current
$i_{pa}=i_{pc}$

(7) Peak potential
E_p is independent of υ

Only the electrochemical processes where the rate of charge transfer is considerably faster than the rate of mass transport have been considered so far, i.e. a Nernstian equilibrium can be maintained at the electrode surface throughout the experiment. However situations where this is not the case do occur and give rise to either **Quasi-reversible** or **Irreversible** electrochemical responses.

2A.2.2 Quasi-reversible[10,11]

A quasi-reversible trace is observed when there is mixed control of kinetic (charge transfer) and thermodynamic (diffusion) parameters for the electrochemical process.

Systems which are seen to be reversible can readily exhibit quasi-reversibility as scan rate increases, because the rate of electron transfer with respect to mass transport decreases with increasing scan rate (i.e a Nernstian equilibrium is harder to achieve as scan rate increases). Typical cyclic voltammograms of this process occurring can be seen in Fig 3. The first cyclic voltammogram (a), is of a typical reversible couple. As scan rate is increased the separation between the two peaks is seen to increase, i.e greater than 59/n mV, which signifies that this system is now quasi-reversible, (b-d).

Compared to reversible systems, the peaks of quasi-reversible systems become more drawn out, (i.e. further apart) as the system tends towards irreversibility. Also, the slope of the concentration profile or peak for a quasi-reversible system will be less steep too. This is due to the concentration of the electroactive species changing more slowly with potential for a quasi-reversible couple than for a reversible one.

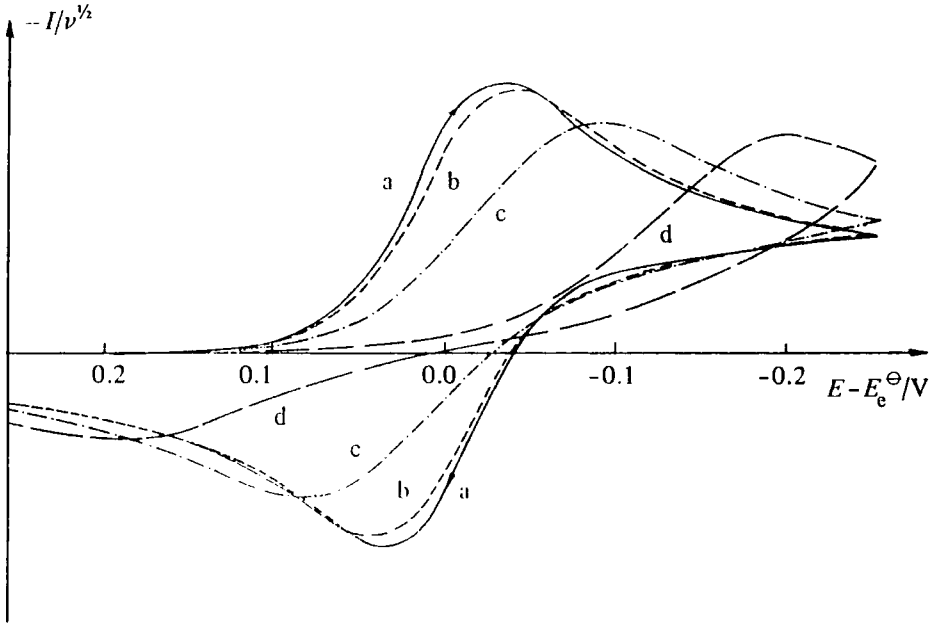

Fig 3. Cyclic voltammograms of a reversible couple, (a), which becomes quasi-reversible, (b-d), with increasing scan rate.

The cyclic voltammograms for quasi-reversible species are similar in appearance to a reversible couple but differ for the following diagnostic features:-

---

(1) Half wave
$\Delta E = | E_{pa} - E_{pc} | > 2.2(RT/nF)$ and increases with υ

(2) Scan rate
i_p increases with $\upsilon^{1/2}$ but is not proportional to it.

(3) Peak height
$i_{pa} = i_{pc}$ provided that activity coefficients $\alpha_c = \alpha_a = 0.5$

(4) Peak potential
E_{pc} shifts negatively with increasing υ

The technique for measuring current and peak potential values from a quasi-reversible cyclic voltammogram is the same as that for a reversible case, see section 2A.2.1. However, accurate assessments of these values for quasi-reversible systems are harder to achieve, as the peaks are much broader than those for a reversible couple. The effect peak broadening has on individual measurements is now described in more detail.

For peak potentials, this broadening or flattening of the peak makes it harder to pin point accurately where the maxima of the voltammogram lie and thus more difficult to determine these potentials accurately. The reliability of the other measurements depends on the accuracy of the cathodic and anodic base lines drawn. Determination of the cathodic base line involves extrapolation of the base line trace before the electrochemical reduction process has occurred. However, determination of the anodic base line is further complicated by the effect that the peak broadening has on the shape of the reverse wave, thus making assessment of this base line harder. Therefore, the cathodic base line is generally the most accurate of the two. Consequently, cathodic measurements, especially $E_{pc/2}$ values, are often quoted as they are subject to smaller errors than the other measurements.

Quasi-reversibility can also occur if the electroactive species is involved in a chemical reaction whose rate is significant with regards to the speed of the scan, i.e. there is enough time for the chemical reaction to occur. The presence of such a competing chemical reaction results in a reduction in concentration at the surface of the electrode of the electroactive species and hence a smaller corresponding

peak current is observed. Therefore i_{pc}/i_{pa} does not equal unity. This effect is reduced as scan rate is increased. Greater detail on this topic is covered in the adjoining section 2A.2.3.

As previously mentioned, the peak to peak width for a quasi-reversible couple is found to be greater than the ideal value for a reversible system of 59/n mV at 25°C and i_{pc}/i_{pa} doesn't always equal one. Hence accurate measurements of $E_{1/2}$ can not be deduced using methods for reversible couples. By examining how the peak to peak separation or peak height varies with scan rate, the kinetics of the electron transfer process or chemical reaction can be calculated; further details can be found in references 15-19.

Often effects of adsorption at the electrode surface are mistaken for a quasi-reversible response. Details on this subject can be found in section 2A.2.4.

The electrochemical scenario where no reverse process occurs, commonly known as irreversibility, will be considered now.

2A.2.3 Irreversible[10,11,20]

This is characterised by the absence of a reverse peak. It occurs when the rate of charge transfer is insufficient to maintain an equilibrium at the surface of the electrode. The cause for irreversibility is often not solely due to an irreversible charge transfer process but due to the presence of a competing chemical reaction whose rate constant is much larger than that for charge transfer.

The most simple case is an **EC** reaction, i.e. an Electrochemical process followed by a Chemical process. It involves a fast electron transfer followed by an irreversible first order reaction[21].

EC mechanism

$$O + ne^- \underset{k_b}{\overset{k_f}{\rightleftharpoons}} R \qquad k_c >> k_b$$

$$R \xrightarrow{k_c} X$$

where O=oxidised species, R=reduced species, X=species produced by competing chemical process and $k_{f,b \text{ and } c}$ are the rate constants for the forward, backward and chemical processes.

Other mechanisms include **ECE**, **EEC** and **CE** and are self explanatory as for the above **EC** mechanism. Also observed are catalytic reactions, eg **EC'**.

EC′ mechanism

$$O + ne^- \underset{k_b}{\overset{k_f}{\rightleftharpoons}} R \qquad k_c'>>k_b$$

$$R + Y \xrightarrow{k_c'} O + Z$$

where Y is a species (in excess) which reacts with R to form the oxidised species O.

The diagnostic features of an irreversible cyclic voltammogram are given below.

---

(1) Wave shape
No reverse peak is observed

(2) Peak height
$i_{px} \propto \upsilon^{1/2}$

(3) Peak potential
E_{px} shifts negatively by $30/\alpha_x n_\alpha$ mV for each decade increase in υ at 25°C.
α=activity coefficient

(4) Half peak
$|E_{px}-E_{px/2}| = 48/\alpha n_\alpha$ mV at 25°C

2A.2.4. Adsorption[22]

Adsorption is said to occur when there is electrostatic interaction or orbital overlap between the electrode and an electroactive species (adsorbate). A typical example of this is the reduction of protons at a platinum electrode[23].

The term adsorption can not be used to describe an electrochemical process where one of the electroactive species is highly insoluble and precipitates onto the electrode surface. This process is more commonly known as deposition[24].

The effect adsorption of a electroactive species has on the shape of the cyclic voltammogram depends on how strongly the reactant and/or product is adsorbed at the electrode surface[25]. A brief description of each type of process will now follow.

Examples of typical CV responses for reversible systems where the reactant and the product are weakly adsorbed can be seen in Fig 4 and 5. Looking firstly at the case where the reactant is weakly adsorbed, a characteristic enhancement of the cathodic wave is observed. If the scan rate is increased for this process, the cathodic peak is seen to increase to a greater extent than the anodic wave. This is due to the ratio of adsorbed material to diffusing material increases with scan rate. Interestingly, the anodic wave is seen to increase with scan rate for this process. This is due to the relationship $i_p \propto \upsilon^{1/2}$ from Eqn 2 and because adsorption leads to a higher concentration of reactants which results in a higher concentration of products. Therefore as the scan rate increases the reduced species has less time to diffuse away from the surface of the electrode before the reverse scan and hence this enhancement in concentration of the product, due to reactant adsorption, can contribute to enhancement of the anodic wave. At fast enough scan rates both peak currents have a set contribution from the adsorbed material and i_{pc}/i_{pa} becomes constant, but not usually unity. Altering the concentration of the analyte rather than scan rate results in an identical response to Fig 4 being observed. However, for this case, adsorption increases as concentration of the analyte decreases. This is attributed to the ratio of diffusing material to adsorbed material decreasing with concentration. Peak potentials are also seen to shift to more cathodic potentials with increased adsorption of the reactant. This is due to the adsorbed material being harder to reduce and therefore the free energy of the system rises with increased adsorption.

For a system where the product is now weakly adsorbed an opposite response to the above is observed, i.e. a large anodic peak is observed, see Fig 5. This is attributed to concentration of product at the surface of the electrode being higher than that required for the Nernstian equilibrium. This also explains why peaks shift towards more anodic potentials. Weak product adsorption increases with increasing scan rate and decreasing concentration, for the same reasons as the previous case.

Electroactive species can also be strongly adsorbed. Two post peaks and pre-peaks are observed when reactant and product are strongly adsorbed respectively. More detail on this subject can be found in reference 22.

The above examples are based on reversible systems suffering one type of adsorption. However, combination where both reactants and products adsorb

and the system is quasi-reversible or irreversible do exist but are not considered here as they are obviously more complicated than the above cases.

Clearly, weak adsorption at the surface of the electrode can be mis-interpreted as being a quasi-reversible process as two peaks are observed and i_{pc}/i_{pa} is not unity. However, adsorption can usually be identified from other processes by the increased symmetry of the peaks and their characteristic shapes.

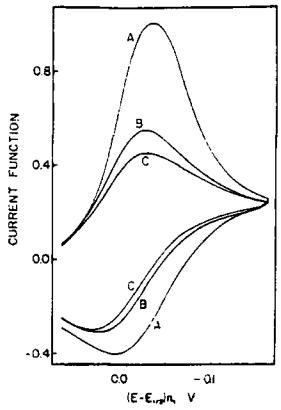

Stationary electrode polarograms with reactant weakly adsorbed—Variation with scan rate

$P_{O\varphi O}$ = 0.01. A, P_O = 5.0; B, P_O = 1.0; C, P_O = 0.1. Corresponding to relative scan rates, υ, of 2500, 100, and 1

Fig 4. Reactant weakly adsorbed, $i_{pc\text{-reactant}} >> i_{pa\text{-product}}$.

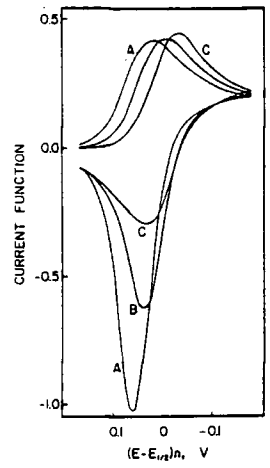

Stationary electrode polarograms with product weakly adsorbed—variation with scan rate

$P_{R\varphi R}$ = 0.01. A, P_R = 20.0; B, P_R = 5.0; C, P_R = 0.1. Relative scan rates are 4 × 10^4, 2.5 × 10^3, and 1

Fig 5. Product weakly adsorbed, $i_{pc\text{-reactant}} << i_{pa\text{-product}}$.

2A.2.5 Conclusion

In summary, cyclic voltammetry is a convenient way of confirming thermodynamic reversibility. It is also an excellent method for deducing reaction pathways, formal redox potentials and kinetic parameters of systems[26].

In the following section, the practical electrochemical considerations are discussed, particularly in relation to the apparatus used to study both aryl 1,2,3,5 and aryl 1,3,2,4 dithiadiazolylium salts.

2A.3 Practical considerations for CV [26]

2A.3.1 The Cell

In solution and solid state, dithiadiazolylium salts and related compounds are air and moisture sensitive. Therefore to avoid decay of the samples, a special cell, designed by Dr. Z.V.Hauptman[27] , was used which enabled the samples to be loaded into the cell and electrochemical runs to be conducted under an inert atmosphere, see chapter 4. This cell also has the unique capability of being able to contain pressured liquid gases whose vapour pressure doesn't exceed 5atm, e.g. liq SO_2.

2A.3.2 Resistances

Resistances within the electrochemical cell are known to reduce the accuracy of the electrochemical measurements in CV[28,29]. In the forward sweep, an unknown resistance term R_u affects the value of $E_{(measured)}$ by the following relationship:

$$E_{(measured)} = E_{(initial)} + \upsilon t + iR_u$$

Fortunately, this resistance term R_u can be eradicated by connecting a device called a potentiostat to the cell. This device has a positive feedback circuit incorporated, which results in a cancellation of iR_u term, hence $E_{(real)}=E_{(initial)}+\upsilon t$. A similar set up was used for all the cyclic voltammetry measurements for these sulphur nitrogen species.

A further potential source of variable resistances is variations in relative positions of the three electrodes of the cell between scans. This source of error was easily avoided, as they were mounted the same distance for all experiments.

2A.3.3 Solvent

It was essential to use a suitable solvent. Acetonitrile (MeCN) was the natural choice here because (1) the sulphur nitrogen materials to be studied are stable and readily soluble in it, (2) the solvent is stable in the potential window of interest, ±2V vs S.S.C.E (see section 2A.3.6), (3) it possesses a reasonable dielectric constant, ε=37, (4) it is easy to handle and (5) it exists as a liquid within the temperature ranges of the measurements.

2A.3.4 Concentration[30,31]

The concentration at which the samples were to be electrochemically studied was the next decision. A concentration of $1x10^{-3}$M was chosen as it was considered large enough so that the sulphur nitrogen analytes could be observed

and low enough that freely solvated ions were present rather than ion pairs and neutral monomeric radicals rather than dimers existed. However at this concentration the solution is not conductive enough and convection becomes the main method of transport and not diffusion. This is overcome by adding supporting electrolyte, in excess, which increases the conductivity of the solution.

2A.3.5 Supporting electrolyte

Supporting electrolytes are salts which are inert in the potential window used, readily soluble in the solvent and inert to the solvent and substrate. For these measurements tetrabutylammonium tetrafluoroborate, $TBABF_4$ fitted the criteria. The supporting electrolyte was added in excess, (0.1M), as this forces the sole mode of mass transport to be by the desired process of diffusion, and not by convection or migration.

2A.3.6 Reference electrode

The reference electrode designed for the cell was an Ag/Ag^+ (0.01M $AgAsF_6$, MeCN) system and this is one of the few reference electrodes that is stable in MeCN, see chapter 4. Using this electrode enabled the working system to contain the same solvent throughout. This electrode was referenced to the standard saturated calomel electrode S.S.C.E after every experiment in order to have potential values that could be quoted relative to a well established and recognised standard[32]. Unfortunately this practice does introduce unknown junction potentials but they are assumed to be constant throughout the series of experiments. The S.S.C.E couldn't be used as a direct reference electrode as it is one of many that don't behave ideally in MeCN[33].

2A.3.7 Scans

During continuous CV scans of these types of materials, it is often observed that very mild changes in the shape of cyclic voltammograms begin to appear, probably due to competing chemical reactions occurring to a small degree. Therefore it was decided that only graphical information from the first scan would be recorded, so that all processes were at the initial stages of development.

The errors of these CV experiments encompassed apparatus sensitivity and accuracy of manual measurements of potentials from the graphs. From the electrochemical results obtained by previous students and myself, using an analogous experimental set up, $E_{pc/2}$ and E_{px} values had an associated error of $\pm$5mV and $\pm$10mV respectively[34]. $E_{pa/2}$ and i_{pa} values had a variable error

associated with them due to the inherent inaccuracy in assessing a correct reverse scan base line. However, errors did not exceed ±30mV and 8% of the current value respectively, see chapter 2B. Typical error of i_{pc}/i_{pa} was 15%.

2A.3.8 CV[35]

Variations of the following factors are known to affect, to differing degrees, the shape and position of a cyclic voltammogram. These are (1) scan rate υ, (2) temperature T, (3) concentration of analyte, (4) supporting electrolyte, (5) solvent, (6) electrodes and (7) associated counter ions of studied ionic analytes[36].

From previous experiences with similar sulphur nitrogen compounds, analysed electrochemically by the same CV apparatus used for these experiments, it was often found that to obtain a sharp cyclic voltammogram it was necessary to vary scan rates from sample to sample[34]. Therefore a study on how υ affects CV data was conducted for this series of dithiadiazolylium compounds so that the precision of the measurements could be estimated, see Eqn (2). Along the same vein of thought, measurements at variable temperature were also undertaken to see if this had any effect on CV response too.

The effect the variables (3) to (7) had on the electrochemistry of these compounds was not investigated and they were kept constant during the experiments.

Taking into account how (1)-(7) can affect potentials, (see section 2A.2.1), comparisons between CV data of the dithiadiazolylium salts and other systems (including and excluding dithiadiazolylium salts), could only be made when experimental conditions (1)-(7) were closely similar.

2A.3.9 Electrodes

It is well known in the field of electrochemistry that the condition of the electrodes can effect the cyclic voltammetric response observed. Therefore all the electrodes used in these experiments were maintained to a high quality in order to ensure reproducibility of results. The working electrode was 1mm platinum disc which was regularly polished in order to retain the quality of the surface. The counter electrode was a platinum coil which was cleaned before every experiment using nitric acid and "flamed" until it was white hot. Finally the reference electrode [Ag/Ag^+, 0.01M $AgAsF_6$, MeCN] was regularly topped up with the appropriate standard solution of $AgAsF_6$ from a reservoir incorporated into the cell, chapter 4. This electrode was stored in this solution, under an inert atmosphere of nitrogen, in order to prevent moisture entering into the system.

2A.4 Conclusion

So far the theory and practical elements of cyclic voltammetry have been discussed. Now in the following sub-chapters the attention is turned to describing and explaining the cyclic voltammetric experimental results obtained for the several series of substituted aryl 1,2,3,5 and 1,3,2,4 dithiadiazolylium hexafluoroarsenate salts and related compounds. **Note that synthetic aspects for the above synthesised compounds are considered in the synthetic experimental section, chapter 4.**

As the para derivatives were the most characterised systems and their chemistries were found to be similar for each isomer, it made sense to study their electrochemistry first of all.

ΩΩΩΩΩΩΩΩΩΩΩΩΩΩΩΩΩΩΩΩΩΩΩΩΩΩΩΩΩΩΩΩΩΩΩΩΩΩΩΩΩ

Section 2B.1

ΩΩΩΩΩΩΩΩΩΩΩΩΩΩΩΩΩΩΩΩΩΩΩΩΩΩΩΩΩΩΩΩΩΩΩΩΩΩΩΩΩ

2B.1 The Electrochemistry of *Para* Substituted Phenyl 1,2,3,5 Dithiadiazolylium Hexafluoroarsenate Salts.

2B.1.1 Phenyl 1,2,3,5 dithiadiazolylium salt

The simplest type of aryl 1,2,3,5 dithiadiazolylium hexafluoroarsenate salt, $PhCNSSN^+AsF_6^-$, was studied first. When CV was conducted at -15°C, over a potential range of +1.2V to -0.5V, on a $1x10^{-3}$ M solution of phenyl 1,2,3,5 dithiadiazolylium salt, (sample A), in acetonitrile two peaks were observed, see Fig 6.

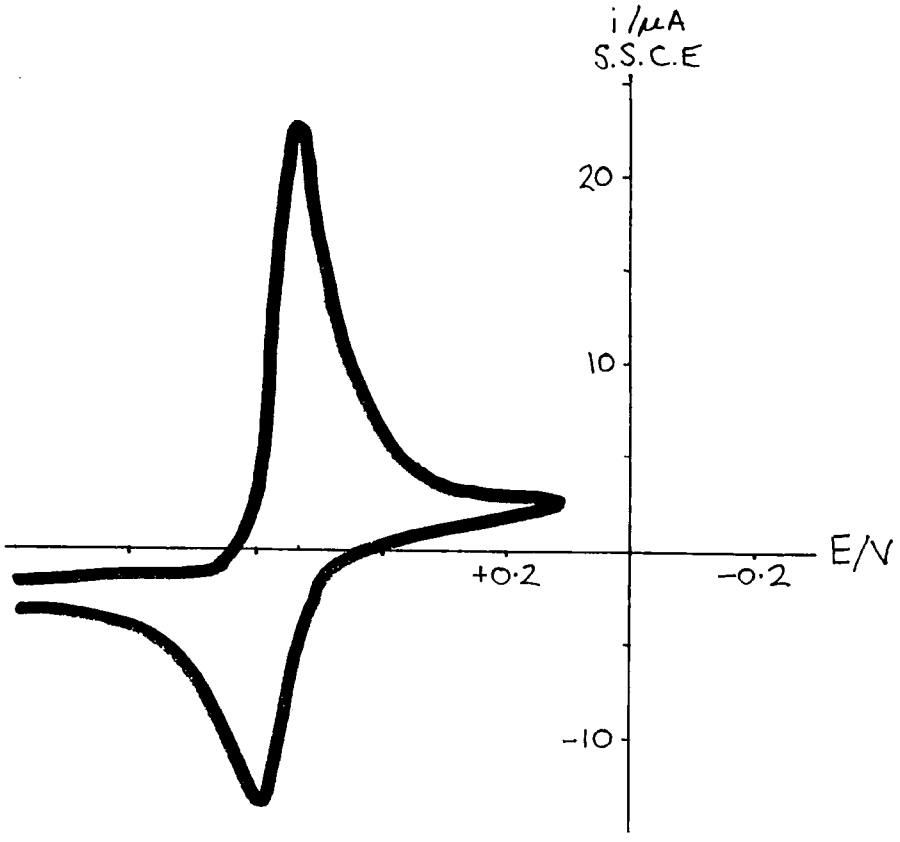

Fig 6. Cyclic voltammogram of sample A in acetonitrile at -15°C, supporting electrolyte $TBABF_4$ $1x10^{-1}$M, scan rate υ=576mVs^{-1}.

The cathodic peak corresponds to the following reduction process

$R\text{-}C_6H_4\text{-}CNSSN^+ + e^- \text{-----> } R\text{-}C_6H_4\text{-}CNSSN^\bullet$ where R=H

and the anodic peak relates to the reverse oxidation process

$R\text{-}C_6H_4\text{-}CNSSN^\bullet - e^- \text{-----> } R\text{-}C_6H_4\text{-}CNSSN^+$ where R=H

As mentioned previously in section 2A.3.7 all the $E_{p/2}$ and E_p potentials quoted from here onwards are accurate to ±5mV and ±10mV respectively.

From the above cyclic voltammogram of sample A, the cathodic peak potential E_{pc} was found to be 530mV and $E_{pc/2}$ was equal to 580mV and hence a difference of 50mV. The last value agrees with that expected for an electrochemically reversible system at -15°C *viz* ca. 49/n mV where n=1. Examination of the anodic wave reveals that E_{pa}=610mV, $E_{pa/2}$=510mV and hence E_{pa}-$E_{pa/2}$=100mV. In this case the last value is too high to belong to a reversible couple. But as assignment of the reverse scan base line in order to measure the anodic half peak potential is fraught with error, the reliability of $E_{pa/2}$ and associated calculations is questionable. The same errors naturally apply for peak current ratios. For this sample i_{pc}/i_{pa} was 1.52. Despite the errors associated with this ratio (15%), the value can be said to be larger than the ideal value of unity observed for a reversible couple.

So far, only a fraction of the data retrieved from the cyclic voltammogram in Fig 6 of sample A has been discussed. But the information already assembled does not conclusively prove one way or another if this system is reversible or not. This was finally decided by investigating the value of $|E_{pc}-E_{pa}|$. For total reversibility this value must be ~50mV. But for this system it was found to be 80mV, which strongly indicates that this sample is electrochemically **quasi-reversible**.

In order to investigate the nature of this redox process further, variable temperature measurements were made. Two independent samples were run to check the reproducibility of these results.

2B.1.2 Variable Temperature CV Measurements

Variations in temperature are known to affect the shape and position of cyclic voltammograms[35]. Therefore a variable temperature investigation was conducted on two samples (A and B) of phenyl 1,2,3,5 dithiadiazolylium hexafluoroarsenate to see how their CV's were affected. This was achieved by slowly warming each sample up and recording scans at regular temperature intervals. The results are displayed in Table 1 overleaf. Discussion on how temperature affects these results will be split into two parts, one that deals with potentials and the other with current values.

Potential

Examination of the E_{pa}-E_{pc} values of both samples over these temperature ranges were examined first of all in order to identify if these samples were quasi-reversible or not under these conditions. If these samples were reversible, between the temperature range of the experiments (-15°C to 8°C), values of

between 0.049V and 0.054V respectively, (with an error of ±10mV associated with them), would be observed. If weak adsorption of a reversible couple was happening the peaks would be more symmetrical, i.e. E_{pa}-E_{pc} is than the ideal value of ~0.05V. However for these samples the values were almost double that required for a reversible couple and this feature alone distinguishes these compounds as being quasi-reversible. The lowest and highest E_{pa}-E_{pc} value was 80mV and 100mV respectively.

For these samples, the cathodic and anodic peak potentials were seen to slightly increase with increasing temperature. These shifts in potential for both samples can be explained by the direct relationship between the Gibbs free energy, potential and temperature that exists. Therefore as the temperature increases so do the above two factors, i.e the process becomes more favourable. These potential values for sample A were within experimental error of the corresponding values for those of other sample (B) at similar temperatures, which indicates the results are reproducible between samples.

The cathodic half peak potentials were found to increase with temperature but all the values were within experimental error of each other (±5mV). Values of E_{pc}-$E_{pc/2}$ were found to be just within and outside experimental error of the value required for the system to be reversible. A typically value for sample A and B over this temperature range was 60mV. E_{pc} and $E_{pc/2}$ were found to be typically 530mV and 590mV respectively.

For the anodic half peak potential no obvious trend between potential and temperature was found to exist for these two samples. Analysis of the E_{pa}-$E_{pa/2}$ values for both samples revealed that they are quite different. For samples A and B these values vary from 90mV to 130mV and 60mV to 70 mV respectively. As the E_{pa} values between samples were all found to be within experimental error of each other it is the differences in their $E_{pa/2}$ values which contribute to these differences in anodic half peak widths. These differences of $E_{pa/2}$ values between samples can readily occur due to difficulties in the correct assessment of the reverse scan base line and subtle difference in the amount of impurities in solution, concentrations and electrode surface affecting the shape of the anodic wave between samples. (How these differences in wave shape can arise will be explained in greater detail at the end of this sub-section).

The $(E_{pa}+E_{pc})/2$ value is known to be equal to the standard reduction potential, E°, for reversible systems. For these two quasi-reversible samples, A and B, over this temperature range this assumption is invalid. The $(E_{pa}+E_{pc})/2$ value for both samples was seen to increase with increasing temperature by 20mV. This value is not as consistent as the E_{pc} and $E_{pc/2}$ over this temperature

Sample	Temperature °C	E_{pc} mV	$E_{pc/2}$ mV	i_{pc} μA	E_{pc}-$E_{pc/2}$ mV	E_{pa} mV	$E_{pa/2}$ mV	i_{pa} μA	E_{pa}-$E_{pa/2}$ mV	i_{pc}/i_{pa} μA	E_{pa}-E_{pc} mV	$(E_{pa}+E_{pc})/2$ mV
A	-15	530	580	25.8	50	610	510	17.0	100	1.52	80	570
	-13.5	520	590	22.4	70	610	520	16.4	90	1.37	90	565
	-7.5	530	590	16.8	60	620	520	16.4	100	1.02	90	575
	-2	530	590	11.6	60	630	500	18.0	130	0.64	100	580
	2	530	590	10.0	60	630	500	20.4	130	0.49	100	580
B	-15	530	590	33.0	60	620	555	33.4	65	0.99	90	575
	-13	520	590	28.8	70	610	550	29.9	60	0.97	90	565
	-3	535	600	16.8	65	620	550	20.0	70	0.84	85	577.5
	3	540	600	13.2	60	620	550	17.6	70	0.75	80	580
	8	540	600	9.0	60	630	560	15.0	70	0.60	90	585
C	-13.5	530	590	20.5	60	610	510	54.0	100	1.52	80	570
D	7	530	590	10.8	60	620	555	23.6	65	0.92	90	575

Table 1. Cyclic voltammetric variable temperature data for four samples of ~$1x10^{-3}$M phenyl-1,2,3,5-dithiadiazolylium hexafluoroarsenate in MeCN, supporting electrolyte $TBABF_4$, scan rate υ=576mVs^{-1}.

range and hence the later cathodic potentials are a better source for reference potentials for these samples.

Now follow the results from the analysis of how temperature affected the corresponding current values of these samples.

Current

For samples A and B, their i_{pc} values were found to decrease with increasing temperature and this is in agreement with the Randles-Sevcik equation, Eqn(2), which shows that $i_p \propto T^{-1/2}$ for a diffusion controlled process. When i_{pc} and $T^{-1/2}$ values for these two samples are plotted against each other, two analogous linear relationships are found to exist, with all points within two ESD's of the line, see Fig 7.

The i_{pa} values were found to be inconsistent. This is attributed to the quasi-reversible nature of the two systems, see section 2A.2.2.

Despite i_{pa} values following no predictable trend, the peak current ratio was found to consistently decrease with increasing temperature for each sample. This will be discussed in more detail later.

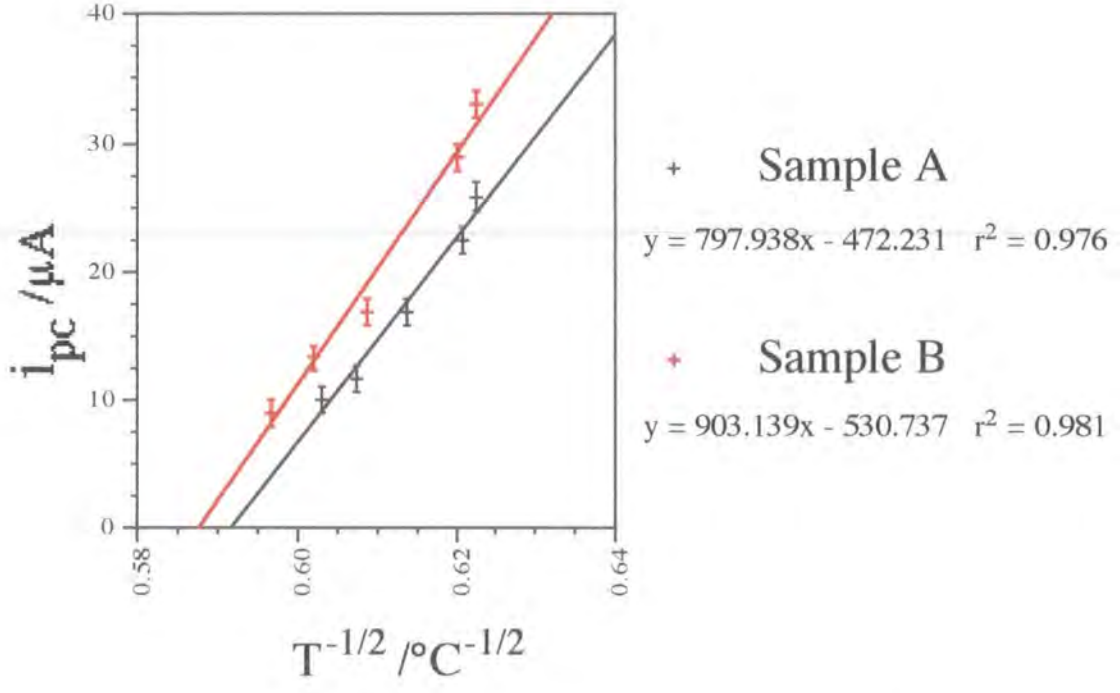

Fig 7. i_{pc} *vs* $T^{-1/2}$ plot for two samples,(A and B), of phenyl 1,2,3,5 dithiadiazolylium hexafluoroarsenate studied by cyclic voltammetry.

Samples C and D

Two additional fresh samples (C and D) of this compound were examined by CV, one at -13.5°C and the other at 7°C, to test if the results were truly reproducible. Both gave identical cyclic voltammograms with those obtained already, i.e. E_{pc} and $E_{pc/2}$ values were found to be characteristically 0.53V and 0.59V respectively, and the systems were quasi-reversible as E_{pa}-E_{pc}>0.055V.

All Four Samples

CV measurements over this temperature range reveal that the peak potentials and cathodic half peak potentials of samples of $PhCNSSN^+AsF_6^-$ at similar temperatures are equivalent, (i.e. within experimental error). The size of E_{pa}-E_{pc} values for all the samples in this experiment, (greater than 55mV), clearly indicates that the samples are quasi-reversible in nature.

The anodic half wave potentials are less predictable over this temperature range and the i_p values of these four samples at similar temperatures are found not to be comparable to each other. Why these differences occur will now be tackled, starting with peak current values first of all.

Using Eqn(2) it can be seen that i_p is not only proportional to $T^{-1/2}$ but also to the concentration of the analyte. Therefore slight differences in concentration between the samples would aid to explain this variable i_p phenomenon. Error assessment on the concentration of the samples now follows.

Despite careful preparations, the concentration and purity of the solutions can only be guaranteed to $1x10^{-3}M \pm 2x10^{-4}M$ and a maximum of 99% respectively. The errors of the molarity of the solution arise from the sample weights and volume of solvent used were only accurate to 0.2mg and 0.5ml respectively. Also the presence of minor impurities will contribute to a lower concentration of the analyte than calculated being present in solution. Therefore it is evident that these minor variations in concentration and purity could readily contribute to small deviations in current values between samples.

During the synthesis and electrochemical procedures of the analyte the presence of a low level of impurities is unavoidable. Impurities can arise due to the limitations of the purification methods employed. They can also be generated by reactions involving these air and water sensitive analytes with trace moisture. Alternatively, the analyte could react with impurities present to form new impurities. Therefore, to keep impurities at a minimum very dry solvent, nitrogen and glassware was used in the preparation of samples of phenyl 1,2,3,5 dithiadiazolylium hexafluoroarsenate. Also purity of solvent and materials is also important for the same reason. Throughout the electrochemical survey on

samples of this derivative meticulous attention to experimental details was undertaken in order to keep the amount of impurities and moisture to an absolute minimum in order to achieve solutions of accurate concentrations (see chapter 4).

The concentration of the supporting electrolyte in CV influences the conductivity of the solution and therefore variations in molarity can affect observed i_p current values. However, for these four cases the error associated with this supporting electrolyte concentration, (0.100M ± 0.001M), is considered too small to have a noticeable effect on current values.

Another factor that can affect i_p values is minor differences in the electrode surface between sample runs. This is assumed to be a minor contribution in this case, as identical electrode preparation was undertaken for all the runs, see section 2A.3.9.

These variations in concentration between samples appear to have a negligible effect on the position and shape of the cathodic wave as cathodic half peak width, E_{pc}-$E_{pc/2}$, is typically 60mV ±10mV for all samples. On the other hand these variations are not solely responsible for the anodic portion varying between 60mV to 130mV among these samples. This trend can be partially explained due to large errors in assessment of the correct reverse scan base line and associated anodic measurements. Also the fact that the i_{pc}/i_{pa} ratios are seen to range from being greater than one to less than one with increasing temperature strongly indicates that another process(es) other than the main quasi-reversible charge transfer process is in operation.

If a competing process which was more sensitive to temperature than quasi-reversible charge transfer was occurring, then as temperature increased the competing process would progressively influence the electrochemistry and ultimately relative peak heights to a larger degree with increasing temperature, i.e. a trend between peak current ratio with temperature would exist as observed with these compounds. For these compounds any possible competing process present obviously effects the shape and position of the anodic wave to a greater extent than the cathodic wave over this temperature range. Also, only two peaks of the product were observed in the potential window which indicates that any foreign reagents or side products of any possible reaction are either at a low concentration or are not electroactive in this potential window viewed or are electroactive in the same region as the analyte. Possible competing processes that may be present will now be discussed.

One such process that could occur is a competing chemical reaction. It is possible that the dithiadiazolylium or dithiadiazolyl moiety could react with the small amount of impurities in solution over the time period of the experiment.

This would result in a small reduction in concentration of one of these species at the surface of the electrode during measurements and hence reduction in height of the corresponding peak. However, this is considered to be a minor process as impurities were kept to a minimum and noticeable peaks corresponding to reaction products were not observed.

Alternatively, the analyte could electrochemically cleave in some way such that the new components can go on to form new compounds. However, this process is highly unlikely as both the cationic and radical PhCNSSN derivatives have been shown to be very stable in solution and during their synthesis. This is further supported by the absence of other peaks corresponding to these side products.

If impurities or side products of the above reaction were present and electroactive in the same potential regions as the $PhCNSSN^{+/\bullet}$ couple, (their corresponding CV's overlapped), then changes in peak shape and height, i.e. deviations from simple quasi-reversibility, would be observed. This is considered to be highly unlikely especially as these additional materials would be very different to the analyte, i.e. different electronic factors affecting the electrochemistry.

Therefore, for the above processes to be valid options to explain variations in CV responses between samples of $PhCNSSN^{+}AsF_6^{-}$ the concentration of impurities or side products would have to be low as no additional peaks were observed over this temperature range. Elemental analysis confirmed impurities to be at a minimum (<1%). Also, if a side product of a reaction was highly insoluble a CV trace for this material would not necessarily be detected. This can be ruled out in this case as it is anticipated that such side reactions involving the analyte would result in materials with an organic framework being produced, which would be expected to readily dissolve in MeCN.

If a sparingly soluble reduced electrochemically generated species became more soluble as temperature increases in this experiment, i.e. deposition of material is reduced, this would contribute to reduction of the anodic peak with temperature. This is not observed and therefore can be ignored especially as radical and salt of this derivative is sufficiently soluble in this solvent.

Adsorption could also be contributing to peak enhancement. As only two peaks are observed, the type of adsorption that could possibly be present must be weak, see section 2A.2.4. Also the process must be adsorption of a quasi-reversible couple as the peaks are not symmetrical enough, (E_{pa}-E_{pc}>55mV). In the literature quasi-reversible systems suffering from weak adsorption in conjunction with other competing processes is not covered as it is considered too

complicated. Therefore, no rationalisation of what type of adsorption maybe occurring will be undertaken as it is considered to be a minor process relative to quasi-reversible charge transfer, as the differences of the cyclic voltammograms between the samples are relatively small. This also applies to other possible competing processes mentioned earlier which are considered to be minor contribution.

Due to the limitations of this experiment a more precise answer to which of the above processes are competing with quasi-reversible charge transfer can't be deduced.

In summary, these results show that electrochemistry is an extremely sensitive technique as subtle differences between these samples of $PhCNSSN^+AsF_6^-$ are significant enough to effect the shape of the anodic wave between samples. Despite the sensitivity of this technique, measurements involving the cathodic wave were very reproducible and the system was shown to be electrochemically quasi-reversible under these experimental conditions. Further examination of factors effecting the shape of the anodic wave were not attempted as the primary interest was the various potentials of the reduction process which had been shown to be very insensitive to temperature and sample deviations.

2B.1.3 Variable Scan Rate CV Measurements

Following along a similar vein of thought, an investigation into how change of scan rate affected the CV of phenyl 1,2,3,5 dithiadiazolylium hexafluoroarsenate was conducted, with all other experimental conditions remaining constant.

Just one sample of the phenyl derivative was examined, with scan rates varying from 10^2 to $30^2 mVs^{-1}$. At these scan rates the sample exhibited electrochemical quasi-reversibility as $E_{pc}-E_{pa}>0.055V$, see Table 2.

The following trends, (characteristic of a quasi-reversible couple), were also observed:- (1) E_{pc} decreases with scan rate and E_{pa} increased with scan rate by 20mV and 30mV respectively per 9 fold increase in scan rate, (2) $E_{pc/2}$ and $E_{pa/2}$ were consistently 590mV and 550mV ±5mV respectively, (3) $E_p-E_{p/2}$ increased with scan rate from 60mV to 80mV per 9 fold increase in scan rate, (4) peak to peak separation increased by 50mV over the scan rate range and (5) i_p increases with increasing scan rate. The i_{pc}/i_{pa} ratio was constant during this study and was seen to be approximately one throughout even though peak separation was seen to increase with scan rate. This feature too is typical of a

$\upsilon^{1/2}$ $(mV/s)^{1/2}$	E_{pc} mV	$E_{pc/2}$ mV	$E_{pc}-E_{pc/2}$ mV	i_{pc} µA	E_{pa} mV	$E_{pa/2}$ mV	$E_{pa}-E_{pa/2}$ mV	i_{pa} µA	$E_{pa}-E_{pc}$ mV	i_{pc}/i_{pa}	$(E_{pa}+E_{pc})/2$ mV
10	540	590	50	11.2	610	550	60	12.0	85	1.02	312.5
15	530	590	60	15.2	615	550	60	17.2	90	0.98	315
18	535	590	55	17.6	615	550	65	20.4	100	0.97	310
20	530	590	60	19.2	615	550	70	23.6	115	0.99	312.5
23	530	590	60	22.4	615	550	70	25.2	110	1.00	315
25	530	590	60	26.8	620	550	75	26.0	125	1.04	312.5
28	525	590	65	28.8	620	550	75	28.4	130	1.04	315
30	525	590	65	31.2	630	555	75	32.8	130	0.98	315

Table 2. Variable scan rate CV measurements for a sample of phenyl-1,2,3,5-dithiadiazolylium hexafluoroarsenate in MeCN, concentration 1×10^{-3} M, supporting electrolyte $TBABF_4$ and temperature -15°C.

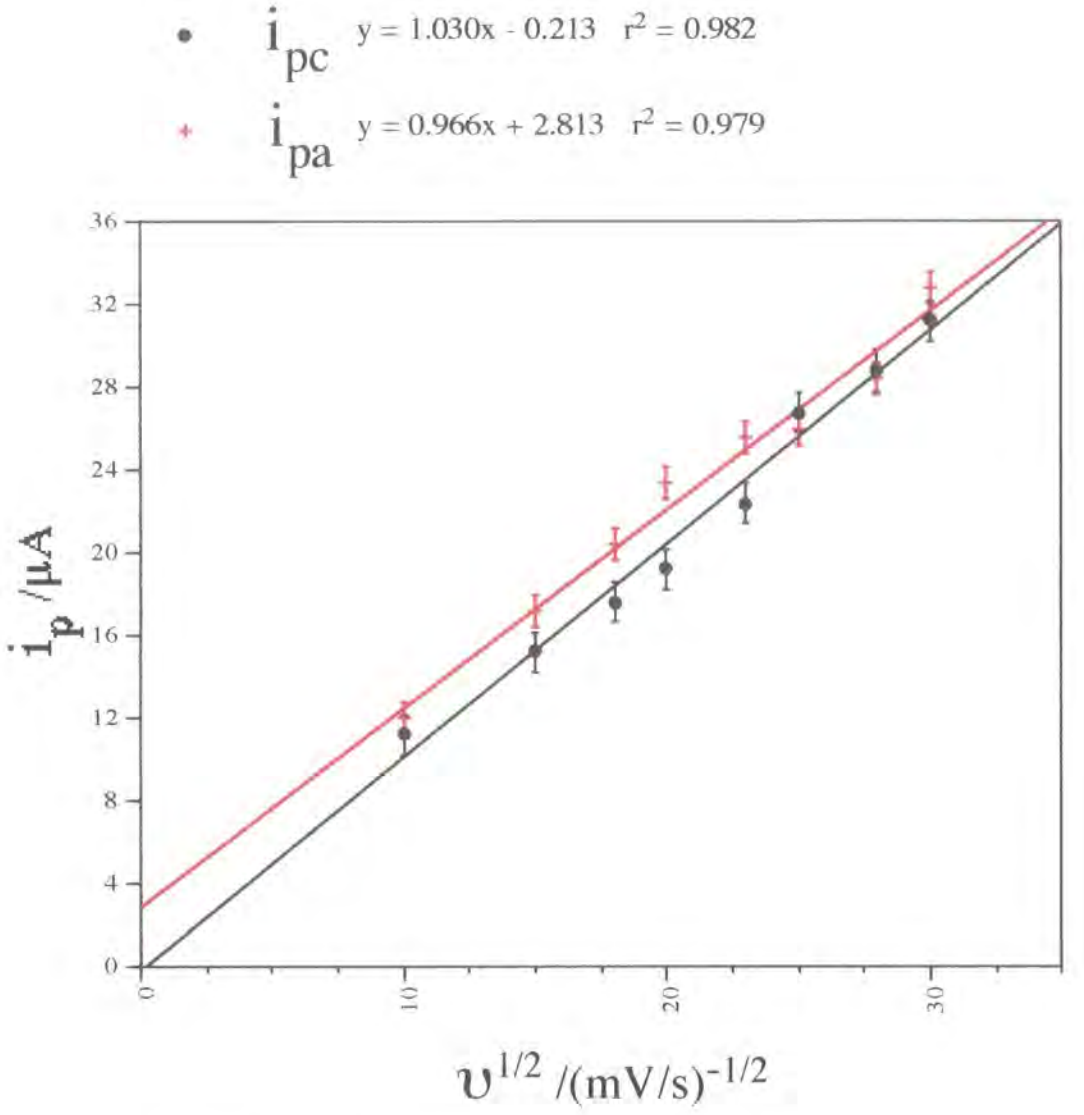

Fig 8. i_p *vs* $\upsilon^{1/2}$ plot for a sample of phenyl-1,2,3,5-dithiadiazolylium hexafluoroarsenate studied by cyclic voltammetry.

classical quasi-reversible couple and an example of this can be seen in section 2A.2.2.

According to the Randles-Sevcik equation, Eqn(2), $i_p \propto \upsilon^{1/2}$ for a diffusion controlled or reversible process. When i_p versus $\upsilon^{1/2}$ was plotted for this set of data a linear relationship was observed, see Fig 8. None of the lines passed through the origin, but the plot for the cathodic wave came very close. This shows that i_p does increases with $\upsilon^{1/2}$ by a constant value over this range of scan rates (10^2 to $30^2 mVs^{-1}$).

The electrochemical responses observed for these variable scan rate measurements are a good example of a classical electrochemical quasi-reversible couple as seen in section 2A.2.2.

The anodic half peak width was found to be just within or outside of that of the corresponding cathodic value. As these differences between the peaks are so small it is assumed that discrepancies are due to a higher error associated with measurements involving a reverse scan base line, see section 2A. 2.2.

For phenyl-1,2,3,5-dithiadiazolylium hexafluoroarsenate it has been shown that varying temperature and scan rate under these experimental conditions has a minimal effect on the E_{pc} and $E_{pc/2}$ values especially. But how different would the electrochemical behaviour be for a range of *para* substituted phenyl 1,2,3,5 dithiadiazolylium hexafluoroarsenate salts? Derivatives with an electron donating or accepting group in the *para* position were successfully synthesised so that an answer could be provided for this electrochemical quandary. The electrochemical properties of examples possessing electron withdrawing and donating groups are described below.

2B.1.4 Derivatives Possessing Electron Withdrawing Groups

The derivatives chosen to be studied by CV possessed substituent groups with a wide range of electron withdrawing ability, (*viz.* NO_2, CF_3, CN, Br, Cl and F). Therefore, the influence that the strength of the acceptor group has on the redox chemistry of these materials could be thoroughly examined, including quantitative analysis of results.

The CV methods, previously reported for the unsubstituted phenyl derivative, were used in this investigation, see sections 2B.1.1-3.

Trifluoromethyl

The first compound examined was *para* trifluoromethylphenyl-1,2,3,5-dithiadiazolylium hexafluoroarsenate. The first sample was run at -15°C with small variations in scan rate. The peak potentials and derivative potentials were found to be extremely similar and within experimental error of each other, see Table 3. In each case the current ratio was slightly less than one and the difference in the peak potentials was greater than 0.049V, which are both characteristic of a quasi-reversible system. The peak current, i_{pc}, was found to increase with increasing scan rate. More detailed examination of this compound was unnecessary as the system was obviously quasi-reversible like the unsubstituted phenyl derivative previously studied.

A similar CV investigation was conducted on another sample of this compound, but this time the temperature was 0°C during measurements. This sample too exhibited quasi-reversibility of the type observed in the previous

Sample		Temp °C	Scan rate mVs^{-1}	E_{pc} mV	$E_{pc/2}$ mV	i_{pc} μA	$E_{pc}-E_{pc/2}$ mV	E_{pa} mV	$E_{pa/2}$ mV	i_{pa} μA	$E_{pa}-E_{pa/2}$ mV	i_{pc}/i_{pa} μA	$E_{pa}-E_{pc}$ mV	$(E_{pa}+E_{pc})/2$ mV
CF3	A	-15	676	590	650	15.8	60	670	600	17.8	70	0.89	80	630
		-15	576	590	650	15.4	60	665	600	17.4	65	0.89	75	627.5
	B	0	676	590	650	5.1	60	670	610	5.4	60	0.94	80	630
		0	196	590	650	2.56	60	665	605	2.88	60	0.89	75	627.5
F	A	0	784	545	605	18.5	60	620	560	20.5	60	0.90	75	582.5
		0	324	550	605	13.5	55	630	570	12.5	60	1.08	80	590
		0	100	550	600	7.9	50	620	560	6.9	60	1.14	70	585
	B	-15	576	550	600	39.2	50	620	580	33.2	40	1.18	70	585
	C	0	324	550	600	12.25	50	630	530	16.0	100	0.77	80	590
	D	-15	144	550	600	4.6	50	630	570	4.6	60	1.00	80	590
MeS	A	-11	484	510	585	35.6	75	645	565	37.2	80	0.96	135	577.5
	B	-11	484	510	590	30.0	80	630	510	18.4	120	1.63	120	570
	C	-13	676	530	595	10.0	65	630	520	9.0	110	1.10	100	580
Me	A	0	484	520	580	18	60	605	550	18.0	55	1.00	85	562.5
		-15	484	515	580	35.4	65	595	540	32.8	55	1.08	80	555
MeO	A	0	100	505	570	9.25	65	580	525	8.25	55	1.12	75	542.5
	B	-13	576	510	570	34	60	585	535	36.8	50	0.92	75	547.5

Table 3. Cyclic voltammetric data for *para* substituted phenyl - 1,2,3,5 - dithiadiazolylium hexafluoroarsenate in MeCN, concentration 1×10^{-3} M, supporting electrolyte $TBABF_4$.

Sample	Temp. °C	Scan rate mVs^{-1}	E_{pc} mV	$E_{pc/2}$ mV	i_{pc} μA	$E_{pc}-E_{pc/2}$ mV	E_{pa} mV	$E_{pa/2}$ mV	i_{pa} μA	$E_{pa}-E_{pa/2}$ mV	i_{pc}/i_{pa} μA	$E_{pa}-E_{pc}$ mV	$(E_{pa}+E_{pc})/2$ mV
NO_2	-15	576	610	675	15.6	65	705	635	8.6	70	1.81	95	657.5
CN	-15	576	600	660	27.2	60	685	625	32.8	60	0.83	85	642.5
Br	-15	576	570	625	10.6	55	640	580	10.6	60	1.00	70	605
Cl	-15	576	560	620	54.0	60	670	600	54.0	70	1.00	110	615
CO_2Me	0	676	580	640	25.6	60	660	600	27.2	60	0.94	80	620
	0	676	575	640	24.0	65	670	610	25.6	60	0.94	95	622.5
CF_3O	-14	576	560	630	16.25	70	665	600	13.25	65	1.23	105	612.5
	-14	576	570	630	28.5	60	660	540	17.7	120	1.63	90	615

Table 4. Cyclic voltammetric data for *para* substituted phenyl - 1,2,3,5 - dithiadiazolylium hexafluoroarsenates in MeCN, concentration $1x10^{-3}M$, supporting electrolyte $TBABF_4$.

example. The reproducibility of E_{pc} and $E_{pc/2}$ values between these samples was excellent with consistent values of 0.59V and 0.65V respectively.

The presence of the trifluoromethyl group relative to a hydrogen at the *para* position resulted in an increase in cathodic potentials of 60mV. Despite this difference between the cathodic potentials of these derivatives they are found to have the following electrochemical features in common with each other, e.g. E_{pc}-$E_{pc/2}$ is typically 60mV, E_{pa}-E_{pc}>0.05V, i_{pc}/i_{pa} does not equal one unless $\alpha_c=\alpha_a=0.5$ and i_p increases with υ.

Anodic potentials were not considered due to errors associated with measurement of the reverse scan portion of the cyclic voltammograms of quasi-reversible systems. Further details can be found in sections 2B.1.1-3 and 2A.2.2.

Fluoro

The fluoro derivative was the next to be examined by CV using variable scan rates. Measurements at 0°C revealed that E_{pc}-$E_{pc/2}$=0.05V, which is the result expected from a reversible couple, see Table 3. Contrary to this evidence, this derivative is quasi-reversible to the same degree as for H and CF_3 derivatives due to the following being observed: E_{pa}-E_{pc}>0.05V, i_p increases with υ and i_{pc}/i_{pa} is approximately unity.

Analogous measurements on a new sample of this material, (B), at -15°C were found to be akin to those of the previous sample examined at 0°C.

Two further samples, (C and D), at the temperatures and scan rate ranges as A and B, were run to test the reproducibility of these results. Both were found to be quasi-reversible to the same extent as A and B from the relative size of their potentials.

Therefore, for this derivative, under the above experimental conditions, E_{pc} and $E_{pc/2}$ are 550mV and 600mV respectively.

The size of the $E_{pc/2}$ potentials for the compounds studied so far was CF_3>F>H. A possible trend was starting to emerge: the greater the electron withdrawing ability of the substituent group the larger or more positive are the potentials.

Others

CV investigations on *para* NO_2, CN, Br and Cl phenyl 1,2,3,5-hexafluoroarsenate salts showed that they exhibit the same quasi-reversible properties as the above, i.e. E_{pc}-$E_{pc/2}$ ~0.06V, E_{pa}-E_{pc}>0.055V and i_{pc}/i_{pa} does not equal one unless $\alpha_c=\alpha_a=0.5$, see Table 4.

By examining the $E_{pc/2}$ potentials of all the six *para* substituted derivatives, it is apparent that the acceptor strength of the substituent group is directly connected to the potential of the dithiadiazolylium ring. Hence the following order of cathodic potentials is observed:

$$\mathbf{H < F < Cl < Br < CF_3 < CN < NO_2}$$

Looking at the $(E_{pc}-E_{pa})/2$ values of these compounds, a similar trend is observed with values being ~15(±5)mV less than the corresponding $E_{pc/2}$ values.

2B.1.5 Derivatives Possessing Electron Donating Groups

Para MeS, Me and MeO derivatives were successfully synthesised. At variable temperature, -15°C and 0°C, all three materials produced a quasi-reversible response identical to that of the electron withdrawing analogues, see Table 3. Also, the strength of the donor substituent was found to be inversely related to the half peak reduction potential and half wave potential of the dithiadiazolylium moiety. Hence the following order in cathodic potentials is observed:

$$\mathbf{MeO < Me < MeS < H}$$

2B.1.6 All *Para* Substituted Derivatives

For all the derivatives, containing donor and acceptor substituents groups, the following common features were apparent.

Quasi reversible effects

(1) $E_{pc}-E_{pc/2} \sim 0.06V$

(2) i_{pc} decreases with increasing temperature

(3) i_{pc} increases with increasing scan rate

(4) $E_{pc}-E_{pa} > 0.055V$

(5) i_{pc}/i_{pa} only equals unity if $\alpha_c=\alpha_a=0.5$

(6) Cathodic potentials are more reproducible than anodic potentials

Donor/acceptor affects

(7) The greater the electron accepting ability of the substituent group the more positive is the cathodic potential.

Points (1) to (6) suggest that a similar quasi-reversible electrochemical reduction mechanism applies to all of these *para* derivatives. This is consistent with the similar chemistries of these derivatives.

Results from the cathodic portion of the wave for all the derivatives show that $E_{pc}-E_{pc/2}$ is typically 60-80mV. The $E_{pa}-E_{pc}$ values for the MeS and Cl derivatives ranged from 100-135mV and for the other derivatives ranged from 65-95mV. This difference is attributed to broader anodic waves being observed for these two examples due to additional competing minor processes, (other than simple quasi-reversible charge transfer), effecting anodic wave shape. Investigation into identifying what additional processes were occurring was not attempted as it was the cathodic measurements that were the main focus of interest and these were seen to be unaffected by these additional processes.

Point (7) can be readily rationalised by examining the electrochemical process taking place. Since the free energy for the process can be expressed as $\Delta G^\circ=-nE^\circ F$, the more positive the potential becomes the more negative ΔG° gets and hence the process becomes more preferable[37]. Therefore, the more stable the electrochemical product is in relation to other reduced species, the higher the value of the standard reduction potential E° will be.

From these simple CV studies E° could not be calculated. However, it is important to note that $E_{pc/2}$, which was found to be the most reliable potential, is not equal to the standard potential but proportional to it. Therefore, this value

could be used instead to gauge the relative Gibbs free energy of these compounds.

So, by looking at the range in $E_{pc/2}$ reduction potentials of these *para* substituted phenyl-1,2,3,5-dithiadiazolylium salts and above relationship, it can be deduced that ΔG° of this reduction process becomes more favourable,(i.e product becomes more energetically stable), as does the reduction potential, as the electron withdrawing ability of the substituent group increases.

The product of the electrochemical reduction process occurring for the *para* substituted phenyl dithiadiazolylium derivatives is the corresponding 7π dithiadiazolyl radical. Therefore, the stronger the electron withdrawing ability of the substituent group the more stable the produced radical is.

This trend is observed because the stronger the donor ability of the *para* substituent group, the more it will destabilise the dithiadiazolyl ring as it is placing more charge into anti-bonding orbitals and hence making the ring more anti-aromatic in nature. This has been confirmed by MO calculations conducted on substituted aryl dithiadiazolylium species by Boere *et al*[38], who showed that the addition of a stronger donor group increased the energy level of the LUMO, (SOMO for dithiadiazolyl) to a greater extent than compared with that of the corresponding HOMO. This indicates that product stability is the main driving force for the reaction and not the stability of the reactant. Also, the energy required to place an electron into the LUMO, i.e reduce the cation, increases with donor capacity of a *para* substituent group. Hence ΔG° and E° become less favourable or decrease accordingly, for derivatives possessing electron donating side groups too[39,40].

2B.1.7 Hammett[40,41]

The Gibbs free energy of a system can also be represented as $\Delta G'^{\circ}-\Delta G'^{\circ}_{o}=-2.303RT\sigma_p\rho$, where σ_p=Hammett constant for *para* substituents, ρ=constant specific for experimental conditions and $\Delta G'^{\circ}$= Gibbs free energy for conditions different to those used in the Hammett measurements. Therefore E° can be related to σ_p through their relationship with $\Delta G'^{\circ}$ [42].

The Hammett value, σ_p, is a measure of the degree that a substituent group assists or hinders the ionisation of aryl carboxylic acids in water at 25°C. *Para* substituent groups influence this by inductive and resonance contributions[43].

Linear free energy relationships have been achieved by plotting σ_p values of carboxylic acid derivatives against potentials of analogous substituted compounds possessing different reaction centres. This only occurs when the electronic effects of the substituents on these reaction centres are analogous.

Para substituted aryl 1,2,3,5 dithiadiazolylium/zolyl derivatives have a similar skeleton to benzoic acids and their dissociated salts; hence similar inductive and resonance pathways could be anticipated.

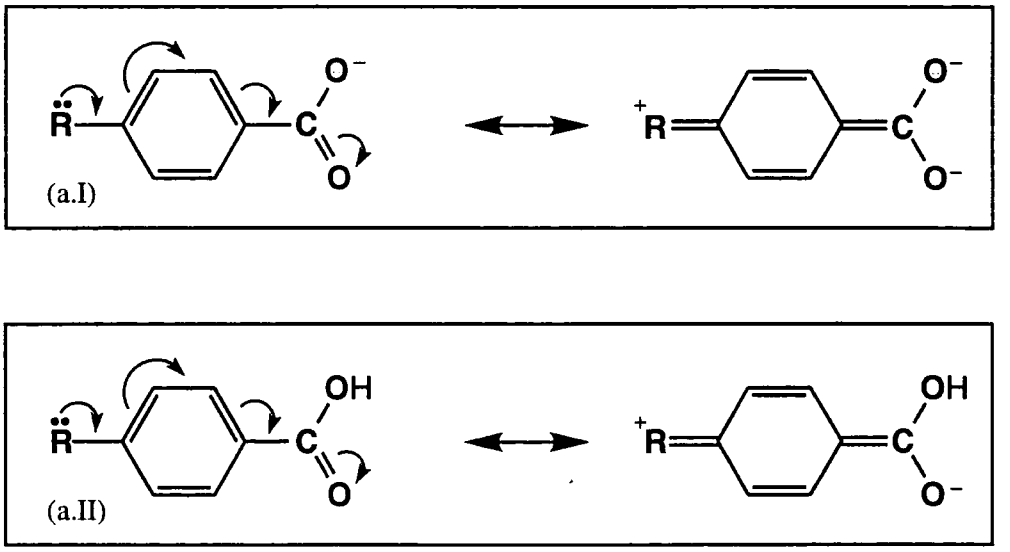

Fig 9. Resonance canonical forms aryl benzoates (a.I) and benzoic acids (a.II) possessing *para* electron donating groups.

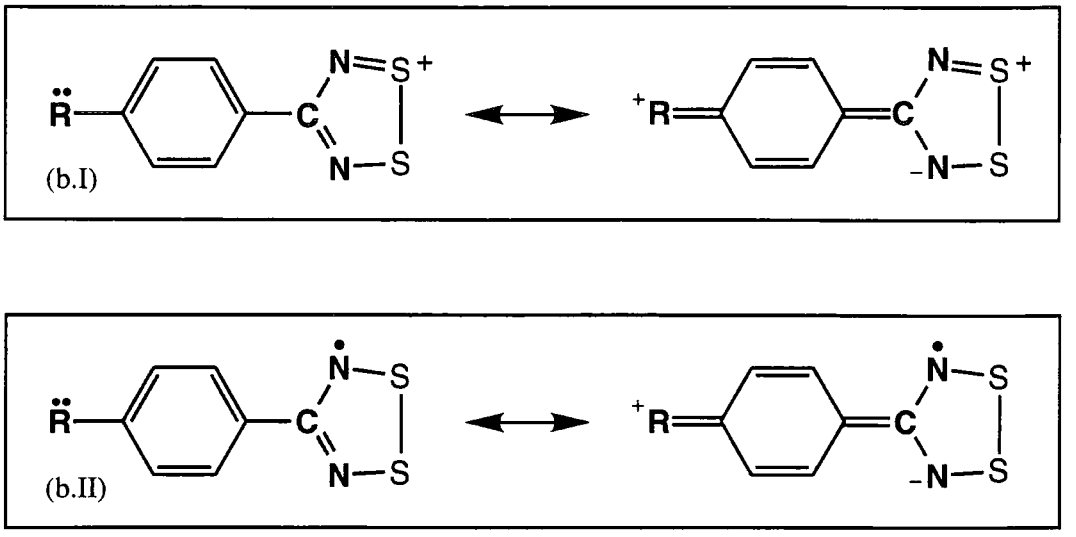

Fig 10. Resonance canonical forms of aryl 1,2,3,5 dithiadiazolylium (b.I) and (b.II) dithiadiazolyl moieties possessing *para* electron donating groups.

This is further supported by looking at the resonance pathways of these four types of *para* substituted compounds in detail. Figs 9 and 10 show the possible resonance canonicals for derivatives possessing electron donating *para* derivatives and they are all found to form similar quinoid type canonicals with the charge being placed at the second atom of the reaction centre.

If the reverse situation is examined when electron withdrawing groups are present, it is impossible for charge to be transferred away from these reaction centres, (except for the dithiadiazolyl species), via the mesomeric effect as it results in extremely unsound chemical systems being drawn up, e.g.. monovalent positive oxygen and positive divalent nitrogen or two positive sulphurs bonded together, see Figs 11 and 12. However, from the resonance diagrams of dithiadiazolyls possessing electron withdrawing groups, there is no way of telling the size of this resonance contribution to the overall energy of the system and the effect it has on the electronic environment of the ring, see Fig 12.

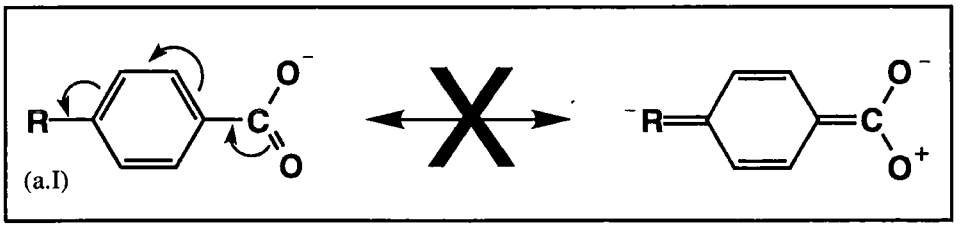

Fig 11a. Resonance canonical form for a benzoate derivative (a.I) possessing a *para* electron withdrawing group.

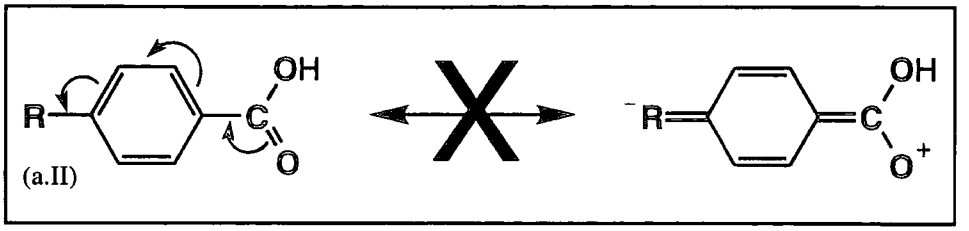

Fig 11b. Resonance canonical form of a benzoic acid derivative (a.II) possessing a *para* electron withdrawing group.

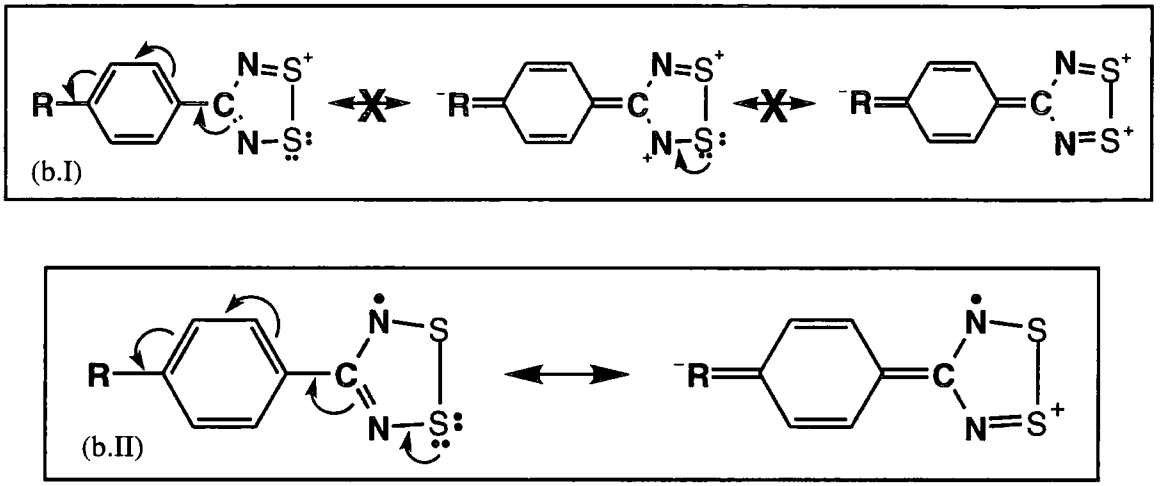

Fig 12. The disfavoured and favoured resonance canonical forms of aryl 1,2,3,5 dithiadiazolylium (b.I) and dithiadiazolyl (bII) moieties possessing *para* electron withdrawing groups respectively.

Due to these similarities in resonance pathways, it seemed a good idea to investigate if a linear free energy linear relationship existed between a series of *para* substituted aryl dithiadiazolylium derivatives and corresponding carboxylic acids. There was no guarantee that such a relationship would exist as measurements are conducted in different solvents (H_2O & MeCN), hence differing solvent effects between these two series of compounds, which influence these measurements, may not be comparable[40,41].

More detail on Hammett values and constant can be found in section 2C.1.

Linear Free Energy Plot

When $E_{pc/2}$ values of these *para* substituted phenyl 1,2,3,5 dithiadiazolylium salts were plotted against corresponding Hammett σ_p values an excellent linear free energy relationship was found to exist, therefore the suspicion that these two parameters were related was confirmed, see Fig 13 and Table 5. The very high r^2 value of 0.990 of this plot shows that the errors associated with this linear relationship are very small.

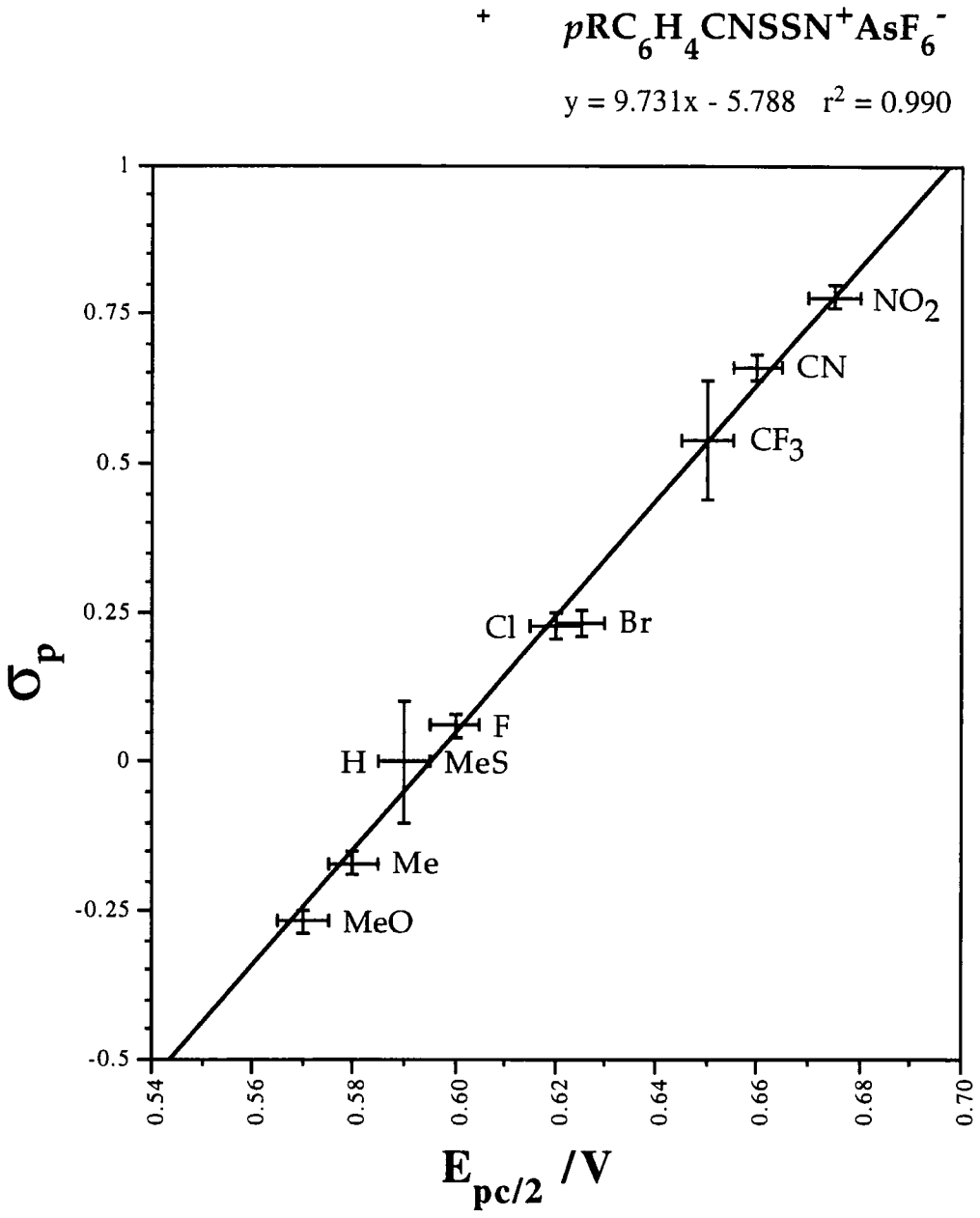

Fig 13. A plot of $E_{pc/2}$ values of some *para* substituted phenyl 1,2,3,5-dithiadiazolylium hexafluoroarsenate salts versus Hammett σ_p values.

Sample	$E_{pc/2}$ /mV	σ_p
NO_2	675	0.778 +/- 0.02
CN	660	0.660 +/- 0.02
CF_3	650	0.54+/- 0.1
Br	630	0.232 +/- 0.02
Cl	620	0.227 +/- 0.02
F	600	0.062 +/- 0.02
H	590	0.00
MeS	590	0.00 +/- 0.1
Me	580	-0.170 +/- 0.02
MeO	570	-0.268 +/- 0.02
CO_2Me	640	0.45 +/- 0.1
CF_3O	630	0.35 +/- 0.02

Table 5. $E_{pc/2}$ CV data and related Hammett σ_p values for several *para* substituted phenyl 1,2,3,5 dithiadiazolylium hexafluoroarsenate salts[44,45].

The gradient of the graph was positive which indicates that electron withdrawing groups help stabilise products of the ionization of benzoic acids and reduction of dithiadiazolylium species. Electron donating groups have the opposite effect (see section 2C.1).

The plot involves a comparison of two different physical responses in different solvents. The electronic environment of these reaction centres is not only sensitive to substituent groups but also solvent interactions. Solvent interactions with a medium will naturally differ if the medium or solvent is changed. As the gradient of the plot is constant, this suggests that comparable solvent effects are present among these *para* substituted phenyl 1,2,3,5 dithiadiazolylium and carboxylic acid derivatives. Therefore, the gradient of this plot is an indication of a ratio of effects that substituents place on the dithiadiazolylium and carboxylic acid reaction centre under these experimental conditions.

It was not possible to make a direct comparison between the Hammett values or reduction potentials of both types of derivatives for the following two

reasons: Firstly it is envisaged that obtaining reduction potentials for these carboxylic acids would be difficult. This is because of the possibility of side reactions occurring during the CV experiment, thus complicating the electrochemistry[26]. Secondly Hammett values calculated directly from the ionization of dithiadiazolylium derivatives in acidic media could not be attempted as these compounds would decompose in the presence of protons.

From these plots its can be deduced that (i) similar electronic effects operate in *para* substituted aryl carboxylic acids and 1,2,3,5 dithiadiazolylium salts and (ii) similar electrochemical reaction mechanisms for the reduction of the 1,2,3,5 dithiadiazolylium cations exist.

As this relationship is so good, could $E_{pc/2}$ values of other *para* substituted phenyl 1,2,3,5 dithiadiazolylium salts be predicted from this plot using known Hammett σ_p values?

CF_3O and CO_2Me

CF_3O and CO_2Me derivatives were therefore synthesised in order to address this question. CV investigations revealed that these compounds gave responses typical of their sister compounds, see Table 4. Their experimental $E_{pc/2}$ values were found to be 0.63V and 0.64V respectively. These values are in good agreement with those predicted from the linear free energy plot, see Fig 14 and Table 5.

Clearly this is a reliable method of evaluating $E_{pc/2}$ values for this system. But would the same electrochemical behaviour be observed for the analogous isomeric 1,3,2,4 dithiadiazolylium salts? This is now discussed in the following chapter.

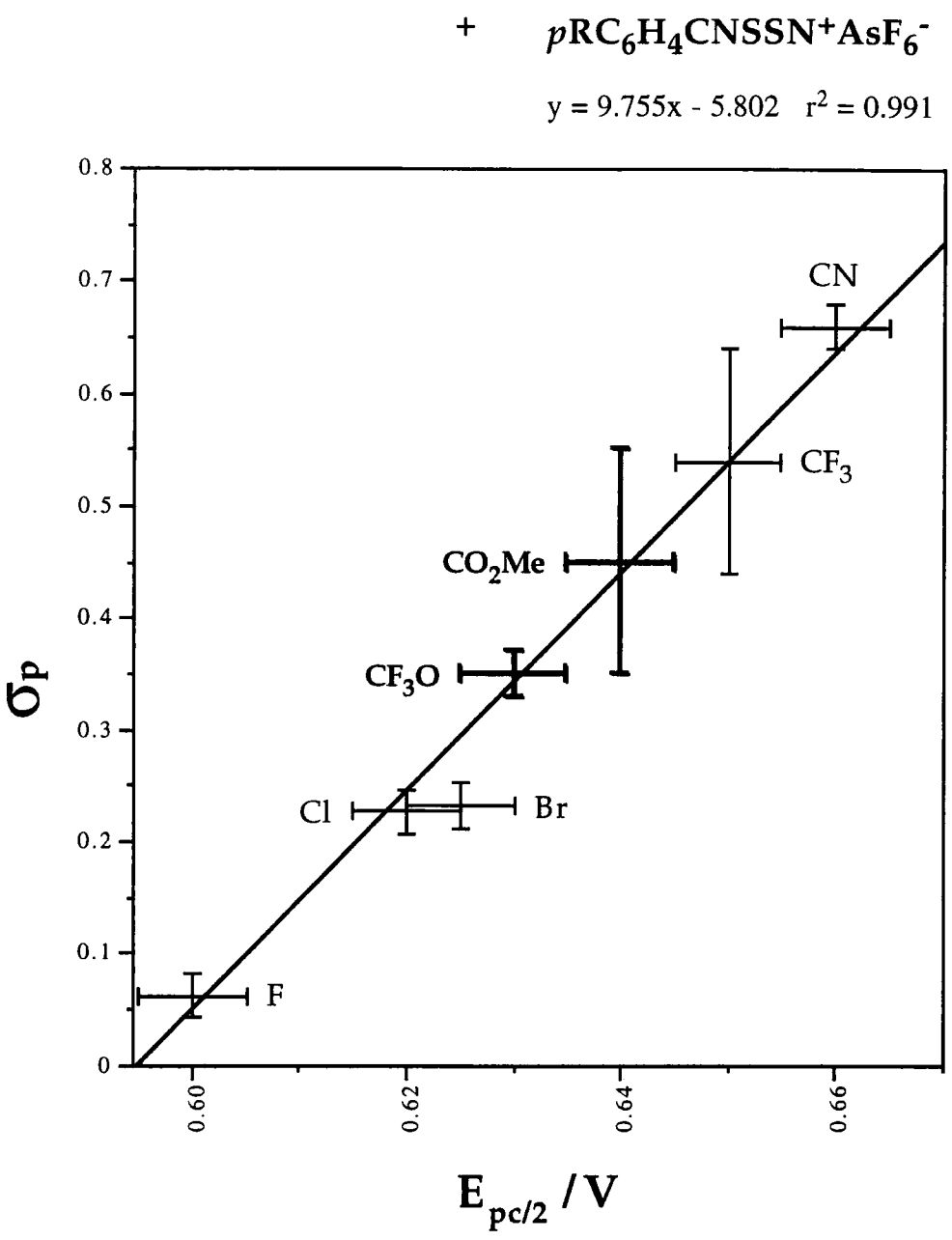

Fig 14. A plot of $E_{pc/2}$ values of some *para* substituted phenyl 1,2,3,5 dithiadiazolylium hexafluoroarsenate salts versus corresponding Hammett σ_p values, which include CF_3O and CO_2Me derivatives.

Section 2B.2

2B.2 The Electrochemistry of *Para* Substituted Phenyl 1,3,2,4 Dithiadiazolylium Hexafluoroarsenate Salts

2B.2.1 Phenyl 1,3,2,4 dithiadiazolylium salt

An investigation, identical to that undertaken for *para* substituted phenyl 1,2,3,5 dithiadiazolylium hexafluoroarsenate salts,(section 2B.1), was conducted on isomeric 1,3,2,4 dithiadiazolylium analogues so that their electrochemistries could be readily compared. Naturally the parent compound was examined first, i.e. phenyl 1,3,2,4 dithiadiazolylium hexafluoroarsenate.

This compound gave a cyclic voltammogram trace with two peaks, a picture of the trace is shown in Fig 15.

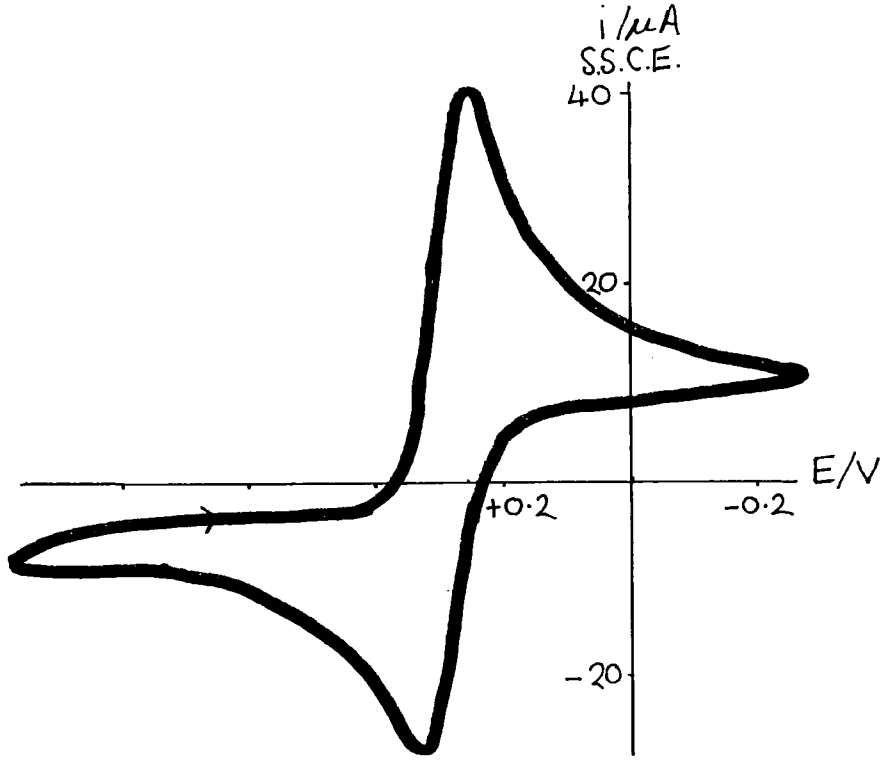

Fig 15. Cyclic voltammogram of $1x10^{-3}$M phenyl 1,3,2,4 dithiadiazolylium hexafluoroarsenate in MeCN, at -15°C, scan rate $576mVs^{-1}$, supporting electrolyte $TBABF_4$ at $1x10^{-1}$M.

The shape of the above pictured cyclic voltammogram is extremely similar to that given by isomeric 1,2,3,5 dithiadiazolylium analogues. Other coincidences include E_{pa}-E_{pc}>0.055V, E_{pc}-$E_{pc/2}$ ~60-70mV and i_{pc}/i_{pa} ratio is not necessarily unity (in this case 1.39), i.e. a quasi-reversible system. The most noticeable difference between the isomers was the shift in the potentials. The observed cathodic peak and half peak potentials for this 1,3,2,4 derivative were 0.260V and

0.330V respectively. The same values for the 1,2,3,5 dithiadiazolylium sister compound are found to be larger, with values typically 0.530V and 0.590V respectively. Discussion on why there is a difference in these values can be found later on in section 2B.2.7.

Another feature of this voltammogram is that the half peak widths of both waves are found each to be 70mV. Anodic measurements have only briefly been mentioned because the information tendered is sufficient to readily diagnose this system as being quasi-reversible and the main source of interest is the cathodic or reduction potentials of this derivative.

The electrochemical behaviour of this 1,3,2,4 dithiadiazolylium salt and related *para* substituted analogues was explored further, in a manner analogous to that described in section 2B.1.

2B.2.2 Variable Temperature CV Measurements

The exploration commenced with a variable temperature CV scan, (-15°C to +10°C), on a fresh sample of phenyl 1,3,2,4 dithiadiazolylium hexafluoroarsenate.

Potentials

Results revealed that all of the peak and related potentials steadily increased with increasing temperature, see Table 6. The smallest shift in potentials, over this temperature range, was observed for half peak potentials of 10mV compared with 20mV for peak potentials and $(E_{pa}+E_{pc})/2$. Also these ranges were equal to the limits of the experimental error associated with these measurements. The average values of E_{pc} and $E_{pc/2}$ were 260mV ±10mV and 330mV ±5mV which correspond nicely with the results obtained from Fig 15.

The system was found to be quasi-reversible over this temperature range as E_{pa}-E_{pc} was consistently larger than 55mV (maximum ideal reversible couple value at 10°C).

The cathodic half peak width was found to be within experimental error of that of the corresponding anodic value and was typically 70mV.

Current

The values of the peak currents and peak current ratios were found to decrease with increasing temperature. (Therefore $(E_{pa}+E_{pc})/2$ values are not equal to the standard reduction potential of this system, see section 2B.1.2). A plot of i_{pc} *vs* $T^{-1/2}$ revealed that these two values were indeed proportional to each other, see Fig 16, and did obey the Randles-Sevcik equation for a diffusion controlled process, see Eqn 2 in section 2A.2.1.

Temperature °C	E_{pc} mV	$E_{pc/2}$ mV	$E_{pc}-E_{pc/2}$ mV	i_{pc} µA	E_{pa} mV	$E_{pa/2}$ mV	$E_{pa}-E_{pa/2}$ mV	i_{pa} µA	$E_{pa}-E_{pc}$ mV	i_{pc}/i_{pa}	$(E_{pa}+E_{pc})/2$ mV
-15	260	330	70	42.0	350	280	70	30.2	90	1.39	305
-12	255	330	75	36.4	340	275	65	27.0	85	1.35	297.5
-4	260	330	70	26.4	350	280	70	21.2	90	1.29	305
0	260	330	70	23.0	360	290	70	19.6	100	1.23	310
6	275	340	65	19.5	360	290	70	17.0	85	1.15	317.5
10	270	335	65	17.0	370	290	80	16.8	100	1.01	320

Table 6. CV data for a sample of phenyl - 1,3,2,4 - dithiadiazolylium hexafluoroarsenate collected at increasing temperature, scan rate 576mVs^{-1}.

$\upsilon^{1/2}$ $(mV/s)^{1/2}$	E_{pc} mV	$E_{pc/2}$ mV	$E_{pc}-E_{pc/2}$ mV	i_{pc} µA	E_{pa} mV	$E_{pa/2}$ mV	$E_{pa}-E_{pa/2}$ mV	i_{pa} µA	$E_{pa}-E_{pc}$ mV	i_{pc}/i_{pa}	$(E_{pa}+E_{pc})/2$ mV
10	270	330	60	23.0	355	295	60	22.5	85	1.02	312.5
13	270	330	60	28.5	360	300	60	29.0	90	0.98	315
15	260	330	70	32.5	360	295	65	33.5	100	0.97	310
18	255	330	75	40.5	370	300	70	41.0	115	0.99	312.5
20	260	330	70	45.0	370	300	70	45.0	110	1.00	315
23	250	325	75	53.0	375	300	75	51.0	125	1.04	312.5
25	250	330	80	57.0	380	305	75	55.0	130	1.04	315
27	250	325	75	59.0	380	305	75	60.0	130	0.98	315
30	245	325	80	66.0	380	300	80	64.0	135	1.03	312.5

Table 7. CV data for a sample of phenyl - 1,3,2,4 - dithiadiazolylium hexafluoroarsenate conducted at various scan rates, temperature at 0°C.

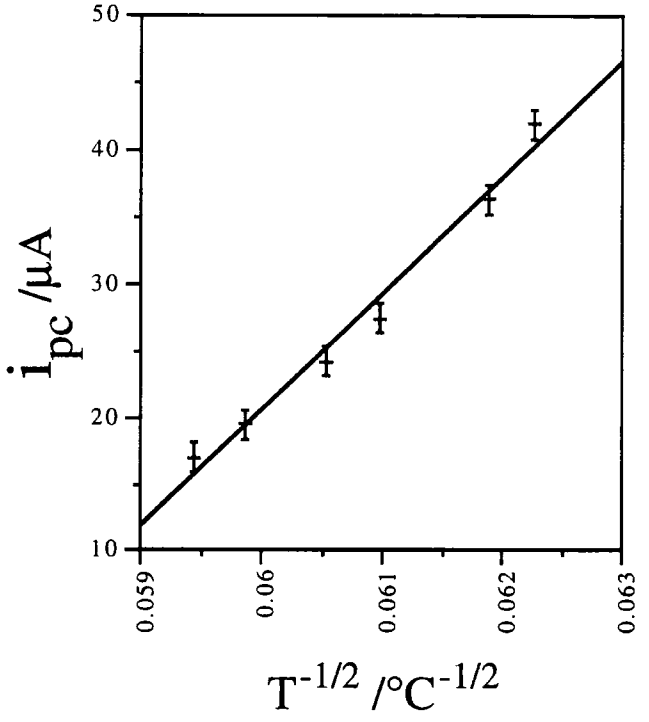

+ C_6H_5-CNSSN $^+AsF_6^-$

y = 8707.752x - 501.916
r^2 = 0.982

Fig 16. i_{pc} *vs* $T^{-1/2}$ plot for phenyl 1,3,2,4 dithiadiazolylium hexafluoroarsenate, scan rate 576mVs^{-1}, concentration 1x10^{-3}M, supporting electrolyte $TBABF_4$, solvent MeCN.

General

All of the above trends were also observed for the phenyl 1,2,3,5 dithiadiazolylium salt under similar conditions and are described in slightly more detail in section 2B.1.2. Greater attention has been paid to the cathodic wave and quasi-reversibility of the system as these are the main areas of interest.

2B.2.3 Variable Scan Rate CV Measurements

Potential

Next, the same investigation was repeated with fresh material, constant temperature (0°C) and variable scan rates in the range 100 to 900mVs^{-1}. This CV study revealed that $E_{p/2}$ values were constant to within experimental error of ±5mV; $E_{pc/2}$ was 330mV and $E_{pa/2}$ was 300mV, see Table 7. The cathodic and anodic peak potentials were observed to decrease and increase respectively with increasing scan rate, each by a maximum of 0.025V over a nine fold change in scan rate. E_{pa}-E_{pc} and E_p-$E_{p/2}$ were seen to increase with scan rate by 50mV and

20mV respectively. Again E_{pa}-E_{pc} and E_p-$E_{p/2}$ were found to be greater than 0.055V and so this run also displayed quasi-reversibility.

Current

The current, i_p, was found to increase with increasing scan rate. On the basis of Eqn(2) of section 2A.2.1, a plot of i_p versus $\upsilon^{1/2}$ was drawn and a linear relationship was discovered to exist, see Fig 17. If the errors on the gradient of these graphs are taken into account it can be said that these lines do pass through the origin and therefore i_p is proportional to $\upsilon^{1/2}$.

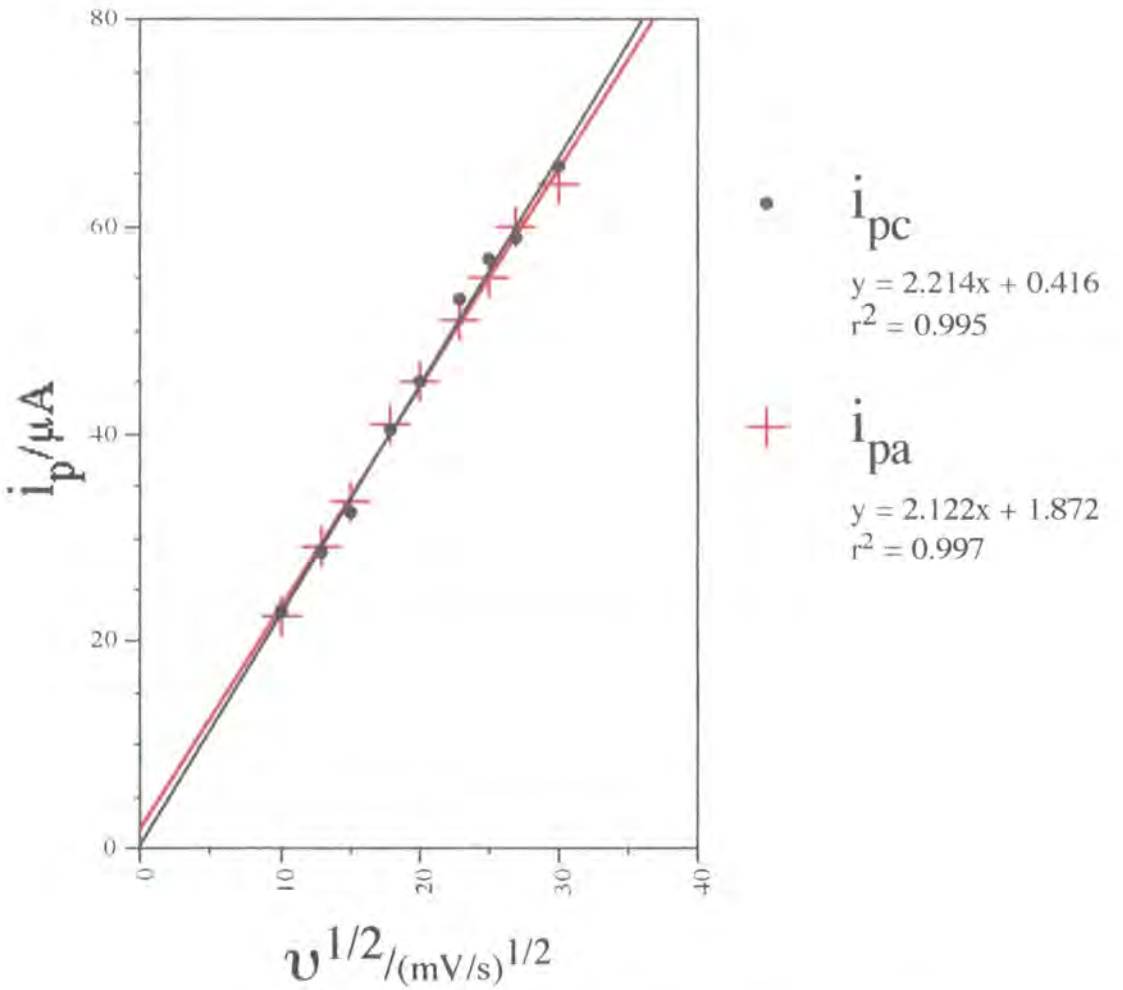

Fig 17. i_p *vs* $\upsilon^{1/2}$ plot for phenyl 1,3,2,4 dithiadiazolylium hexafluoroarsenate at 0°C, concentration $1x10^{-3}$M, supporting electrolyte $TBABF_4$, solvent MeCN.

The i_{pc}/i_{pa} current ratios were found to be approximately unity throughout the experiment and no obvious relationship between them and scan rate was evident.

General

All of the above trends were also observed for the phenyl 1,2,3,5 dithiadiazolylium salt under similar conditions and are described in slightly more detail in section 2B.1.3.

2B.2.4 Comparison of the electrochemistry between phenyl 1,2,3,5 and 1,3,2,4 dithiadiazolylium isomers.

When the trends observed in the above CV investigations of phenyl 1,3,2,4 dithiadiazolylium hexafluoroarsenate are compared with those already drawn up for the 1,2,3,5 dithiadiazolylium analogue there are many striking resemblances:-

---

(1) The redox process is quasi-reversible as -
$E_{pc}-E_{pc/2}>0.055V$
$E_{pa}-E_{pc}>0.055V$
i_{pc}/i_{pa} ratio decreases with increasing temperature
$0<i_{pc}/i_{pa}>1$

(2) $i_p \propto \upsilon^{1/2}$ over a range of 10^2 to $30^2 mVs^{-1}$

(3) $i_p \propto T^{-1/2}$ over a range of -15°C to +10°C

Earlier, an electrochemical investigation of *para* substituted aryl 1,2,3,5 dithiadiazolylium salts revealed that the donor/acceptor ability was directly related to the size of potential of the reaction centre and that all of them exhibited similar quasi-reversible responses, see section 2B.1.4-6.

So far it has been seen that phenyl 1,2,3,4 and 1,3,2,4 derivatives behave in a complementary manner to each other. Therefore, several substituted 1,3,2,4 dithiadiazolylium analogues were synthesised to see if electrochemical similarities between the isomers extend to substituted derivatives as well.

2B.2.5 Derivatives Possessing Electron Withdrawing Groups

The substituted aryl derivatives possessing the electron withdrawing *para* substituents, NO_2, CF_3, Br, Cl and F, were studied first of all. The results are shown in Table 8.

Beginning with the NO_2 derivative, a very simple variable scan rate and temperature examination revealed that this compound behaved in an electrochemical quasi-reversible manner reminiscent to that observed for the analogous unsubstituted relative, i.e. E_{pa}-E_{pc}>0.055V, i_p increases with scan rate and $E_{pc/2}$ was consistent to within ±5mV. $E_{pc/2}$ was found to be 400mV.

Next, three batches of Br and F derivative were tested by CV, (at variable temperatures and scan rates), in order to test if the measurements were within experimental error of each other despite varying conditions. Of particular interest was the reproducibility of $E_{pc/2}$ potential. All the $E_{pc/2}$ values for Br and F derivatives were found to be consistently 350mV and 340mV respectively. The survey revealed that both were quasi-reversible under these conditions and possessed the same characteristic electrochemical features as the above NO_2 derivative.

Finally, a less detailed examination of the CF_3 and Cl derivatives showed that they too exhibited the same quasi-reversibility as their sister compounds. $E_{pc/2}$ values for these two groups were found to be 380mV and 350mV respectively.

Looking at the $E_{pc/2}$ values for all of these substituted 1,3,2,4 derivatives it is evident that electron withdrawing ability of the substituent group is related to the size of this potential. Hence, the order is as follows,

$$\mathbf{H < F < Cl \leq Br < CF_3 < NO_2} \qquad \mathbf{E_{pc/2} / mV}$$

The same trend in the relative size of $(E_{pa}+E_{pc})/2$ values were also observed. But as stated in section 2B.1.2 this is not equivalent to the E° standard reduction potential of these compounds as they are found to be quasi-reversible and referring back to section 2B.2.2. these potentials are not as reliable as the cathodic potentials.

2B.2.6 Derivatives Possessing Electron Donating Groups

An identical investigation was carried out for *para* Me, MeO and MeS derivatives. A variable temperature scan of the Me derivative showed that, under identical conditions, this material had the same electrochemical qualities as those

Sample		Temp °C	Scan rate mVs^{-1}	E_{pc} mV	$E_{pc/2}$ mV	i_{pc} μA	$E_{pc}-E_{pc/2}$ mV	E_{pa} mV	$E_{pa/2}$ mV	i_{pa} μA	$E_{pa}-E_{pa/2}$ mV	i_{pc}/i_{pa} μA	$E_{pa}-E_{pc}$ mV	$(E_{pa}+E_{pc})/2$ mV
NO_2	A	0	729	330	395	18.8	65	425	355	14.8	70	1.27	95	377.5
		0	576	340	395	17.6	55	420	355	13.6	65	1.29	80	380
		0	484	345	405	17.2	60	430	360	14.0	70	1.23	85	387.5
	B	-15	484	335	405	30.8	70	430	355	25.6	75	1.20	130	382.5
CF_3	A	-14.5	484	320	380	17.6	60	430	350	13.6	80	1.29	110	375
Br	A	-15.5	400	275	350	16.6	75	425	340	13.2	85	1.26	150	350
	B	-15	400	280	350	14.95	70	415	335	12.4	80	1.21	135	347.5
	C	-15	576	275	350	10.2	75	415	335	8.8	85	1.16	140	345
Cl	A	-15.5	400	275	350	17.2	75	410	335	12.2	75	1.41	135	342.5
F	A	-13	256	270	340	40.8	70	375	340	36.8	55	1.11	105	322.5
	B	-15	576	280	340	26.4	60	380	315	17.2	65	1.53	100	330
	C	-13	576	280	340	29.2	60	380	320	22.2	60	1.31	100	330
MeS	A	-13	144	260	310	10.6	50	330	265	6.8	65	1.56	70	295
Me	A	0	484	230	300	23.5	70	350	280	23.2	70	1.01	120	290
		-13	484	240	300	36.8	60	340	280	28.4	60	1.30	100	290
	B	0	324	225	300	20.2	75	345	275	19.8	70	1.02	120	285
MeO	A	0	400	230	290	18.0	60	310	250	16.2	60	1.11	80	270
		0	484	230	285	19.4	55	310	250	16.6	60	1.17	80	270
		0	100	245	295	8.9	50	305	245	6.3	60	1.41	60	275

Table 8. Cyclic voltammetric data for *para* substituted phenyl - 1,3,2,4 - dithiadiazolylium hexafluoroarsenate in MeCN, concentration 1×10^{-3} M, supporting electrolyte $TBABF_4$.

of the analogous unsubstituted and electron withdrawing compounds, see Table 8. $E_{pc/2}$ was found to be 300mV.

A variable scan rate test on the MeO derivative showed that it too exhibited the same characteristics as above, 2B.2.5, with an average $E_{pc/2}$ value of 290V.

Finally, CV conducted on the MeS derivative revealed that it was quasi-reversible to the same degree as the two previous derivatives studied. $E_{pc/2}$ value for this derivative was found to be 310mV.

The $E_{pc/2}$ and $(E_{pa}+E_{pc})/2$ values for these derivatives confirmed that these potential are inversely related to the acceptor strength of the electron donating group.

General

Therefore the following trend exists.

MeO < Me < MeS < H < F < Cl ≤ Br < CF_3 < NO_2 **$E_{pc/2}$ in mV**

Electron donating ⇐ **⇒Electron accepting**

This CV survey revealed that these *para* substituted phenyl dithiadiazolylium salts all possess the same electrochemical quasi-reversible characteristics. This indicates that the electrochemical reduction mechanism and the degree of mixed control between charge transfer and mass transport in existence are very similar among these isomers.

2B.2.7 Electrochemical Comparison Between *Para* Substituted Phenyl 1,2,3,5 and 1,3,2,4 Dithiadiazolylium Salts.

How does the electrochemistry between the two isomeric series compare? A list of comparisons is given below.

Similarities

(1) Quasi-reversibility

$E_{pc}-E_{pc/2} > 55mV$

$E_{pa}-E_{pc} > 55mV$

i_{pc} increases with $\upsilon^{1/2}$

i_{pc} increases with $T^{-1/2}$

i_{pc}/i_{pa} decreases with increasing temperature

(2) $\Delta E_{pc/2}(NO_2\text{-MeO})$ similar, e.g. $\Delta E_{1.2.3.5}$=105mV and $\Delta E_{1,3,2,4}$=100mV±5mV

(3) $E_{pc/2}$ more reproducible than other potential measurements.

(4) The size of $E_{pc/2}$ is related to the electron withdrawing strength of the substituent group attached.

Differences

(1) 1,2,3,5 potentials higher than 1,3,2,4 potentials by 260-280mV

(2) For the 1,2,3,5 isomer $0 \leq i_{pc}/i_{pa} \geq 1$ but for the 1,3,2,4 isomer $i_{pc}/i_{pa} \geq 1$

From the above Table it can be seen that many similarities between the electrochemistry of these two isomers exist and this is basically due to the following three features being common to both isomers.

Firstly, the electrochemical process studied, for both series of compounds involved the redox reaction between cationic 6π and radical 7π species. Secondly, these materials have similar chemistries. Thirdly, both types of phenyl dithiadiazolylium salts studied have a similar bonding framework. These aspect will now be elaborated upon to explain the above listed electrochemical trends fully.

The molecular bonding framework of both types of isomers as cations and radicals can be seen in figs 18a, b and c. In addition, associated resonance canonical forms possible for the cationic derivatives are included in the first two diagrams. From examination of these three figures, it can be clearly seen that very

similar resonance effects are present among these types of isomers. For instance, *para* substituent of dithiadiazolylium species can push electron charge into the cationic ring by analogous π systems, (resonance effect), but the reverse process can't happen. For the radical species, it is possible for the resonance effect to operate in both directions, i.e. either push or pull charge out of the ring depending on the substituent, see Fig 18c and section 2B.1.7. It is important to note that from these diagrams the size of the contribution of these resonance forms have on the electronic environment of the ring is unknown. However, the inductive effect from *para* substituents is likely to be comparable for the two isomers. Therefore, if each *para* phenyl substituent influences the electronic environment of both rings by the same order of magnitude (i.e. the resonance and inductive contributions are the same), then the ΔE's for both series would be expected to be close to one another and this is indeed observed.

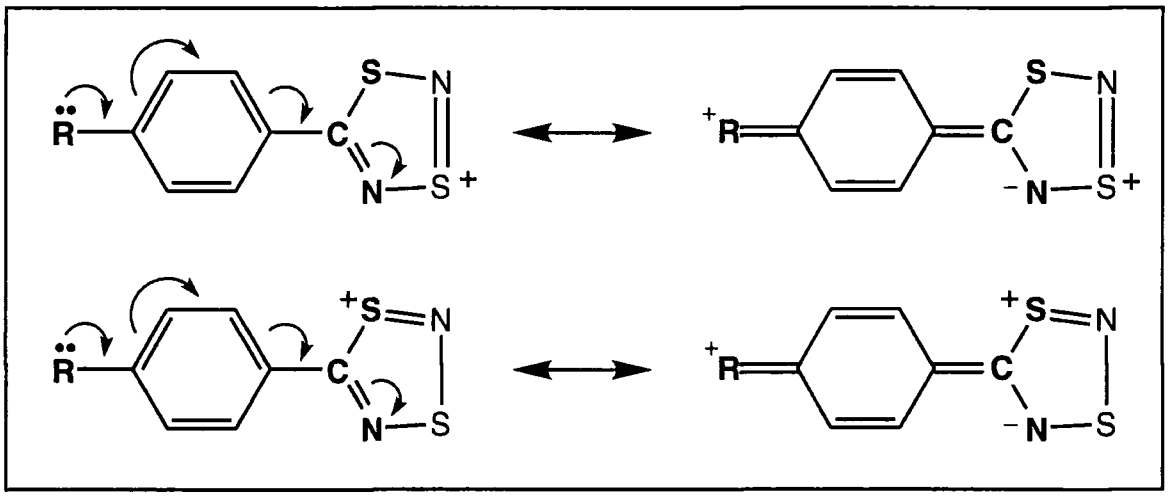

Fig 18a. Resonance canonicals of a substituted aryl 1,3,2,4 dithiadiazolylium derivative possessing a *para* electron donating group.

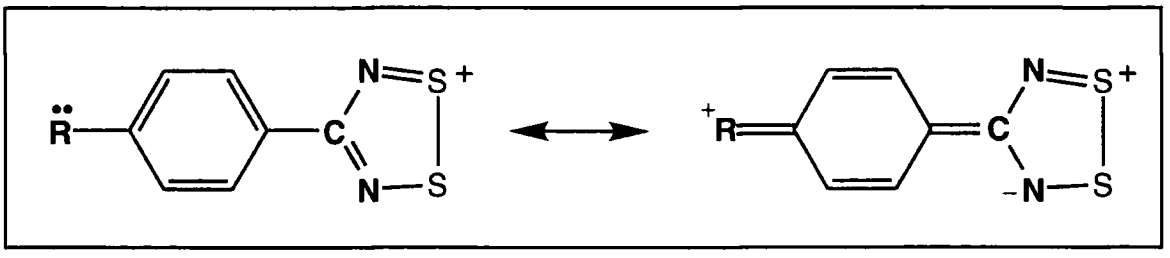

Fig 18b. Resonance canonicals of a substituted aryl 1,2,3,5 dithiadiazolylium derivative possessing a *para* electron donating group.

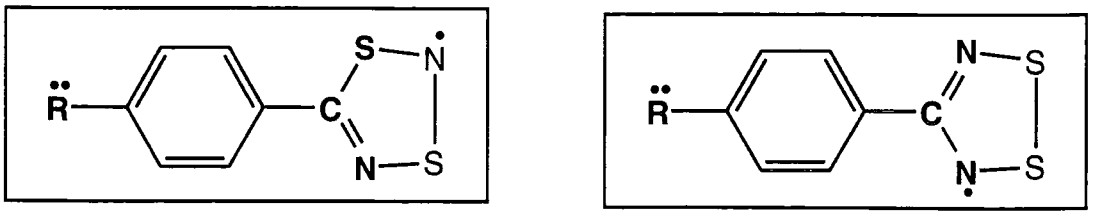

Fig 18c. *Para* substituted aryl 1,3,2,4 and 1,2,3,5 dithiadiazolyls

Why do the cathodic potentials increase with increasing electron acceptor strength of the substituent group? The answer to this relies on considering the process involved. For both analogues the cathodic process involves the 6π ring being reduced to a 7π radical. These radicals are destabilized by substituents which push excess charge towards them and hence making them more 8π or anti-aromatic in nature[38]. Therefore, using the relationship $\Delta G^{\circ}=-nE^{\circ}F$, the smaller the potential the more energetically unfavourable the reduction process, i.e. the more stable the product is relative to other analogues. Therefore it is expected that electron-donating groups that push excess charge into the ring will have lower potentials than their electron withdrawing counterparts and this is observed.

From the measurements of both isomers, the $E_{pc/2}$ values have been found to be the most accurate or reproducible under these experimental conditions and hence is the main potential referenced. This is not unique to these systems. In general electrochemistry, $E_{pc/2}$ is generally found to be more reliable than E_{pc} due to the larger error associated with the maximum than with the slope of the cyclic voltammogram[46].

Differences

Only two differences between the electrochemical response of these compounds were observed.

Starting with the differences in the potentials of the 1,2,3,5 and 1,3,2,4 analogues, this can be readily explained by studying relevant MO diagrams[34]. For this discussion the MO's of analogous H-$CN_2S_2^+$ systems will be used, see Fig 19. This is because MO orbital diagrams are generally more accurate when the atoms involved have a low atomic number and a smaller number of atoms. Also, it is assumed that the MO's of $HCN_2S_2^+$ will not be perturbed greatly by replacing the hydrogen substituent by a phenyl group.

The HOMO and LUMO for the 1,2,3,5 cationic ring are lower in energy than those of the analogous 1,3,2,4 ring. Also, if a cation is reduced, (i.e. an electron is placed into this LUMO), 8.52eV is required for the 1,2,3,5 system compared with a larger value of 9.23eV for the 1,3,2,4 system. Therefore reduction

of the 1,2,3,5 dithiadiazolylium ring is energetically more favourable relative to the isomeric 1,3,2,4 moiety. Using the relationship $\Delta G^{\circ}=-nE^{\circ}F$ the potential at which the 1,2,3,5 cation reduces would be expected to be higher than the 1,3,2,4 analogue and this is what's observed in practice.

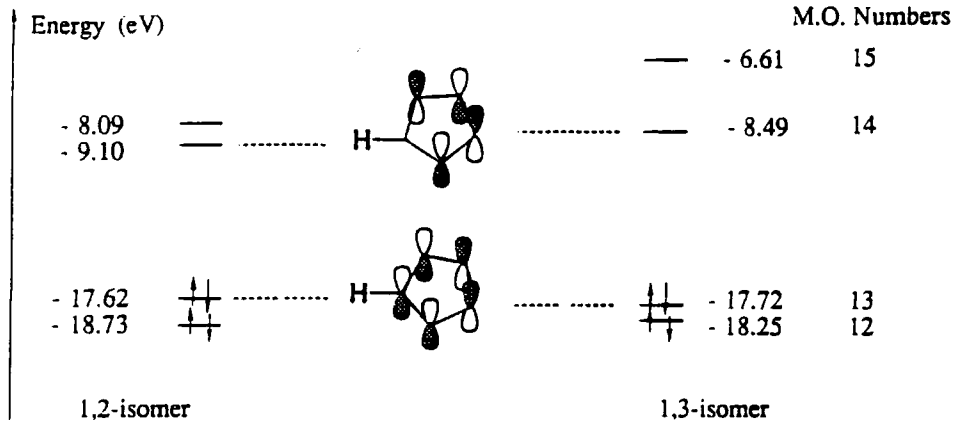

Fig 19. HOMO and LUMO energy levels for 1,3,2,4 and 1,2,3,5 dithiadiazolylium ring.

The other difference observed was in the size of the peak current ratios between the two series of substituted isomers. For the *para* substituted phenyl 1,2,3,5 dithiadiazolylium hexafluoroarsenate $0 \leq i_{pc}/i_{pa} \geq 1$, but for the analogous 1,3,2,4 salts $i_{pc} \geq 1$.

To assess this situation certain similarities between these two series of compounds need to be considered.

These systems were identified as being quasi-reversible, due to slow charge transfer, as the cathodic and anodic peaks were seen to move to more anodic potentials with increasing temperature and peak separation increased with increasing scan rate. Even though the peak current ratios were not necessarily one and differed slightly for both sets of compounds they were seen to decrease with increasing temperature and remain reasonably constant with increasing scan rate. Also, the cathodic potentials of each sample of these two series of compounds were reproducible within experimental error over the temperature and scan rate ranges used in this electrochemical study.

The current ratios did not necessarily equal one for these series of compounds. This indicates that another process(es) other than quasi-reversible charge transfer is in operation to some degree. The process(es) affecting peak height for both appears to be more sensitive to temperature (thermodynamic parameter) than to scan rate (kinetic parameter). Of particular interest is the fact at the beginning of the variable temperature measurements cathodic peak current is larger than the anodic value but as the temperature rises the reverse situation gradually develops. These additional processes have little impact on cathodic peak potentials which are the main source of interest but do influence to a minor degree peak height and shape of the anodic wave. These two last bits of information are major clues to uncovering what the process(es) is.

Such processes that can cause these effects are (1) weak absorption at the electrode surface, (2) differing solubility/ precipitation and (3) a competing chemical reaction. The electrochemical information gathered is not extensive enough to identify which process or processes are responsible for this phenomenon but the validity of each will be discussed in turn.

(1) From the shape of the voltammograms of both series of compounds the only possible adsorption that can occur is weak adsorption of a quasi-reversible couple. In the literature this is not covered in any great detail as assessing the relationship between rate of charge transfer and adsorption is considered too complicated. Therefore, no further in-depth discussion of this subject will be attempted.

(2) If the oxidised and reduced species have differing solubilities, such that the most insoluble species is precipitated during the scan then the peak current ratio will be affected due to a build up of this species at the surface of the electrode. If the reduced species is deposited or precipitated then the anodic wave is enhanced. The same effect on the cathodic wave will be observed if the oxidised species is the least soluble. This effect will be less pronounced as temperature increases as the solubility of the least soluble species will increase too. The enhanced peaks formed by this process are often referred to as 'stripping peaks'.

For these compounds the salts are generally more soluble than the radicals in MeCN. Therefore, at low temperature if the radical was being precipitated an enhancement of the reverse wave would be expected. As the temperature increases the anodic peak height would decrease relative to the cathodic peak due to increased solubility of the radical. Overall this would result in an increase in the peak current ratio with increasing temperature. However the ratio would not exceed one. The opposite trend in peak current ratios for these compounds is observed. If the oxidised species precipitated out then this trend would be

observed but in this case this doesn't happen as the oxidised species is readily soluble in the solution. Therefore deposition can be ruled out as a feasible option.

(3) What possible chemical reactions can occur, which would contribute to the trends in peak current ratios and peak shapes between these series of compounds? As the peak current ratios slightly differ in size between the two sets of isomeric derivatives then the chemical reactions between them can differ also.

The most obvious chemical difference between the 1,2,3,5 and 1,3,2,4 isomers is the radical species of the later can rearrange in solution to the 1,2,3,5 isomer[47]. This process is readily initiated by light and heat.

If the 1,3,2,4 radical species produced during the cathodic scan began to rearrange before the anodic peak is reached, this would reduce the concentration of the 1,3,2,4 radical at the surface of the electrode. Hence a lower i_{pa} value and higher peak current ratio would be observed. This process would become more pronounced with increasing temperature and thus peak current ratios would increase accordingly. Also, if this was occurring an anodic peak corresponding to the 1,2,3,5 side product would also be observed. However, none of the *para* substituted phenyl 1,3,2,4 dithiadiazolylium salts studied possessed voltammograms with the above distinguishing features characteristic for the rearrangement. Hence this process is negligible in solution during these CV measurements.

Another possible source of a chemical reaction could be due to the materials possessing undetectable trace impurities which react with the analyte to form a multitude of materials whose redox processes are either not observed in the potential window scan in these measurements or they overlap those of the dithiadiazolylium species.

If the impurities are reacting with electroactive species then they will naturally become more reactive with increasing temperature. As the cathodic portion of the wave is generally more constant between runs than the anodic wave this suggests that the reactions involve the radical species. If this was the case for these samples the peak current ratio would increase with increasing temperature as the concentration of the reduced species declined but this is not observed for these samples. It is unlikely that the reverse process, involving the cationic species, is in operation as only small potential shifts in the cathodic wave are observed.

If impurities are electrochemically active in the same region as the species of interest, such that both voltammograms overlap, then they can contribute to peak enhancement of a sample. However this is considered to be a minor process as it is extremely unlikely that impurities will do this, especially if you consider

that 1,2,3,4 and 1,3,2,4 derivatives are similar but their potentials are significantly different.

In summary, these systems are both predominantly quasi-reversible due to slow charge transfer which is complicated by other minor processes competing which can't be identified from this simple electrochemical investigation. No attempt was made to conduct a more detailed electrochemical analysis as the main focus of the experiment was the size of the relative cathodic potentials of the samples, which had been shown to be sufficiently reproducible under these experimental conditions.

As there are many similarities between the electrochemistries of the *para* substituted phenyl 1,2,3,5 and 1,3,2,4 dithiadiazolylium species further questions arise; would a linear free energy relationship be observed for the latter species also? This is now discussed in section 2B.2.8.

2B.2.8 Hammett

E° is related to $\sigma\rho$ by a linear free energy relationship (see section 2C.1). When $E_{pc/2}$ potentials of the *para* substituted phenyl 1,3,2,4 derivatives were plotted against corresponding Hammett σ_p values such a relationship was indeed found to exist analogous with that found for the sister 1,2,3,5 isomeric compounds in section 2B.1.7, see Table 9 and Fig 20.

Sample	$E_{pc/2}$ /mV	σ_p
NO_2	400	0.778 +/- 0.02
CF_3	380	0.54+/- 0.1
Br	350	0.232 +/- 0.02
Cl	350	0.227 +/- 0.02
F	340	0.062 +/- 0.02
H	330	0.00
MeS	310	0.00 +/- 0.1
Me	300	-0.170 +/- 0.02
MeO	290	-0.268 +/- 0.02

Table 9. $E_{pc/2}$ and related Hammett σ_p values for several *para* substituted phenyl 1,3,2,4 dithiadiazolylium hexafluoroarsenate salts[44].

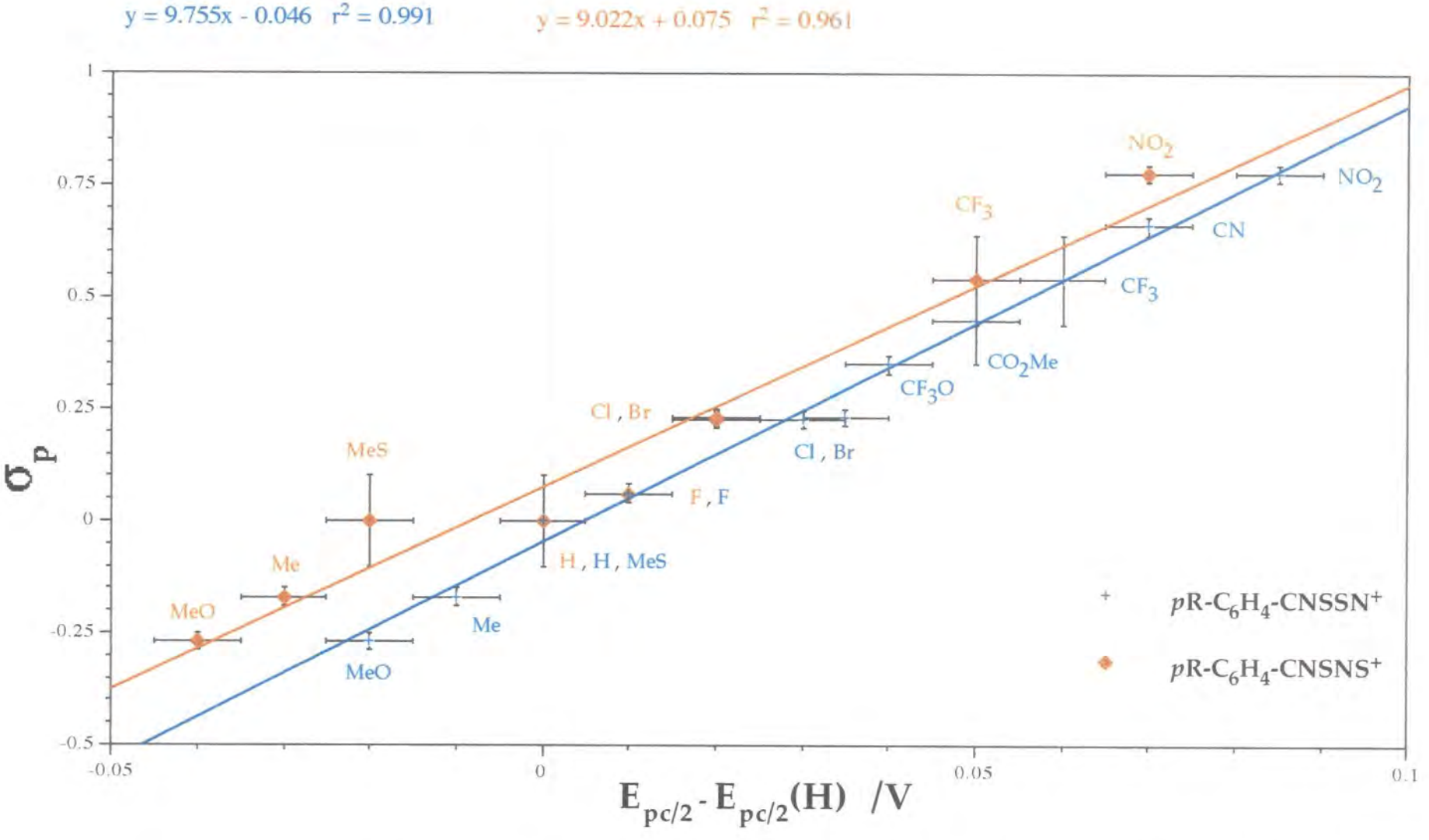

Fig 20. Linear free energy plot for a series of *para* substituted aryl 1,3,2,4 and 1,2,3,5 dithiadiazolylium hexafluoroarsenate salts.

The gradient for this graph is found to be $9.022V^{-1}$, (r^2 0.961). The positive gradient signifies that electron withdrawing groups favour the reduction process. This is further supported by detailed examination of resonance canonical forms, see 2B.2.7. Similar findings were found for the previous analogous study on isomeric 1,2,3,5 dithiadiazolylium derivatives, see 2B.1.7.

Using the modified Hammett equation $\Delta E=\sigma\rho$, (ρ is a measure of the susceptibility of a reaction or equilibrium to substituents effects), the ρ value for this plot is 0.106V, see Fig 35. The ρ value for the analogous plot for 1,2,3,5 derivatives is within experimental error of this value (0.102V, $r^2$0.991), see Fig 35. This indicates that *para* substituents have a similar effect on the electronic environment of both types of dithiadiazolylium reaction centres. Furthermore, the substituent effect of these compounds is comparable to that observed for the ionisation of *para* substituted benzoic acids.

The r^2 value for this 1,3,2,4 plot is larger than that for the 1,2,3,5 plot discussed in section 2B.1.7. A reason for this could be due to the electronic effects of *para* substituents of benzoic acids are more similar to those of 1,2,3,5 dithiadiazolylium analogues than for 1,3,2,4 isomers. The inductive effects of substituents for the above compounds are assumed to be the same (excluding external influences) as benzoic acid, benzoate, phenyl dithiadiazolylium cation and phenyl dithiadiazolyl have a similar π bonding framework, see section 2B.2.7. However investigation of the mesomeric pathways of charge transfer between the substituent and reaction centres in these groups of compounds did reveal slight discrepancies.

For the 1,2,3,5 dithiadiazolylium and benzoic acids derivatives bearing electron-donating substituents two similar resonance canonicals could be drawn, see 2B.1.7. In the case of 1,3,2,4 analogues the reaction centre is not symmetrical unlike the previous examples and hence two distinct resonance canonical forms can be drawn, see section 2B.2.7.

If the reverse situation is reviewed, where the substituents are electron withdrawing, one resonance canonical form can be drawn for derivatives possessing a dithiadiazolyl moiety, see 2B.1.7. and 2B.2.7.

At this point it is important to stress that the influence all these resonance contributions have on the bonding nature or electronic environment of each relevant system can't be gauged by just looking at the resonance diagrams. However their influence on certain physical responses of derivatives can, e.g. redox potentials. The size of the resonance contribution is ultimately determined by the type of interaction between bonding atoms and orbital overlap (especially π orbitals).

As the resonance diagrams involving *para* substituent of benzoic acids are more similar to 1,2,3,5 dithiadiazolylium derivatives than 1,3,2,4 analogues, it is likely that their substituent effects are more comparable and hence errors for the linear free energy relationship of the 1,2,3,5 compounds are less than for the analogous 1,3,2,4 plot.

Also, solvent interactions can influence observed potentials as they can assist in stabilising a reaction centre and making the process more favourable or vice versa. Solvent interactions of 1,2,3,5 and 1,3,2,4 rings will not necessarily be the same, as the charge distribution and atomic arrangement between these isomers differs. Therefore, if different solvent contributions are present between analogues of these isomers, the solvent effects for one isomer will be more comparable with those present in the dissociation of benzoic acids than the other one will. Therefore, if the odd one out is the 1,3,2,4 derivative then differing solvent interactions could assist in explain why a better linear free energy relationship is observed for analogous 1,2,3,5.

In summary, an excellent linear relationship exists for these *para* substituted aryl 1,3,2,4 dithiadiazolylium salts. The over-all electronic effect a *para* substituent influences the electronic environment of the 1,3,2,4 cationic heterocyclic ring is comparable to that observed for benzoic acid derivatives.

2B.2.9 Radicals

So far the discussion has centred on the reduction process of 1,2,3,5 and 1,3,2,4 dithiadiazolylium derivatives to the corresponding neutral radical species. However, if the potential window is expanded to encompass -2V *vs* S.S.C.E a second reduction process is observed at -1.6V which corresponds to the formation of the dithiadiazolylide anion[48], see Fig 21.

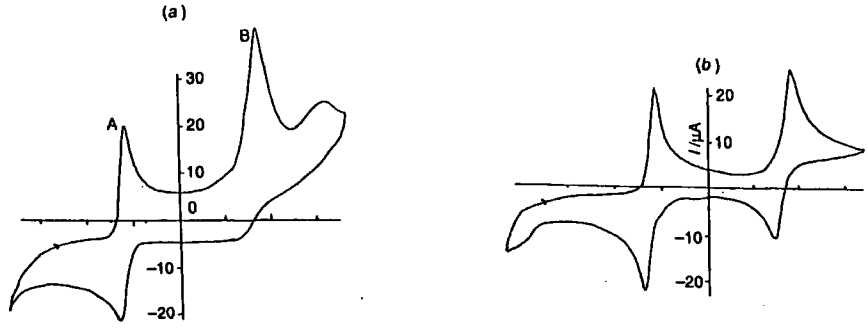

Fig 21. CV of (a) 1,2,3,5 phenyl dithiadiazolylium salt and (b) analogous radical, showing the two reduction processes which correspond to the cationic species being reduced to the dithiadiazolylide anion via the dithiadiazolyl radical.

This second reduction peak is found to be electrochemically irreversible for a sample of $PhCNSSN^+AsF_6^-$ but quasi-reversible for a sample of $PhCNSSN^\bullet$. This can be readily rationalised by considering what species are present in the bulk solution and at the surface of the electrode.

$$PhCNSSN^-_{(surface)} + PhCNSSN^+_{(bulk)} \text{ ----------> } 2PhCNSSN^\bullet$$

$$PhCNSSN^-_{(surface)} + PhCNSSN^\bullet_{(bulk)} \text{ -------X-------> }$$

Therefore, using the above equations, it can be seen that for the sample of $PhCNSSN^+$, the electrochemically generated anion can undergo a chemical reaction with the cations in the bulk solution. But because this process can occur to completion before the reverse scan is conducted no reverse wave is seen, i.e. a cross between an EC and EC' mechanism exists, refer to section 2A.2.3.

However, this EC/EC' type reaction can't occur when cyclic voltammetry is conducted on a sample of $PhCNSSN^\bullet$.

No rearrangement processes of any sort are observed for 1,2,3,5 radicals in solution. Results recently published by R.T.Boere *et al* have shown that analogous radicals, analogous to the *para* substituted aryl 1,2,3,5 dithiadiazolylium salts

discussed in chapter 2B.1, give comparable electrochemical results, i.e. they have the same quasi-reversible characteristics[38]. Cyclic voltammetry work previously conducted on PhCNSSN$^{\bullet}$ by previous students and myself[48], (using the CV experimental set up used for the cations studied here), showed that there is no difference within experimental error between the quasi-reversible characteristics and $E_{pc/2}$ values for analogous *para* substituted aryl dithiadiazolylium hexafluoroarsenate salts and associated radicals.

The phenyl 1,2,3,5 dithiadiazolylide anion has been isolated chemically as a sodium crown ether salt by the Banister group[48]. Unfortunately, this compound is found to be extremely air sensitive. This is because the negatively charged nitrogen of the ring can act as a base with moisture in the air, which results in the formation of N-H species and secondly S-O species, which ultimately leads to ring fragmentation[49]. This decomposition process is favoured as the anion, which possesses 8π electrons, is energetically more unstable than the decomposition products.

Work involving these anion derivatives possessing electron withdrawing groups has also been attempted by this group as it was considered that these types of substituent group would pull charge away from the ring, via induction and resonance effects, so making the ring less basic and 8π in nature, i.e. reducing the reactivity and increasing the stability of the ring. Unfortunately, no other dithiadiazolylide anion apart from the phenyl derivative has been isolated to date.

A similar electrochemical investigation was conducted on a sample of phenyl 1,3,2,4 dithiadiazolylium hexafluoroarsenate. For this derivative, no second reduction peak was observed within the constraints of the potential window of -2V *vs* S.S.C.E. This observation strongly suggests that anion formation is a less favoured process for the 1,3,2,4 than the 1,2,3,5, as no reduction potential for the 1,3,2,4 radical is observed at a more positive potential than that of the 1,2,3,5 isomer. This is further confirmed by MO calculations as the energy required for an electron to enter the SOMO is greater for the 1,3,2,4 than the 1,2,3,5 radical, see section 2B.2.7.

Electrochemistry was not conducted on solutions of 1,3,2,4 radicals as they rearrange in light and heat to 1,2,3,5 derivatives, see section 1.5.

For this study the electrochemical reduction process going from neutral radical to negative species was not examined as the main focus of the investigation was to compare the electrochemistries, synthesis and solid state structure of cations and radicals. Attempts at anion formation was avoided because of the inherent air sensitivity of the compounds.

2B.2.10 Conclusion

So, far it has been shown that *para* substituted aryl 1,2,3,5 and 1,3,2,4 dithiadiazolylium hexafluoroarsenate salts and associated radicals have comparable quasi-reversible characteristics. The 1,2,3,5 derivatives reduce at higher potentials than 1,3,2,4 analogues and this is related to the differences in energy between their HOMO and LUMO's. Both series of isomer form excellent linear free energy relationships when their $E_{pc/2}$ values are plotted against corresponding Hammett σ_p values.

Therefore, these two pieces of information indicate that both isomers undergo a similar electrochemical reduction process and that substituents groups have comparable effects on the electronic environment of the dithiadiazolylium / dithiadiazolyl ring of both isomers.

How would the *meta* and *ortho* systems compare? This is now discussed in the following chapter.

Section 2C

2C *Meta* and *ortho* substituted phenyl 1,2,3,5 and 1,3,2,4 dithiadiazolylium species and related compounds

2C.1 The Hammett Equation

2.C.1.1 Introduction

In the previous chapter, linear relationships were found to exist between $E_{pc/2}$ reduction potentials of several *para* substituted phenyl 1,2,3,5 and 1,3,2,4 dithiadiazolylium hexafluoroarsenate salts and corresponding Hammett σ_p values of analogous *para* substituted benzoic acids. An examination of how σ_p is derived has not been covered in any detail so far. Below is some background information on Hammett values which will assist in clarifying why such linear relationships exist and why it was decided to investigate if similar linear relationships exists for the *meta* and *ortho* aryl dithiadiazolylium derivatives.

2.C.1.2 Hammett σ values[40-43, 50, 51]

Hammett σ_p values are calculated, using Eqn (3), from the acid dissociation constant, Ka, of substituted benzoic acids in water at 25°C .

$$\log_{10} \frac{\mathbf{Ka}(pRC_6H_4COOH)}{\mathbf{Ka}(C_6H_5COOH)} = \boldsymbol{\sigma}_p \qquad \text{Eqn (3)}$$

The Ka of the substituted benzoic acids is a measure of how well the R group stabilises the dissociated $RC_6H_4COO^-$ anion.

$$pR\text{-}C_6H_4COOH + H_2O \rightleftharpoons pR\text{-}C_6H_4COO^- + H_3O^+ \qquad Ka = \frac{[RCOO^-][H_3O^+]}{[RCOOH][H_2O]}$$

Therefore R groups that are electron withdrawing will help to stabilise $RCOO^-$ anions. This results in the equilibria being pushed further to the right hand side and hence larger Ka and σ_p values. The reverse is true for electron donating groups.

For these types of substituted *para* derivatives the substituent can affect the environment of the reaction centre via the sigma and pi bonding framework, commonly known as inductive and resonance (or mesomeric effect) respectively.

Ka for the standard reaction will change if the reaction centre, solvent or temperature are altered, thus resulting in new K'a constants being observed. Therefore, if comparable electronic and steric effects, influencing the environment of the reaction centre, are in effect under these new conditions relative to the standard then the following relationship will exist, see Eqn (4)

$$\log_{10} \frac{K'_{a(\text{unsubstituted})}}{K'_{a(\text{substituted})}} = \rho\sigma_p \qquad \text{Eqn (4)}$$

where ρ is a constant that is specific for a set of reaction conditions and is equal to unity for the standard reaction, i.e., the dissociation of substituted benzoic acids in H_2O at 25°C.

It is important to stress that the Hammett σ_p value of this equation is the same as the one in Eqn (3) under standard conditions and therefore doesn't alter as conditions alter, it is the ρ factor which is the variable.

If $pK_a = -\log_{10} K_a$ then $\rho\sigma_p = \Delta pK'_a$

Therefore if ΔpK_a or $\Delta pK'_a$ of a reaction is plotted against corresponding Hammett σ_p values a linear plot will be observed if similar electronic and steric factors are in operation. From these plots the ρ value can be deduced as it will be equal to the gradient.

If ρ is positive Electron withdrawing groups increase rate of reaction or equilibrium constant of the substrate, i.e. like that observed for benzoic acids.

ρ is negative Electron donating groups increase rate of reaction or equilibrium constant of the substrate.

The above method can be used to determine analogous Hammett σ values for *ortho* and *meta* derivatives too, but of course the new Hammett values (σ_o and σ_m) reflect different electronic (inductive and resonance) and steric effects:

Ortho	Steric, resonance and inductive
Meta	Inductive
Para	Resonance and inductive

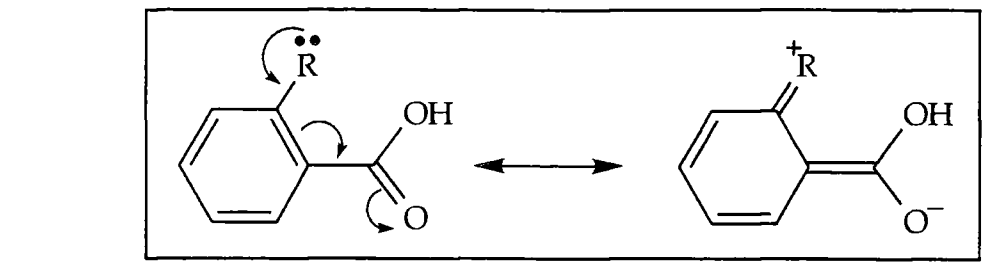

(a)

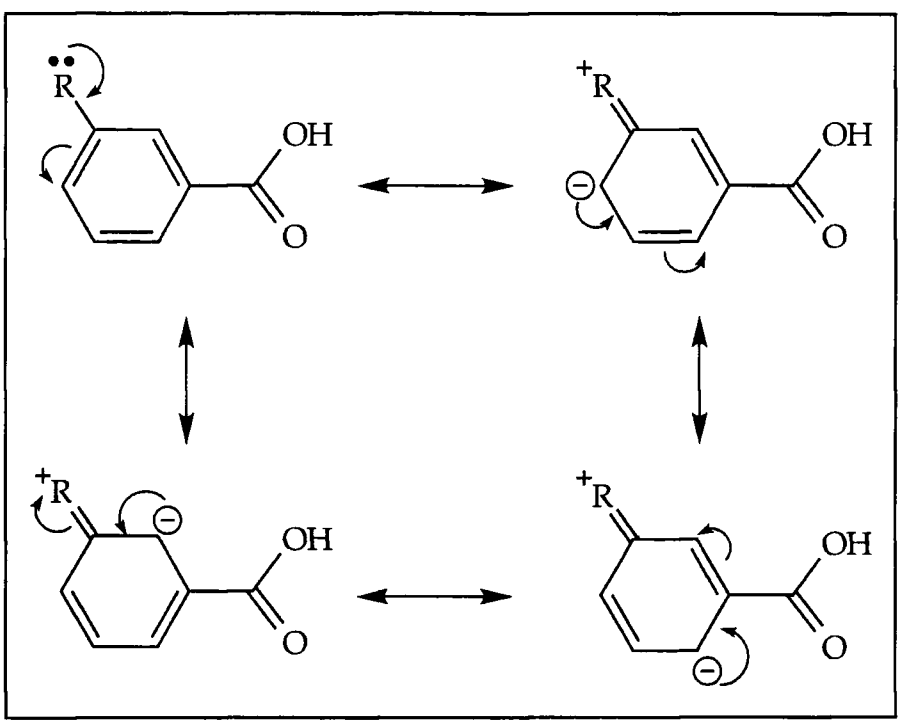

(b)

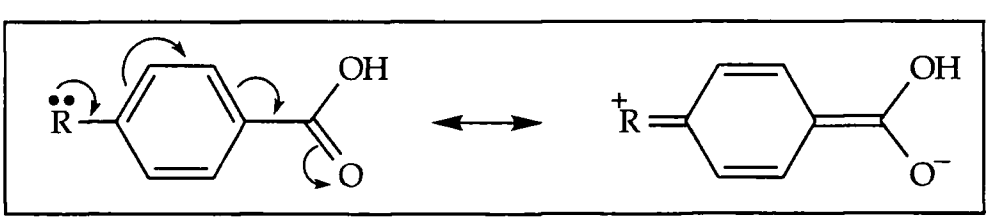

(c)

Fig 22. Resonance canonicals of (a) *ortho*, (b) *meta* and (c) *para* substituted benzoic acids.

All three types of positional derivatives have an inductive electronic contribution as this is transmitted along the sigma bond framework. However, only two of the three possess a resonance contribution and the reason for this can be found with studying the pi framework. In Fig 22 possible resonance canonicals involving benzoic acids with electron donating substituents in the three different positions are shown. From these diagrams it can be readily seen that all bar the

meta example can form resonance canonicals involving the substituent and reaction centre via the pi framework. Lastly, steric effects are only observed for *ortho* derivatives because basically the substituents in this position are closer to the reaction centre relative to the other positions and can thus interact favourably or unfavourably with the reaction centre.

2C.1.3 Linear Free Energy Relationships[41, 42, 53]

Hammett σ values are related to the Gibbs free energy term as follows.

The Gibbs free energy term for benzoic acid under standard conditions is

$$\Delta G^{\circ}_{o}=-2.303RT.\log_{10}K_a$$

and for a substituted derivative at standard conditions

$$\Delta G^{\circ}=-2.303RT.\log_{10}K_a$$

hence $\Delta G^{\circ}-\Delta G^{\circ}_{o}=-2.303RT\sigma$ under standard conditions

For an analogous system under different conditions

$$\Delta G'^{\circ}-\Delta G'^{\circ}_{o}=-2.303RT\sigma\rho$$

It is also known that $\Delta G^{\circ}= -nE^{\circ}F$

(where E° is the standard reduction potential of species and F is the Faraday constant)

Therefore combination of these two equations leads to a modified Hammett equation[54-56],

$$\Delta E^{\circ}=\sigma\rho$$

If E° for a series of compounds and corresponding Hammett σ values are plotted against each other two possible outcomes can be observed.

If a linear plot is observed, this implies that the electronic and steric contributions for individual substituent groups are affecting the stabilisation of the reaction centres for the dissociation of carboxylic acids and potentials of a series of compounds by comparable degrees[57-60]. This type of linear plot also tends to suggest that the same electrochemical process is occurring among the analysed series of compounds too. This can be further confirmed by examination of the individual electrochemical responses of each compound involved in the plot.

However not all systems give rise to linear free energy plots[61]. These occur when intramolecular charge transfer mechanisms differ by varying degrees between the benzoic acids and the investigated series of compounds. An example

of this is NO_2-C_6H_4-OH and NO_2-C_6H_4-COOH [42]. A discrepancy occurs because the NO_2 group can stabilise the hydroxyl anion but can't stabilise the carboxylic anion by through resonance.

To accommodate deviations from the Hammett σ value, many other σ constants have been derived[62], e.g. -

σ^- These are derived from data of phenols. This term is usually used when there are through resonance contributions between reaction site that becomes electron rich and an electron withdrawing substituent[63].

σ^+ These are derived from cumyl chlorides in 90% acetone. They are used when there is through resonance between reaction site that is electron deficient and an electron donor substituent[64].

σ^* These are Hammett σ values for aliphatic systems, often observe large steric contributions[65].

σ^I These are Hammett σ values for 4'norbornane carboxylic acid derivative, used as a measure of inductive effects[66].

2C1.4 Linear Free Energy Relationships of substituted *para* phenyl 1,2,3,5 and 1,3,2,4 dithiadiazolylium hexafluoroarsenate salts

An excellent linear free energy relationship was found to exist for the $E_{pc/2}$ *para* substituted phenyl 1,2,3,4 and 1,3,2,4 dithiadiazolylium salts and corresponding Hammett σ_p values. This is not surprising as these compounds have comparable inductive and resonance features to those of the benzoic acids used for the Hammett values, as both possess a similar π system for charge to be transmitted through, see sections 2B.1.7 and 2B.2.7.

The above linear relationship would not exist if the alternative σ constants were used instead because different charge transfer mechanisms are in operation. These differences are due to the dithiadiazolylium reaction centre possesses no excess negative charge for (σ^-), the positive charge doesn't sit on the carbon of the reaction centre directly attached to the benzene ring for (σ^+), differing steric and inductive contributions for (σ^*) and finally even for the *meta* system which is supposedly solely inductive differences will occur due to a small degree of resonance contribution into the polarisable benzene system for (σ^I) comparisons.

Even though two excellent linear free energy relationships are observed, see chapter 2B, why are slight deviations in the plot apparent? There are several reasons for this:

(1) The two functionalities being compared, (carboxylic and dithiadiazolylium), differ by the delocalisation of charges of differing sign present

in them. Also, as the 1,2,3,5 and 1,3,2,4 dithiadiazolylium/zolyl rings are different, their solvent interactions are likely to be different too. Therefore, slight discrepancies can occur due to differing solvent stabilisation contributions.

(2) The F derivatives stray from the line. This could be due to differing degrees of charge back donation of the F atom (part of the synergic effect) or hydrogen bonding of fluorobenzoic acid relative to that of fluorophenyl dithiadiazolylium.

(3) The N and O atoms of 1,2,3,5 dithiadiazolylium and carboxylic groups both carry a δ- charge with respect to the central carbon and are equivalent. For the 1,3,2,4 dithiadiazolylium ring this is not the case as the two ring N atoms exist in two different environments. Therefore, a better plot is observed for the 1,2,3,5 than the 1,3,2,4 derivatives as the resonance contributions between analogous 1,2,3,5 and benzoic acid derivatives are more similar due to the greater similarities in the bonding framework relative to the 1,3,2,4 scenario.

These effects are relatively minor and from these linear free energy plots excellent predictions of quantitative $E_{pc/2}$ values from known σ_p values can be determined, see chapter 2B. Would the same electrochemical properties and linear free energy relationships exist for the *ortho* and *meta* substituted phenyl dithiadiazolylium derivatives and related compounds? In order to test this, the syntheses of several *ortho* and *meta* derivatives were undertaken.

The initial focus was on the *meta* series as only simple inductive effects from substituent group on the substrate would be involved unlike the *ortho* systems which would be more complex due to added steric intramolecular interactions. In conjunction with these studies, structural investigations were conducted on many of the *meta* radical derivatives as little was known about the solid state packing of these types of substituted phenyl dithiadiazolyls, see chapter 3.

2C.2. The Electrochemistry of *meta* substituted phenyl 1,2,3,5 dithiadiazolylium species and related compounds

2C.2.1 Introduction

A CV study of the above compounds was initiated so that a comparison could be made with the electrochemistry of the *para* analogues. Previous investigations of *para* 1,2,3,5 derivatives had shown that the analogous cation and radical samples give identical $E_{pc/2}$ values and similar electrochemical properties, therefore this property was also examined for the *meta* analogue.

As several *meta* substituted phenyl 1,2,3,5 dithiadiazolyl radicals were readily available, (they had already been synthesised for structural investigations), it seemed sensible to study these materials before the salts.

Similar investigative CV procedures were followed to those used during the study of the unsubstituted phenyl 1,2,3,5 derivative. As this simple derivative was also a point of reference for the *meta* derivatives, the results obtained in the previous section, 2B.1, could be carried over. So, the survey began with studying the effects that electron withdrawing groups have on the redox chemistries of *meta* substituted phenyl 1,2,3,5 dithiadiazolyls.

2C.2.2 Electrochemistry of substituted 1,2,3,5 dithiadiazolyl derivatives

Derivatives Possessing Electron Withdrawing Groups

The following 1,2,3,5 radical derivatives were studied, CN, CF_3, Br, Cl and F. Beginning with the CN derivative, it was found that a sample of this material possessed quasi-reversible electrochemical properties, (at variable scan rates), akin to the *para* derivatives, i.e. the cathodic half wave potential was reproducible within experimental error of ±5mV, i_p increased with υ, $E_{pc}-E_{pc/2} > 0.055V$, i_{pc}/i_{pa} was approximately equal to unity and $E_{pa}-E_{pc} > 0.055V$, see Table 10. Another sample was run and the results confirmed that the data were reproducible. $E_{pc/2}$ for this derivative is 0.655V under these conditions. Similar variable scan rate and/or sample investigations were conducted on halogen derivatives (Br, Cl, F) and CF_3, these materials also gave the same characteristic quasi-reversible response, see Table 10.

Derivatives Possessing Electron donating Groups

Unfortunately, purification problems were involved in the synthesis of the Me and MeO radical derivatives, so no comparison with electron donating groups could be made.

Sample		Scan rate mVs^{-1}	E_{pc} mV	$E_{pc/2}$ mV	i_{pc} μA	$E_{pc}-E_{pc/2}$ mV	E_{pa} mV	$E_{pa/2}$ mV	i_{pa} μA	$E_{pa}-E_{pa/2}$ mV	i_{pc}/i_{pa} μA	$E_{pa}-E_{pc}$ mV	$(E_{pa}+E_{pc})/2$ mV
CN	A	324	590	650	24.0	60	680	620	22.75	60	0.92	90	635
		576	590	660	39.0	70	680	610	43.5	70	0.90	90	635
		729	590	660	43.0	70	670	590	48.0	80	0.90	80	630
	B	576	590	655	28.5	65	690	620	30.5	70	0.93	100	640
CF_3	A	256	590	645	35.2	55	665	600	38.4	65	0.92	75	627.5
Br	A	196	590	640	5.8	60	655	580	7.1	75	0.82	65	622.5
		324	580	640	7.1	60	655	590	7.9	65	0.90	75	617.5
		784	570	640	16.5	70	660	590	18.0	70	0.92	90	615
	B	324	560	640	25.0	80	660	580	25.0	80	1.00	100	610
Cl	A	484	570	635	37.5	65	670	600	38.5	70	0.97	100	620
		784	565	630	38.0	65	670	605	35.5	70	0.94	105	617.5
	B	196	580	640	17.25	60	660	600	18.0	60	0.96	80	620
		400	570	640	23.0	70	660	595	24.75	65	0.93	90	615
F	A	484	570	630	34.8	60	660	590	35.6	70	0.98	90	615
	B	256	570	630	48.0	60	660	590	48.0	70	1.00	90	615
	C	576	570	630	46.5	60	660	590	48.5	70	0.96	90	615
		676	570	630	67.0	60	660	590	65.0	70	1.03	90	615
	D	256	570	635	53.5	65	670	595	56.5	75	0.95	100	620
		784	550	630	84.0	80	670	600	88.0	70	0.95	120	610
	E	256	570	630	46.5	65	665	600	49.0	65	0.95	95	617.5
		324	575	635	53.5	65	660	590	54.6	70	0.98	85	617.5
	F	484	565	630	34.4	65	660	590	35.6	70	0.97	95	612.5

Table 10. Cyclic voltammetric data of *meta* substituted phenyl-1,2,3,5-dithiadiazolyl radicals in MeCN at 0°C, concentration 1×10^{-3} M, supporting electrolyte $TBABF_4$.

General

Looking at the magnitude of the half peak potentials, including that of the unsubstituted derivative, see Table 11, it can be readily seen that the size of these potentials are related to the electron withdrawing ability of the substituent group, as displayed below.

$$H > F > Cl > Br > CF_3 > CN \qquad E_{pc/2}\ /mV$$

Hammett

So far, the *meta* compounds had electrochemically behaved similarly to their *para* cousins. Therefore, the next step was to draw a free energy plot which resulted in a superb correlation being unearthed, see Table 11 and Fig 23.

Sample	$E_{pc/2}$ /mV	σ_m
CN	660	0.56 ±0.05
CF_3	645	0.43 ±0.1
Br	640	0.391 ±0.02
Cl	635	0.373 ±0.02
F	630	0.337 ±0.02
H	590	0.00

Table 11. $E_{pc/2}$ CV data and related Hammett σ_m values for several *meta* substituted phenyl 1,2,3,5 dithiadiazolyls[44].

The extremely high r^2 value of this graph indicates that this correlation is even better than the already excellent linear free energy relationship found for the *para* derivatives, see sections 2B.1.7 and 2B.2.8.

Next, CV was conducted on some *meta* substituted phenyl 1,2,3,5 hexafluoroarsenate salts to see if their electrochemistries were similar to the radicals and in particular to observe the behaviour of the readily available electron donating substituent groups MeO and Me.

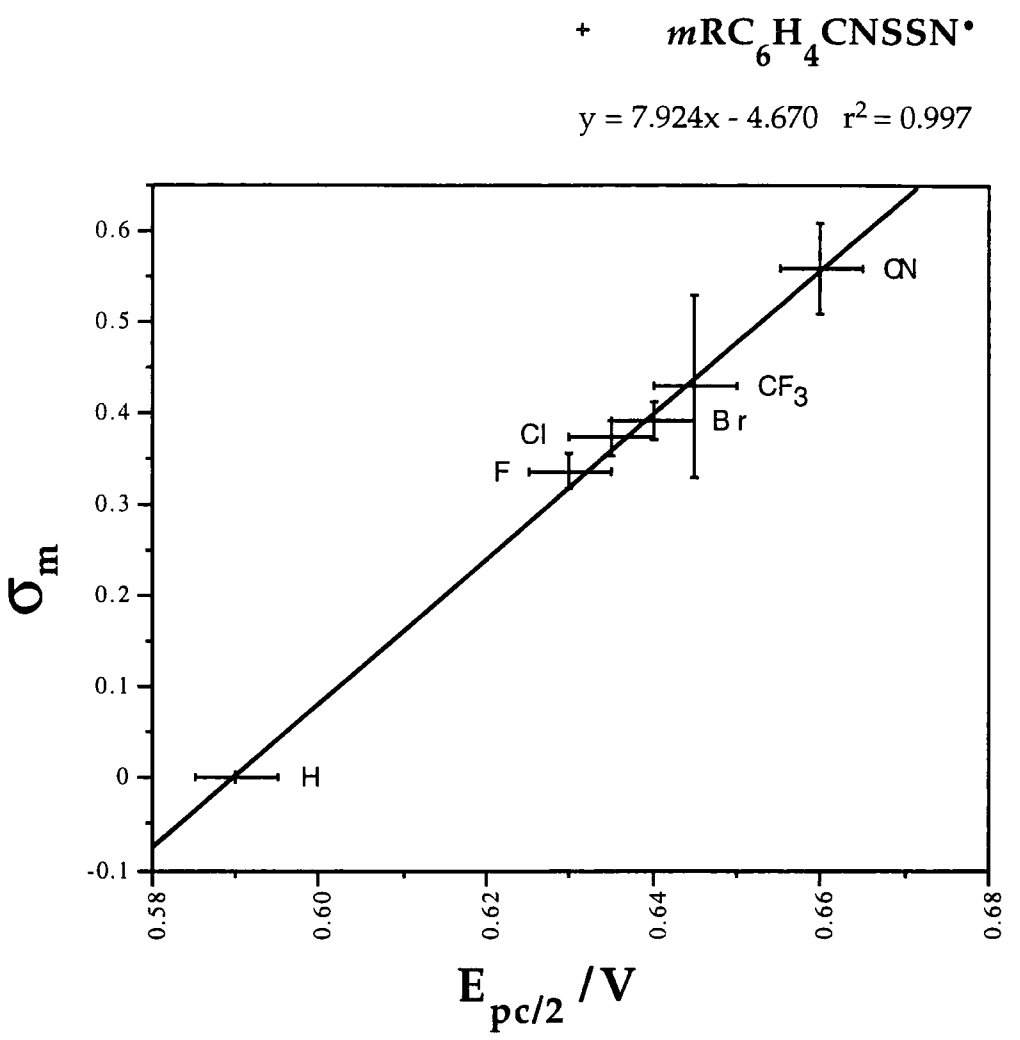

Fig 23. Plot of $E_{pc/2}$ potential of several *meta* substituted phenyl 1,2,3,5 dithiadiazolyls versus Hammett σ_m values.

2C.2.3. Electrochemistry of substituted 1,2,3,5 dithiadiazolylium hexafluoroarsenate derivatives

A CV study of a few salts was carried out to see if any electrochemical differences would be observed compared with that of the radicals. An experimental approach like that of the previous investigation was followed.

The results revealed that the samples with electron withdrawing substituents gave results almost identical to those of their radical analogues, see Table 12. Each sample showed the same quasi-reversible features as the radical analogues: $E_{pc/2}$ was consistent within experimental error, $E_{pc}-E_{pc/2} > 0.055V$, $E_{pa}-E_{pc} > 0.055V$, i_{pc} increased with υ and i_{pc}/i_{pa} only equal to unity under special conditions.

Sample		Scan rate mVs^{-1}	E_{pc} mV	$E_{pc/2}$ mV	i_{pc} μA	$E_{pc}-E_{pc/2}$ mV	E_{pa} mV	$E_{pa/2}$ mV	i_{pa} μA	$E_{pa}-E_{pa/2}$ mV	i_{pc}/i_{pa} μA	$E_{pa}-E_{pc}$ mV	$(E_{pa}+E_{pc})/2$ mV
CF_3	A	196	565	645	44.0	80	700	625	48.0	75	0.92	135	632.5
Cl	A	196	570	630	24.0	60	645	580	19.0	65	1.26	75	607.7
		324	570	635	42.5	65	660	590	43.0	60	0.99	90	615
MeO	A	324	530	595	55.0	65	650	550	75.0	100	0.73	120	590
		576	525	600	90.0	75	650	570	90.0	80	1.00	125	587.5
	B	484	540	600	16.2	60	620	560	16.4	60	0.99	80	580
		576	540	600	16.4	60	620	560	17.0	60	0.96	80	580
	C	324	530	600	71.0	70	630	560	79.0	70	0.90	100	580
Me	A	100	535	590	7.9	55	595	545	7.8	50	1.01	60	565
		484	530	590	16.8	60	605	550	17.2	55	0.98	75	567.5

Table 12. Cyclic voltammetric data of *meta* substituted phenyl-1,2,3,5-dithiadiazolylium hexafluoroarsenate in MeCN at 0°C, concentration $1x10^{-3}M$, supporting electrolyte $TBABF_4$.

Again the size of the potential was related to the strength of the electron withdrawing ability of the substituent group, the resulting trend is as follows:-

$$\mathbf{Me \leq H < MeO < Cl < CF_3}$$

When $E_{pc/2}$ is plotted against corresponding Hammett σ_m values then a linear free energy relationship is found to exist but the correlation is not as good as for the radical derivatives, see Table 13 and Fig 24.

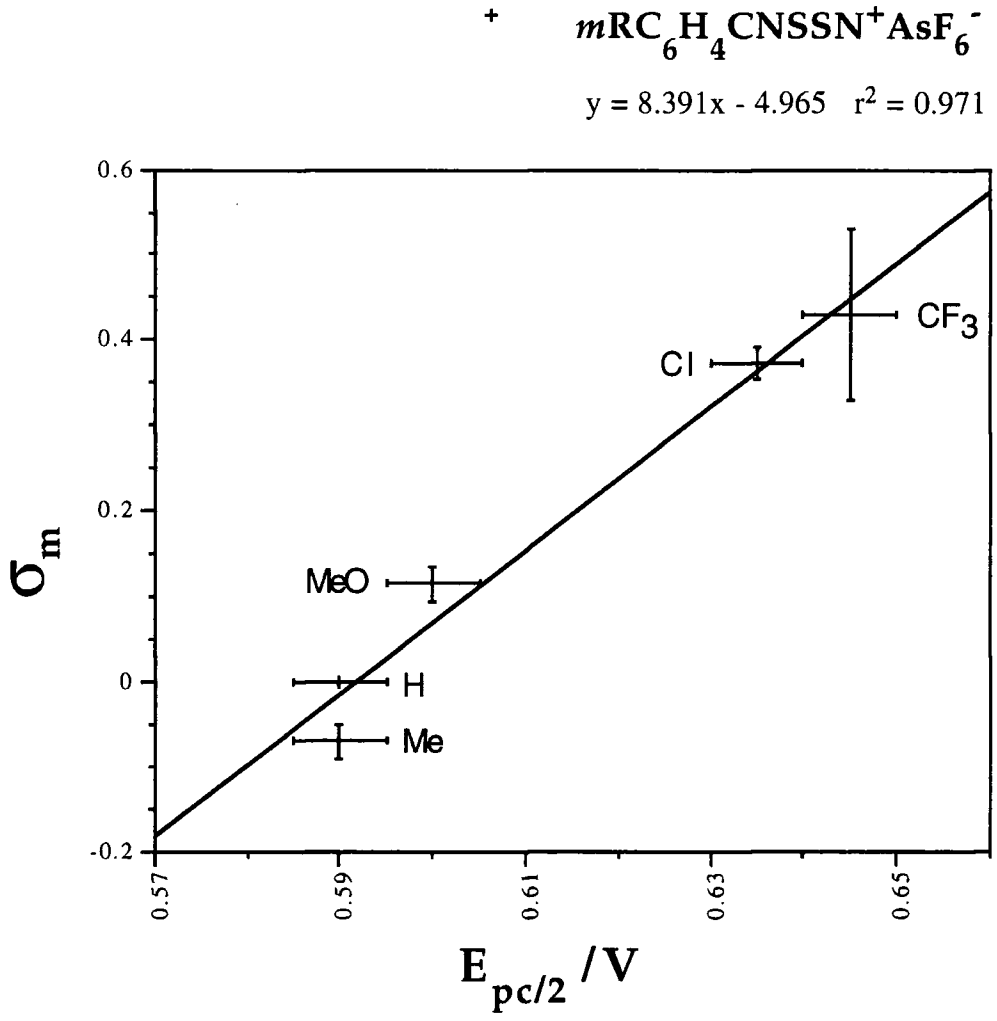

Fig 24. Plot of $E_{pc/2}$ potential of several *meta* substituted phenyl 1,2,3,5 dithiadiazolylium hexafluoroarsenate salts versus Hammett σ_m values.

The gradient of the graphs for Fig 23 and 24 can be said to be the same within in experimental error, also refer to Fig 25b. Knowing that Hammett ρ constant is specific to a set of reaction conditions and is proportional to the gradient; it can therefore be deduced, from the above similarities in gradients, that bulk solutions of dithiadiazolylium cations or associated radicals have similar effects on the diffusion layer surrounding the electrode during the

reduction process. Also, the fact that the gradient is positive indicates that electron withdrawing groups assist in making the reduction process more energetically favourable while the reverse is true for electron donating substituents.

Sample	$E_{pc/2}$ /mV	σ_m
CF_3	645	0.43 ±0.1
Cl	632.5	0.373 ±0.02
MeO	600	0.115 ±0.02
H	590	0.00
Me	590	-0.069 ±0.02

Table 13. $E_{pc/2}$ CV data and related Hammett σ_m values for several *meta* substituted phenyl - 1,2,3,5 - dithiadiazolylium hexafluoroarsenate salts[44].

As the CV responses between these compounds and the *para* derivatives are so alike, the presence of a similar electrochemical processes is indicated. For more details on the electrochemistry of the *meta* derivatives refer to the analogous studies of the *para* derivatives in section 2B.1.

Also, the excellent linear free energy relationships for these *meta* derivatives show that the substituent effects influencing the reduction of dithiadiazolylium cations are comparable to those influencing the ionisation of analogous carboxylic acids. The ρ value for the radicals is 0.126 (r^2 0.997) and for the salts is 0.116 (r^2 0.971), see Fig 35. These values are within experimental error of each other. These ρ values are found to be within experimental error of those values found for *para* substituted analogues as well, see section 2B.2.8 and Fig 35. As all the experiments were carried out under similar experimental conditions, the similarity of these ρ values indicates that the substituent effects of *para* and *meta* substituted carboxylic acids is comparable to that among the analogous series of 1,2,3,5 dithiadiazolylium/zolyls studied.

It is important to note that for *meta* substituted aryl derivatives of dithiadiazolylium, dithiadiazolyl and carboxylic acids the electronic effects are inductive, no through resonance of charge into the reaction centre can occur unlike that of the analogous *para* derivatives, see section 2C.1.

The next question was: would *meta* substituted phenyl 1,3,2,4 hexafluoroarsenate salts also mimic the electrochemical and Hammett responses of their *para* 1,3,2,4 counterparts?

2C.3. The Electrochemistry of *Meta* substituted aryl 1,3,2,4 dithiadiazolylium hexafluoroarsenate salts

2C.3.1 Electrochemistry of substituted 1,3,2,4 dithiadiazolylium hexafluoroarsenate derivatives

A series of *meta* substituted phenyl 1,3,2,4 hexafluoroarsenates, was synthesised successfully in order to probe the CV responses of these materials.

As the unsubstituted derivative was being used as a reference here, the electrochemical results obtained on this compound for the *para* derivatives, section 2B.2, can be used in this survey too.

The following derivatives were examined, NO_2, CF_3, F, MeO and Me. Yet again the same quasi-reversible characteristics, as those exhibited for the previously studied aryl derivatives, were apparent, see Table 14. Also the same differences between the *para* 1,2,3,5 and the 1,3,2,4 derivatives were observed for these *meta* derivatives, i.e, 1,2,3,5 analogue reduces at a potential at least 0.025V higher than for the 1,3,2,4 analogue. The same arguments used in section 2B.2.7. can be used to explain both the *para* and *meta* situations.

2C.3.2 Hammett

The size of the $E_{pc/2}$ potential not surprisingly increases with increasing strength of the electron-withdrawing ability of the substituent group. When these potentials are plotted against the corresponding Hammett σ_m values a fair linear relationship is found to exist, see Table 15 and Fig 25a. The errors associated with this plot are larger compared with the other plots but are still low enough to say that such a relationship does exist. The ρ value for this plot is 0.113V ($r^2 = 0.935$).

Sample	$E_{pc/2}$ /mV	σ_m
NO_2	400	0.71 ±0.02
CF_3	390	0.43 ±0.1
F	370	0.337 ±0.02
MeO	330	0.115 ±0.02
H	330	0.00
Me	320	-0.069 ±0.02

Table 15. $E_{pc/2}$ CV data and related Hammett σ_m values for several *meta* substituted phenyl 1,3,2,4 dithiadiazolylium hexafluoroarsenate salts[44].

Sample		Scan rate mVs^{-1}	E_{pc} mV	$E_{pc/2}$ mV	i_{pc} μA	$E_{pc}-E_{pc/2}$ mV	E_{pa} mV	$E_{pa/2}$ mV	i_{pa} μA	$E_{pa}-E_{pa/2}$ mV	i_{pc}/i_{pa} μA	$E_{pa}-E_{pc}$ mV	$(E_{pa}+E_{pc})/2$ mV
NO_2	A	484	325	400	106	75	440	360	86	80	1.23	115	382.5
		576	330	400	108	70	450	360	89	90	1.21	120	390
CF_3	A	324	325	390	39	65	420	360	32.5	60	1.20	95	372.5
F	A	576	290	370	96	80	415	340	81	75	1.19	125	352.5
		676	290	370	103	80	420	340	88	80	1.17	130	355
MeO	A	324	260	330	40.8	70	350	285	34.4	65	1.19	90	305
		400	265	330	43.6	65	355	295	36.0	60	1.21	90	310
Me	A	324	255	320	31.0	65	370	290	30.5	80	1.02	115	312.5
		484	250	320	50.5	70	355	285	48	70	1.05	105	302.5

Table 14. Cyclic voltammetric data of *meta* substituted phenyl-1,3,2,4-dithiadiazolylium hexafluoroarsenate in MeCN at 0°C, concentration $1x10^{-3}M$, supporting electrolyte $TBABF_4$.

The gradient of this graph is positive and within experimental error of the gradient of the other analogous *para* plot too, see Fig 35. Therefore, it can be deduced that (a) electron-withdrawing groups improve the product stability, i.e. makes the reduction process more favourable and electron donating groups have a counter effect and (b) the difference between how *meta* and *para* substituent group affect the electronic environment of a carboxylic acid is comparable to that between analogous 1,3,2,4 dithiadiazolylium salts, (see section 2C.1 and 2C.2.3).

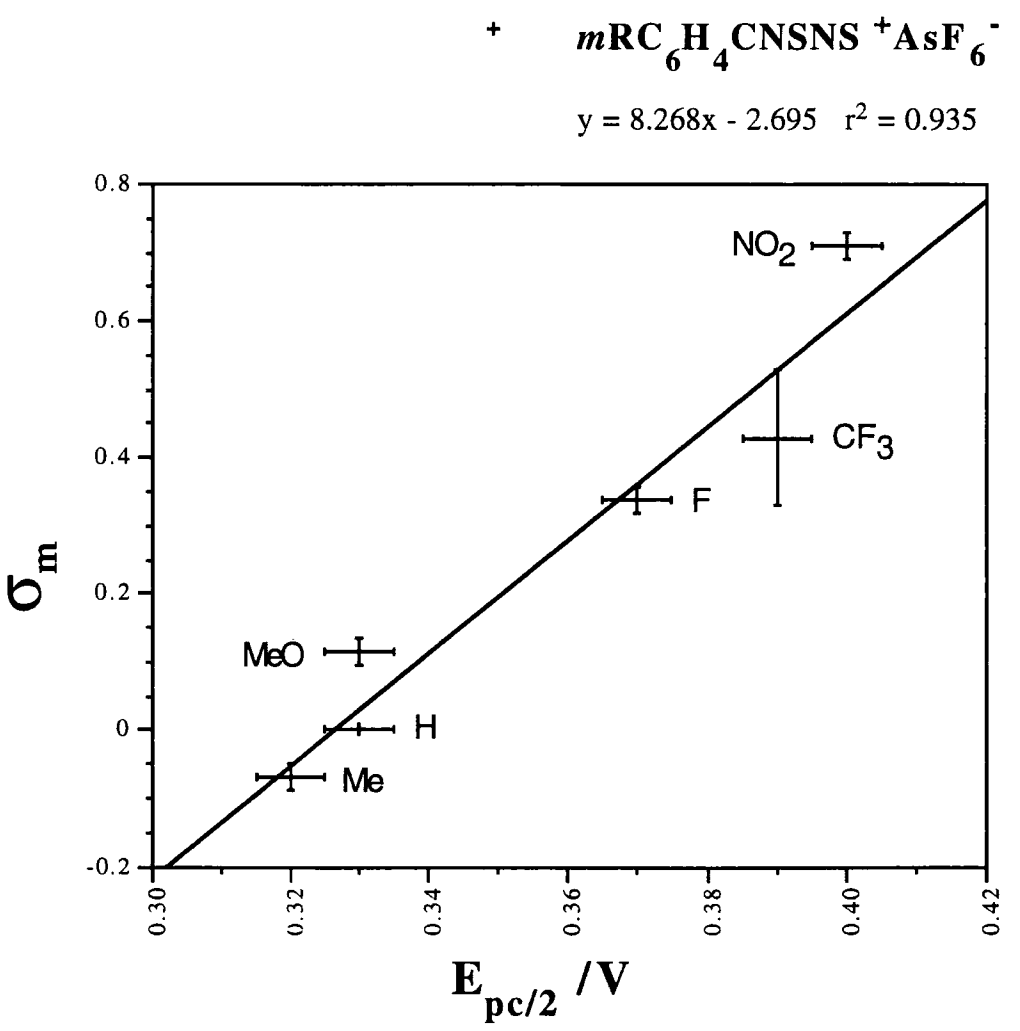

Fig 25a. Plot of $E_{pc/2}$ potential of several *meta* substituted phenyl 1,3,2,4 dithiadiazolylium hexafluoroarsenate salts versus Hammett σ_m values.

2C.4.1. Comparison between *para* and *meta* substituted phenyl 1,2,3,5 and 1,3,2,4 dithiadiazolylium salts and associated radicals.

It can be concluded that the common electrochemical quasi-reversible features, (for the +/• redox process), that exist for the *para* substituted aryl dithiadiazolylium cations and 1,2,3,5 dithiadiazolyls are also in operation for the *meta* analogues.

If the linear free energy correlations are also compared among this group, the plots are seen to overlap one another such that the gradients of the graphs are approximately the same, see Figs 20, 25b & 35. As the ρ values of these linear free energy relationships are within experimental error of each other, this indicates that the substituent effects of these dithiadiazolylium/zolyl compounds are (i) comparable to those of analogous benzoic acid derivatives and (ii) the same under these sets of experimental conditions, refer to Fig 35. The positive sign of the gradient indicates that the stronger the electron withdrawing ability of a substituent the more stable the product becomes and hence the reduction process is more favoured.

Below is the difference in $E_{pc/2}$ potentials, ΔE, for *meta* and *para* derivatives possessing the substituent groups printed in the brackets.

	Meta	*Para*
1,3,2,4 dithiadiazolylium	$\Delta E_{(NO_2\text{-}Me)}$=80mV	$\Delta E_{(NO_2\text{-}Me)}$=100mV
1,2,3,5 dithiadiazolyl	$\Delta E_{(CF_3\text{-}Me)}$=55mV	$\Delta E_{(CF_3\text{-}Me)}$=70mV
1,2,3,5 dithiadiazolylium	$\Delta E_{(CN\text{-}F)}$=30mV $\Delta E_{(CN\text{-}H)}$=70mV	$\Delta E_{(CN\text{-}F)}$= 50mV $\Delta E_{(CN\text{-}H)}$= 70mV

If the ΔE values with **Me**thyl and **F**luoro derivatives are studied it can be clearly see that the *para* derivatives are larger than the *meta* derivatives, (the experimental error associated with ΔE is ±5mV). However, ΔE for the cyano and unsubstituted phenyl 1,2,3,5 dithiadiazolylium salts, i.e. (CN-H), are the same for both isomers. These observations can be readily explained by looking at the types of electronic effects present.

For the *meta* derivatives substituents can only transfer charge by inductive effects but for the *para* derivatives additional resonance pathways involving only charge transfer between the substituent and the ring are available too, see 2C.1.

No difference for ΔE for (CN-H) of *meta* and *para* analogues is observed. This is partly because the H derivative is the same in both cases and the fact that the inductive effect that analogous *meta* and *para* substituents have on a reaction centre are essentially the same. However it is possible to draw a resonance canonical form involving the *para* CN group and the dithiadiazolyl ring. But as the ΔE values for these *meta* and *para* analogues are the same, this clearly indicates that this additional resonance contribution involving the *para* CN substituent pulling charge out of the reaction centre must have a negligible effect on the energy of the system. This is further supported by results from Hammett plots of *para* derivatives with carboxylic acids and comparisons of their resonance canonical forms, see section 2B.1.7 and 2B.2.7.

If the H is replaced by F, (CN-F), the story is quite different, these *meta* derivatives are now seen to have a smaller ΔE than for the analogous *para* derivatives, even though the inductive effect from analogous *meta* and *para* derivatives are essentially the same. This is because the resonance contribution from the *para* F derivative does contribute significantly to the overall energy of the system, unlike the CN group. The *para* F substituent possesses the ability to back donate charge into the cationic and radical ring by the resonance effect. This extra resonance contribution leads to a decrease in the reduction potential of the ring as the effect of extra charge into the ring renders it less stable. Hence, the observed trend in the ΔE(CN-F) values for *meta* and *para* is seen. If the fluoro substituent is replaced by methyl a similar trend is observed due to the *para* methyl group's ability to push charge into the ring by the mesomeric effect. Again this is further supported by results from Hammett plots of *para* derivatives with carboxylic acids and comparisons of their resonance canonical forms, see section 2B.1.7 and 2B.2.7.

Therefore, this brief comparison of ΔE values shows the importance that mesomeric effects can play in affecting the electronic environment of a reaction centre, especially between *meta* and *para* derivatives. For these analogues in particular, the substituents that can significantly contribute to the mesomeric effect are *para* electron donating groups. These groups contribute to making the reduction process less favourable and hence a larger $\Delta E_{(\text{acceptor-donor group})}$ for *para* derivatives relative to *meta* derivatives is observed.

Finally to complete the electrochemical picture the *ortho* derivatives were studied.

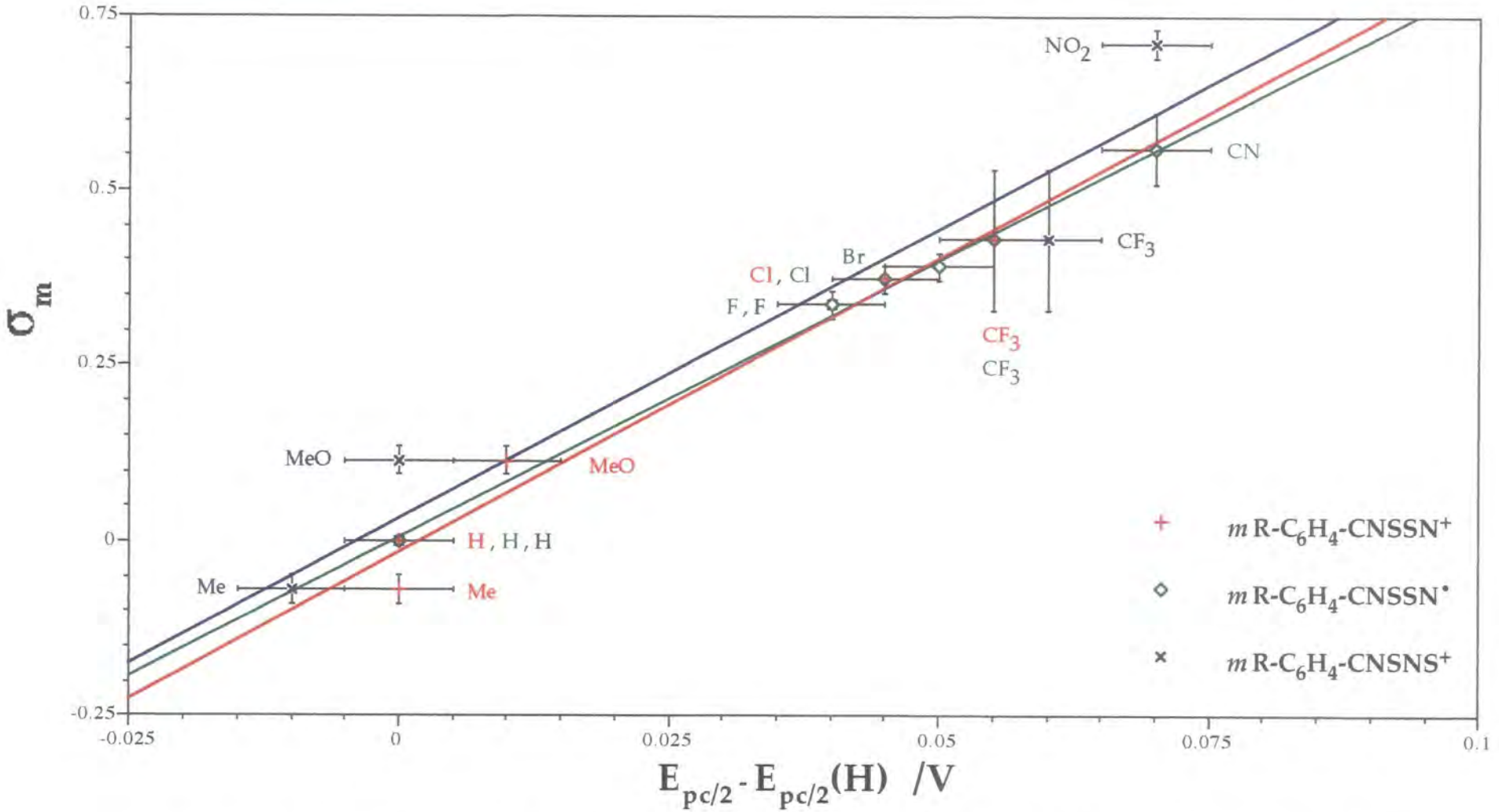

Fig 25b. Plot of $E_{pc/2}$ potential of several *meta* substituted phenyl 1,2,3,5 and 1,3,2,4 dithiadiazolylium hexafluoroarsenate salts and related radicals versus Hammett σ_m values.

2C.5 The Electrochemistry of *Ortho* substituted phenyl 1,2,3,5 and 1,3,2,4 dithiadiazolylium species and related compounds

2.C.5.1 Introduction

It has been proved that *meta* and *para* phenyl 1,2,3,5 and 1,3,2,4 dithiadiazolylium salts have many electrochemical features in common, see 2C.4.1. Prior to these studies little was known about such properties for analogous *ortho* derivatives but it can not be assumed that they would mimic the behaviour of their *meta* and *para* cousins even though electronic contributions from substituent groups are likely to be comparable. This is because additional steric effects occur in *ortho* derivatives which influence the relative positions of the two rings, (*viz.* phenyl and dithiadiazolylium/zolyl), and hence the electronic environment of the CN_2S_2 ring.

Therefore, syntheses of several *ortho* substituted phenyl 1,2,3,5 and 1,3,2,4 dithiadiazolylium salts and related 1,2,3,5 radical species were attempted in order to compare the electrochemical properties of these derivatives with those of their *meta* and *para* analogues.

2.C.5.2 Types of 1,3,2,4 derivatives to study.

The following desired *ortho* substituted aryl 1,3,2,4 salts were successfully made, NO_2, CF_3, Br, Cl, F, Me, MeO and EtO. Synthetic details can be found in the Chapter 4. These derivatives were chosen as they have published Hammett σ_o values (which are scarce), and therefore an $E_{pc/2}$ versus Hammett σ_o free energy plot could be attempted, and compared with the results achieved for the *para* and *meta* derivatives.

2.C.5.3 Electrochemistry of substituted 1,3,2,4 dithiadiazolylium hexafluoroarsenate derivatives

For the above *ortho* 1,3,2,4 derivatives the following trends were observed.

Starting with electron donating substituents, CV on samples of MeO and Me derivatives were found to give similar responses to those observed for the *meta* and *para* analogues, i.e. i_p increased with υ, i_{pc}/i_{pa} was equal or greater than one, E_{pc}-$E_{pc/2}$ was typically 60-70mV, cathodic potentials decreased with scan rate, anodic potentials increased with scan rate, peak potential separation increased with scan rate and $E_{pc/2}$ values were reproducible within experimental error of ±0.005V, see Table 16a. Therefore from these results it can be deduced that under these experimental conditions these derivatives also are electrochemically quasi-reversible, especially as E_{pa}-E_{pc}>0.055V. When less

Sample		Scan rate mVs^{-1}	E_{pc} mV	$E_{pc/2}$ mV	i_{pc} μA	E_{pc}-$E_{pc/2}$ mV	E_{pa} mV	$E_{pa/2}$ mV	i_{pa} μA	E_{pa}-$E_{pa/2}$ mV	i_{pc}/i_{pa} μA	E_{pa}-E_{pc} mV	$(E_{pa}+E_{pc})/2$ mV
NO_2	A	625	320	390	41.5	70	430	360	36.0	70	1.15	110	375
		784	320	390	43.0	70	425	355	36.0	70	1.19	105	372.5
CF_3	A	484	330	405	44.0	75	440	360	41.5	80	1.06	110	385
	B	484	330	400	48.0	70	450	360	46.0	90	1.04	120	390
Br	A	678	270	325	14.8	55	350	280	12.2	70	1.21	80	310
Cl	A	784	260	320	36.0	60	360	290	34.5	70	1.04	100	310
F	A	576	240	310	82	70	360	285	81	75	1.01	120	300
	B	576	240	310	62	70	360	290	63	70	0.98	120	300
	C	576	240	310	59	70	360	290	56	70	1.05	120	300
Me	A	256	250	310	35.2	60	340	280	28.4	60	1.24	90	295
	B	256	250	310	33.6	60	340	280	32.0	60	1.05	90	295
		676	230	300	83	70	350	280	80	70	1.04	120	290
		784	220	300	86	80	350	275	80	75	1.08	130	285
MeO	A	256	100	160	7.4	60	180	120	7.6	60	97	75	140
		676	100	160	42.5	60	195	130	40.5	65	1.05	95	147.5
		784	90	155	44.0	65	195	130	42.5	65	1.04	105	142.5
EtO	A	256	95	160	16.2	65	175	125	16.4	60	0.99	80	135
	B	400	95	160	16.6	65	190	125	15.8	65	1.05	95	142.5
	C	400	105	165	16.2	60	190	130	16.4	60	0.99	85	147.5

Table 16a. Cyclic voltammetric data of *ortho* substituted phenyl-1,3,2,4-dithiadiazolylium hexafluoroarsenate in MeCN at 0°C, concentration 1 x 10^{-3} M, supporting electrolyte $TBABF_4$.

Sample		Scan rate mVs^{-1}	E_{pc} mV	$E_{pc/2}$ mV	i_{pc} μA	E_{pc}-$E_{pc/2}$ mV	E_{pa} mV	$E_{pa/2}$ mV	i_{pa} μA	E_{pa}-$E_{pa/2}$ mV	i_{pc}/i_{pa} μA	E_{pa}-E_{pc} mV	$(E_{pa}+E_{pc})/2$ mV
F	A	676	530	610	70	80	670	590	66	80	1.06	140	600
	B	676	540	610	92	70	650	580	94	70	0.98	110	595

Table 16b. Cyclic voltammetric data of *ortho* fluorophenyl-1,2,3,5-dithiadiazolyl in MeCN at 0°C, concentration 1 x 10^{-3} M, supporting electrolyte $TBABF_4$.

detailed CV was conducted on the remaining *ortho* substituted compounds the same quasi-reversible characteristics were found.

The experiments were repeated to check if the reference electrode had drifted between measurements causing differences in potentials but the results were identical.

Thus, the similarities in electrochemical response between all of the substituted phenyl 1,3,2,4 dithiadiazolylium hexafluoroarsenate species studied so far indicates that the same electrochemical process, quasi-reversible charge transfer, is in operation and is therefore independent of the position of the substituent group.

The spread in $E_{pc/2}$ potentials, $\Delta E_{(acceptor\text{-}donor\ group)}$, for these *ortho* compounds, ranging from 157.5mV for the MeO derivative to 390mV for the NO_2 derivative, is at least three times larger than that observed for either the *para* or *meta* analogues. Also, it is important to remember that the spread in potentials for the *para* compounds has been found to be ~20mV larger than for the *meta* analogues, see section 2C.4.1.

The relative size of $E_{pc/2}$ is related to the electronic environment of the dithiadiazolylium/zolyl ring. The above trend shows that the influence substituents place on the electronic environment of the ring differs with position. Therefore, this trend can be readily explained when electronic factors of the three types of positional derivatives are examined. The reason why $\Delta E_{(acceptor\text{-}donor\ group)}$ for *para* is greater than for *meta* has already been explained in section 2C.4.1 and is due to additional resonance contributions present in *para* derivatives, (the inductive effects from both positions being approximately equal). The ΔE value for the *ortho* scenario is the largest simply due to the closer proximity of its substituents to the reaction centre. Thus, *ortho* groups have a stronger inductive effect on the reaction centre compared with the other two situations. Also, particular *ortho* groups have the ability to sterically interfere or interact through space with the reaction centre which can affect the resonance or inductive contribution. Evidence that steric forces are present among these *ortho* substituted derivatives can be found by looking at the relative sizes of the potentials of certain positional isomers.

It is interesting to notice that the $E_{pc/2}$ values of derivatives possessing a strong electron withdrawing group, at any position on the aryl ring, are approximately all the same. However, these values differ among analogues possessing strong electron donating groups.

The potentials of *meta* and *para* derivatives possessing electron-withdrawing substituents are the same due to (i) the inductive effect of these

substituents are approximately the same and (ii) the mesomeric effect of the substituent on the reaction centre is non-existant for both sets of compounds, refer to section 2C.2.7 and 2C.1.2.

The potentials of *meta* and *para* derivatives with analogous electron withdrawing substituents are the same due to resonance contributions (involving these substituent groups and the radical centre) do not contribute significantly to the overall energy of the system, and the fact that the inductive effects for analogous *meta* and *para* substituents are about the same, see section 2C.4.1. However, for derivatives possessing an electron donating group, the resonance contribution from a *para* substituent does contribute significantly to the energy of the system and therefore reduction potentials of these *meta* and *para* analogues will differ. For all *ortho* derivatives the inductive effect will be greater than that observed for *meta* analogues. However, the potentials of *ortho* derivatives possessing strong electron-withdrawing substituents are not observed to be greater than those of the other positional analogues. This trend is also observed for derivatives possessing a Me group, (an electron donating group), for which potentials of all positional isomers are found to be approximately the same size too. This is evidence that additional steric effects between groups *ortho* to each other are in play and affecting the environment of the reaction centres. For other electron withdrawing groups like MeO, the potential of the *ortho* derivative is considerably lower than *para* or *meta* derivatives. Again suspicions of steric involvement between groups *ortho* to each other are aroused as such a large downward shift of the *ortho* derivatives is not expected.

Closer examination in the relative size of the $E_{pc/2}$ values of individual *ortho* derivatives reveals that the halogen substituted derivatives have lower values than the plain unsubstituted phenyl 1,3,2,4 dithiadiazolylium derivative. The reverse situation is expected as the stronger electron withdrawing inductive contribution of the halogen groups, relative to the hydrogen, on the reaction centre should result in the larger potential values being observed for the halogen derivatives as observed for the *meta* and *para* analogues. The most likely reason for this trend is a change in environment of the ring due to steric factors being present. If repulsive steric forces are present the molecule will twist and the resonance contribution will decrease. Alternatively, if attractive forces between the reaction centre and *ortho* group are present the electronic environment of the ring will be altered too by this process and hence influence the observed potential. This topic will be expanded upon in the next section.

2.C.5.4 Hammett

When the $E_{pc/2}$ values for all these *ortho* 1,3,2,4 derivatives are plotted against the corresponding Hammett σ_o values, a simple linear free energy relationship is not seen to exist; instead there are three possible lines that can be drawn, **(I)**, **(II)** and **(III)**, see Fig 26 and Table 17. It is obvious from these results that this system doesn't possess the same ratio of electronic and steric contributions as the substituted benzoic acids used to derive the Hammett constants.

Sample	$E_{pc/2}$ /mV	σ_o
NO_2	390	1.99
CF_3	402.5	-
Br	325	1.35
Cl	320	1.28
F	310	0.93
Me	305	0.29
MeO	157.5	0.12
H	330	0.00
EtO	162.5	-0.01

Table 17. $E_{pc/2}$ CV data and related Hammett σ_o values for several *ortho* substituted phenyl 1,3,2,4 dithiadiazolylium hexafluoroarsenate salts[67].

Notice that the unsubstituted H derivative, that has been used in the previous *meta* and *para* plots, has been included here too. It is assumed that its $E_{pc/2}$ potential value is accurate to ±5mV and this is confirmed by the excellent free energy relationships that exist for analogous series of *meta* and *para* derivatives.

The validity of each possible plot will now be discussed in turn.

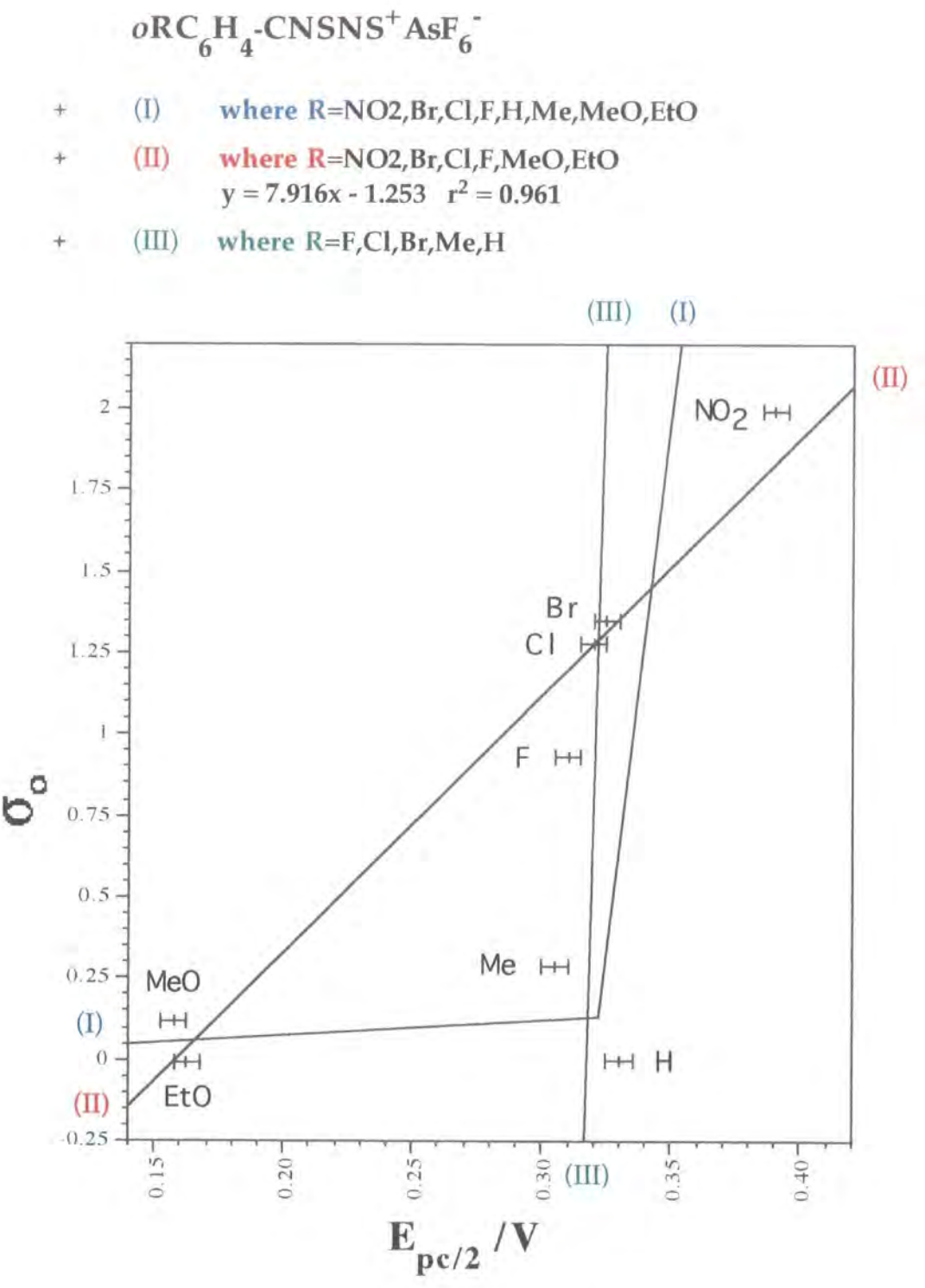

Fig 26. Plot of $E_{pc/2}$ potential of several *ortho* substituted phenyl 1,3,2,4 dithiadiazolylium hexafluoroarsenate salts versus Hammett σ_o values.

Plot (I)

The shape of this plot at first tends to suggest that a change in the reduction mechanism of these materials could be occurring, i.e. electron donating groups favour one process and electron withdrawing groups favour another process resulting a plot possessing two distinct gradients. An example of this is the hydrolysis of substituted ethyl benzoates in 99.9% H_2SO_4 where formation of ethanol or the ethyl cation is favoured by electron donating or electron withdrawing groups respectively[68]. However, for these processes the gradients are of opposite sign and this is not observed in plot (I). Therefore, a change in the reduction mechanism of these materials can be readily discounted.

Further evidence to support this can be found in studying the electrochemical responses for these materials too. Firstly, the electrochemical quasi-reversible response for these *ortho* compounds are all found to be the same as those observed for the *meta* and *para* analogues. For the latter two examples the reduction process is known to involves the reduction of cationic species to analogous radicals. This tends to suggest a similar electrochemical mechanism is in operation for all and a competing chemical reaction as in the above example is not present.

Alternatively, a change in solvent interactions with δ+ sulphur or δ- nitrogen of the ring could be responsible for altering the electronic environment of the ring relative to that observed for carboxylic acids, thus resulting in this trend. For this to occur the electron density of one of these ring atoms must be sufficiently changed such that a different or preferred orientation of the solvent molecules arises as the substituents go from being electron donors to acceptors. Therefore between these two different solvent interactions, one of them must stabilise the ring to a greater extent than the other. The electrochemical results for the *meta* and *para* analogues have shown that the size of the potential signifies the degree of charge stabilisation of the ring. However, if this type of changing solvent interactions were in operation then steric bulk of some of the side groups would also be expected to influence these solvent interactions. However, the maximum and minimum values or extremes of the plot are both as sterically bulky as each other, which seriously flaws this argument.

Similar looking plots were observed for the ionization for *meta* and *para* substituted Ar_3C-Cl derivatives in liquid SO_2 [69]. The *meta* derivatives were seen to give linear Hammett plots whereas the *para* plot became increasingly curved. The reason for this deviation is due to increased conjugation interaction with lone-pair substituents in the *para* position developing, much greater than that measured in dissociation of benzoic acids, i.e. enhanced resonance. For both *meta*

and *para* substituted dithiadiazolylium salts excellent linear free energy plots are observed and therefore an enhanced resonance theory doesn't explain plot (I) either.

The *ortho* system differs from the *meta* and *para* derivatives as it possesses steric factors which influences its electronic environment. Going from electron withdrawing to electron donating groups there is definitely no gradual increase in steric bulk of the *ortho* substituent groups and therefore changing steric interactions can't be responsible for a subtle change in reduction mechanism and change in gradient of this plot.

Therefore all the above discussions tend to discount this plot as being a valid option.

As mentioned previously in the cyclic voltammetry discussion of these *ortho* substituted phenyl 1,3,2,4 dithiadiazolylium derivatives, the halogen substituted analogues have a smaller $E_{pc/2}$ potential or make the reduction product more stable compared to the hydrogen derivative. The opposite trend is observed for analogous *meta* and *para* derivatives. From the Hammett values of *ortho, meta* and *para* substituted benzoic acids, all the halogen derivatives assist dissociation of the acid more than the hydrogen analogue. Therefore, as suggested earlier, these differences in the above trends are due to additional steric forces being present in the *ortho* derivatives. Rationalisation of the next two plots focuses on this idea.

Plot (II)

This line is the computer generated best fit line and includes all the derivatives except the Me and H derivatives. The gradient of this line was found to be $7.916V^{-1}$ (r^2=0.961). From section 2C.1.1, it was shown that the gradient of the line is proportional to the Hammett ρ factor which is specific for a set of reaction conditions and independent of position of substituent. When gradients of the *ortho, meta* (section 2C.3.1) and *para* (section 2B.2.8) derivatives were compared all together it was found that their gradients were within experimental error of each other. At first glance this does not seem a surprising result as the measurements were all conducted under the same experimental conditions.

However, for these types of Hammett plots the main reference point or origin is the hydrogen derivative, and therefore the line should pass close to or through this point, but in this case it doesn't. Therefore, for this plot to be valid the H and the Me derivative must not possess features common to the other derivatives.

When bulky *ortho* groups are introduced on to a planar delocalised molecule, any resulting steric repulsions, between both groups *ortho* to each other,

leads to deviations from planarity which ultimately reduce the amount of π orbital overlap that can occur in these types of molecules. Hence this leads to a reduction in the resonance contribution from the *ortho* group and ultimately a change in the electron density distribution in the reaction centre. On the other hand favourable electrostatic interactions through space can lead to a change in charge distribution in the ring and induction effect of the substituent group as well, see Fig 27.

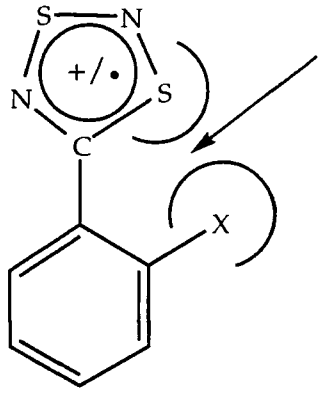

Potential for steric repulsions and electrostatic attractions to exist depending on what X is.

Fig27. *Ortho* substituted dithiadiazolylium/zolyl

For plot(II) to exist the dithiadiazolylium derivatives that lie on or within experimental error of the line, must possess *ortho* substituents which have comparable steric, inductive and resonance effects, on the electronic environment of the reaction centre, as those for the analogous benzoic acid derivatives. Therefore, the deviation of the H and Me derivatives from this plot signify this is not the case for these particular compounds.

Due to these observed deviations from linearity, a simple free energy relationship can't be said to exist, like those already seen for the *meta* and *para* analogues. The only other difference between the three analogues is the *ortho* group is the only one to possess a steric component. Therefore, these additional steric contributions must be responsible for these discrepancies and this is supported by research by other workers on different *ortho* systems.

The discussion will focus on Me and H derivatives first of all and then move onto the others.

The Methyl derivative

The following observation may account for the Me anomaly. Crystals of a sample of the methyl derivative were grown by T.Hibbert in order to investigate solid state features of this material so that a comparison with the analogous halogen species could be made[70]. These crystals, identified as *o*-Me-C_6H_4-

$CNSNS^+AsF_6^-$, (A), using elemental analysis, were submitted for x-ray structure determination. However, the crystal that was examined had a structure corresponding to the compound 3,5-(*ortho*-tolyl)-1,2-dithia-4-azolium hexafluoroarsenate, $[C_7H_7\text{-}C_2S_2N\text{-}C_7H_7]^+AsF_6^-$, (B). The crystals were grown in CH_2Cl_2 and this solvent may have influenced the rearrangement process of A to B. Alternatively, the crystallographer may have chosen an impure crystal from many pure ones. The CV measurements were conducted in a different solvent, MeCN. Therefore crystals of this material, which again analysed as $Me\text{-}C_6H_4\text{-}CNSNS^+AsF_6^-$, were prepared from MeCN to confirm or disprove which type of compound was being examined by CV. Unfortunately, the crystals "went off" before they could be examined by x-ray crystallography.

If the methyl compound tested by CV was compound (B) rather than (A), then the potential of the Me derivative would be expected to deviate relative to the others. Therefore, this would account for deviations of the Me derivative from plot (II).

Hydrogen and others

It is important to stress again that these types of free energy plots rely on the unsubstituted H derivative as the main reference point. As previously mentioned, a straight line will exist if the steric influence that the *ortho* group places on the electronic environment of the dithiadiazolylium reaction centre, is comparable to that observed for a series of benzoic acid analogues. So far the argument has centred around the H being the odd one out and not following this trend. This topic will now be discussed.

Examination of the distances between the *ortho* groups and the dithiadiazolylium and carboxylic reaction centres showed that they were all within contact distance of each other, when the molecule is planar, see appendix A. When the same investigation was conducted with the reaction centre being 90° out of the plane of the rest of the molecule, it showed that the sum of the van der Waals radii between these groups was exceeded. This shows that unfavourable interactions can be avoided by the molecule twisting or that favourable through space interactions can exist. Therefore, it is not the absence of a steric contribution that can be used to explain the H anomaly. However, the steric influence is the least for the H derivative and so this is likely to contribute to the anomalous position of this compound on the plot.

These van der Waals distances have been calculated using data achieved from crystallographic results and standard tables of van der Waals distances. Also from the crystallographic results there appears to be a preference for the *ortho* group of interest to be in a closer proximity to the sulphur at the 1 position

rather than the nitrogen at the 4 position of the dithiadiazolylium reaction centre[70]. Therefore, the discussion will adopt this bias too.

The following sets of values used in forthcoming discussions can be found in appendix A:- (i) Distance between *ortho* groups and the two reaction centres when in plane and at 90° to each other, (ii) van der Waals radius between particular atoms and (iii) differences in electronegativity between particular atoms.

Steric discussion

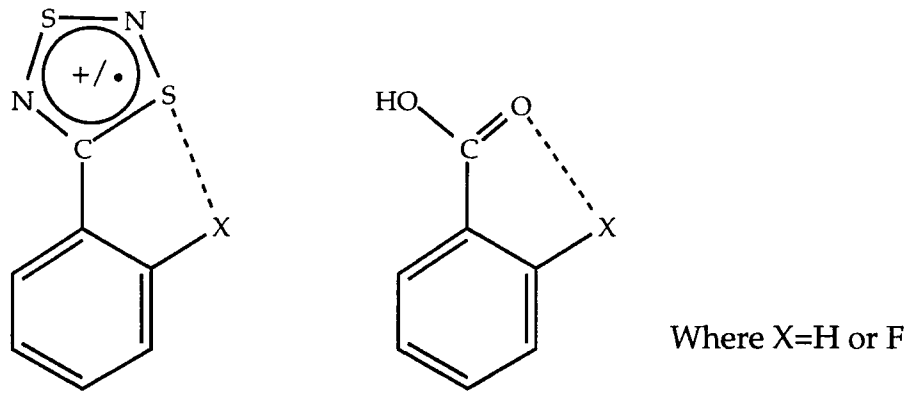

Fig 28. Schematic diagrams of *ortho* substituted benzoic acid and phenyl 1,2,3,5 dithiadiazolylium/zolyl species.

The steric interactions of *ortho* groups with reaction centres of unsubstituted and *ortho* fluoro benzoic acid and phenyl dithiadiazolylium derivatives will be studied first, see Fig 28. From these diagrams the atoms which are likely to be involved in possible steric confrontations are marked by a dotted line, i.e. S···X and O···X are of interest. Therefore, the distances of interest are S····F, O····F, S····H and O····H. When the molecule is planar the values are 2.88-2.56, 2.52, 2.91-2.62, 2.53Å respectively. With the reaction centre 90° out of the plane the distances are now 3.88-3.72, 3.39, 3.81-3.66, 3.32Å respectively. Therefore it can be seen that when the molecules are planar all the *ortho* groups are within van der Waals radii by approximately the same degree, see appendix A. Two types of steric interactions through space can occur, these are repulsions and attractions. A favourable electrostatic interaction will occur when a δ+ δ- dipolar interaction exists. A repulsion will occur from like dipoles being in close proximity to each other, i.e. δ- δ- or δ+ δ+. Therefore, for both fluoro compounds of Fig 28, $S^{\delta+}\cdots F^{\delta-}$ will be a favourable interactions and $O^{\delta-}\cdots F^{\delta-}$ will be a repulsion. The opposite effect will be observed for the unsubstituted H derivatives, $S^{\delta+}\cdots H^{\delta+}$ versus $O^{\delta-}\cdots H^{\delta+}$, therefore differences or shifts in potentials due to difference in charge

distribution will be observed among these two sets of compounds. The differences in electronegativity of S···F, O···F, S···H and O···H are 1.5, 0.5, 0.4 and 1.4 respectively. So, the strength of these repulsions/contacts can be estimated from the size of the differences in electronegativity of the atoms involved.

A similar trend to that observed for the fluoro derivatives is observed when the side group possesses an oxygen group instead, as $S^{\delta+}\cdots O^{\delta-}$ of the dithiadiazolylium is favoured over $O^{\delta-}\cdots O^{\delta-}$ of the benzoic acid, and for exactly the same reasons. When X=Cl, N or Br similar differences in favourable electrostatic attractions between $S^{\delta+}\cdots X^{\delta-}$ and unfavourable $O^{\delta-}\cdots X^{\delta-}$ repulsions exist due to similarities in the differences in electronegativities of the X atoms. Therefore, the H derivative is unique as it is the only situation where a more favourable steric contact exists between the *ortho* group and the carboxylic group than the dithiadiazolylium moiety.

If the Me derivative is allowed back into the discussion, the same rules would apply to this as the H as $O^{\delta-}\cdots H^{\delta+}$ and $S^{\delta+}\cdots H^{\delta+}$ are involved. These are the only derivatives studied which have the potential to form these types of interaction and hence makes them unique with respect to the other derivatives. Therefore, this could be the reason for these two derivatives being excluded from the plot.

This discussion has centred around preference for S rather than N being involved with electrostatic discussions. Again using the data in appendix A, this observation can be rationalised by looking at the electronegativities. The sulphur of the dithiadiazolylium/zolyl ring will be more electropositive than the nitrogen atoms due to possessing a smaller electronegavity value. As all the substituents except the H derivative will be more electronegative than the carbon atom they are bonded to and will have a negative dipole. Therefore, favourable $S^{\delta+}\cdots X^{\delta-}$ electrostatic interactions will be favoured over $N^{\delta-}\cdots X^{\delta-}$ repulsions. So, the preference for the sulphur is energetically more favourable. Therefore, N interactions will not be discussed in further detail. This readily explains the trend for *ortho* halogen groups to pack in the solid state with the *ortho* group on the side of the 1-S of the dithiadiazolylium ring[70].

For the analogous carboxylic acid derivatives the only steric interactions/repulsions that can exist are between carboxyl oxygen atoms and the *ortho* group.

All the above *ortho* benzoic acid and dithiadiazolylium derivatives discussed also possess an *ortho* hydrogen in addition to the *ortho* substituent of interest. Therefore, $O^{\delta-}\cdots H^{\delta+}$ and $N^{\delta-}\cdots H^{\delta+}$ attractive forces will exist for both and

are assumed to have a constant effect throughout these series in order for a linear plot to be observed.

Plot three will now follows.

Plot (III)

This plot suggest that the NO_2, EtO and MeO derivatives are anomalies. The three things these groups instantly have in common are that they are the biggest and hence have the largest potential to interact favourably and unfavourably with the neighbouring ring. However, relevant van der Waals distances and crystallography results show that the R group of the RO species, (where R=Et or Me), points away from the reaction centre and hence only the oxygen is involved. The steric involvement of the oxygen is no different in magnitude compared to the other groups. So this argument is flawed.

However another feature these two groups have in common is that they involve S···O interactions. The arguments used here will contradict many of those used for (II). For the analogous carboxylic acid derivatives unfavourable $O^{\delta-}\cdots O^{\delta-}$ steric forces exist but in the dithiadiazolyliums more favourable $S^{\delta+}\cdots O^{\delta-}$ steric forces are in action. Therefore the greater strength of these repulsive forces relative to the others present could assist in discrepancies occurring.

2C.5.5 Conclusions

Plot (I) was readily discounted. Arguments in support of (II) and (III) have centred around supporting arguments from solid state investigations and electronegativities. The rationalisations for either plot (II) or (III) revolves around differences in favourable and unfavourable electrostatic interactions of unsubstituted or oxygen containing *ortho* groups relative to the other derivatives and the effect this places on the electronic environment of the reaction centres. It is difficult to separate these two as both are equal in strength.

In these discussions, crystallography results have been used as crude tool to draw molecular templates which were used to gain insight into intramolecular interactions in solution. The range of structures used was very small (15). The bond angles and lengths used were averages obtained from all the known structures of these compounds and their sizes will naturally be influenced by solid state interactions. These molecular templates when used to describe effects in solution do not take into account that the molecules can freely rotate in solution and that solvent interactions can influence the shape of the molecules. Therefore, errors in the discussion can occur with the assumption that the geometry of the molecule in solution is the same as that in the solid state.

The key to this puzzle really lies in synthesising more derivatives to observe a larger range of effects. The CF_3 derivative was made and examined by CV which showed it to be quasi-reversible to the same degree as the other derivatives. This derivative was also found to have a larger $E_{pc/2}$ than the NO_2 compound. This trend signifies that the CF_3 group is better at stabilising an *ortho* positioned dithiadiazolyl than the NO_2 functionality. But due to the lack of a relevant Hammett value it can't be used to assess this situation. Therefore more Hammett σ_o values will have to be produced in order to further this study.

The $E_{pc/2}$ values for the above two derivatives contradicts results achieved from analogous *meta* and *para* derivatives which showed that the NO_2 group is better at making the electronic environment of the reaction centre less electron rich (i.e. favouring the reduction process more) than compared with the CF_3 derivative. Therefore, steric factors must be influencing the electronic environment of the ring in the *ortho* derivatives in order for this deviation to occur. Alternatively, the *ortho* CF_3 derivative may be behaving in a similar manner to that of the Me derivative, i.e. existing as 3,5-(*ortho* trifluoromethyl phenyl)-1,2-dithia-4-azolium hexafluoroarsenate, $[C_7H_4F_3\text{-}C_2S_2N\text{-}C_7H_4F_3]^+AsF_6^-$.

Without further investigations on new derivatives (e.g. calculating their relevant Hammett σ_o values and parallel crystallographic studies, especially of the supposed *o*Me-C_6H_4-CNSNS$^+AsF_6^-$ derivative) there is not enough evidence to suggest exactly which theory or theories can explain which relationship or combination exists. Clearly, the electronic environment of the ring in solution is an energy trade off between solvent interactions, steric repulsive forces, and the strength of through space attractive interactions (field effects).

Therefore, none of the plots can be selected due to difficulties of quantitative recognition of the contribution of steric factors and electrical effects in contrast to the proportional variation of these effects for *meta* and *para* substituents. This effect is commonly described in physical organic chemistry as the "the *ortho* effect" [40, 41].

In order to overcome this *ortho* effect problem with Hammett plots the Hammett equation can be written as $\log k_X/k_H = \rho\sigma_{(o,m,p)} + \delta E_s + fF$, where E_s is the Taft steric constant, F is a field parameter and δ and f are constants for selected reactions[71]. The field effect is propagated through space. Therefore, δE_s and fF are negligible for *meta* and *para* derivatives. For *ortho* derivatives these extra terms will differ from substituent to substituent and reaction type. Therefore, the above results from the $E_{pc/2}$ plots versus Hammett σ_o values clearly indicates that *ortho* substituted benzoic acid and analogous 1,3,2,4 dithiadiazolylium derivatives have very different δE_s and fF values.

2.C.5.6 Electrochemistry of substituted 1,2,3,5 dithiadiazolylium hexafluoroarsenate derivatives

Limited success was achieved with the synthesis of the *ortho* substituted aryl 1,2,3,5 dithiadiazolylium/zolyl derivatives; only the fluoro and chloro salt derivative and fluoro radical were successfully made. Discussion on why other syntheses failed is in chapter 4.

CV study of *ortho* fluoro phenyl 1,2,3,5 dithiadiazolyl revealed that it too gave quasi-reversible responses similar to those for *meta* and *para* dithiadiazolyls previously studied, see Table 16b. The observed $E_{pc/2}$ value was found to be 610mV.

No meaningful linear free energy plot could be attempted as there were only two points. Even though in the past *meta* and *para* 1,2,3,5 and 1,3,2,4 have been comparable, it would be unwise to assume that this correlation would also exist for the *ortho* systems, especially as the *ortho* 1,3,2,4 plot has not been fully rationalised.

The 1,2,3,5 dithiadiazolyls are more similar to the carboxylic acid derivatives than the 1,3,2,4 as only one type of atom with a δ- charge is involved in steric relations with *ortho* groups (e.g. 3,5 dithiadiazolylium nitrogens and carboxyl oxygens). Therefore, it is not unreasonable to propose that a better linear free energy relationship would be anticipated for *ortho* substituted phenyl 1,2,3,5 dithiadiazolylium derivatives with analogous substituted benzoic acids than compared to that observed for the isomeric 1,3,2,4 derivatives.

Further evidence to support this comes from examining the $E_{pc/2}$ potential of *ortho* fluoro phenyl dithiadiazolylium/zolyl derivatives relative to unsubstituted and positional derivatives. For the *ortho* fluoro 1,2,3,5 derivative the potential is found to be larger than that of the unsubstituted derivative and hence the fluoro group assists the reduction process. For the 1,3,2,4 analogue the opposite effect was observed. (The *meta* and *para* fluoro analogues of both isomers have been shown to reduce at a larger potential than the unsubstituted derivative, see section 2B and 2C). If the effect the position of a fluoro group has on the dissociation of analogous aryl carboxylic acids is now examined, (by looking at the size of the corresponding Hammett values), it can been seen that addition of a fluoro group enhances the dissociation process relative to the unsubstituted derivative. Therefore, the presence of a fluoro substituent on a phenyl 1,2,3,5 dithiadiazolylium/zolyl or benzoic acid contributes towards making the above reduction and dissociation processes more favourable, respectively. This can't be said for the 1,3,2,4 derivatives where the *ortho* derivatives are the exception due to

very differing steric forces present. Hence the above observed similarities support the theory that a linear relationship could exist for 1,2,3,5 *ortho* derivatives.

The electrochemical results achieved indicate that other *ortho* 1,2,3,5 and 1,3,2,4 would be expected to give the same quasi-reversible responses as those for *meta* and *para* analogues.

2.C.6 Conclusion

2.C.6.1 Electrochemistry

A detailed cyclic voltammetric survey of substituted phenyl 1,2,3,4 and 1,3,2,4 dithiadiazolylium hexafluoroarsenate salts and related 1,2,3,5 dithiadiazolyls revealed that they all exhibit the following characteristic electrochemical features. These similarities are highly suggestive that the same reduction mechanism is in operation for all of the them.

---

(1) Randles Sevcik
Obey equations (1) and (2)

(2) Peak separation
$E_{pc}-E_{pa}>0.055V$

(3) Half peak
$E_{pc}-E_{pc/2}$ is typically 60 to 70mV

(4) Potentials
$E_{pc/2}$ is the most consistent potential

(5) Scan rate
i_p increases with υ

(6) Peak current
i_{pc}/i_{pa} doesn't equal unity unless $\alpha_c=\alpha_a=0.5$

(7) Potential
For 1,3,2,4 dithiadiazolylium moiety $i_{pc}/i_{pa}>1$ and for the 1,2,3,5 isomer $0<i_{pc}/i_{pa}>1$

(8) Half peak
$E_{pc/2}$ is the same for 1,2,3,5 cations and their analogous radical species

(9) Potentials
If $\Delta E=E_{(\text{electron withdrawing group})}-E_{(\text{a electron donating group})}$ then *ortho>>para>meta* in decreasing size of ΔE

2.C.6.2 Hammett

Excellent linear free energy relationships were found to exist for *meta* and *para* substituted phenyl dithiadiazolylium/zolyl derivatives when their $E_{pc/2}$ values are plotted against corresponding Hammett σ values. From these plots, $E_{pc/2}$ values for these types of derivatives can be predicted reliably from known Hammett σ values. Also this information can be used to assess donor/acceptor properties of substituents groups.

For the *ortho* derivatives steric effects result in deviations from linearity of these free energy plots. Further work has to be conducted on new *ortho* derivatives before a better assessment of these steric effects can be made.

Section 2D

2D Electrochemistry of Di-substituted phenyl 1,2,3,5 and 1,3,2,4 dithiadiazolylium salts and related radicals.

2D.1.1 Introduction

The synthesis, structures and electrochemical properties of mono substituted phenyl 1,2,3,5 and 1,3,2,4 salts have already been investigated thoroughly, refer to chapters 2C, 2D, 3 and 4. But very little analogous information is known for multi-functionalised derivatives.

Therefore, to widen our understanding of the properties of such compounds several di-substituted aryl species were synthesised. In this chapter electrochemical measurements and comparisons with Hammett values, similar to those conducted on the monosubstituted derivatives, are discussed. Additional chemical and structural information is found in later chapters 3 and 4.

Background information on the Hammett $\Sigma\sigma$ and $\Delta E'$ potential values used later on in this discussion will now follow.

2D.1.2 Hammett $\Sigma\sigma$ linear free energy relationships

Hammett values for the di-substituted groups were not available from the literature, hence relationships between $E_{pc/2}$ and Hammett σ values could not be contrasted with those for the monosubstituted derivatives.

However, there is a method of calculating pK_a values of multifunctionalised compounds by using the sum of the Hammett value of each individual substituent $\Sigma\sigma$ and appropriate **X** and **Y** constants which are specific for a particular set of reaction conditions[50].

$$\therefore \quad \mathbf{pK_a = X - Y\Sigma\sigma}$$

It is known that $E_{pc/2}$ is proportional to pK_a, see section 2C.1. and therefore using the above equation it is also proportional to $\Sigma\sigma$ [72-75].

Knowing this, it is now possible to plot $E_{pc/2}$ of these di-substituted derivatives against the corresponding $\Sigma\sigma$ Hammett function. As **X** and **Y** will be constant, (as the reaction conditions were kept the same), a linear plot will be observed if a linear free energy relationship exists[76].

This method of establishing a free energy relationship is often subject to large errors as the side groups can (i) sterically impinge with each other or (ii) form supplementary or competing resonance contributions between themselves and the reaction centre, thus altering the stabilisation of the carboxylic acid, such that the compound's Hammett value is not proportional to the sum of two separate components[77].

2D.1.3 $\Delta E'$ relationship

From the electrochemical studies conducted on monosubstituted aryl dithiadiazolylium and unrelated species, chapter 2B and 2C, it has been shown that the potential $E_{pc/2}$ is inversely related to the relative energy of the reduced product, i.e the more positive the potential the more favourable is the reduction process.

For two mono substituted compounds with substituents A and B, if the sum of their potentials is calculated and referenced to the unsubstituted derivative (A=B=H), a potential $\Delta E'_{calc}$, can be determined. This can be used to give a measure of the combined resonance and inductive effects of each component on the reaction centre of a di-substituted analogue relative to a standard. However, this value does not encompass steric effects between the two neighbouring substituents. Therefore, when the observed potentials, $\Delta E'_{obs}$, of some di-substituted derivatives is plotted against corresponding $\Delta E'_{calc}$, a linear plot will be observed if steric effects are minimal, i.e. a $\Delta E'$ relationship[78]. Therefore combination of individual mono substituent potentials to give $\Delta E'$ values, is a method of gauging the relative energy of reduction products of the redox process involving di-substituted aryl dithiadiazolylium/zolyl species.

$$\therefore \quad \Delta E'_{obs} \propto \Delta E'_{calc} \text{ where } \Delta E'_{calc}=\Sigma E_{(X \text{ and } Y)}$$

The $\Delta E'$ plot for these compounds, (which involves comparing analogous compounds under the same experimental conditions, i.e. a homogenous technique), is unlike Hammett plots of D1.2; the latter compares experimental measurements on two different types of compounds in different solvents, i.e. a heterogeneous technique.

Hammett plots have been shown to be successful recently for *meta* and *para* substituted dithiadiazolylium/zolyl systems despite the two systems compared being heterogeneous to one another, see Chapter 2B and C. For the *ortho* system this is not found to be so and this is attributed to the presence of steric forces which distort the electronic environment of the reaction centre, see Chapter 2C. Due to the absence of a linear free energy plot for *ortho* substituted analogues, $\Delta E'$ measurements are anticipated as being a better reflection of comparative electronic and steric effects among di-substituted derivatives, especially ones possessing one or two *ortho* groups, than corresponding Hammett values. However this method is subject to error for the same reason as 2D.1.2.

2D.1.4 Choice of disubstituted compounds

Disubstituted aryl 1,2,3,5 and 1,3,2,4 dithiadiazolylium salts possessing identical substituent groups were studied, mainly to observe how the position of the two groups influence the electrochemistry. It was not planned as a comparison between the potentials of the isomers; it was already anticipated that the 1,2,3,5 would reduce at a higher potential than the 1,3,2,4.

Difluoro derivatives were chosen for the first investigation since fluorinated starting materials were readily available. Also the probability of synthesising both isomeric forms seemed high because although there are very few known *ortho* 1,2,3,5 salts that can be synthesised, the fluoro derivatives are amongst them. No problems with the synthesis of the 1,3,2,4 derivatives were anticipated as production of analogous *ortho, meta* and *para* systems had been relatively straight forward.

A second and much smaller investigation was conducted on aryl 1,2,3,5 derivatives which possessed two different substituent groups at the *meta* and *para* positions. The radical derivatives were examined by CV in preference to hexafluoroarsenate salts purely because structural studies of these compounds were also being undertaken, see chapter 4. These derivatives will be discussed much later in section 2D.5.1.

2D.2.1 Electrochemistry of difluoro substituted phenyl 1,2,3,5 dithiadiazolyls.

1,2,3,5 radical derivatives

An electrochemical survey was conducted on the following difluorophenyl 1,2,3,5 dithiadiazolyls: 2,3; 2,5; 3,4 and 3,5. The 2,4 and 2,6 radical derivatives could not be examined due to synthesis problems; further discussion on this subject can be found in chapter 4.

The electrochemical results in Table 18, indicate that these compounds possess the same quasi-reversible characteristics as those observed for the previously studied mono-substituted derivatives, section 2C.6.

1,2,3,5 cationic derivative

Problems were also incurred with the synthesis of the 2,4 difluoro phenyl 1,2,3,5 dithiadiazolylium hexafluoroarsenate but not with the 2,6 analogue. Hence CV was conducted on a sample of this latter material under identical electrochemical experimental conditions as that for the unsubstituted salt. An identical quasi-reversible response was observed for this compound, see Table 18 and section 2C.6.

All five derivatives

So far the CV studies of these 1,2,3,5 difluoro derivatives have revealed that they all give the same quasi-reversible responses, comparable with those observed for their mono substituted cousins, see 2C.6. Therefore, due to these similarities it is not unreasonable to assume that the $E_{pc/2}$ potential for difluoro derivatives will be similar whether it is a salt or a radical (as observed for mono-substituted 1,2,3,5 derivatives). Thus, this assumption allows a comparison to be made between the four difluoro radical derivatives already studied and the 2,6 difluoro cationic derivative.

Other similarities between the difluoro and mono substituted derivatives include the difference between the highest and the lowest observed $E_{pc/2}$ potentials; this is found to be approximately 30mV. Overall, the cathodic half wave potentials observed for the difluoro substituted derivatives (lowest potential of 632.5mV for the 3,4 derivative) are generally higher than those observed for any of the mono substituted F derivatives (*ortho*=610mV, *meta*=630mV and *para*=600mV). This is as expected; the extra F atom pulls more charge away from the ring, aiding radical ring stabilisation and hence increasing the observed potentials.

Sample		Scan rate mVs^{-1}	E_{pc} mV	$E_{pc/2}$ mV	i_{pc} μA	$E_{pc}-E_{pc/2}$ mV	E_{pa} mV	$E_{pa/2}$ mV	i_{pa} μA	$E_{pa}-E_{pa/2}$ mV	i_{pc}/i_{pa} μA	$E_{pa}-E_{pc}$ mV	$(E_{pa}+E_{pc})/2$ mV
2,3	A[a]	400	580	645	46.5	65	680	610	48.0	70	0.97	100	630
	B[a]	676	590	650	67.0	60	680	600	61.0	80	1.10	90	635
		784	580	650	76.0	70	680	610	79.0	70	0.96	100	630
	C[a]	786	585	655	43.5	70	690	615	44.5	75	0.98	105	637.5
	D[a]	324	585	650	42.0	65	680	610	44.0	70	0.95	95	632.5
	E[a]	121	595	650	26.0	55	675	615	27.0	60	0.96	80	635
		144	590	650	29.0	60	680	610	29.0	60	1.00	90	635
2,5	A[a]	144	580	650	82.0	70	705	620	84.0	85	0.98	125	642.5
		196	585	650	95.0	65	705	630	97.0	75	0.98	120	645
		676	555	645	150.0	90	720	630	145.0	90	1.03	165	637.5
	B[a]	196	585	650	80.0	65	700	625	86.0	75	0.93	115	642.5
2,6	A[b]	196	615	665	6.8	50	690	630	6.9	60	0.99	75	652.5
		196	610	660	7.4	50	680	620	7.4	60	1.00	70	645
3,4	A[a]	256	580	630	35.5	50	670	590	41.0	80	0.87	90	625
		676	570	635	41.5	65	670	600	43.5	70	0.95	100	620
3,5	A[a]	324	595	660	73.0	65	710	635	80.0	75	0.91	115	652.5
		484	590	660	93.0	70	720	640	96.0	80	0.97	130	655

Table 18. Cyclic voltammetric data of difluoro substituted phenyl - 1,2,3,5 - dithiadiazolyls[a] and a dithiadiazolylium hexafluoroarsenate salt[b] in MeCN at 0°C, concentration 1×10^{-3} M, supporting electrolyte $TBABF_4$.

The following order of the $E_{pc/2}$ potentials for these compounds was found, (3,4<2,3=2,5<3,5<2,6). This trend will now be investigated with the assistance of using $\Sigma\sigma$ Hammett values (2D.1.2) and ΔE values (2D.1.3).

2D.2.2 $\Delta E'$

The $\Delta E'$ values were studied first of all, see Table 19. A plot of $\Delta E'_{obs}$ versus $\Delta E'_{calc}$ revealed that for four of the five derivatives a satisfactory relationship exists between $\Delta E'_{obs}$ versus $\Delta E'_{calc}$, see Fig 29. However it is evident that the 2,6 derivative, with an observed $E_{pc/2}$ value of 665mV is anomalous.

This deviation of the 2,6 derivative observed in Fig 29 heavily suggests that electronic influence of the two fluorines is affected by an additional term not included in the sum of the two individual substituent effects. This is supported by the following crystallographic findings and energy diagrams.

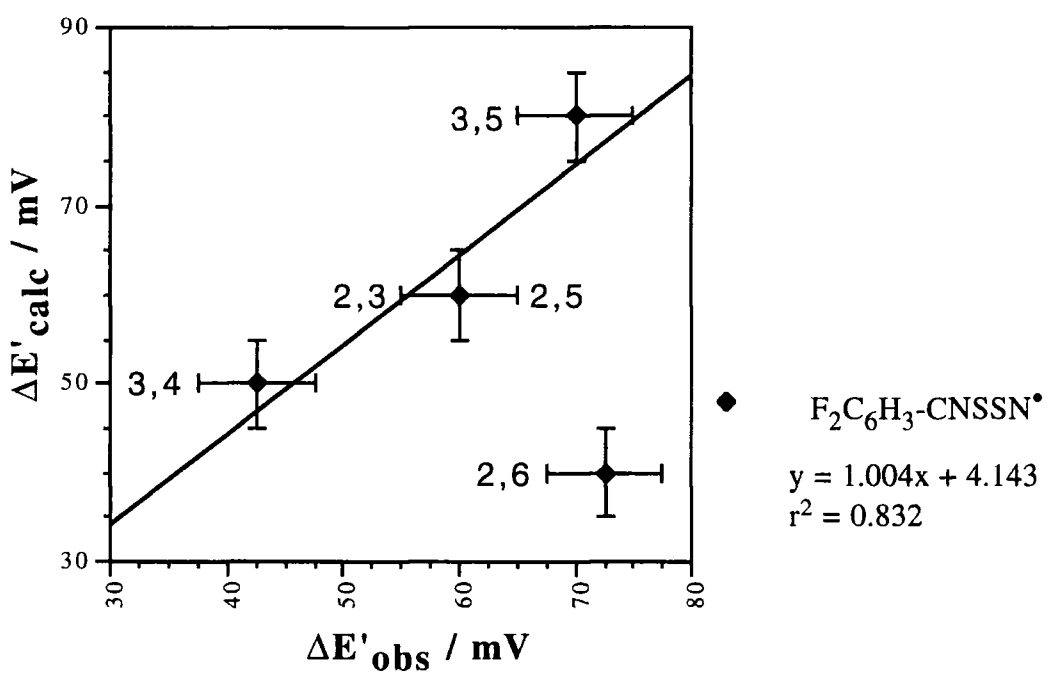

Fig 29. $\Delta E'_{obs}$ versus $\Delta E'_{calc}$ values of some difluoro phenyl 1,2,3,5 dithiadiazolyls and a dithiadiazolylium salt studied by CV, in MeCN, concentration $1x10^{-3}$M, temperature 0°C, supporting electrolyte $TBABF_4$.

It can be shown, using a molecular template of an aryl dithiadiazolyl, (derived from average bond lengths and angles of several aryl dithiadiazolyl derivatives), that if the molecule is planar, an *ortho* fluoro group will be within the van der Waals radius of the neighbouring ring nitrogen, (see section 2C.5.4).

sample	$\Delta E'_{obs}$/mV	$\Delta E'_{calc}$/ mV
2,3[a]	60	60
2,5[a]	60	60
2,6[b]	72.5	40
3,5[a]	70	80
3,4[a]	42.5	50

Table 19. $\Delta E'_{obs/calc}$ values from CV investigation of some difluoro phenyl 1,2,3,5 dithiadiazolylium[a]/zolyls[b], in MeCN, concentration $1x10^{-3}$M, temperature 0°C, supporting electrolyte $TBABF_4$.

As the charge on both the F and N is δ-, they will repel each other and cause the molecule to twist. If the fluorine is replaced by a hydrogen the *ortho* group is still just within the van der Waals radii of the neighbouring ring nitrogen, but this time $N^{\delta-}$ and $H^{\delta+}$ will not repel each other but attract each other very weakly. This is further confirmed by examination of the twist angles of the following analogous derivatives.

Crystal data on phenyl 1,2,3,5 dithiadiazolyl derivatives with two *ortho* fluoro substituents (see chapter 3) show that a large twist angle, in the order of 30°-40°, is observed. A plot of energy vs twist angle between the dithiadiazolyl and the aryl ring of C_6F_5-CNSSN$^{\bullet}$ shows the energy of the system is lowest at this angle range too.

For the analogous unsubstituted derivatives, (i.e. two *ortho* hydrogen), this angle, where the system is at a minimum, is 0°-15°. This is in keeping with the crystallography results too.

Naturally, it is assumed that the observed twist angle for derivatives possessing just one *ortho* fluoro plus an *ortho* hydrogen will be less severe than that observed for derivatives possessing two *ortho* fluoro atoms.

Meta and *para* fluoro substituents will not induce any twisting due to sterics as they are not close enough to the dithiadiazolyl ring.

Therefore, these results support a theory that a much larger twist angle between 1,2,3,5 dithiadiazolyl ring and the benzene ring for the di-*ortho* fluoro will be observed compared with that of difluoro analogues possessing only one fluorine in the *ortho* position or a mono fluoro derivative. The smaller the twist angle the greater the extent of π orbital overlap that occurs between *ortho* fluoro group(s) and the dithiadiazolyl/ium ring. This increase in π overlap results in the resonance effect of the substituent group(s) on the reaction centre becoming more significant. Therefore, the resonance contribution from each fluorine of the 2,6

derivative will be smaller than from an *ortho* fluorine of an analogous di or mono substituted derivative that has a smaller twist angle. As the resonance contribution of fluoro groups contributes to a reduction in ring stability (i.e. a smaller $E_{pc/2}$ value), the 2,6 compound will have a higher $E_{pc/2}$ potential than calculated from mono fluoro components. This is exactly what is observed.

Alternatively, it may not be a valid assumption that the value of $E_{pc/2}$ for the 2,6 salt derivative is identical to that for the not isolated radical (and resultant differences are responsible for this supposed deviation). But this is thought to be highly unlikely as the assumption is based on results from *meta* and *para* derivatives which are chemically very similar in nature.

2D.2.3 Hammett

The sum of the Hammett values for each of these difluoro derivatives was calculated using the method described in section D1.3. These results were then plotted against the corresponding $E_{pc/2}$ values, see Table 20 and Fig 30.

Fig 30 reveals that for four of the five derivatives a good linear relationship exists between these calculated Hammett $\Sigma\sigma$ values and corresponding $E_{pc/2}$ potentials, but why should the 3,5 derivative be an exception?

sample	$E_{pc/2}$ /mV	$\Sigma\sigma$
2,3[a]	650	1.267
2,5[a]	650	1.267
2,6[b]	662.5	1.86
3,5[a]	660	0.674
3,4[a]	632.5	0.399

Table 20. $\Sigma\sigma$ and $E_{pc/2}$ values from CV investigation of some difluoro phenyl 1,2,3,5 dithiadiazolylium[b]/zolyls[a] species, in MeCN, concentration $1x10^{-3}$M, temperature 0°C, supporting electrolyte $TBABF_4$ [44, 67].

There is only one factor that separates the 3,5 derivative from the others: neither of the *meta* substituent can form resonance canonicals which involve the reaction centre. It has already been shown that *meta* or *para* substituted phenyl dithiadiazolylium/zolyl derivatives have comparable electronic environments to analogous carboxylic acids. Therefore, the di-*meta* and *meta/para* would be expected to follow a similar trend to its monosubstituted components. For this plot the 3,4 derivative is seen to fit on the line which is odd as one would expect it to deviate like the 3,5.

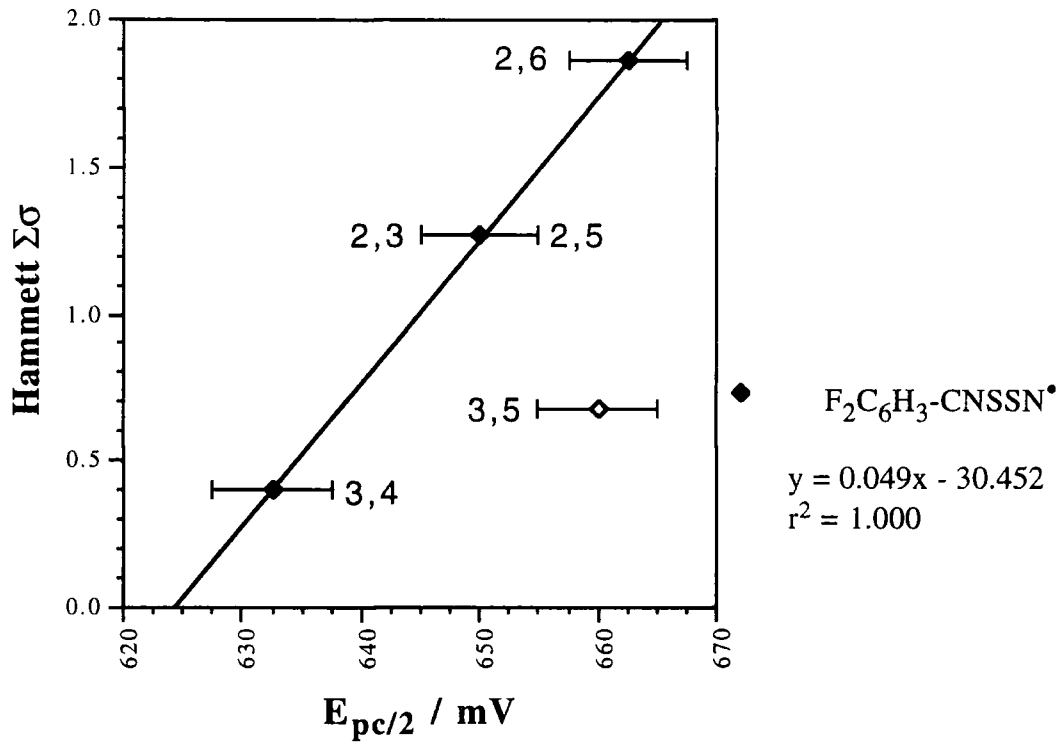

Fig 30. $E_{pc/2}$ versus Hammett $\Sigma\sigma$ values of some difluoro phenyl 1,2,3,5 dithiadiazolyls studied by CV, in MeCN, concentration $1x10^{-3}M$, temperature 0°C, supporting electrolyte $TBABF_4$.

Also the di *ortho* substituted derivative may be producing misleading results as observed for the mono *ortho* derivatives. Again it is important to mention that there is a slim chance that the value of $E_{pc/2}$ for the 2,6 salt derivative is not accurate as it is assumed that its corresponding radical will have the same value as the salt and therefore errors may arise with the above plot. But as previously mentioned this is assumed to be highly unlikely from the electrochemical track record of monosubstituted derivatives.

2D.2.4 Conclusions

For <u>all</u> the associated difluoro phenyl 1,2,3,5 derivatives studied no universal linear relationships were found to exist between $E_{pc/2}$ values and Hammett $\Sigma\sigma$ values or between $\Delta E'_{calc}$ and $\Delta E'_{obs}$ even though all of the derivatives possessed the same quasi-reversible electrochemical responses. This is attributed to errors associated with the determination of the Hammett and $\Delta E'$

values which do not take into account additional electronic and steric effects between functional groups and reaction centres, (see section 2C.5.4).

For fluoro phenyl dithiadiazolylium/zolyls the fluoro group has the ability to form resonance canonicals with the reaction centre when they are at the *ortho* and *para* position. However, for di-substituted fluoro derivatives (depending on the position of the difluoro groups of these dithiadiazolylium/zolyl derivatives) competing resonance canonicals involving either fluoro group and the reaction centre can be drawn. No additional resonance contributions between the two substituents can exist as it would involve the generation of F^+ which is energetically not favoured. The effect of resonance and induction contributions of substituents being able to compete with each other in disubstituted system is not taken into account in the calculated Hammett $\Sigma\sigma$ and $\Delta E'$ values and associated plots. Therefore this can contribute to observed deviations from linearity of these plots.

For each of the above plots it is found that one point obviously deviates from the linear relationship. But as the results for the 2,4 derivative were unobtainable due to problems in synthesis and as the CV measurements of the 2,6 were of a salt and not a radical like the other derivatives it can not be said conclusively which relationships do or do not exist.

Also, these results must not be taken too seriously as the difference in potentials is 30mV; the rationalisations are based on small deviations from linearity.

Problems in the synthesis of these two radicals has obviously hindered these CV investigations. However, for the difluoro phenyl 1,3,2,4 dithiadiazolylium salts, all of the derivatives were readily made and hence a more thorough study could be conducted. Results from these derivatives might help to clear up the uncertainties that exist for the above Hammett and ΔE plots of analogous 1,2,3,5 compounds.

2D3.1 Electrochemistry of difluoro substituted phenyl 1,3,2,4 dithiadiazolylium hexa-fluoroarsenate derivatives

A similar CV investigation was naturally conducted on a series of difluoro substituted phenyl 1,3,2,4 dithiadiazolylium salts. These compounds included all isomers apart from the 2,3 which was assumed would give almost identical results to the 2,5 derivative as observed with the analogous 1,2,3,5 derivatives due to similar electronic resonance and inductive pathways.

For all these difluoro substituted phenyl 1,3,2,4 dithiadiazolylium hexafluoroarsenate salts, CV revealed that their electrochemistries were comparable with that of the already studied mono substituted derivatives as they exhibited similar quasi-reversible responses, see section 2C.6. and Table 21. The same differences that exist between the 1,2,3,5 and 1,3,2,4 mono derivatives were also found to exist for the difluoro derivatives, see section 2C.6.

For the mono substituted 1,3,2,4 derivatives the following cathodic half wave potentials were observed, *ortho*=310mV, *meta*=370mV and *para*=340mV. There is a larger range in these observed potentials (60mV) compared with the corresponding 1,2,3,5 analogues (30mV). Therefore it is not surprising that the potential range (70mV) for the 1,3,2,4 disubstituted derivatives studied is more than double that observed for the corresponding 1,2,3,5 analogues (27.5mV).

The potentials of these difluoro derivatives are about the same size as those observed for the mono fluoro derivatives. The following trend in increasing order of $E_{pc/2}$ and $\Delta E'_{obs}$ potentials is as follows, 2,4 > 2,6 > 2,5 > 3,4 > 3,5.

This larger range in potentials will enable results achieved from the $\Delta E'$ and $\Sigma\sigma$ plots to be assessed to a higher degree of confidence compared with their 1,2,3,5 friends.

2D.3.2 $\Delta E'$

Values of $\Delta E'_{calc}$ and $\Delta E'_{obs}$ are shown in Table 22. When these results were plotted against each other the relationship found Fig 31 was extremely reminiscent of that for analogous difluoro phenyl 1,2,3,5 dithiadiazolyls, see Fig 29. From Fig 31 it is apparent that the 2,6 derivative does not follow the trend observed for the other derivatives. The same argument, as used for the 1,2,3,5 derivative, of increased steric repulsive forces between the two *ortho* fluoro groups with the dithiadiazolylium ring in solution, can be used to rationalise this anomaly.

If the same plot is drawn but without the 2,6 derivative, a much improved relationship is found as indicated by the increase in size of the r^2 factor to a respectable 0.915.

Sample		Scan rate mVs^{-1}	E_{pc} mV	$E_{pc/2}$ mV	i_{pc} μA	E_{pc}-$E_{pc/2}$ mV	E_{pa} mV	$E_{pa/2}$ mV	i_{pa} μA	E_{pa}-$E_{pa/2}$ mV	i_{pc}/i_{pa} μA	E_{pa}-E_{pc} mV	$(E_{pa}+E_{pc})/2$ mV
2,4	A	196	255	320	41.0	65	365	295	37.5	70	1.09	110	310
		225	250	325	46.0	75	375	295	42.5	80	1.08	125	312.5
		900	225	320	88.0	95	390	300	85.0	90	1.04	165	307.5
2,5	A	144	285	360	45.0	75	395	320	40.0	75	1.15	110	340
		729	270	355	85.0	85	410	330	80.0	80	1.06	140	340
2,6	A	256	280	345	41.0	65	380	310	38.5	70	1.06	100	330
		676	280	345	53.5	65	380	310	50.0	70	1.07	100	330
3,4	A	144	295	360	48.5	65	415	340	43.0	75	1.13	120	355
		400	270	360	100.0	90	430	340	86.0	90	1.16	160	350
3,5	A	256	330	390	18.2	60	440	365	16.2	75	1.12	110	385

Table 21. Cyclic voltammetric data of difluoro substituted phenyl-1,3,2,4-dithiadiazolylium hexafluoroarsenate in MeCN at 0°C, concentration 1 x 10^{-3} M, supporting electrolyte $TBABF_4$.

sample	$\Delta E'_{obs}$ /mV	$\Delta E'_{calc}$ / mV
2,6	15	-40
2,5	27.5	20
2,4	-10	-10
3,5	60	80
3,4	30	50

Table 22. $\Delta E'_{obs/calc}$ values from CV investigation of some difluoro phenyl 1,3,2,4 dithiadiazolylium hexafluoroarsenate salts, in MeCN, concentration $1x10^{-3}$M, temperature 0°C, supporting electrolyte $TBABF_4$.

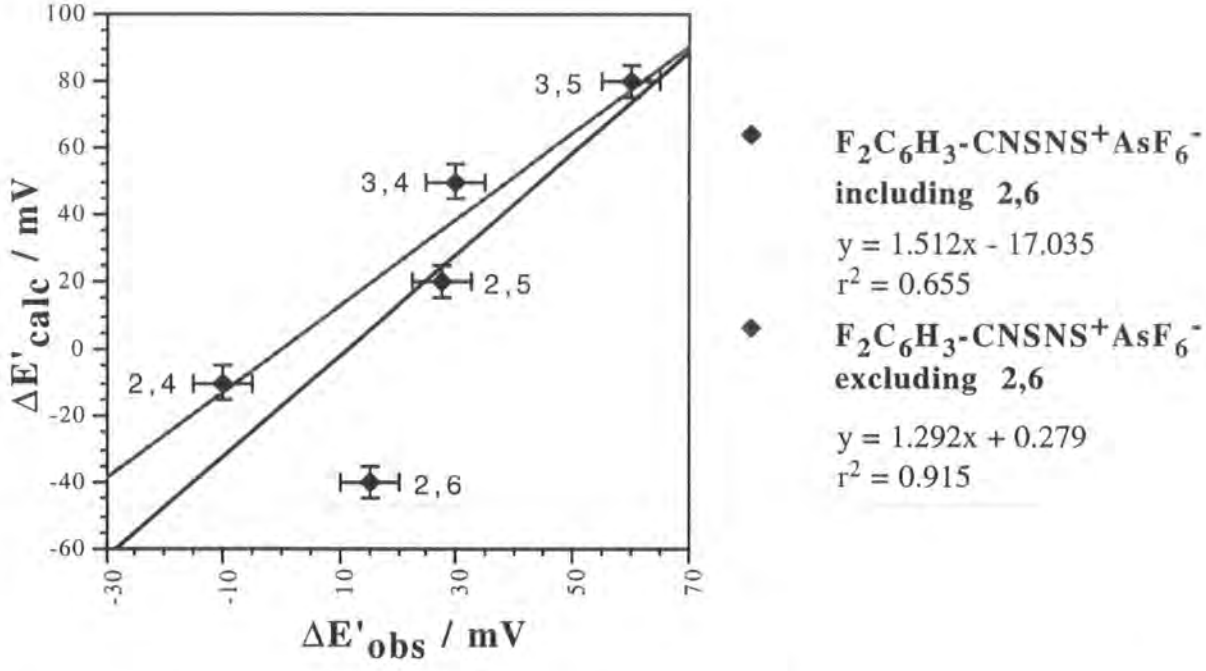

Fig 31. $\Delta E'_{obs}$ versus $\Delta E'_{calc}$ values of some difluoro phenyl 1,3,2,4 dithiadiazolylium hexafluoroarsenate salts studied by CV, in MeCN, concentration $1x10^{-3}$M, temperature 0°C, supporting electrolyte $TBABF_4$.

There is a possibility that an alternative line that passes through the 3,4, 2,5 and 2,6 could be drawn but using the arguments for the 1,2,3,5 case this is strongly disfavoured especially as this line does not fit the data as well as the other one. Also it is not logical that 2,4 and 3,5 would deviate from linearity so much, especially as they don't appear to possess unique electronic and steric properties relative to the others.

2D.3.3 Hammett

If the $E_{pc/2}$ potentials of these compounds are compared with the sum of the Hammett $\Sigma\sigma$ values no correlation is found to exist, see Table 23 and Fig 32.

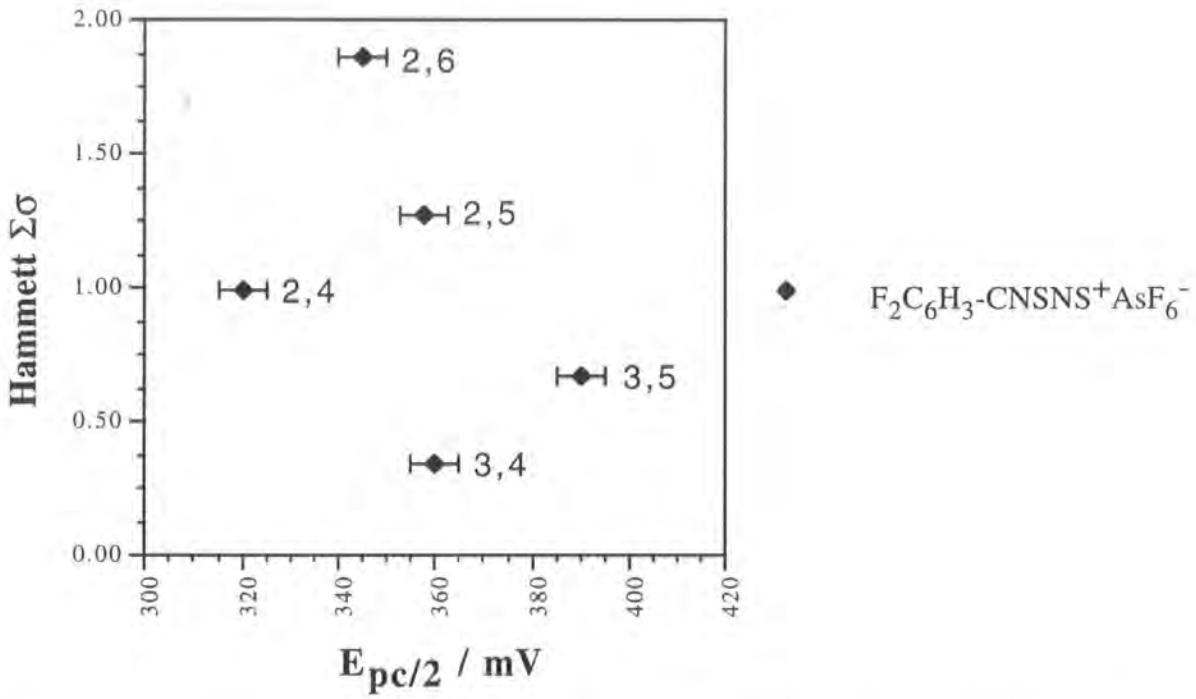

Fig 32. $E_{pc/2}$ versus Hammett $\Sigma\sigma$ values of some difluoro phenyl 1,3,2,4 dithiadiazolylium hexafluoroarsenate salts studied by CV, in MeCN, concentration $1x10^{-3}$M, temperature 0°C, supporting electrolyte $TBABF_4$.

sample	$E_{pc/2}$ /mV	$\Sigma\sigma$
2,6	345	1.86
2,5	357.5	1.267
2,4	320	0.992
3,5	390	0.674
3,4	360	0.399

Table 23. $\Sigma\sigma$ and $E_{pc/2}$ values from CV investigation of some difluoro phenyl 1,3,2,4 dithiadiazolylium hexafluoroarsenate salts, in MeCN, concentration $1x10^{-3}$M, temperature 0°C, supporting electrolyte $TBABF_4$.

This is attributed mainly to the *ortho* carboxylic acid Hammett component not being applicable to describe the influence electronic and steric effects that *ortho* groups place on the reduction of *ortho* dithiadiazolylium derivatives, see previous Hammett section for more details. It is anticipated for this reason that deviation from linearity will be more severe for the 2,6 derivative due to a doubling of this Hammett inaccuracy present, see section 2D2.3. This phenomenon readily explains why a linear relationship is not observed.

2D4.1 Comparison of the electrochemistry between difluoro substituted phenyl 1,2,3,5 and 1,3,2,4 dithiadiazolylium hexafluoroarsentae salts and related radicals.

Difluoro phenyl 1,2,3,5 and 1,3,2,4 dithiadiazolylium salts and related compounds exhibit electrochemical quasi-reversible responses identical to those found for mono substituted aryl 1,2,3,5 and 1,3,2,4 derivatives. The differences in electrochemistries between the difluoro 1,2,3,5 and 1,3,2,4 analogues were akin to those observed for analogous mono substituted derivatives, see 2C.6.

The observed $E_{pc/2}$ potentials for mono and disubstituted fluoro phenyl dithiadiazolylium/zolyl 1,3,2,4 derivatives are the same order of magnitude; however for 1,2,3,5 analogues the disubstituted derivatives generally have larger $E_{pc/2}$ values than the mono substituted derivatives. Therefore, the presence of more electron withdrawing fluorine substituents raising potentials can't be said to occur among all these derivatives.

The potential for the *ortho* fluoro phenyl 1,3,2,4 dithiadiazolylium derivative is found to be lower than for the unsubstituted derivative, but for the 1,2,3,5 analogue it is higher. This has been attributed to differing steric forces influencing the electronic environment of the rings, i.e, $S^{\delta+}\cdots F^{\delta-}$ attractive forces and $N^{\delta-}\cdots F^{\delta-}$ repulsive forces between the *ortho* fluorine substituent and the 1,3,2,4 and 1,2,3,5 rings respectively. For disubstituted analogues possessing two *ortho* fluorines, the steric forces for one of the fluorines is the same as that observed for the above mono substituted analogues, however an additional $N^{\delta-}\cdots F^{\delta-}$ repulsion involving the extra *ortho* fluorine is also present among both isomers. Therefore, a larger twist angle in these disubstituted derivatives than in analogous mono substituted derivatives would be expected due to greater steric repulsive forces being present in the former. (This is supported by crystallography results of similar compounds, see section 2C.5.4). This would result in a smaller resonance contribution from fluorines of di *ortho* substituted derivatives relative to those of a mono *ortho* substituted derivative. Hence a higher reduction potential for the 2,6 difluoro derivatives than predicted using

results from mono substituted derivatives is expected. This trend is observed for both types of 2,6 difluoro derivatives.

Steric forces are assumed to be negligible for *meta* and *para* disubstituted analogues as the groups are small and further away from the reaction centre. Therefore, differing steric forces between mono fluoro and difluoro substituted derivatives can't be used to totally explain why the relative size of the potentials among isomeric analogues of these derivatives isn't connected to the strength of the electron withdrawing ability of the substituent attached to the heterocyclic ring.

Solvent interactions are known to affect the stability of molecules in solution. As these electrochemical measurements were conducted in solution, differing solvent interactions involving the fluorines and/or the two types of isomeric rings could be contributing to the difference in the relative sizes of potentials among derivatives. However, it is important to note the steric effects of *ortho* substituents, as discussed above, will contribute to differences in the electronic environment of the reaction centre and the observed reduction potentials too.

Therefore, the observed potentials between mono and substituted fluoro compounds are clearly influenced by steric forces, solvent interactions and the electron withdrawing ability of the substituent group to varying degrees.

Clear Hammett correlations, for these series of di-fluorinated derivatives, are not achieved because the Hammett values used are derived from monosubstituted compounds which are not compatible with the sum of electronic and steric components in disubstituted compounds. In particular, derivatives possessing *ortho* substituents tend to be the worst offenders due to the influence of steric repulsive forces between substituents. This is supported by similar research conducted on a series of *ortho* substituted phenyl 1,3,2,4 dithiadiazolylium salts, see section 2C.5.4.

Comparing relative calculated potentials $\Delta E'_{calc}$ with observed potentials ΔE_{obs} definitely appears to be a more successful way of estimating the size of the potentials for these derivatives than Hammett $\Sigma\sigma$ versus $E_{pc/2}$ plots. The reasonable $\Delta E'$ plots achieved for all the derivatives except for 2,6 derivatives does suggest that the resonance and inductive contributions of mono substituted derivatives are proportional to those observed for disubstituted. It is interesting to note that this method does fail routinely for di *ortho* substituted derivatives of both isomers. This is attributed to the additional repulsions between the second *ortho* fluorine $F^{\delta-}$ and the ring $N^{\delta-}$ being present for both 2,6 difluoro isomeric derivatives. These repulsive forces result in the molecules twisting more than that

observed for the respective mono *ortho* fluoro analogues, which ultimately reduces the resonance contribution from the fluorines; hence an $E_{pc/2}$ potential larger than expected is observed. However, for the disubstituted derivatives possessing only one *ortho* substituent, the steric effect the *ortho* fluorine has on the ring is comparable to that for an analogous *ortho* mono substituted derivative i.e. similar steric forces are in operation. All these deductions are supported by crystallography data, twist angle versus energy plots and electronegativities of component atoms of these derivatives.

The similarities between the 2,6 derivatives of both isomers also assists in justifying the assumption that potentials of the 2,6 difluoro phenyl 1,2,3,5 salt and associated radical would be identical too.

2D5.1 Electrochemistry of di substituted phenyl 1,2,3,5 dithiadiazolyls.

Structural and CV studies were conducted on 3Cl, 4Me and 3Cl, 4F phenyl 1,2,3,5 dithiadiazolyls.

CV revealed quasi-reversible responses identical to those of other mono and di substituted aryl 1,2,3,5 dithiadiazolyls, see Table 24. Looking at the $E_{pc/2}$ values for 3F, 4F and 3Cl, 4F derivatives, the potential rises from 632.5mV to 650mV respectively, just by replacing the F substituent by a stronger electron withdrawing group, e.g Cl. If the F substituent of the 3Cl, 4F compound is replaced by an electron donating substituent such as Me, a decrease in the potential $E_{pc/2}$ from 650mV to 615mV is observed. Therefore, these preliminary result are comparable with results obtained for *meta* and *para* mono substituted analogues because changing a substituent with a stronger electron withdrawing group results in an increase in $E_{pc/2}$ potential or ring stabilisation of the associated radical and the opposite occurs for replacement by electron donating groups.

Next, the $E_{pc/2}$ values of these compounds were plotted against corresponding $\Delta E'_{calc}$ and Hammett $\Sigma\sigma$ value, (analogous to the survey of isomeric 1,2,3,5 difluoro derivatives previously studied). The results from these plots are now discussed.

2D.5.2 $\Delta E'$

The $\Delta E'_{calc}$ potentials for this selection of di-substituted phenyl 1,2,3,5 dithiadiazolyls were plotted against their corresponding $\Delta E'_{obs}$ and an extremely poor relationship was found, see Table 25 and Fig 33.

However with this limited number of data points it can not be conclusively said that no relationship exists as one of the points could be anomalous. Therefore, further CV investigations are required to confirm or dispute this.

sample		$\Delta E'_{obs}$/mV	$\Delta E'_{calc}$/ mV
3	4		
Cl	Me	25	20
Cl	F	60	40
F	F	30	50

Table 25. $\Delta E'_{obs/calc}$ values from CV investigation of some di-substituted phenyl 1,2,3,5 dithiadiazolyls, in MeCN, concentration $1x10^{-3}$M, temperature 0°C, supporting electrolyte $TBABF_4$.

Sample		Scan rate mVs^{-1}	E_{pc} mV	$E_{pc/2}$ mV	i_{pc} μA	$E_{pc}-E_{pc/2}$ mV	E_{pa} mV	$E_{pa/2}$ mV	i_{pa} μA	$E_{pa}-E_{pa/2}$ mV	i_{pc}/i_{pa} μA	$E_{pa}-E_{pc}$ mV	$(E_{pa}+E_{pc})/2$ mV
Cl,Me	A	144	560	615	4.2	55	630	550	4.7	80	0.89	70	595
		484	555	620	6.7	65	630	565	7.8	65	0.86	75	592.5
		676	560	615	7.5	50	625	560	8.5	65	0.88	65	592.5
	B	676	550	615	16.0	65	630	560	17.2	70	0.93	80	590
		784	550	615	18.0	60	620	550	20	70	0.90	70	585
Cl, F	A	144	610	675	8.8	65	685	620	9.4	65	0.94	75	647.5
		900	610	680	17.0	70	690	630	17.75	60	0.96	80	650
		256	590	650	16.25	60	680	590	17.25	90	0.94	90	635

Table 24. Cyclic voltammetric data of di substituted phenyl-1,2,3,5-dithiadiazolyls in MeCN at 0°C, concentration 1×10^{-3} M, supporting electrolyte $TBABF_4$.

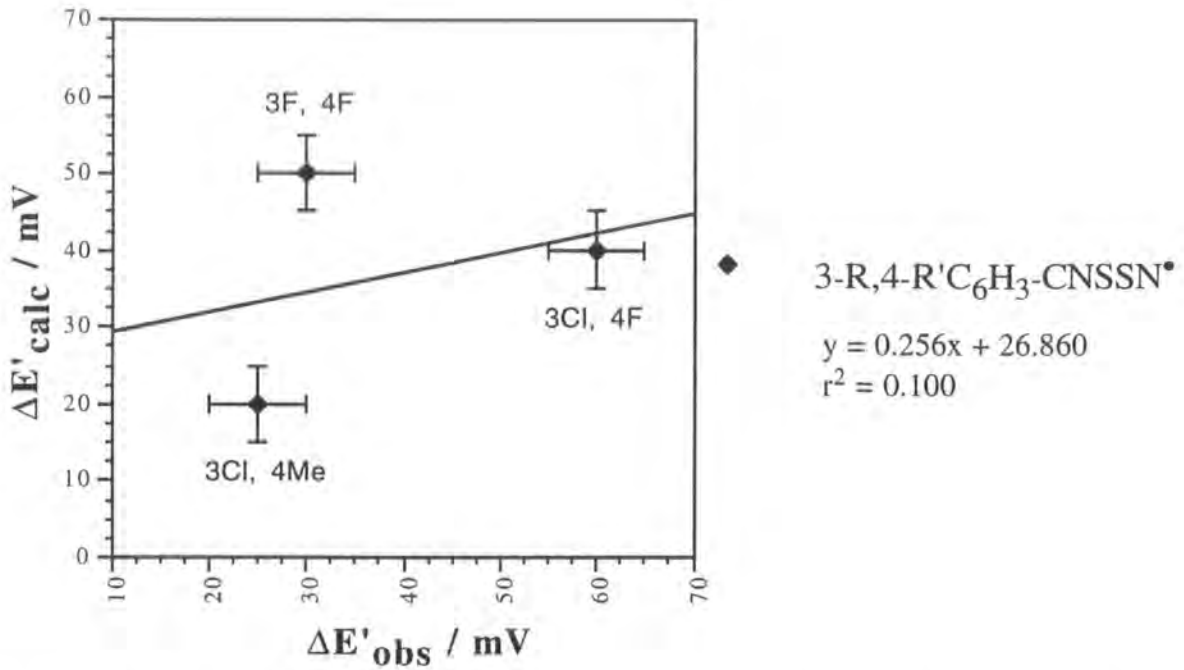

Fig 33. $\Delta E'_{obs}$ versus $\Delta E'_{calc}$ values of some di-substituted phenyl 1,2,3,5 dithiadiazolyls studied by CV, in MeCN, concentration $1x10^{-3}M$, temperature 0°C, supporting electrolyte $TBABF_4$.

2D.5.3 Hammett

When the results in Table 26 were plotted against each other a fair relationship was found, (r^2=0.863), see Fig 34.

Again, as there are so few points the reliability of such a plot is open to question. However there is very strong supporting evidence, as follows.

sample		$E_{pc/2}$ /mV	Σσ
3	4		
Cl	Me	615	0.203
F	F	632.5	0.399
Cl	F	650	0.435

Table 26. Σσ and $E_{pc/2}$ values from CV investigation of some di-substituted phenyl 1,2,3,5 dithiadiazolyls, in MeCN, concentration $1x10^{-3}M$, temperature 0°C, supporting electrolyte $TBABF_4$.

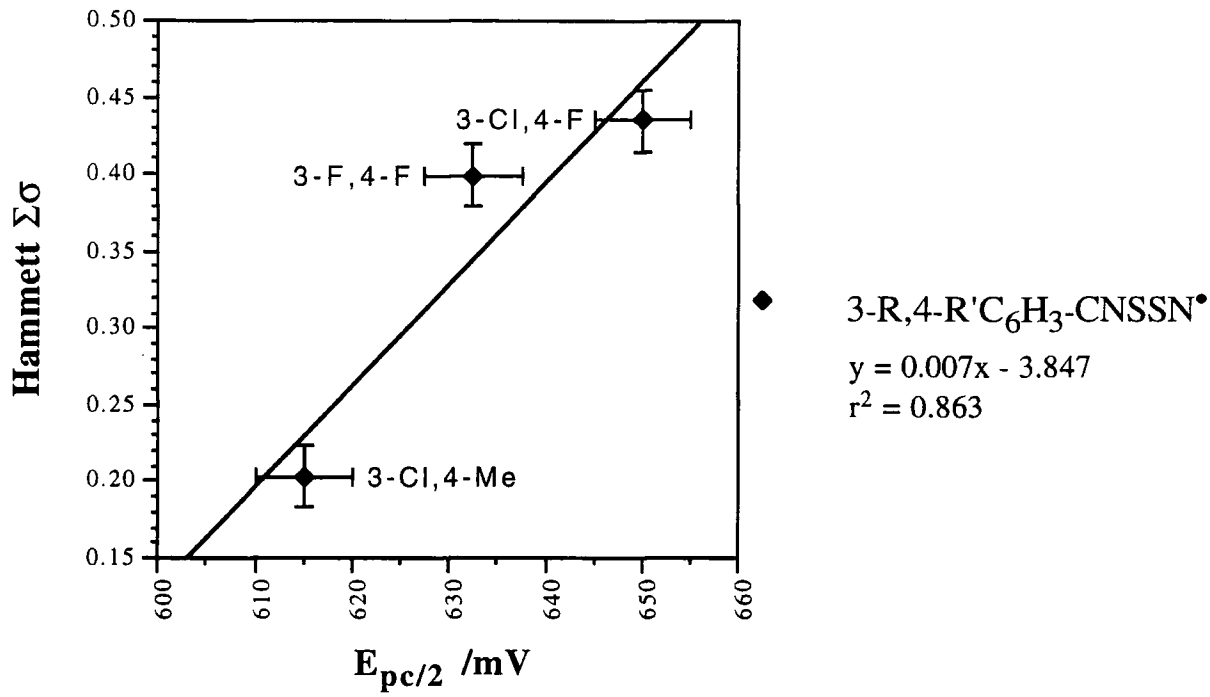

Fig 34. $E_{pc/2}$ versus Hammett Σσ values of some di-substituted phenyl 1,2,3,5 dithiadiazolyl derivatives studied by CV, in MeCN, concentration $1x10^{-3}$M, temperature 0°C, supporting electrolyte $TBABF_4$.

Looking back at the earlier results obtained from *para* and *meta* derivatives of these compounds in chapter 2B and 2C, excellent linear free energy relationships of this type were found to exist. It is known from studying the *ortho* and difluoro analogues that steric interactions can effect Hammett plots due to different electronic effects substituents place on the electronic environment of reaction centres. Therefore as these derivatives are in the *meta* and *para* positions and possess groups which do not sterically interact with each other it is extremely likely that such a free energy relationship can exist. Slight deviations from linearity are readily explained using the same arguments as for the *para* and *meta* mono substituted derivatives and by minor resonance contributions that can exist between the disubstituted derivatives.

As mentioned before with the ΔE' plots, data from other di-substituted analogues are required in order to make a conclusive judgement as to whether such relationships do exist for *meta* and *para* di-substituted phenyl 1,2,3,5 dithiadiazolyls.

2D.6.1 Conclusions

All of the di-substituted compounds studied were found to exhibit the same electrochemical quasi-reversible response as those of their mono-substituted cousins, therefore this is an indication that they all undergo a similar electrochemical reduction mechanism.

These preliminary results suggest that for a family of disubstituted derivatives, containing the same substituent groups, a satisfactory trend between $\Delta E'_{calc}$ and $\Delta E'_{obs}$ is to be expected, except for 2,6 derivatives or for very bulky substituents when additional steric interactions affect the electronic environment of the ring. The same compounds would not be expected to form a relationship between $E_{pc/2}$ values and corresponding Hammett $\Sigma\sigma$ values, mainly due to the difference in electronic and steric influence of these groups on the carboxylic acid and the dithiadiazolylium functional groups.

For the preliminary CV study on the 3,4 di-substituted derivatives the reverse of the above is observed, i.e, good Hammett and negligible $\Delta E'$ relationships exist. But due to the limited number of data points further investigation is required in order to establish such correlations. Referring back to the excellent analogous results for *meta* and *para* monosubstituted derivatives, it is not unreasonable to assume a linear free energy relationship could exist for disubstituted derivatives possessing only *meta* and *para* substituents too. However deviations could occur due to some substituent groups sterically impinging upon each other and supplementary resonance contributions between the substituents.

ΩΩΩΩΩΩΩΩΩΩΩΩΩΩΩΩΩΩΩΩΩΩΩΩΩΩΩΩΩΩΩΩΩΩΩΩΩΩΩ

Section 2E

ΩΩΩΩΩΩΩΩΩΩΩΩΩΩΩΩΩΩΩΩΩΩΩΩΩΩΩΩΩΩΩΩΩΩΩΩΩΩΩ

2E Electrochemistry of pyridyl 1,2,3,5 dithiadiazolylium and dithiadiazolyl derivatives.

2E.1.1 Introduction

The last set of CV investigations centred around the electrochemistry of pyridyl 1,2,3,5 dithiadiazolylium salts and related compounds. This enabled an investigation into the effect that the replacement of one of the aryl carbons by a heteroatom had on the electrochemistry of these dithiadiazolylium/zolyl species.

2E.1.2 CV measurements conducted in MeCN

The plan was to investigate the successfully synthesised para and meta pyridyl 1,2,3,5 dithiadiazolyls by CV. These two derivatives were found to be virtually insoluble in MeCN and hence other alternative avenues had to be explored. This included synthesising the 2,3,5,6 tetrafluoro 4-pyridyl derivative which was found to be extremely soluble as a radical or salt. Therefore this was ideal for an electrochemical investigation of the type previously conducted in Chapter 2A-D.

The CV results of the radical and the hexafluoroarsenate salt derivatives of this pyridyl tetrafluoro species revealed that their $E_{pc/2}$ values were almost identical to each other, 785mV and 790mV respectively, see Table 27, as these values are within the experimental error of 5mV of each other. They also exhibit the same quasi-reversible electrochemical responses. The above behaviour is typical of that observed for substituted phenyl 1,2,3,5 derivatives.

CV was conducted on a sample of 2,3,5,6 tetrafluoro 4-cyano phenyl 1,2,3,5 dithiadiazolyl to gauge the influence of the fluorines and the heteroatom place on the size of the $E_{pc/2}$ reduction potential. For this tetra fluoro cyano derivative the same quasi-reversible response was seen as for the analogous pyridyl derivative; an $E_{pc/2}$ value of 770V was recorded. Therefore the presence of four additional fluorines on para cyano phenyl 1,2,3,5 dithiadiazolyl raises the potential by some 110mV, (660mV). The act of changing the cyano group and a phenyl carbon by a heteroatom causes a further increase in potential of 15mV. Therefore the heteroatom acts as a better electron withdrawing group than the cyano derivative (assuming solvent effects are compatible). The meta analogue was not synthesised as the appropriate starting material was unavailable.

Sample		Scan rate mVs^{-1}	E_{pc} mV	$E_{pc/2}$ mV	i_{pc} μA	$E_{pc}-E_{pc/2}$ mV	E_{pa} mV	$E_{pa/2}$ mV	i_{pa} μA	$E_{pa}-E_{pa/2}$ mV	i_{pc}/i_{pa} μA	$E_{pa}-E_{pc}$ mV	$(E_{pa}+E_{pc})/2$ mV
pCN^F radical	A	324	710	770	33	60	800	710	28	90	1.18	110	755
		484	710	775	49	65	815	740	53	75	0.92	105	762.5
		576	700	770	53	70	820	740	62	80	0.85	120	760
ppy^F radical	A	400	710	780	30	70	810	730	35	80	0.86	100	760
		676	720	785	42.5	65	820	750	48	70	0.89	100	770
		729	720	785	44	65	820	750	49	70	0.90	100	770
ppy^F	A	324	735	795	34.4	60	825	765	36	60	0.96	90	780
AsF_6	B	324	730	790	45.2	60	820	760	46	60	0.98	90	775
salt	C	324	730	790	55.2	60	830	770	56.8	60	0.97	100	780

Table 27. Cyclic voltammetric data of 2,3,5,6 tetrafluoro 4-cyano phenyl-1,2,3,5-dithiadiazolyl (pCN^F) and 2,3,5,6-tetrafluoro 4-pyridyl dithiadiazolylium/dithiadiazolyl species (ppy^F) in MeCN at 0°C, concentration 1 x 10^{-3} M, supporting electrolyte $TBABF_4$.

2E.1.3 CV measurements conducted in SO_2

To overcome the problem of the solubility of the unfluorinated pyridyl derivatives a different solvent system was used for the electrochemical measurements. Out of many suitable solvents investigated none were found to dissolve the 4-pyridyl derivative, a discussion on why this is so can be found in the DSC section of chapter 4. However the meta analogue was found to readily dissolve in liquid SO_2 as did the already studied fluoro pyridyl derivatives[79].

Meta pyridyl 1,2,3,5 dithiadiazolylium chloride in liquid SO_2 gave a quasi-reversible electrochemical response. The peak to peak separation, E_{pa}-E_{pc} was shown to be on average twice as large as that observed for other derivatives studied in MeCN. Therefore in SO_2 the rate of charge transfer is slower and more irreversible in nature than in MeCN for substituted aryl dithiadiazolylium/zolyls, see Table 28.

An analogous CV study conducted on the para tetrafluoro derivative revealed electrochemical behaviour, similar to that for the previous compound. The $E_{pc/2}$ value for this compound was found to be 747.5mV, which is 17.5mV higher than that observed under similar conditions for the aforementioned meta analogue ($E_{pc/2}$=730mV).

CV studies of the hexafluoroarsenate and radical derivatives of the tetrafluoro pyridyl derivative in SO_2 gave similar quasi-reversible responses to the above compounds already studied in the solvent. They revealed the $E_{pc/2}$ value is highest for the hexafluoroarsenate salt (833mV), then the radical derivative (818mV) and lowest for the chloride salt (730mV). These results reveal that the hexafluoroarsenate is easiest to reduce and the chloride is the hardest derivative to reduce. This can be attributed to the favourable chloride ion interactions with the electropositive sulphurs of the cation, therefore reduction of the ring would severely weaken this association and hence this process is energetically not favoured. The difference between the potentials of the radical and hexafluoroarsenate salts is less obvious. As the hexafluoroarsenate is a spectator ion, it is assumed that both dithiadiazolylium/zolyls exist as monomeric species in the solution. However, the rings are not sufficiently different such that differing solvent effects, which are contributing to this trend, can readily be explained.

Sample		Scan rate mVs^{-1}	E_{pc} mV	$E_{pc/2}$ mV	i_{pc} µA	$E_{pc}-E_{pc/2}$ mV	E_{pa} mV	$E_{pa/2}$ mV	i_{pa} µA	$E_{pa}-E_{pa/2}$ mV	i_{pc}/i_{pa} µA	$E_{pa}-E_{pc}$ mV	$(E_{pa}+E_{pc})/2$ mV
mpy^H Cl-	A	400	640	730	176	90	845	745	178	100	0.99	205	742.5
	B	400	630	730	202	100	850	750	212	100	0.98	220	740
	C	841	620	720	205	100	850	750	220	100	1.15	230	735
ppy^F Cl-	A	196	650	750	116	100	850	750	106	100	1.09	200	750
		900	620	745	225	75	920	785	210	135	1.07	300	770
ppy^F radical	A	256	720	820	110	100	950	845	114	105	0.96	230	835
	B	676	740	815	54	75	900	835	44	95	1.23	160	820
ppy^F AsF_6	A	576	770	835	50	65	880	810	49.5	70	1.01	110	825
	B	676	765	830	49.5	65	880	810	48.5	70	1.02	115	822.5

Table 28. Cyclic voltammetric data of 2,3,5,6-tetrafluoro (ppy^F) and *meta* (mpy^H) pyridyl-1,2,3,5-dithiadiazolylium /dithiadiazolyl species in liquid SO_2 at **-15°C**, concentration ~1 x 10^{-3} M, supporting electrolyte $TBABF_4$.

2E.14 Conclusion

Comparing the $E_{pc/2}$ values obtained by CV for 2,3,5,6 tetrafluoro 4-pyridyl dithiadiazolylium salts and dithiadiazolyl it can be seen that higher $E_{pc/2}$ values are observed when measurements are conducted in SO_2 rather than MeCN. These can be due to two reasons: (i) These materials reduce more easily in SO_2 than the other solvent. The electronegativity of S, O and N are 2.5, 3.5 and 3.0 respectively (see Appendix A), hence electrostatic interactions involving S···O atoms will be stronger than S-N due to the greater difference in electronegativity values. Therefore, compared to MeCN, SO_2 is a more polar solvent which can interact more strongly with the ring system (via stronger S···O rather than S···N associations) resulting in better stabilisation of excess charge of the dithiadiazolyl ring. (ii) The CV responses of these materials are more quasi-reversible in SO_2 than MeCN. Therefore as the peaks spread out the cathodic wave will naturally go to higher potentials. The shape of the voltammogram traces indicate that charge transfer is slower in SO_2 than in MeCN for these compounds. Therefore, one would expect a greater shift of cathodic potentials to more positive potentials as observed. This is attributed to either SO_2 being more viscous or the compounds interacting better with this solvent than with MeCN under these experimental conditions, thus slowing down the charge transfer mechanism.

The range of the i_{pc} and i_{pa} values for some of the materials in SO_2 is greater than that observed in MeCN. Another difference is that it is harder to obtain solutions of samples of concentration $1x10^{-3}M$ in SO_2 than MeCN, particularly as the former solvent has to be condensed into the cell so that the exact volume of solvent is often difficult to gauge compared with the latter solvent for which a known volume can be syringed in to the cell. Looking at the Randles-Sevcik equation , Eqn (2), it is evident that i_{px} is proportional to the concentration of the material studied and hence the larger errors associated with the concentrations of solutions in SO_2, $1x10^{-3}M \pm 5x10^{-4}M$ than MeCN, $\pm 2x10^{-4}M$, readily explain why the range in i_{px} values is observed in SO_2 than the other solvent.

These pyridyl derivatives give similar quasi-reversible CV responses in MeCN to those observed for mono and disubstituted 1,2,3,5 phenyl dithiadiazolylium salts and related species. However in SO_2 these derivatives exhibit a higher degree of electrochemical quasi-reversibility (i.e. tending more towards irreversibility) and more positive $E_{pc/2}$ values than in MeCN.

Due to the lack of available σ values for pyridyl substituents, no plot between $E_{pc/2}$ potentials of these pyridyl dithiadiazolylium/zolyl derivatives versus corresponding Hammett σ values was undertaken.

ΩΩΩΩΩΩΩΩΩΩΩΩΩΩΩΩΩΩΩΩΩΩΩΩΩΩΩΩΩΩΩΩΩΩΩΩΩΩΩΩ

Section 2F

ΩΩΩΩΩΩΩΩΩΩΩΩΩΩΩΩΩΩΩΩΩΩΩΩΩΩΩΩΩΩΩΩΩΩΩΩΩΩΩΩ

2F Conclusion

2F.1 General Trends

The following series of compounds have been studied by CV:

- *Meta* and *para* substituted phenyl 1,2,3,5 dithiadiazolylium hexafluoroarsenate salts and related dithiadiazolyls.
- *Ortho* fluoro phenyl 1,2,3,5 dithiadiazolyl.
- *Ortho, meta* and *para* substituted phenyl 1,3,2,4 dithiadiazolylium hexafluoroarsenate salts.

- Difluoro substituted phenyl 1,2,3,5 dithiadiazolyls and associated 2,6 dithiadiazolylium derivative.
- Difluoro substituted phenyl 1,3,2,4 dithiadiazolylium hexafluoroarsenate salts.

- Disubstituted phenyl 1,2,3,5 dithiadiazolyls.
- Pyridyl 1,2,3,5 dithiadiazolylium and related dithiadiazolyl derivatives.

The following diagnostic features were observed for all of these derivatives:

---

(1) Randles Sevcik
Obey eqns (1) and (2)

(2) Half peak
E_{pc}-$E_{pc/2}$ is typically 60-70mV

(3) Peak separation
E_{pc}-E_{pa} > 59mV

(4) Scan rate
i_{pc}increases with υ

(5) Peak current
i_{pc}/i_{pa} does not always equal unity

(6) Potentials
E_{pc} and $E_{pc/2}$ decrease with increasing scan rate. The opposite occurs for the anodic potentials.

(7) Potentials
$E_{pc/2}$ most reproducible potential.

(8) 1,2,3,5 and 1,3,2,4 isomer
$i_{pc}/i_{pa} \geq 1$ for the 1,3,2,4 derivatives but $0<i_{pc}/i_{pa}>1$ for the 1,2,3,5 derivatives.

The above similarities in electrochemical process are highly suggestive that the same electrochemical mechanism is in operation for all of these derivatives regardless of the type, position and number of substituent group(s).

2F.2 Individual groups of compounds

2F.2.1 *Meta* and *para* derivatives

The potentials for all of the derivatives, with substituents that are *meta*, *para* or both increase with increasing electron withdrawing ability of the functional group(s).

The linear free energy relationships between $E_{pc/2}$ for *meta* and *para* derivatives and corresponding Hammett σ values found were excellent. The gradients of these plots were positive, signifying that electron-withdrawing substituent groups favour the reduction process. The ρ values of these plots were found to be within experimental error of each other, see Fig 35. This indicates that the substituent effect of *meta* and *para* groups of these 1,2,3,5 and 1,3,2,4 dithidiazolylium/zolyl systems are the same and comparable to those of benzoic acid analogues.

2F.2.2 *Ortho* derivatives

The failure of linear free energy relationships between *ortho* substituted benzoic acid and phenyl dithiadiazolylium/zolyl systems (Fig 35) is attributed to the steric intramolecular forces between these two groups of compounds are not comparable.

2F.2.3 Di-substituted derivatives

For the difluoro and disubstituted derivatives using the sum of the potentials of mono components can be used to gauge the order in which their potentials occur. The only failure of this method routinely occurs for di-*ortho* systems where steric interactions appear to distort the results.

For the 3,4 disubstituted derivatives more data are required before predictions in potentials, for these types of compounds, can be made with corresponding Hammett $\Sigma\sigma$ or $\Delta E'$ values.

2F.2.4 Pyridyl derivatives

For the pyridyl compounds it was shown for the tetrafluoro *para* derivative that the pyridyl nitrogen acts as a stronger electron withdrawing centre than a corresponding cyano group. Also, the pyridyl derivatives exhibited larger peak separations when studied electrochemically in SO_2 than in MeCN, i.e more quasi-reversible in nature.

2F.3 Conclusion

In summary, it can be ascertained from these electrochemical results that the quasi-reversible electrochemical characteristic of aryl 1,2,3,5 and 1,3,2,4 dithiadiazolylium and associated radicals is independent of position or number of substituents on the aryl ring when measurements are conducted under the following conditions: concentration ~$1x10^{-3}$M, supporting electrolyte $TBABF_4$ $1x10^{-1}$M, solvent MeCN at -15° to 0°C or solvent SO_2 at -15°C.

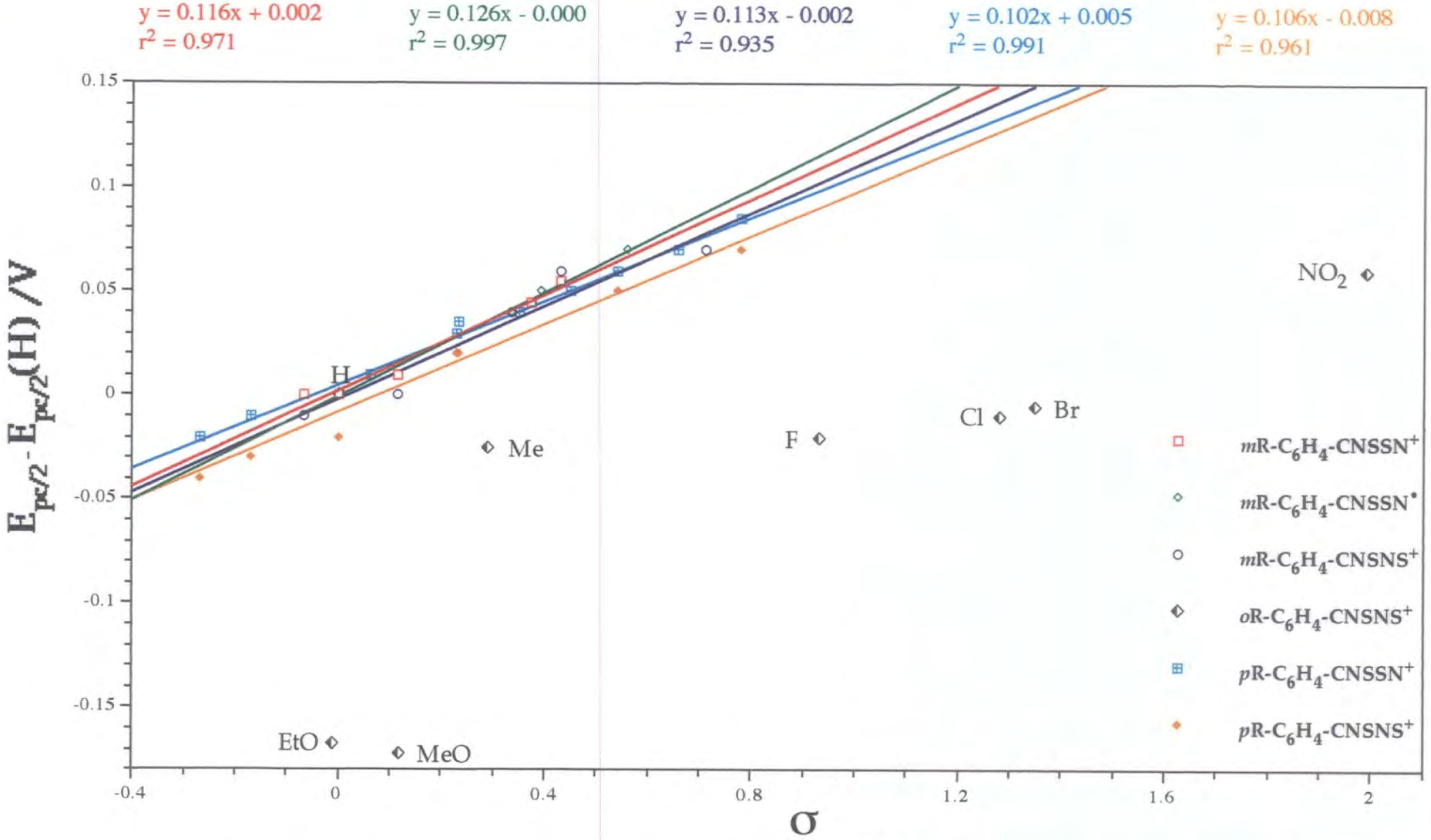

Fig 35. A plot of $E_{pc/2}$ values of some substituted phenyl 1,2,3,5 and 1,3,2,4 dithiadiazolylium salts and associated radicals versus Hammett σ values.

NB error bars not shown for clarity. For σ errors see sections 2B.1.7/2.8 & 2C.2.2/2.3/3.2/5.4. Standard error for $E_{pc/2}$ measurements are ± 5mV.

References :

1 (a) A. J. Banister and J. M. Rawson, *The Chemistry of Inorganic Ring Systems*, Ed., R. Steudel, Elsevier, Amsterdam, 1992, 323.
(b) A. W. Cordes, R. C. Haddon and R. T. Oakley, *The Chemistry of Inorganic Ring Systems*, Ed., R. Steudel, Elsevier, Amsterdam, 1992, 295.

2 (a) A. J. Banister and J. M. Rawson, *Chem. Br.*, 1992, 148.
A. J. Banister, I. Lavender, J. M. Rawson and W. Clegg, *J. Chem. Soc., Dalton Trans.*, 1992, 859.
(b) C. M. Aherne, A. J. Banister, A. W. Luke, J. M. Rawson and R. J. Whitehead, *J. Chem. Soc., Dalton Trans.*, 1992, 1277.
(c) A. J. Banister, I. Lavender, J. M. Rawson and R. J. Whitehead, *J. Chem. Soc., Dalton Trans.*, 1992, 1449.

3 S. Parsons, J. Passmore, M. J. Schriver and P. S. White, *J. Chem. Soc., Chem. Commun.*, 1991, 369.

4 (a) A. W. Cordes, R. C. Haddon, R. T. Oakley, L. F. Schneemeyer, J. V. Waszczak, K. M. Young and N. M. Zimmerman, *J. Am. Chem. Soc.*, 1991, 113, 582.
(b) M. P. Andrews, A. W. Cordes, D. C. Douglass, R. M. Fleming, S. H. Glarum, R. C. Haddon, P. Marsh, R. T. Oakley, T. T. M. Palstra, L. F. Schneemeyer, G. W. Trucks, R. Tycko, J. V. Waszczak, K. M. Young and N. M. Zimmerman, *J. Am. Chem. Soc.*, 1991, 113, 3559.
(c) A. W. Cordes, R. C. Haddon, R. G. Hicks, D. K. Kennepohl, R. T. Oakley, L. F. Schneemyer and J. V. Waszczak, *Inorg. chem.*, 1993, 32, 1554.

5 (a) A. J. Banister, M. I. Hansford, Z. V. Hauptman, A. W. Luke, S. T. Wait, W. Clegg and K. A. Jørgensen, *J. Chem. Soc., Dalton Trans.*, 1990, 2793.
(b) C. D. Bryan, A. W. Cordes, R. C. Haddon, R. G. Hicks, R. T. Oakley, T. T. M. Palstra, A. S. Perel and S. R. Scott, *Chem. Mater.*, 1994, 6, 508.

6 A. J. Banister, N. Bricklebank, W. Clegg, M. Elsegood, C. I. Gregory, I. Lavender, J. M. Rawson and B. Tanner, *manuscript submitted for publication* 1995.

7 A. W. Cordes, C. D. Bryan, W. M. Davis, R. H. de Laat, S. H. Glarum, J. D. Goddard, R. C. Haddon, R. G. Hicks, D. K. Kennepohl, R. T. Oakley, S. R. Scott and N. P. C. Westwood, *J. Am. Chem. Soc.*, 1993, 115, 7232.

8 Y. Miura, A. Yamamoto and M. Kinoshita, *Electrochimica Acta*, 1984, 29, No 12, 1731.

9 M. R. Bryce, *J. Chem. Soc., Perkin Trans. I*, 1985, 1675.

10 The Southampton Electrochemistry Group, *Instrumental Methods in Electrochemistry*, Ellis Horwood Ltd, Chichester, 1985.

11 A. J. Bard and L. R. Faulkner, *Electrochemical Methods*, John Wiley and Sons, N.Y., 1980.

12 B. S. Jensen and V. D. Parker, *J. Am. Chem. Soc.*, 1975, 97, No 18, 5211.

13 R. Varma and J. R. Selman, *Techniques for Characterisation of Electrodes and Electrochemical Processes*, John Wiley and Sons, N. Y., 1991.

14 D. H. Evans, K. M. O'Connell, R. A. Petersen and M. J. Kelly, *J. Chem. Education*, 1983, 60, No. 4, 290.

15 R. S. Nicholson, *Anal. Chem.*, 1965, 37, No. 11, 1351.

16 T. Lund and S. U. Pedersen, *J. Electroanal. Chem.*, 1993, 362, 109.

17 R. S. Nicholson and I. Shain, *Anal. Chem.*, 1964, 36, No 4, 706.

18 G. Q. Lu and Z. B. Hu, *Bull. Electrochem.*, 1988, 4(8), 763.
19 D. Osella, M. Ravera, S. V. Kukharenko, V. V. Strelets and C. E. Housecroft, *J. Orgmet. Chem.*, 1991, 417(3), 421.
20 P. H. Rieger, *Electrochemistry*, 2nd Edn, Chapman and Hall, N.Y., 1994.
21 R. R. Gupta, *Physical Methods in Heterocyclic Chemistry*, J. Wiley and Sons, N. Y., 1984.
22 R. H. Wopschall and I. Shain, *Analytical Chemistry*, 1967, 39, No. 13, (a) 1514 , 1527 and 1535.
23 J. Koryta, J. Dvorak and L. Kavan, *Principles of Electrochemistry*, 2nd Edn, John Wiley and Sons, Chichester, 1993.
24 A. M. Bond and M. A. Khalifa, *Inorg. Chem.*, 1987, 26, 413.
25 C. Sridevi and S. J. Reddy, *Bull. Electrochem.*, 1990, 6(10), 847.
26 H. Lund and M. M. Baizer, *Organic Electrochemistry*, Marcel Dekker Inc., N. Y., 1991.
27 A. J. Banister, Z. V. Hauptman, A. G. Kendrick and R. W. H. Small, *J. Chem. Soc., Dalton Trans.*, 1987, 915.
28 (a) R. S. Nicholson, *Anal. Chem.*, 1965, 37, 667.
(b) W. T. de Vries and E. Dalen, *J. Electroanal. Chem.*, 1965, 10, 183.
29 Y. Zhang, C. D. Baer, C. Camaioni-Neto, P. O'Brien and D. A. Sweigart, *Inorg. Chem.*, 1991, 30, 1682.
30 A. Kapyurkiewicz and B. Behr, *Inorganica Chim. Acta*, 1983, 69, 247.
31 M. Lapkowski and W. Szulbinski, *Bull. Electrochem.*, 1992, 8(9), 436.
32 H. H. Williams, L. L. Merritt and J. A. Dean, *Instrumental Methods of Analysis*, Van Nostrand-Reinhold, N. Y., 1965.
33 C. K. Mann and K. K. Barnes, *Electrochemical Reactions in Nonaqueous Systems*, Marcel Dekker, N. Y., 1970.
34 M. I. Hansford, Ph.D Thesis, Durham, England, 1989
35 D. Dubois, G. Moninot, W. Kutner, M. T. Jones and K. M. Kadish, *J. Phys. Chem.*, 1992, 96, 7137.
36 C. Swistak and K. M. Kadish, *Inorg. Chem.*, 1987, 26, 405.
37 E. B. Smith, *Basic Chemical Thermodynamics*, 3rd Edn, Oxford University Press, N. Y. 1982.
38 R. T. Boeré, K. H. Moock and M. Parvez, *Z. anorg. allg. Chem.*, 1994, 620, 1589.
39 (a) F. D. Saeva, G. R. Olin, *J. Am. Chem. Soc.*, 1980, 102, No. 1, 299.
(b) S. Bank, C. L. Ehrlich and J. A. Zubieta, *J. Org. Chem.*, 1979, 44, No. 9, 1454.
40 N. S. Isaacs, *Physical Organic Chemistry*, Longman Scientific and Technical, U.K., 1987.
41 C. D. Johnson, *The Hammet Equation*, Cambridge University Press, 1973.
42 T. H. Lowry and K. S. Richardson, *Mechanism and Theory in Organic Chemistry*, 3rd Edn, Harper and Row, N. Y., 1987.
43 L. P. Hammett, *Physical Organic Chemistry*, McGraw-Hill Book Co. Inc., N. Y., 1940, 186.
44 (a) D. H. McDaniel and H. C. Brown, *J. Org. Chem.*, 1958, 23, 420.
(b) C. G. Swain and E. C. Lupton Jr., *J. Am. Chem. Soc.*, 1968, 90, 4328.
45 W. A. Sheppard, *J. Am. Chem. Soc.*, 1961, 83, 4860.
46 A. Aalstad and V. D. Park, *J. Electroanal. Chem.*, 1980, 112, 163.
47 (a) C. Aherne, A. J. Banister, A. W. Luke, J. M. Rawson and R. J. Whitehead, *J. Chem. Soc., Dalton Trans.*, 1992, 1277.

(b) N. Burford, J. Passmore and M. J. Schriver, *J. Chem. Soc., Chem. Commun.*, 1986, 140.
48 C. M. Aherne, A. J. Banister, I. B. Gorrel, A. W. Luke, M. I. Hansford, Z. V. Hauptman and J. M. Rawson, *J. Chem. Soc., Dalton Trans.*, 1993, 967.
49 *A. W. Luke, Ph. D Thesis, Durham, England, 1992*
50 J. Clark, D. D. Perrin, *Quart. Rev.*, 1964, 18, 295.
51 R. Jones, *Physical and Mechanistic Organic Chemistry*, 2nd Edn, Cambridge University Press, Cambridge, 1985
52 L. P. Hammett, *J. Am. Chem. Soc.*, 1937, 59, 96.
53 P. W. Atkins, *Physical Chemistry*, 3rd Edn, Oxford University Press, Oxford, 1987.
54 R. W. Brockman and D. E. Pearson, *J. Am. Chem. Soc.*, 1952, 74, 4128.
55 R. W. Taft Jr. and I. C. Lewis, *J. Am. Chem. Soc.*, 1959, 81, 5343.
56 A. H. Maki and D. H. Geske, *J. Am. Chem. Soc.*, 1961, 83, 1852.
57 S. V. Jovanovic, M. Tosic and M. G. Simic, *J. Phys. Chem.*, 1991, 95, 10824.
58 R. Muller, B. Dakova, L. Lamberts and M. Evers, *Electrochim. Acta*, 1994, 39, No. 13, 1961.
59 B. Dakova, J. M. Kauffman, M. Evers, L. Lamberts and G. J. Patriarche, *Electrochim. Acta*, 1990, 35, No. 7, 1133.
60 B. Dakova, L. Lamberts, M. Evers and N. Dereu, *Electrochim. Acta*, 1991, 36, No. 314, 631.
61 (a) P. Zuman and D. J. Voaden, *Tetrahedron*, 1961, 16, 130.
(b) M. Fields, C. Valle and M. Kane, *J. Am. Chem. Soc.*, 1949, 71, 421
62 Cohen, Streitwieser and Taft, Ed, *Progress in Physical Organic Chemistry*, Vol 2, John Wiley and Sons, 1964, p323.
63 C. A. Grob, *Acc. Chem. Res.*, 1983, 16, 426.
64 (a) A. C. Nixon, G. E. K. Branch, *J. Am. Chem. Soc.*, 1936, 58, 492.
(b) H. C. Brown and Y. Okamoto, *J. Am. Chem. Soc.*, 1958, 80, 4979.
65 (a) R. W. Taft Jr., *J. Am. Chem. Soc.*, 1952, 74, 2729.
(b) R. W. Taft Jr., *J. Am. Chem. Soc.*, 1953, 75, 3120.
66 H. H. Jaffé, *Chem. Rev.*, 1953, 53, 191.
67 G. B. Barlin and D. D. Perrin, *Chem. Soc. Quart. Rev.*, 1966, 75.
68 J. E. Leffer and E. Greenwald, *Rates and Equilibria of Organic Reactions*, Wiley, N. Y., 1963.
69 Y. Okamoto, T. Inukai and H. C. Brown, *J. Am, Chem. Soc.*, 1958, 50, 4972.
70 T. Hibbert, MSc. Thesis, Durham, England, 1993.
71 (a) T. Fujita and T. Nishioka, *Prog. Phys. Org. Chem.*, 1976, 12, 49.
(b) M. Charton, *Prog. Phys. Org. Chem.*, 1971, 8, 235.
72 V. Lopez, J. Catalan, R. M. Claramunt, C. Lopez, E. Cayon and J. Elguero, *Can. J. Chem.*, 1990, 68, 958.
73 K. V. Reddy and S. Reddy, *Bull. Electrochem.*, 1986, 2(5), 481.
74 M. J. Bausch, C. Guadalupe-Fasano and A. Koohang, *J. Phys. Chem.*, 1991, 95, 3420.
75 B. Juan, J. Schwarz and R. Breslow, *J. Am. Chem. Soc.*, 1980, 102, 5741.
76 Y. Miura and A. Tanak, *Electrochim. Acta.*, 1992, 37, No. 11, 2095.
77 J. F. J. Dippy and S. R. C. Hughes, *Tetrahedron*, 1963, 19, 1527.
78 D. H. Geske, J. L. Ragle, M. A. Bambenek and A. L. Balch, *J. Am. Chem. Soc.*, 1964, 86, 987.
79 J. B. Chlistunoff and A. J. Bard, *Inorg. Chem.*, 1992, 31, 4582.

Chapter 3

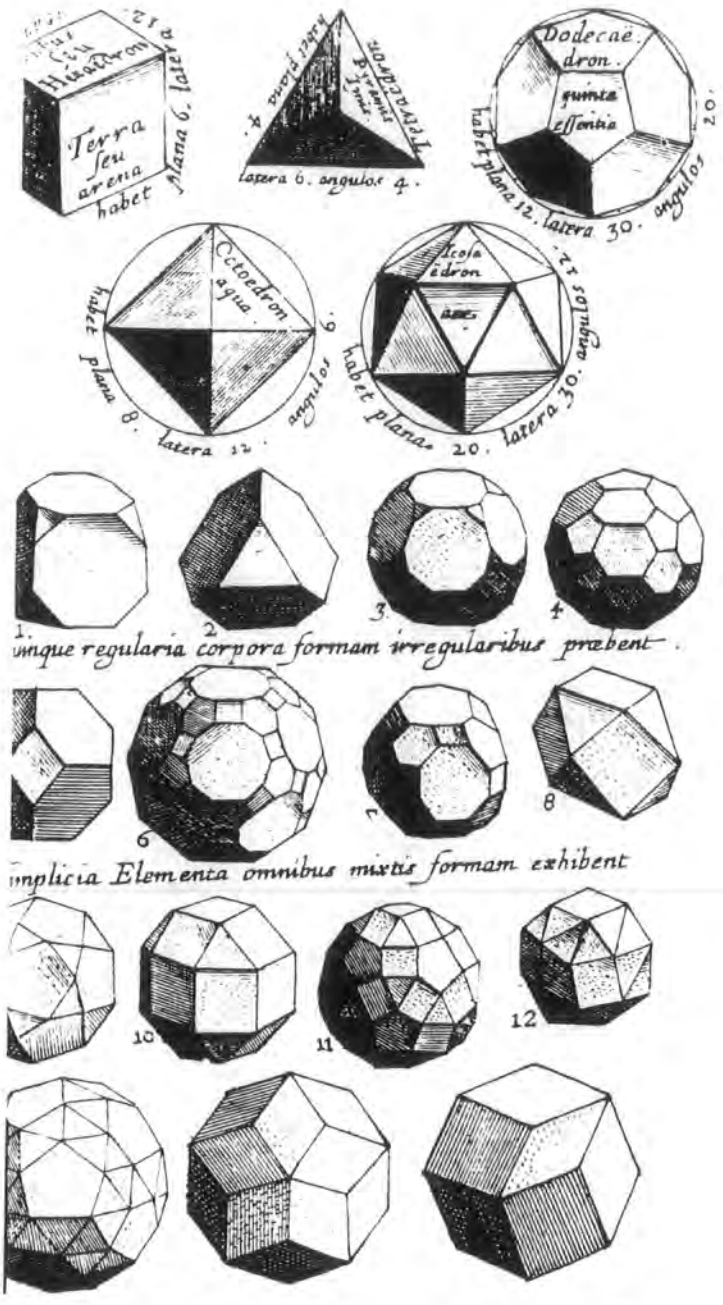

VI WM. DAVISSON'S SCHEME FOR ANALYZING SUBSTANCES IN TERMS OF THE FIVE 'PERFECT' SOLID FIGURES

From his *Philosophia pyrotechnica*, Pt. III, Paris, 1642

3A Introduction

This chapter is solely dedicated to structural analysis of 1,2,3,5 dithiadiazolyl derivatives. Here follows a brief structural history of these compounds. (N.B. esd's are given whenever possible).

3A.1.1 Crystallographic History of Dithiadiazolyls

The first reported structure, on one of these compounds, was that of the phenyl derivative, by Banister et al in 1980[1]. The structure revealed that its molecules exist as dimers via four centred S···S interactions involving 2π electrons, see Fig 1a. The average S···S intradimer distance is found to be 3.112(4)Å. These dimers were found to pack perpendicular to each other with interdimer S···N and S···S contacts of 3.090(7)Å and 3.402(4)Å respectively, see Fig 1b.

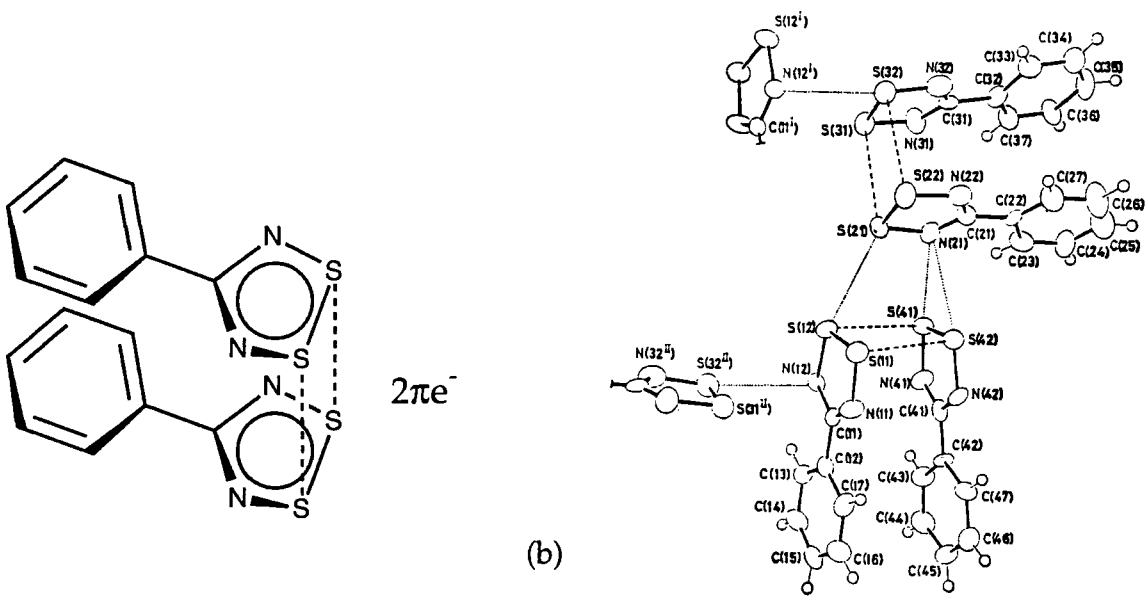

Fig 1. (a) Dimer unit and (b) molecular packing of phenyl 1,2,3,5 dithiadiazolyl

Some 5-10 years later, the next solid state investigations involved the following substituted 1,2,3,5 dithiadiazolyls, containing CF_3[2], Me[3] or NMe_2[4] at the 4-position. These three compounds were found to exist as dimers via just one S···S interaction of 2.988(2)Å, 3.108(2)Å and 3.036(1)Å respectively, see Fig 2a, b and c. This observed difference in the mode of dimerization, relative to the phenyl derivative, is almost certainly due to greater steric repulsions between these substituent groups which prevent the molecules of the dimer packing in the cisoid fashion of the phenyl compound.

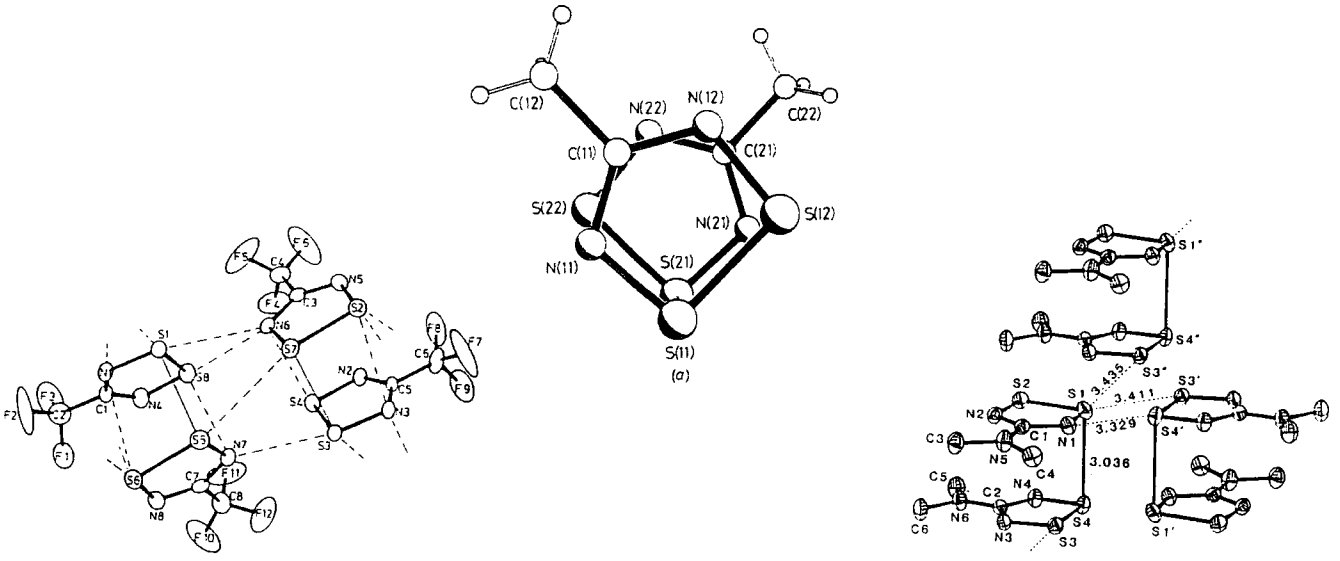

(a) (b) (c)

Fig 2 Molecular packing of (a) trifluoromethyl, (b) methyl and (c) dimethylamino 1,2,3,5 dithiadiazolyls.

It was evident from these studies that molecular substitution had a significant effect on the interactions and molecular packing arrangement of these types of compounds. Using this information, in conjunction with the knowledge that these moieties possess an unpaired electron and have the ability to form interesting S···S interactions, it was apparent that derivatives of these compounds might exhibit interesting conducting and magnetic properties. Below is a list of packing criteria for such materials.

Conduction

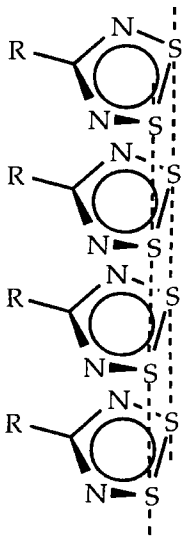

Molecules need to form vertical arrays with S···S interactions running down the stack so that a conduction band involving π-electrons forms[5].

If the S···S interactions are close and relatively evenly spaced a conducting material will result.

If the molecules stack but tend to form dimers so that inter and intra dimer distances differ then the molecule suffers from Peierls distortions and is usually a semiconductor.

An insulator is obtained when the S···S interdimer interactions along the stack are greater than the van der Waals radii or when no vertical stacking occurs.

Magnetism

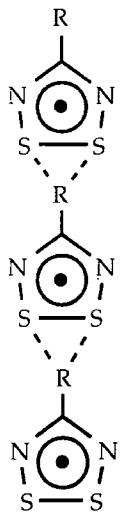

A major requirement for these materials to exhibit interesting magnetic properties is that the radicals must retain their free radical/paramagnetic nature in the solid state, i.e. exist as monomers[6]. The type of spin-spin exchange between radicals determines the bulk magnetic behaviour leading to ferro or anti-ferromagnetism. Spin-spin exchange for a system is influenced by solid state arrangement of the molecules and is favourable when the monomers pack in parallel ribbon type arrays.

The four compounds discussed so far were all shown to be poor conductors and weakly magnetic. These results can be attributed to their individual molecular packing. Of these four compounds, the molecules of the phenyl derivative came closest to achieving ideal packing required for a conducting or magnetic material, as it was the only one to form cisoid dimers involving four-centred S···S interactions. It was also apparent from looking at the other three structures that steric hindrance from the small substituents groups was responsible for them packing differently relative to the phenyl derivative. Therefore, with a view to achieving conducting and magnetic materials modification of the phenyl derivative, by the addition of substituent groups, in order to promote favourable planar monomeric or polymeric packing, definitely appeared to be a very attractive option at this stage.

Hence research in this area in the 1990's has heavily focused towards aryl derivatives of this type. Other types of dithiadiazolyls were not considered due to constraints in synthesis, e.g. vinyl groups.

Investigations on dithiadiazolylium charge transfer salts were also conducted and findings can be found in references 7. Now follows a discussion on structural developments for substituted aryl dithiadiazolyls over the past six years.

One of the initial structures determined on one of these types of compounds was that of the *para* chloro phenyl 1,2,3,5 dithiadiazolyl, from crystals grown by I.Lavender[8]. This compound was found to form co-facial dimers which pack perpendicular to each other forming sheets like its phenyl analogue. But, the similarity ends here as adjacent dimers of the chloro

derivative align anti-parallel to each other which facilitates two parallel S···N interactions between two dithiadiazolyl rings in this plane, see Fig 3.

Work conducted around the same time by Oakley and co-workers had centred around cyano and bis aryl dithia- and diseleno- diazolyls. Diselenodiazolyl derivatives[9] will not be discussed further as the main focus here is on the analogous sulphur derivatives.

The first two published structures were the 1,4 and 1,3 phenylene bis dithiadiazolyls[10]. The 1,4 species was found to pack as cis-oid dimers in herring bone arrays, see Fig 4a.

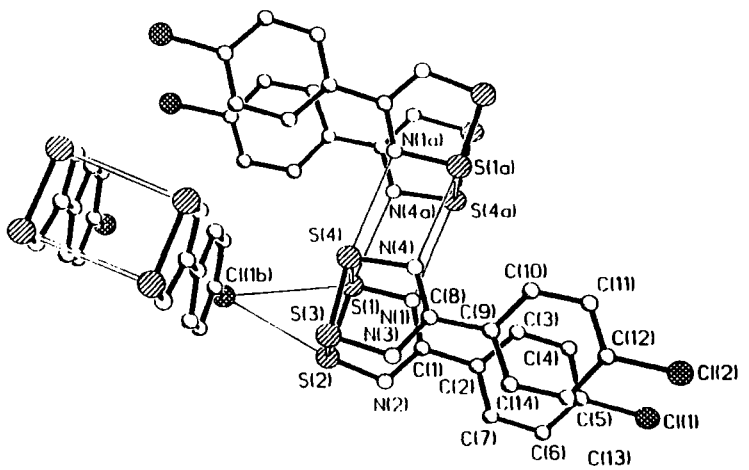

Fig 3. *Para* chloro phenyl 1,2,3,5 dithiadiazolyl

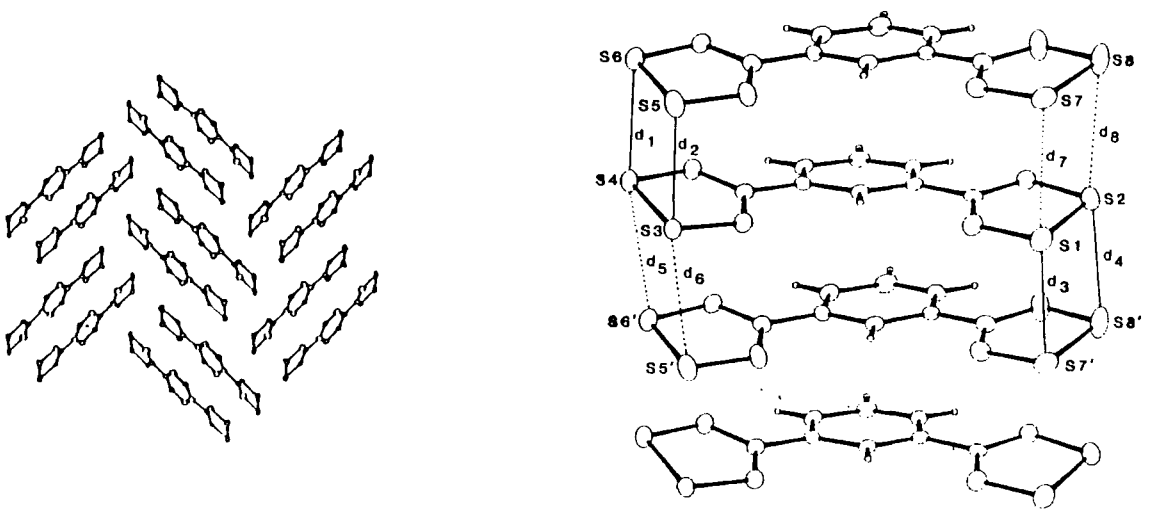

(a) (b)

Fig 4. Packing diagrams of (a) 1,4 and (b) 1,3-phenylene bis 1,2,3,5-dithiadiazolyl.

However, for the 1,3 compound, its co-facial dimers were found to stack on top of one another with S···S interactions running down the stack. Closer examination of the S···S inter and intra dimer stack interactions reveals, that between two molecules in a stack both types of dimer interactions are present and that this pattern alternates down the stack between either end, see Fig 4b. These sulphur contacts are typically 3.966Å and 3.140Å respectively. Consequently, this material suffers from Peierls distortions[11] (i.e. prone to dimerise) and is found to be an insulator (conductivity ~10^{-7}Scm^{-1} at 470K). These columns are arranged in a pin wheel packing pattern.

Further work, by this Canadian group, on *meta* and *para* cyano derivatives revealed some interesting new packing arrangements[12]. These compounds all packed head to tail with interactions between the nitrile nitrogen and the two sulphurs. The *para* derivative formed parallel rows of dimers which packed anti-parallel with neighbouring adjacent rows. This derivative did form stacks but they too were arranged anti-parallel to each other. The *meta* derivative existed as two phases. The α phase formed snake like ribbons which overlapped each other to form vertical dimer stacks, see Fig 5a. Again this compound like the 1,3 bis analogue suffered from Peierls distortions and is an insulator. For the additional β-*meta* phase the snake like ribbons consist of trans anti-facial dimer pairs which do not stack, see Fig 5b.

The formation of these two radical phases is further evidence that there are only small energy differences between different solid state arrangements, especially with regards to dimerization energies and other secondary contacts[13]. Therefore, minor changes in the substituent groups may drastically change the nature and type of molecular packing.

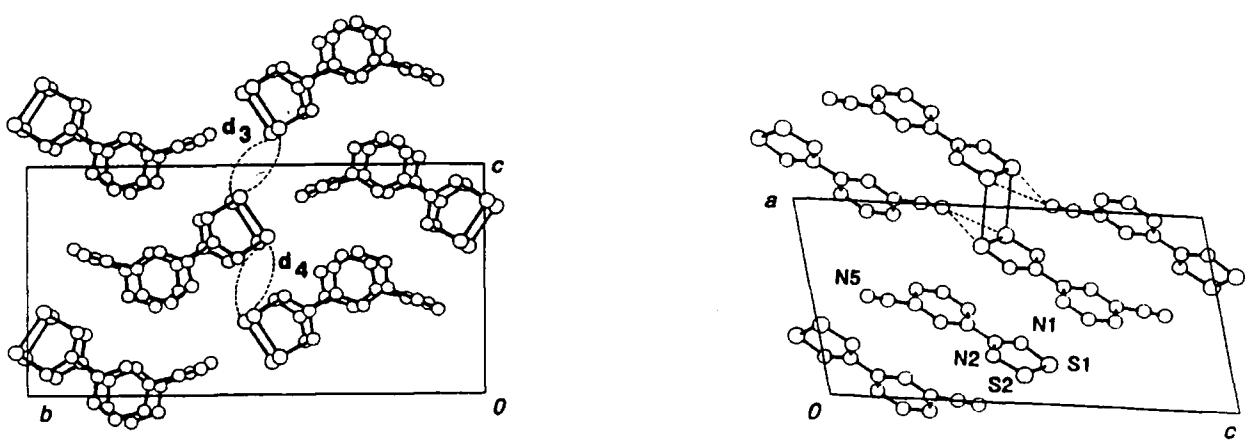

Fig 5. Packing diagrams of (a) α and (b) β-*meta* cyano phenyl dithiadiazolyls

Three aryl derivatives containing heteroatoms, (triazine tris, 2-cyano furanyl 5- and 2,5 furanyl bis dithiadiazolyls), have also been studied briefly by this group in their search for a conducting material[14]. All exist as dimers. The first compound forms linear ribbons whose dimers do not stack. The second compound packs in herring bone arrays and the last one packs similar to the α-*meta* cyano phenyl analogue.

For these furanyl compounds the oxygen heteroatom in the aryl ring is sterically hindered by *ortho* positioned dithiadiazolyl or cyano groups and therefore has negligible influence on the packing arrangements of these compounds.

Some of the continuing work by the Banister research group in this field has centred around aryl perfluorinated systems,

These were primarily investigated to see the effect that electron withdrawing groups would have on the S-S bond length and S···S intradimer distance. Preliminary ESR studies on Ph-CNSSN•, CH_3-CNSSN• and their perfluorinated analogues showed that the fluoro electron withdrawing groups pull charge away from the nitrogens towards the molecular extremities, including the sulphurs[15]. Consequent x-ray structures of these compounds revealed that they exist as dimers in which the intradimer S···S distance is shorter in the fluoro compounds than in the hydrogen analogues [C_6F_5-CNSSN• 3.067(2) and PhCNSSN• 3.109(5)]. Therefore, it was considered that greater S···S overlap or conductivity could be achieved using fluorinated and other electron-withdrawing substituents. Now follows more detailed description of the compounds examined.

The structure of the perfluorinated phenyl derivative revealed that its molecules existed as dimers which packed head to tail to form ribbons[16]. Adjacent ribbons packed anti-parallel, with the dithiadiazolyl rings packing side by side and close enough for S···N interactions to link them together, see Fig 6. This packing was dissimilar to that observed for PhCNSSN• analogue. There also exists a large twist angle between the dithiadiazolyl and aryl ring of 38.2(4)°, (the typical twist angle for the previous aryl derivatives is less than 15°). This helps to minimise $F^{\delta-}\cdots F^{\delta-}$ repulsions and allows preferable S···N, S···S and S···F interactions to occur.

Analogous studies of the 2,3,5,6-tetrafluoro-1,4-phenylene - bis 1,2,3,5 dithiadiazolyl showed that it too existed as a dimer but it didn't pack in a herring bone arrays like its hydrogen analogue[17]. Instead, the molecules pack

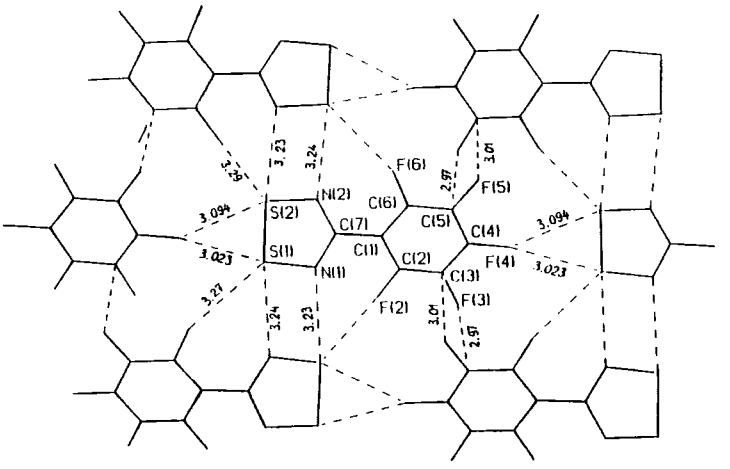

Fig 6a. Above view of molecular packing of perfluoro phenyl 1,2,3,5 dithiadiazolyl.

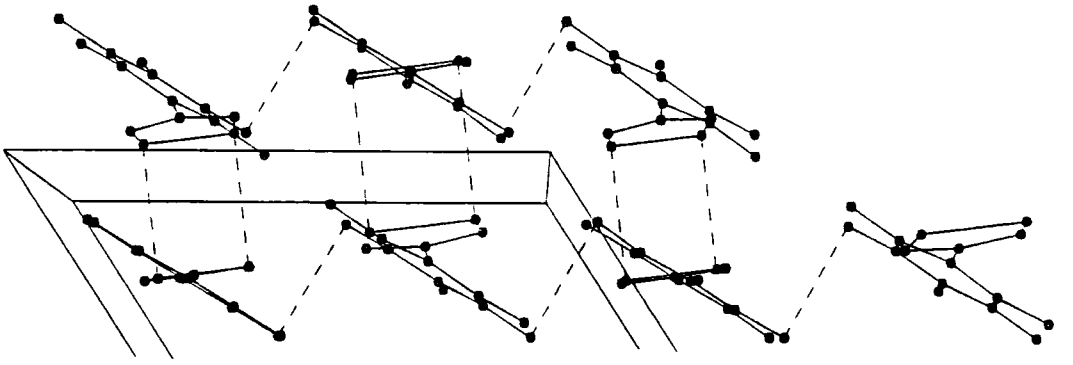

Fig 6b. Side view of molecular packing of perfluoro phenyl 1,2,3,5 dithiadiazolyl.

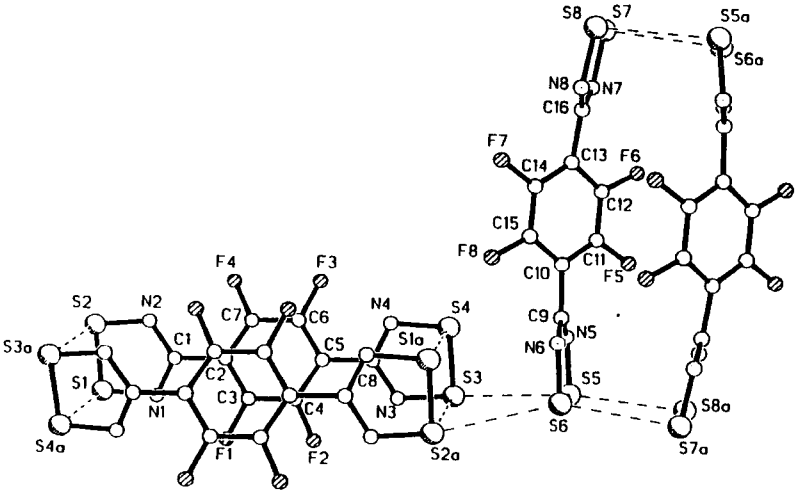

Fig 7. S···S interactions of •NSSNC-C_6F_4-CNSSN•.

perpendicular to each other such that the distance between the sulphurs involved in one intradimer interaction and the two sulphurs bonded together in a neighbouring dimer molecule is smaller than the sum of their van der Waals radii, i.e. S···S contacts exist, see Fig 7. A large twist angle between the phenyl and both dithiadiazolyl rings is also observed, (25.9(6)° and 42.7(6)° for A and B of Fig 8 respectively).

The following compound was found to have a remarkable and unique solid state packing. The *para*-cyano-tetrafluorophenyl dithiadiazolyl was found to exist as a monomer[18]. This is the only dithiadiazolyl to date that has ever been reported to exist as a monomer in the solid state at RTP. It exists in two phases, needles and blocks. The monomers of both form ribbons which pack adjacent to each other, in which the molecules pack head to tail via nitrile nitrogen and sulphur interactions, (c.f. *m* and *p* cyanophenyl analogues). These ribbons are found to pack anti-parallel and parallel to each other in the blocks and needles respectively, see Fig 8. These monomeric ribbons stack on top of one another, such that the S···S distance is 4.6Å which is 0.4A outside the sum of the van der Waals radii. The energy difference between the two phases is small, as observed with the α and β phases of the *meta* cyano phenyl derivative. The twist angle between dithiadiazolyl and aryl ring of α and β phases is 38.2° and 58.0° respectively.

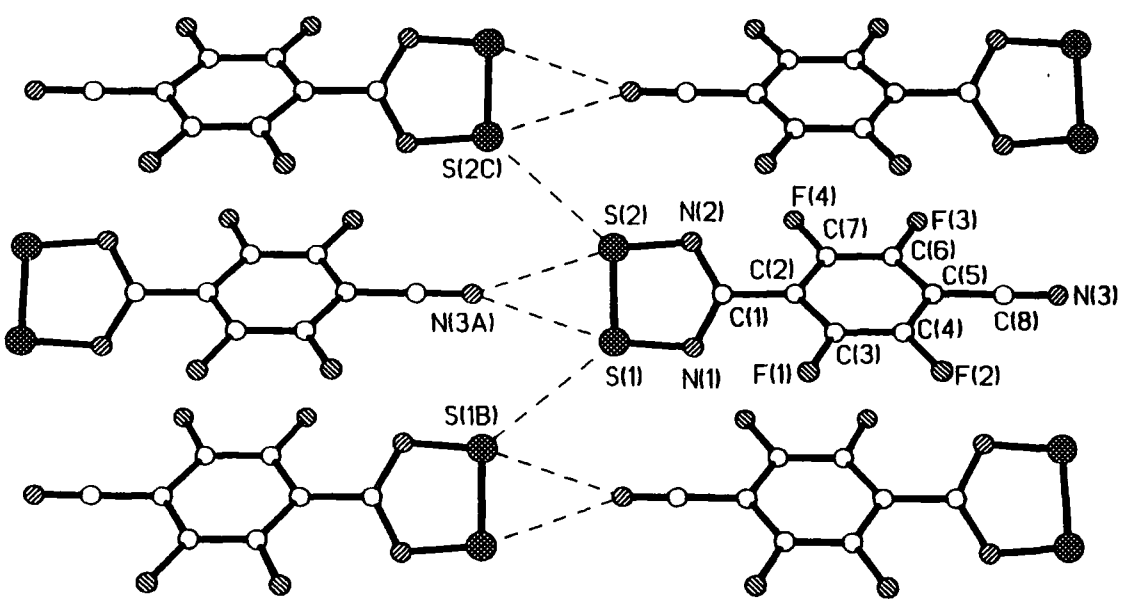

Fig 8. Packing diagram showing ribbons of α-NC-C_6F_4-CNSSN• molecules.

The magnetic results are as follows: (1) The α-phase is anti-ferromagnetically coupled with a Néel temperature of ~9K at which bulk anti-ferrimagnetism sets in. (2) The β-phase is also anti-ferromagnetically coupled but long range order occurs at 60K. On cooling, a phase transition occurs at 38K to a spin-centred anti-ferromagnetic (or weak ferromagnetic) state.

From the data collected so far, cyano derivatives show a strong desire to interact between nitrile nitrogen and sulphur, which gives rise to ribbons of dimers. For bis systems the interdimer sulphur sulphur interactions are dominant such that stacking or herring bone packing arrangements are observed. For the perfluoro systems there is a large twist angle between the sulphur nitrogen ring and the benzene ring which deters unfavourable F···F interactions and contacts.

Clearly, from the available structural information from the compounds mentioned thus far, it is possible to make predictions of the types of S-N, S-S interactions and twist angles which are likely to occur when dithiadiazolyls possess bulky, aryl cyano or perfluorinated dithiadiazolyls. Therefore, this is valuable information with regards to designing molecules for target applications.

3A.1.2. Structural investigation of several dithiadiazolyls

It is evident from these studies that molecular tailoring of dithiadiazolyls with desired solid state packing, has a large degree of unpredictability associated with it. To help rectify this situation, an investigation of how type(s) and position(s) of substituent(s) affects the solid state packing of a variety of aryl and pyridyl dithiadiazolyl derivatives was undertaken. It was envisaged that this would lead to a rationalisation of the packing preferences within this family of compounds.

This involved attempting to synthesise and prepare crystalline samples of *ortho, meta, para,* mixed and pyridyl systems so that both diverse and subtle changes in molecular packing could be studied. Synthesis of these compounds was generally successful, but producing suitable crystals for X-ray structure determination was an entirely different matter altogether. Details on this aspect can be found in the experimental chapter. Associated electrochemical studies on these compounds can be found in chapter 2.

The following compounds were successfully characterised by X-ray crystallography.

para

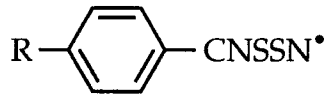

R = MeS, F, CF_3 and NO_2

meta

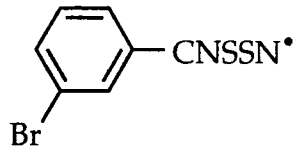

meta,para

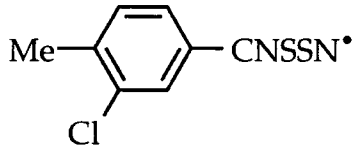

pyridyl

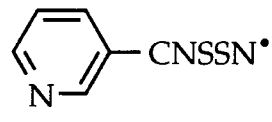

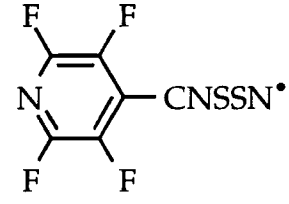

Now follows an individual discussion of each structure and this will include very brief comparisons of other structures. Major comparisons between themselves and other reported structures will be discussed afterwards.

No attempt to rationalise space groups will be conducted, but packing styles and how they are related by substituent molecular interactions will be discussed.

Throughout these discussions the sum of the van der Waals radii between two neighbouring atoms will be quoted and extreme limits of these distances can be found directly below. These values were drawn up by Nyburg and Faerman. They showed that the van der Waals radius of an atom is not spherically constant, but is probably rather smaller along the line of the bonds to that atom and larger perpendicular to them[19].

	Parallel	Perpendicular
S···S	3.20	4.06
S···N	3.20	3.63
S···F	2.90	3.41
S···Cl	3.18	3.81
S···Br	3.14	3.87
S···O	3.14	3.57
N···F	2.90	2.98
N···Cl	3.18	3.38
N···Br	3.14	3.44
F···F	2.60	2.76
Cl···Cl	3.16	3.56

Before the discussion begins, one important packing feature common to them is that they exist as dimers.

In the following discussion the 'eclipse', 'clam' and 'twist' angles of particular dithiadiazolyl molecules will be given. A brief description in order to clarify what these angles refer to can be found overleaf.

'Eclipse'

It is the angle that two molecules of a dimer unit overlap each other.

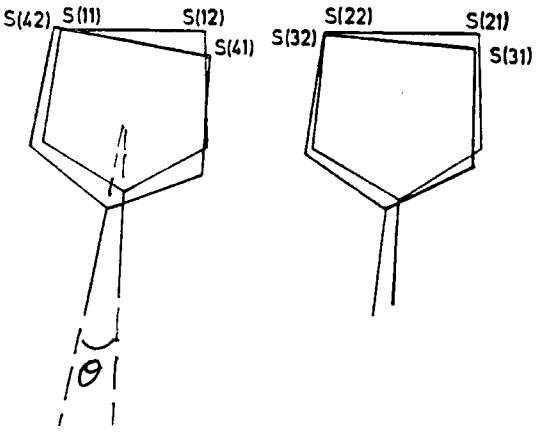

'Clam'

This is the angle between the two mean planes of the molecules in a dimer unit, i.e. a measure of how wedge shaped the dimer unit is.

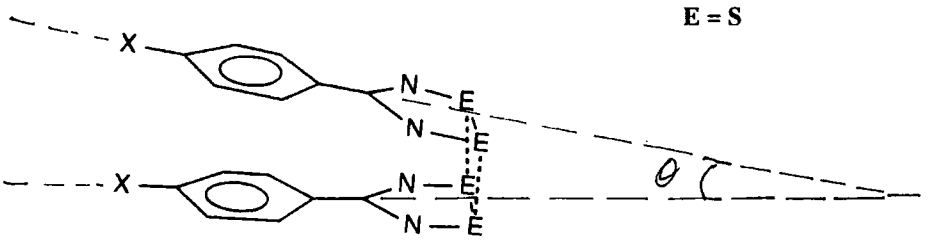

'Twist'

The twist angle for these derivatives refers to the angle between the mean plane of a dithiadiazolyl ring and the aryl ring bonded to it. Therefore, a dimer will possess two twist angles as it is made up of two molecules.

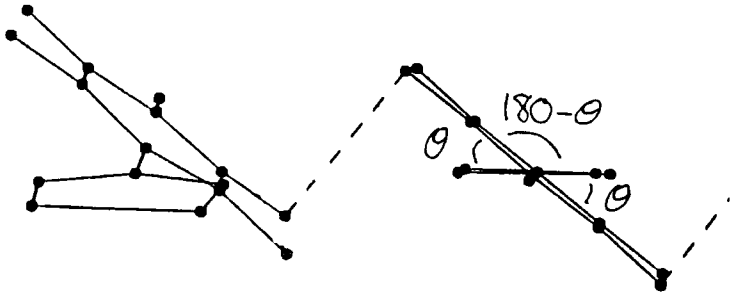

3B.1.1 $pMeS\text{-}C_6H_4\text{-}CNSSN^{\bullet}$

The dimer unit of the pMeS derivative is shown in Fig 10a with associated atom labels corresponding with structural data in Table 1a-h. It can be readily seen from Fig 10a and 10d that the methyl groups are trans to each other and that the two molecules are almost eclipsed, with a skew angle of 7.6°(8). The angle between the mean plane of the molecules of the dimer unit, or clam angle, is -4.5°(8). This geometry minimises the steric repulsions between the Me groups and allows S···H interactions, (2.970(2)Å), between each thioether sulphur and a methyl hydrogen from its twin half. The average S···S intradimer distance is found to be 3.061(2)Å.

The dihedral angle between aryl and heterocycle mean plains is found to be 18.8(5)° and 9.7(5)° for each molecule of the dimer unit. The torsion angle between C(6)-C(5)-S(3)-C(8) and C(12)-C(13)-S(6)-C(16) is 5.3(4)° and 6.0(4)° respectively.

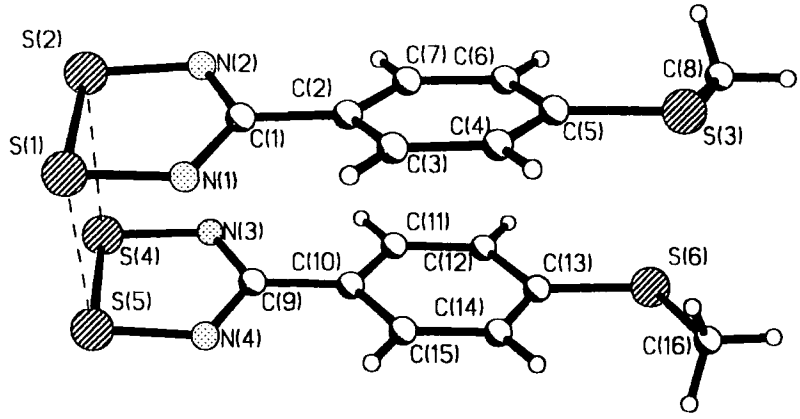

Fig 10a *Para* Trimethylthio phenyl 1,2,3,5 dithiadiazolyl dimer unit.

The dimers pack in planar herring-bone arrays perpendicular to the x axis, see Fig 10b. One thioether sulphur, from each dimer pair, is found to be well within (i.e less than) the sum of the van der Waals radii of two dithiadiazolyl sulphurs of a neighbouring dimer pair. Thus, three-centred S···S interactions of 3.242(2) and 3.382(2)Å are present. This is shown more clearly in Fig 10c.

Referring back to both types of S···S interactions displayed in Fig 10c, there is a step-like pattern of sulphur interactions, which run down the plane of the page. Also present are S···H contact between dithiadiazolyl sulphurs and methyl hydrogens which range from 2.800(2) to 3.096(2)Å.

These planar sheets align such that adjacent molecules almost overlap, which allows S···N inter-sheet contacts of 3.268(4)-3.527(4)Å to exist, as shown in Fig 10d.

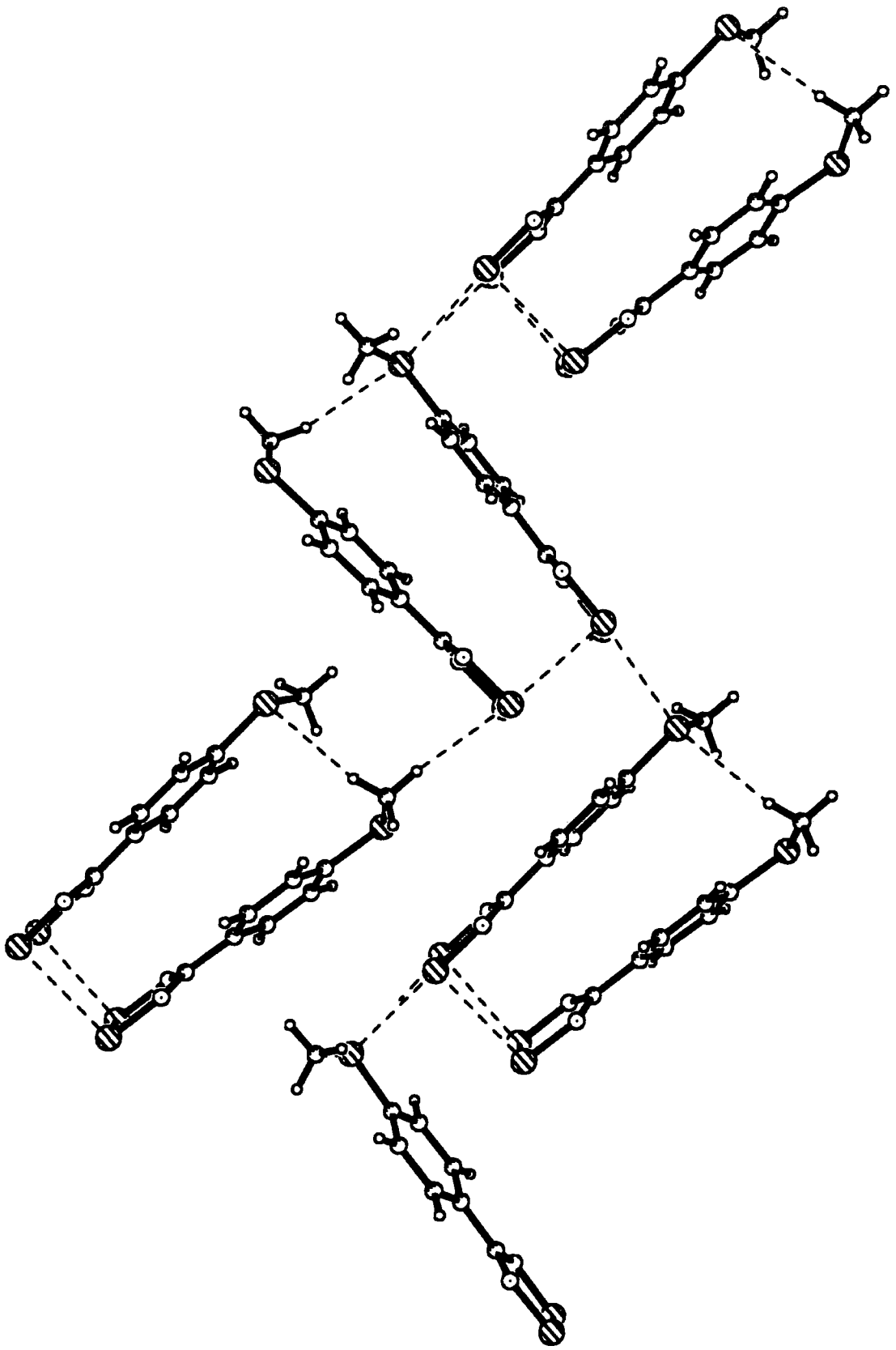

Fig 10b. One layer of dimers packing in a herring bone array.

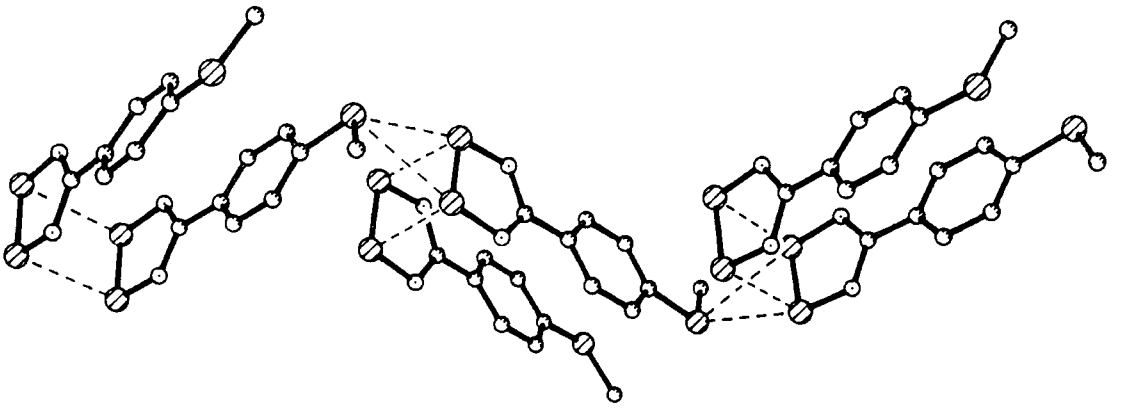

Fig 10c. Diagram showing the S···S intra and inter molecular attractions

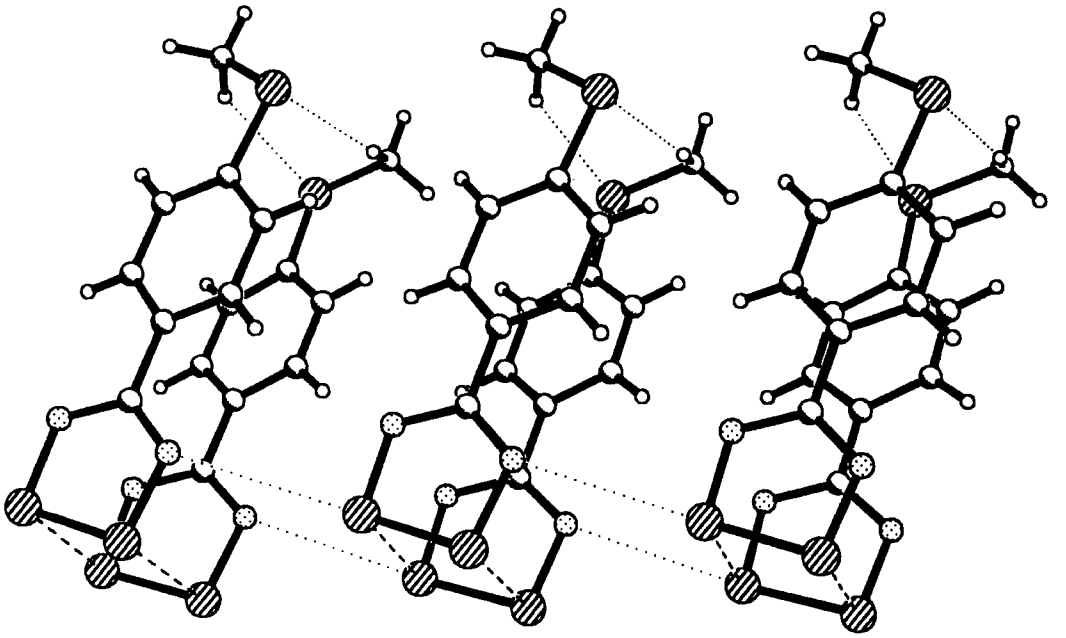

Fig 10d. Packing arrangement perpendicular to the plane of the herring bone arrays.

Table 1a. Crystal Data

Empirical Formula

$C_9 H_7 N_2 S_3$

Color; Habit	DARK RED SQUARE PLATE
Crystal Size (mm)	.3 .4 .2
Crystal System	Monoclinic
Space Group	$P2_1$
Unit Cell Dimensions	**a** = 5.679(2) Å
	b = 17.321(4) Å
	c = 9.646(2) Å
	β = 101.85(2)°
Volume	928.6(4) $Å^3$
Z	4
Formula Weight	227.3
Density(calc.)	1.626 Mg/m^3
Absorption Coefficient	0.746 mm^{-1}
F(000)	468

Table 1b. Data Collection

Diffractometer Used	Rigaku AFC6S
Radiation	MoKα (λ = 0.71073 Å)
Temperature (K)	403
Monochromator	Highly oriented graphite crystal
2θ Range	0.0 to 60.0°
Scan Type	2θ-θ
Scan Speed	Variable; 2.00 to 8.00°/min. in ω
Scan Range (ω)	1.90° plus Kα-separation
Background Measurement	Stationary crystal and stationary counter at beginning and end of scan, each for 25.0% of total scan time
Standard Reflections	3 measured every 150 reflections
Index Ranges	$0 \leq h \leq 7$, $0 \leq k \leq 22$
	$-12 \leq l \leq 12$
Reflections Collected	2393
Independent Reflections	2174 (R_{int} = 3.40%)
Observed Reflections	2005 ($F \geq 3.0\sigma(F)$)
Absorption Correction	N/A

Table 1c.

Solution and Refinement

System Used	Siemens SHELXTL PLUS (VMS)
Solution	Direct Methods
Refinement Method	Full-Matrix Least-Squares
Quantity Minimized	$\Sigma w(F_o-F_c)^2$
Absolute Structure	N/A
Extinction Correction	χ = 0.00047(9), where $F^* = F [1 + 0.002\chi F^2/\sin(2\theta)]^{-1/4}$
Hydrogen Atoms	Riding model, fixed isotropic U
Weighting Scheme	$w^{-1} = \sigma^2(F) + 0.0000F^2$
Number of Parameters Refined	248
Final R Indices (obs. data)	R = 3.15 %, wR = 3.05 %
R Indices (all data)	R = 3.62 %, wR = 3.21 %
Goodness-of-Fit	2.05
Largest and Mean Δ/σ	0.002, 0.000
Data-to-Parameter Ratio	8.1:1
Largest Difference Peak	0.36 eÅ^{-3}
Largest Difference Hole	-0.59 eÅ^{-3}

Table 1d.

Atomic coordinates (x10^4) and equivalent isotropic displacement coefficients (Å^{2}x10^3)

	x	y	z	U(eq)
S(1)	1845(2)	567	3900(1)	20(1)
S(2)	-1330(2)	643(1)	4703(1)	22(1)
S(3)	-5900(2)	-2529(1)	-1927(1)	25(1)
N(1)	751(6)	-59(2)	2683(3)	20(1)
N(2)	-2793(6)	11(2)	3579(4)	22(1)
C(1)	-1553(7)	-275(2)	2665(4)	17(1)
C(2)	-2672(7)	-831(3)	1576(4)	17(1)
C(3)	-1685(7)	-957(3)	379(4)	19(1)
C(4)	-2719(7)	-1464(3)	-664(4)	21(1)
C(5)	-4768(7)	-1886(3)	-535(4)	18(1)
C(6)	-5767(8)	-1764(3)	654(4)	19(1)
C(7)	-4758(7)	-1241(3)	1695(4)	19(1)
C(8)	-8336(8)	-3020(3)	-1347(5)	31(2)
S(4)	867(2)	-580(1)	6996(1)	21(1)
S(5)	3799(2)	-659(1)	6007(1)	19(1)
S(6)	-4499(2)	-4227(1)	1560(1)	23(1)
N(3)	-618(6)	-1279(2)	6082(3)	21(1)
N(4)	2649(6)	-1347(2)	4937(4)	18(1)
C(9)	456(7)	-1596(3)	5117(5)	19(1)
C(10)	-683(7)	-2243(3)	4257(4)	17(1)
C(11)	-2757(7)	-2591(3)	4548(4)	19(1)
C(12)	-3863(7)	-3193(3)	3699(4)	19(1)
C(13)	-2933(7)	-3459(3)	2551(4)	18(1)
C(14)	-858(7)	-3113(3)	2261(4)	21(1)
C(15)	243(7)	-2516(3)	3113(4)	20(1)
C(16)	-2985(7)	-4336(3)	97(5)	28(1)

* Equivalent isotropic U defined as one third of the trace of the orthogonalized U_{ij} tensor

Table 1e. Bond lengths (Å)

S(1)-S(2)	2.107 (2)	S(1)-N(1)	1.625 (4)
S(2)-N(2)	1.642 (4)	S(3)-C(5)	1.761 (4)
S(3)-C(8)	1.808 (5)	N(1)-C(1)	1.358 (5)
N(2)-C(1)	1.332 (6)	C(1)-C(2)	1.470 (6)
C(2)-C(3)	1.400 (6)	C(2)-C(7)	1.406 (6)
C(3)-C(4)	1.374 (6)	C(4)-C(5)	1.402 (6)
C(5)-C(6)	1.396 (6)	C(6)-C(7)	1.386 (6)
S(4)-S(5)	2.087 (2)	S(4)-N(3)	1.627 (4)
S(5)-N(4)	1.624 (4)	S(6)-C(13)	1.767 (4)
S(6)-C(16)	1.807 (5)	N(3)-C(9)	1.332 (6)
N(4)-C(9)	1.362 (6)	C(9)-C(10)	1.464 (6)
C(10)-C(11)	1.402 (6)	C(10)-C(15)	1.399 (6)
C(11)-C(12)	1.394 (6)	C(12)-C(13)	1.399 (6)
C(13)-C(14)	1.402 (6)	C(14)-C(15)	1.386 (6)

Table 1f. Bond angles (°)

S(2)-S(1)-N(1)	94.5(1)	S(1)-S(2)-N(2)	94.1(1)
C(5)-S(3)-C(8)	104.1(2)	S(1)-N(1)-C(1)	114.7(3)
S(2)-N(2)-C(1)	114.9(3)	N(1)-C(1)-N(2)	121.9(4)
N(1)-C(1)-C(2)	117.6(4)	N(2)-C(1)-C(2)	120.5(4)
C(1)-C(2)-C(3)	120.2(4)	C(1)-C(2)-C(7)	121.3(4)
C(3)-C(2)-C(7)	118.4(4)	C(2)-C(3)-C(4)	121.4(4)
C(3)-C(4)-C(5)	120.4(4)	S(3)-C(5)-C(4)	116.2(3)
S(3)-C(5)-C(6)	125.2(3)	C(4)-C(5)-C(6)	118.6(4)
C(5)-C(6)-C(7)	121.1(4)	C(2)-C(7)-C(6)	120.0(4)
S(5)-S(4)-N(3)	94.4(1)	S(4)-S(5)-N(4)	94.8(1)
C(13)-S(6)-C(16)	103.5(2)	S(4)-N(3)-C(9)	115.1(3)
S(5)-N(4)-C(9)	114.2(3)	N(3)-C(9)-N(4)	121.4(4)
N(3)-C(9)-C(10)	120.0(4)	N(4)-C(9)-C(10)	118.6(4)
C(9)-C(10)-C(11)	120.5(4)	C(9)-C(10)-C(15)	120.8(4)
C(11)-C(10)-C(15)	118.7(4)	C(10)-C(11)-C(12)	120.0(4)
C(11)-C(12)-C(13)	120.9(4)	S(6)-C(13)-C(12)	116.5(3)
S(6)-C(13)-C(14)	124.4(3)	C(12)-C(13)-C(14)	119.1(4)
C(13)-C(14)-C(15)	119.8(4)	C(10)-C(15)-C(14)	121.5(4)

Table 1g. Anisotropic displacement coefficients ($Å^2x10^3$)

	U_{11}	U_{22}	U_{33}	U_{12}	U_{13}	U_{23}
S(1)	19(1)	20(1)	20(1)	-2(1)	4(1)	-1(1)
S(2)	19(1)	24(1)	24(1)	2(1)	5(1)	-7(1)
S(3)	32(1)	25(1)	18(1)	-5(1)	4(1)	-4(1)
N(1)	17(2)	25(2)	18(2)	-1(1)	5(1)	-2(2)
N(2)	19(2)	23(2)	27(2)	1(2)	7(2)	-10(2)
C(1)	15(2)	18(2)	17(2)	3(2)	3(2)	4(2)
C(2)	17(2)	17(2)	17(2)	2(2)	0(2)	2(2)
C(3)	18(2)	22(2)	19(2)	-2(2)	6(2)	0(2)
C(4)	22(2)	24(2)	18(2)	2(2)	10(2)	3(2)
C(5)	20(2)	17(2)	16(2)	0(2)	0(2)	-1(2)
C(6)	19(2)	20(2)	19(2)	-2(2)	5(2)	2(2)
C(7)	16(2)	22(2)	19(2)	4(2)	8(2)	2(2)
C(8)	30(3)	30(3)	33(3)	-11(2)	3(2)	-7(2)
S(4)	23(1)	24(1)	19(1)	-2(1)	9(1)	-4(1)
S(5)	17(1)	22(1)	19(1)	1(1)	5(1)	-1(1)
S(6)	24(1)	20(1)	26(1)	-3(1)	4(1)	-2(1)
N(3)	19(2)	25(2)	21(2)	-1(2)	9(1)	-4(2)
N(4)	13(2)	20(2)	21(2)	2(1)	7(1)	1(2)
C(9)	18(2)	18(2)	20(2)	4(2)	6(2)	5(2)
C(10)	19(2)	17(2)	17(2)	4(2)	5(2)	6(2)
C(11)	20(2)	19(2)	22(2)	5(2)	10(2)	5(2)
C(12)	18(2)	18(2)	22(2)	1(2)	5(2)	5(2)
C(13)	22(2)	14(2)	17(2)	1(2)	1(2)	1(2)
C(14)	21(2)	27(3)	17(2)	2(2)	8(2)	1(2)
C(15)	19(2)	20(2)	21(2)	2(2)	6(2)	1(2)
C(16)	31(2)	25(3)	27(2)	-3(2)	6(2)	-4(2)

The anisotropic displacement factor exponent takes the form:

$-2\pi^2(h^2a^{*2}U_{11} + \ldots + 2hka^*b^*U_{12})$

Table 1h. H-Atom coordinates ($x10^4$) and isotropic displacement coefficients ($Å^2x10^3$)

	x	y	z	U
H(3)	-261	-681	284	24(12)
H(4)	-2023	-1535	-1482	17(11)
H(6)	-7174	-2050	745	32(14)
H(7)	-5491	-1150	2492	15(11)
H(8C)	-8988	-3410	-2024	56(18)
H(8B)	-9571	-2655	-1266	68(20)
H(8A)	-7741	-3256	-442	20(12)
H(11)	-3419	-2409	5327	25
H(12)	-5277	-3433	3905	47(16)
H(16C)	-212	-3283	1469	25(12)
H(15)	1675	-2283	2919	45(16)
H(16C)	-3800	-4719	-546	20(12)
H(16B)	-1352	-4494	449	66(19)
H(16A)	-3000	-3852	-390	36(15)

3B.1.2 pF-C_6H_4-CNSSN•

The dimer molecules of pF-C_6H_4-CNSSN• are found to be co-planar with mean S···S intradimer interactions at 3.053(4)Å, see Fig 11a and Table 2a-h. The "skew" or eclipse angle between the two dimer molecules is 3.4(13)° and the angle between the mean plane or "clam" angle for these molecules is 5.8(13)°. The twist angle between the mean plane of the dithiadiazolyl and the aryl ring is 6.2(12)° and for the other molecule of the dimer is 7.0(12)°.

The fluorine end of each dimer faces onto the fluorine end of a neighbouring parallel dimer unit, see Fig 11c-d. This will now be described loosely as a 'tetramer' even though no secondary bonding contacts between the two dimers are observed. These 'tetramer' units in turn pack to form herring-bone arrays which give rise to zig-zag S···S interactions between dimers which extend infinitely in the lattice.

Perpendicular to this plane, the molecules of each array are offset from molecules of adjacent arrays and held together through S···N contacts of 3.468(9) and 3.478(9)Å between the adjacent dithiadiazolyl rings, see Fig 11b. This packing is reminiscent of that observed for the previously discussed pMeS derivative.

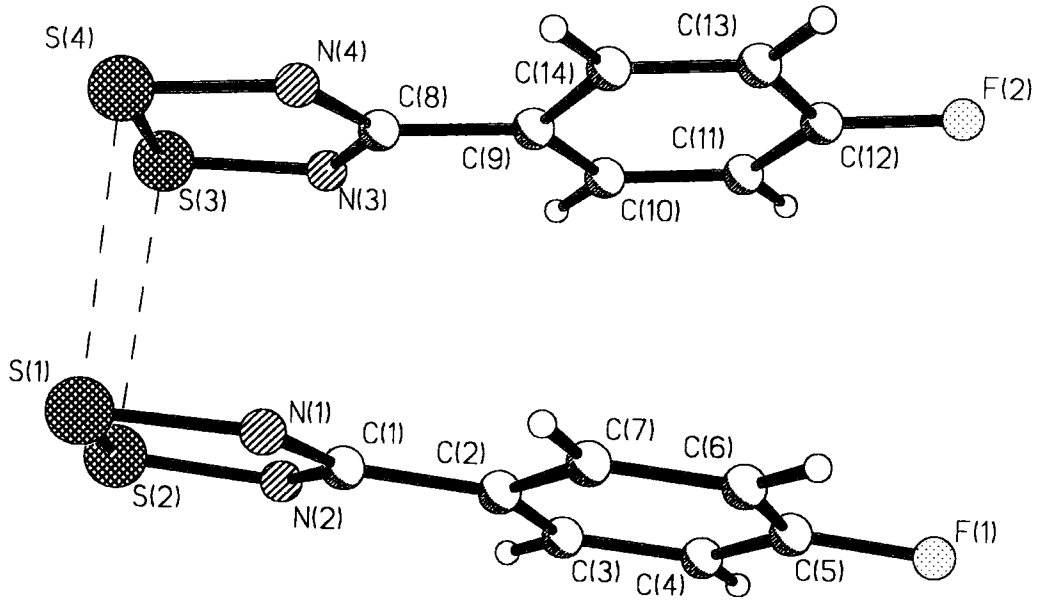

Fig 11a. A dimer

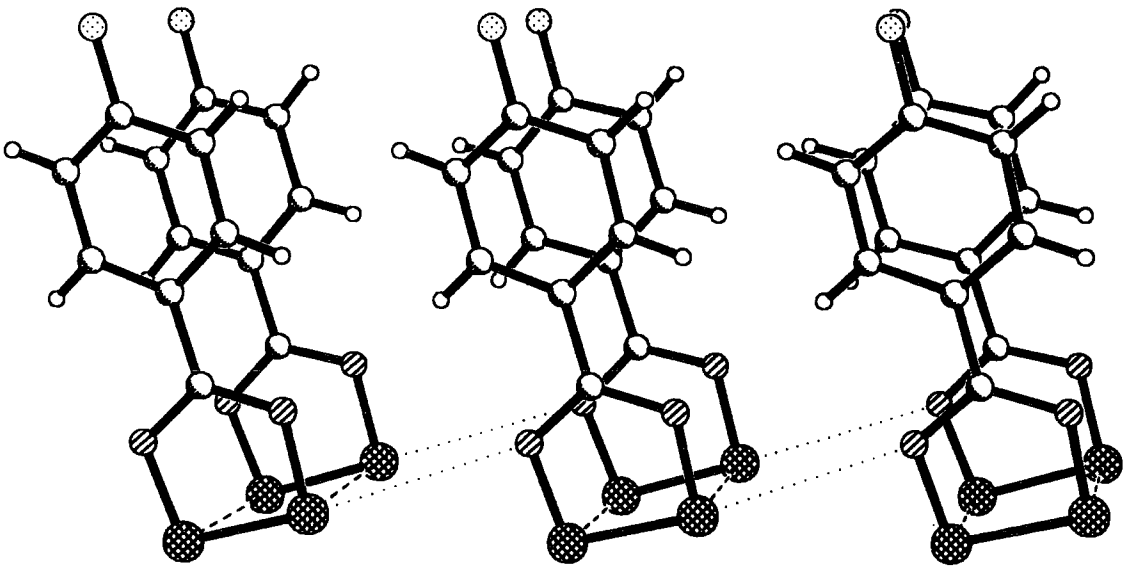

Fig 11b. Packing arrangement perpendicular to the plane of the herring bone arrays.

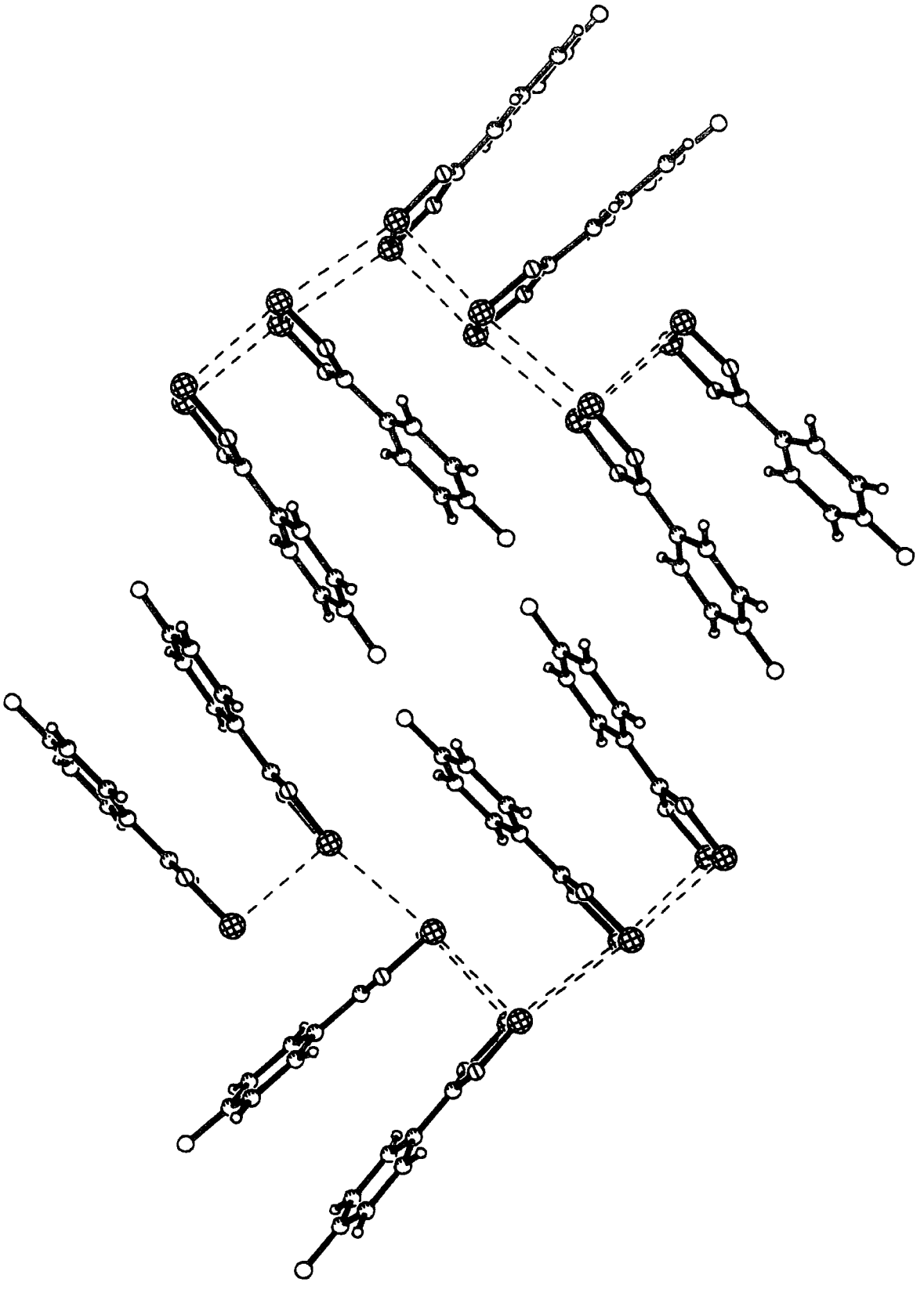

Fig 11c. A layer of dimers packing in a herring bone array.

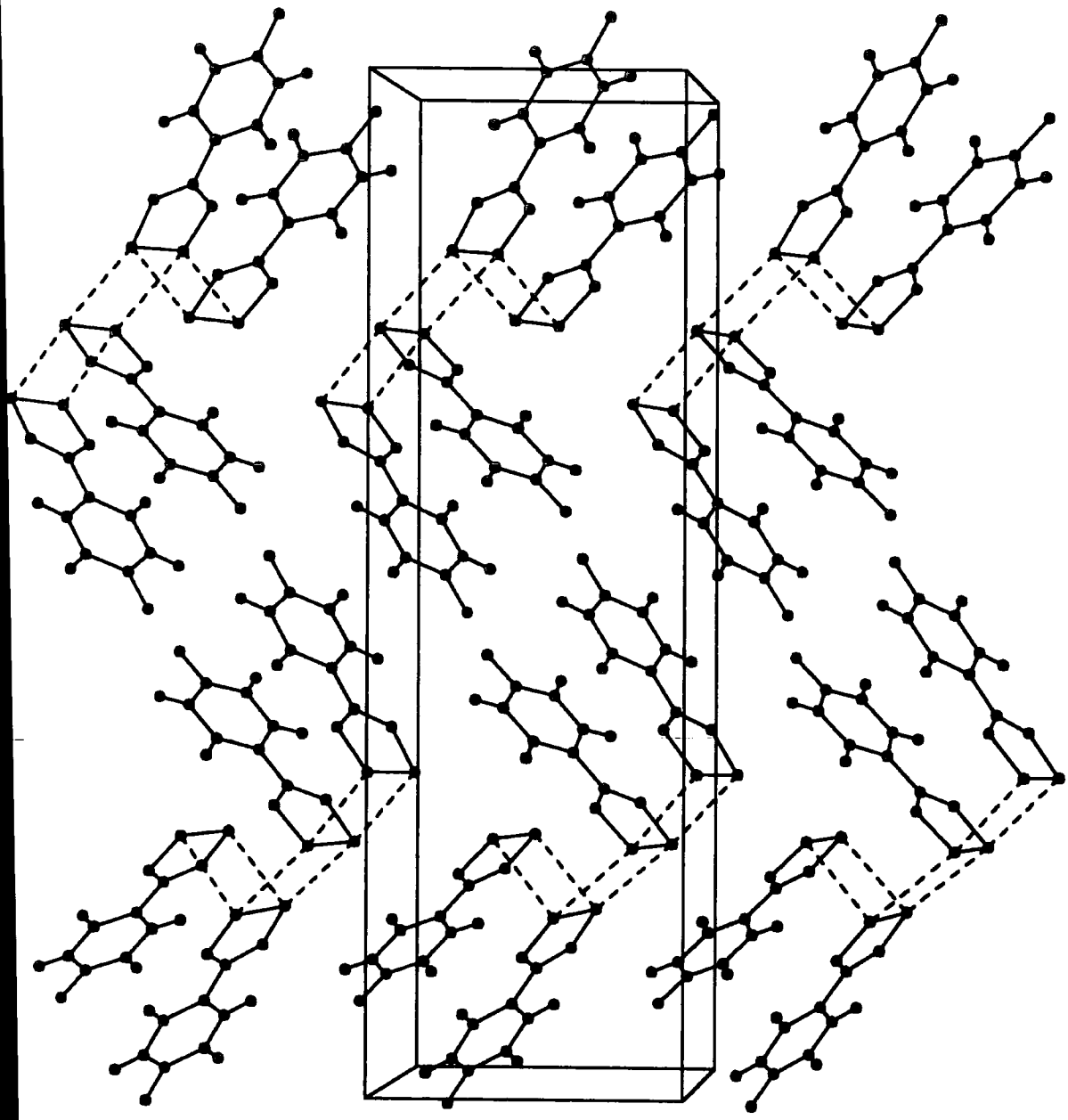

Fig 11d. Diagram clearly showing the S···S intra and inter molecular attractions within the array.

Table 2a. **(b) X-RAY DIFFRACTION OF *PARA*-FLUORO-PHENYL DITHIADIAZOLYL Results.**

Crystal Data

Empirical Formula	$C_7 H_4 F N_2 S_2$
Color; Habit	Dark purple needle
Crystal Size (mm)	0.05 x 0.08 x 0.45
Crystal System	Monoclinic
Space Group	$P2_1/n$
Unit Cell Dimensions	a = 5.794(2) Å
	b = 29.810(11) Å
	c = 9.201(3) Å
	β = 103.01(3)°
Volume	1548.4(10) $Å^3$
Z	8
Formula Weight	199.2
Density(calc.)	1.709 g/cm^3
Absorption Coefficient	0.639 mm^{-1}
F(000)	808

Table 2b. **Data Collection**

Diffractometer Used	Rigaku AFC6S
Radiation	MoKα (λ = 0.71073 Å)
Temperature (K)	150
Monochromator	Highly oriented graphite crystal
2θ Range	5.0 to 45.0°
Scan Type	ω
Scan Speed	Variable; 1.33 to 8.00°/min. in ω
Scan Range (ω)	1.50°
Background Measurement	Stationary crystal and stationary counter at beginning and end of scan, each for 25.0% of total scan time
Standard Reflections	3 measured every 150 reflections
Index Ranges	$-6 \leq h \leq 6$, $0 \leq k \leq 32$
	$-9 \leq l \leq 6$
Reflections Collected	2219
Independent Reflections	2026 (R_{int} = 2.89%)
Observed Reflections	880 ($F \geq 4.0\sigma(F)$)
Absorption Correction	N/A

Solution and Refinement

Table 2c.

System Used	Siemens SHELXTL PLUS (VMS)
Solution	Direct Methods
Refinement Method	Full-Matrix Least-Squares
Quantity Minimized	$\Sigma w(F_o-F_c)^2$
Absolute Structure	N/A
Extinction Correction	N/A
Hydrogen Atoms	Riding model, fixed isotropic U
Weighting Scheme	$w^{-1} = \sigma^2(F) + 0.0002F^2$
Number of Parameters Refined	127
Final R Indices (obs. data)	R = 5.16 %, wR = 5.30 %
R Indices (all data)	R = 16.64 %, wR = 6.65 %
Goodness-of-Fit	1.18
Largest and Mean Δ/σ	0.003, 0.001
Data-to-Parameter Ratio	6.9:1
Largest Difference Peak	0.37 eÅ^{-3}
Largest Difference Hole	-0.38 eÅ^{-3}

Table 2d.

Atomic coordinates (x10^4) and equivalent isotropic displacement coefficients (Å^{2}x10^3)

	x	y	z	U(eq)
S(1)	1749(5)	2501(1)	6238(3)	30(1)
S(2)	4792(5)	2504(1)	5339(3)	32(1)
S(3)	-421(5)	1769(1)	4031(3)	30(1)
S(4)	2504(5)	1800(1)	3054(3)	31(1)
N(1)	2777(14)	3131(3)	7495(9)	25(2)
N(2)	6194(14)	2125(3)	6502(9)	26(2)
N(3)	650(14)	1361(3)	5155(8)	25(2)
N(4)	3903(14)	1335(3)	4032(9)	28(2)
F(1)	8909(11)	701(2)	11773(7)	44(2)
F(2)	6674(11)	-268(2)	8433(8)	55(3)
C(1)	4952(18)	1976(3)	7494(11)	22(2)
C(2)	6058(18)	1641(3)	8617(11)	20(2)
C(3)	4898(18)	1523(3)	9728(10)	20(3)
C(4)	5819(17)	1206(3)	10794(11)	24(3)
C(5)	7943(18)	1010(3)	10714(11)	28(3)
C(6)	9140(18)	1111(3)	9640(11)	26(3)
C(7)	8180(17)	1430(3)	8578(11)	23(3)
C(8)	2748(17)	1208(3)	4998(11)	22(2)
C(9)	3834(17)	820(3)	5915(11)	24(3)
C(10)	2722(19)	648(3)	6988(11)	28(3)
C(11)	3692(19)	280(3)	7834(12)	37(3)
C(12)	5766(19)	94(4)	7604(12)	35(3)
C(13)	6833(19)	257(3)	6526(11)	35(3)
C(14)	5885(17)	618(3)	5689(11)	25(3)

* Equivalent isotropic U defined as one third of the trace of the orthogonalized U_{ij} tensor

Table 2e. Bond lengths (Å)

S(1)-S(2)	2.110 (4)	S(1)-N(1)	1.613 (8)
S(2)-N(2)	1.641 (8)	S(3)-S(4)	2.091 (5)
S(3)-N(3)	1.626 (8)	S(4)-N(4)	1.635 (8)
N(1)-C(1)	1.342 (13)	N(2)-C(1)	1.358 (14)
N(3)-C(8)	1.336 (13)	N(4)-C(8)	1.335 (14)
F(1)-C(5)	1.365 (11)	F(2)-C(12)	1.356 (12)
C(1)-C(2)	1.476 (13)	C(2)-C(3)	1.389 (15)
C(2)-C(7)	1.388 (15)	C(3)-C(4)	1.380 (13)
C(4)-C(5)	1.380 (15)	C(5)-C(6)	1.362 (16)
C(6)-C(7)	1.387 (13)	C(8)-C(9)	1.487 (13)
C(9)-C(10)	1.391 (16)	C(9)-C(14)	1.388 (15)
C(10)-C(11)	1.389 (14)	C(11)-C(12)	1.383 (16)
C(12)-C(13)	1.372 (17)	C(13)-C(14)	1.365 (14)

Table 2f. Bond angles (°)

S(2)-S(1)-N(1)	94.4(4)	S(1)-S(2)-N(2)	94.4(3)
S(4)-S(3)-N(3)	94.3(4)	S(3)-S(4)-N(4)	94.6(4)
S(1)-N(1)-C(1)	115.5(7)	S(2)-N(2)-C(1)	113.9(7)
S(3)-N(3)-C(8)	114.4(7)	S(4)-N(4)-C(8)	113.8(7)
N(1)-C(1)-N(2)	121.8(8)	N(1)-C(1)-C(2)	119.5(9)
N(2)-C(1)-C(2)	118.7(9)	C(1)-C(2)-C(3)	118.7(9)
C(1)-C(2)-C(7)	122.4(10)	C(3)-C(2)-C(7)	118.8(8)
C(2)-C(3)-C(4)	121.5(9)	C(3)-C(4)-C(5)	117.3(10)
F(1)-C(5)-C(4)	118.4(9)	F(1)-C(5)-C(6)	118.2(9)
C(4)-C(5)-C(6)	123.4(9)	C(5)-C(6)-C(7)	118.3(10)
C(2)-C(7)-C(6)	120.6(10)	N(3)-C(8)-N(4)	122.8(8)
N(3)-C(8)-C(9)	118.9(9)	N(4)-C(8)-C(9)	118.2(9)
C(8)-C(9)-C(10)	119.0(9)	C(8)-C(9)-C(14)	121.3(9)
C(10)-C(9)-C(14)	119.7(9)	C(9)-C(10)-C(11)	119.6(10)
C(10)-C(11)-C(12)	119.2(11)	F(2)-C(12)-C(11)	118.3(10)
F(2)-C(12)-C(13)	120.5(10)	C(11)-C(12)-C(13)	121.1(10)
C(12)-C(13)-C(14)	119.9(11)	C(9)-C(14)-C(13)	120.4(10)

Table 2g. Anisotropic displacement coefficients ($Å^2x10^3$)

	U_{11}	U_{22}	U_{33}	U_{12}	U_{13}	U_{23}
S(1)	34(2)	30(2)	27(2)	9(2)	8(1)	0(2)
S(2)	32(2)	33(2)	32(2)	-5(1)	6(1)	8(2)
S(3)	25(2)	36(2)	27(2)	-1(1)	5(1)	6(1)
S(4)	33(2)	34(2)	28(2)	4(2)	12(1)	5(2)
F(1)	41(4)	47(4)	43(4)	18(3)	8(3)	20(4)
F(2)	46(5)	42(4)	75(5)	13(3)	12(4)	24(4)

The anisotropic displacement factor exponent takes the form:

$-2\pi^2(h^2a^{*2}U_{11} + \ldots + 2hka^*b^*U_{12})$

Table 2h. H-Atom coordinates ($x10^4$) and isotropic displacement coefficients ($Å^2x10^3$)

	x	y	z	U
H(3)	3426	1667	9751	25
H(4)	5018	1122	11560	30
H(6)	10620	967	9635	32
H(7)	8967	1506	7799	28
H(10)	1288	786	7125	35
H(11)	2954	157	8580	40
H(13)	8246	115	6372	42
H(14)	6641	742	4951	30

3B.1.3 pCF_3-C_6H_4-CNSSN•

For this derivative the "eclipse" and "clam" angles for the molecules of the dimer unit are **7.0(15)°** and **6.2(15)°** respectively. There is also a twist angle of **7.2(13)°** and **10.2(13)°** between the benzene and dithiadiazolyl rings. The torsion angles for N(4)-C(9)-C(10)-C(15) and N(3)-C(9)-C(10)-C(11) are **6.1(15)°** and 11.4**(15)°**. The S···S intradimer interactions are 3.075(5) and 3.104(5)Å, see Fig 12a.

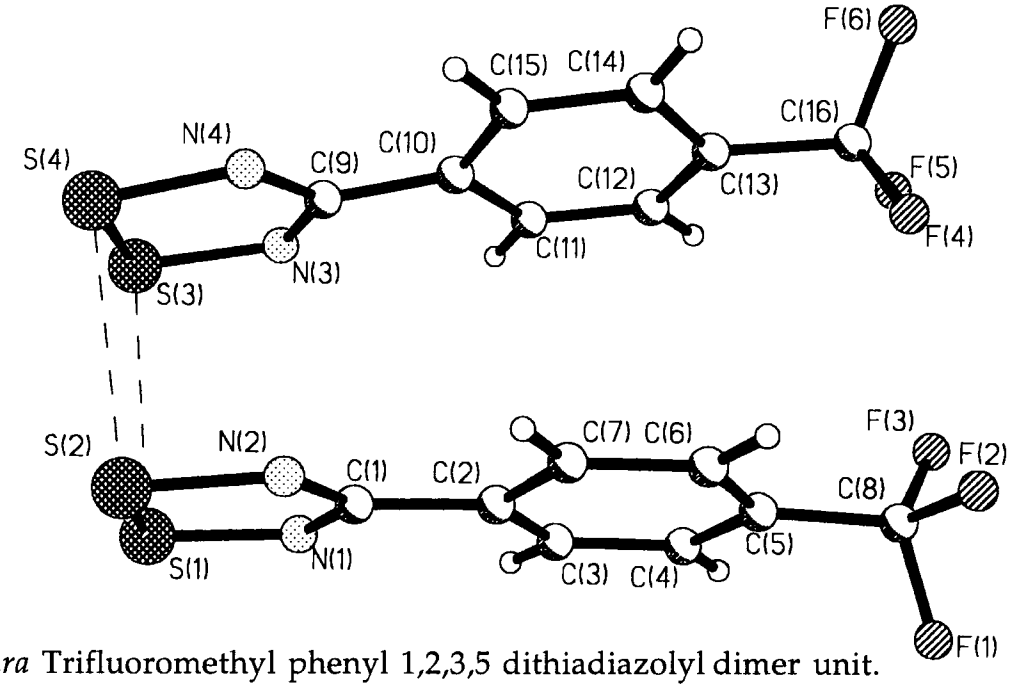

Fig 12a *Para* Trifluoromethyl phenyl 1,2,3,5 dithiadiazolyl dimer unit.

Looking down the x-axis, the dimer packs head to tail, to form ribbons. Along these ribbons two fluorines from the CF_3 group from one half of a dimer each form one S···F contact, (mean 3.290(9)Å), with the neighbouring sulphurs of an in-plane dimer molecule, see Fig 12c and d.

These ribbons pack adjacent and parallel to each other, with the dimers between rows almost overlapping each other. This arrangement allows S···N mean contacts of 3.429(11)Å between the ribbons, see Fig 12b and e. These contacts are similar to those observed in the pMeS and pF structures, see 3B.1.1-2.

These sheets in turn pack on top of one another such that an ABCD type stacking arrangement of dimers is seen. This packing is illustrated in Fig 12d and e, where the dithiadiazolyl ring points in (A) into and to the left, (B) out of and left, (C) into and right and (D) out of and right of the page and so on.

Also observed between every second layer, (A&D, B&C), are unfavourable $F^{\delta-}\cdots F^{\delta-}$ contacts of 2.814(11)Å.

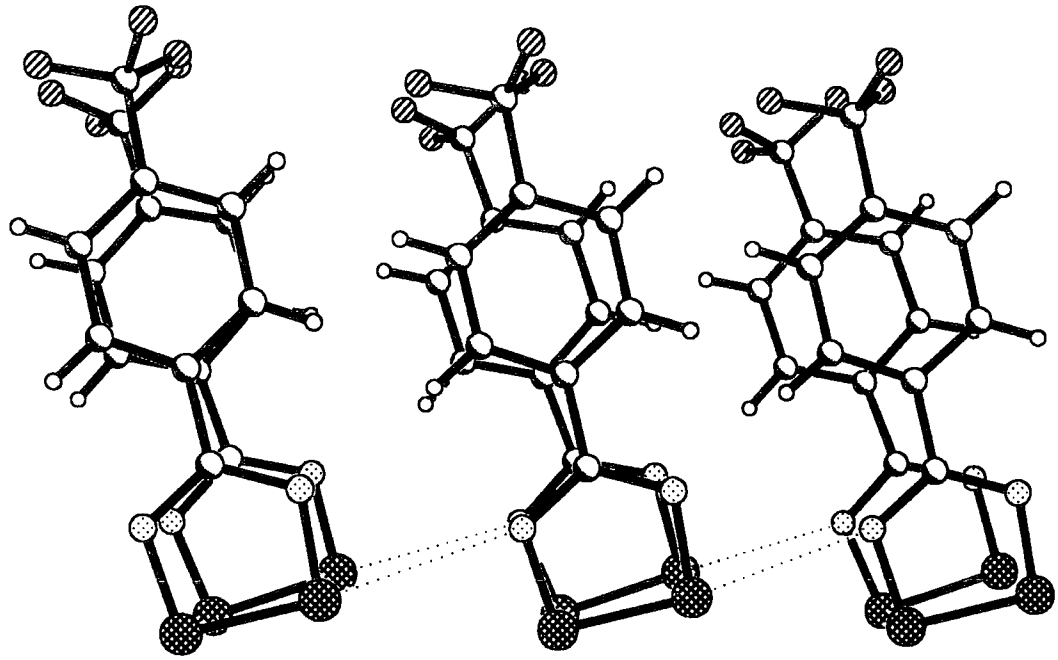

Fig 12b. Packing arrangement between the dimers of adjacent ribbons.

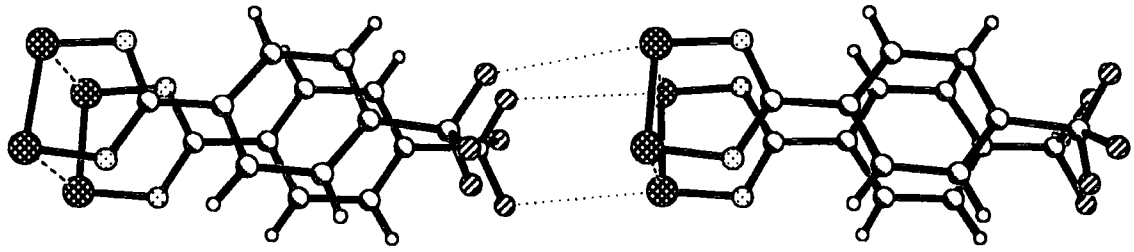

Fig 12c. Diagram showing the S···F ribbon contacts along the axis of the ribbon.

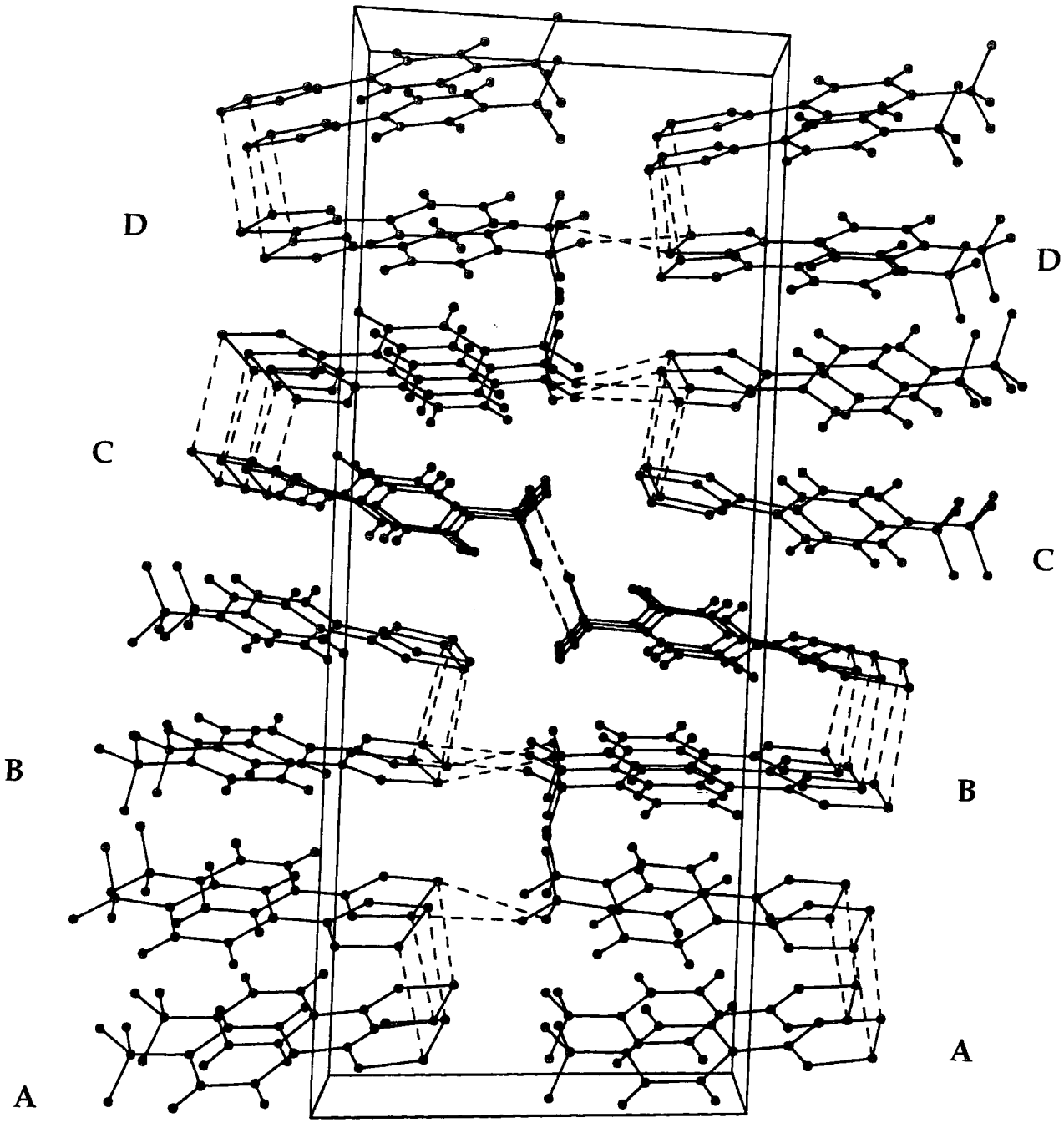

Fig 12d. Diagram showing how the ribbons pack on top of one another.

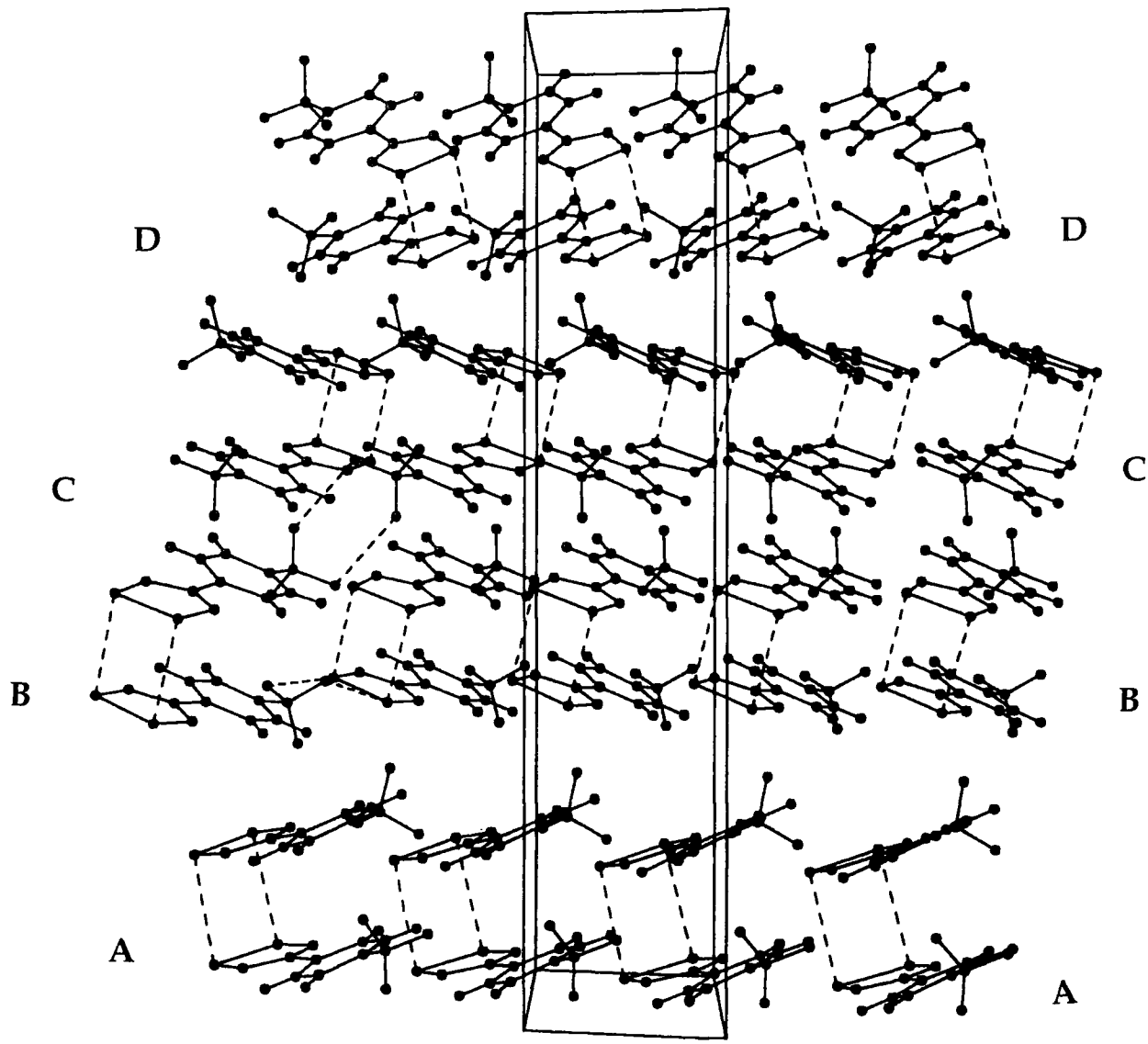

Fig 12e. Diagram showing the ABCD packing of the dimer molecules.

Table 3a. Crystal data, structure solution and refinement for ajb40.

Identification code	ajb40
Chemical formula	$C_{16}H_8F_6N_4S_4$
Formula weight	498.50
Temperature	160(2) K
Radiation and wavelength	MoKα, 0.71073 Å
Crystal system, space group	monoclinic, $P2_1/n$
Unit cell dimensions	a = 11.353(2) Å α = 90° b = 28.148(8) Å β = 100.36(2)° c = 5.722(3) Å γ = 90°
Volume	1798.8(10) $Å^3$
Z	4
Density (calculated)	1.841 g/cm^3
Absorption coefficient μ	0.601 mm^{-1}
F(000)	1000
Reflections for cell refinement	27 (θ range 8.70 to 10.56°)
Crystal colour	dark red
Crystal size	0.18 × 0.10 × 0.09 mm
Data collection method	Stoe-Siemens diffractometer. ω/θ scans
θ range for data collection	2.84 to 22.48°
Index ranges	$-12 \le h \le 12$, $-30 \le k \le 9$, $-6 \le \ell \le 6$
Standard reflections	4 every 60 minutes
Intensity decay of standards	0%
Reflections collected	3412
Independent reflections	2337 (R_{int} = 0.1050)
Reflections with $I>2\sigma(I)$	933
Absorption correction	none
Structure solution	Patterson synthesis
Refinement method	full-matrix least-squares on F^2
Weighting parameters a, b	0.0676, 5.7017
Data / restraints / parameters	2310 / 12 / 271
Goodness-of-fit on F^2	1.099
Final R indices [$I>2\sigma(I)$]	R1 = 0.0595, wR2 = 0.1291
R indices (all data)	R1 = 0.2421, wR2 = 0.2627
Largest and mean shift.esd	0.000 and 0.000
Largest diff. peak and hole	.540 and −.702 $eÅ^{-3}$

Table 3b. **Atomic coordinates (x 10^4) and equivalent isotropic displacement parameters ($Å^2$ x 10^3) for ajb40. U(eq) is defined as one third of the trace of the orthogonalized U_{ij} tensor.**

	x	y	z	U(eq)
S(1)	2519(3)	1986(2)	3131(6)	27.4(10)
S(2)	1987(3)	1730.0(14)	6217(6)	25.2(10)
N(1)	1174(9)	1993(5)	1557(18)	26(3)
N(2)	589(8)	1694(5)	5022(19)	26(3)
C(1)	324(11)	1838(6)	2767(25)	26(4)
C(2)	-937(11)	1847(5)	1469(22)	18(3)
C(3)	-1235(10)	2036(5)	-785(21)	13(3)
C(4)	-2447(11)	2059(5)	-1880(23)	24(4)
C(5)	-3319(10)	1884(5)	-693(20)	13(3)
C(6)	-3038(11)	1679(5)	1495(22)	16(3)
C(7)	-1825(12)	1658(5)	2617(23)	20(3)
C(8)	-4601(11)	1931(5)	-1927(24)	20(3)
F(1)	-4898(6)	2378(3)	-2450(15)	38(2)
F(2)	-5385(6)	1773(3)	-626(13)	33(2)
F(3)	-4827(6)	1697(3)	-4004(13)	36(2)
S(3)	2970(3)	943.5(14)	1758(6)	25.3(10)
S(4)	2588(3)	704(2)	5000(6)	27.1(10)
N(3)	1602(9)	866(4)	287(18)	27(3)
N(4)	1176(8)	595(4)	3946(19)	23(3)
C(9)	838(10)	695(5)	1622(22)	20(3)
C(10)	-406(11)	606(5)	538(23)	19(3)
C(11)	-862(11)	770(6)	-1730(22)	28(4)
C(12)	-2062(11)	726(5)	-2706(25)	23(3)
C(13)	-2824(11)	527(5)	-1400(23)	21(3)
C(14)	-2402(11)	331(5)	824(23)	24(4)
C(15)	-1174(10)	383(5)	1798(22)	23(4)
C(16)	-4154(12)	497(6)	-2361(26)	26(4)
F(4)	-4761(6)	778(3)	-1049(14)	37(2)
F(5)	-4438(6)	669(3)	-4587(14)	37(2)
F(6)	-4609(6)	65(3)	-2300(14)	36(2)

Table 3c. **Bond lengths (Å) and angles (°) for ajb40.**

S(1)-N(1)	1.627(11)	S(1)-S(2)	2.095(5)
S(2)-N(2)	1.614(10)	N(1)-C(1)	1.36(2)
N(2)-C(1)	1.33(2)	C(1)-C(2)	1.49(2)
C(2)-C(3)	1.38(2)	C(2)-C(7)	1.40(2)
C(3)-C(4)	1.41(2)	C(4)-C(5)	1.39(2)
C(5)-C(6)	1.36(2)	C(5)-C(8)	1.50(2)
C(6)-C(7)	1.41(2)	C(8)-F(1)	1.32(2)
C(8)-F(2)	1.335(14)	C(8)-F(3)	1.34(2)
S(3)-N(3)	1.642(11)	S(3)-S(4)	2.091(5)
S(4)-N(4)	1.636(10)	N(3)-C(9)	1.34(2)
N(4)-C(9)	1.35(2)	C(9)-C(10)	1.46(2)
C(10)-C(15)	1.38(2)	C(10)-C(11)	1.39(2)
C(11)-C(12)	1.38(2)	C(12)-C(13)	1.36(2)
C(13)-C(14)	1.39(2)	C(13)-C(16)	1.51(2)
C(14)-C(15)	1.41(2)	C(16)-F(6)	1.32(2)
C(16)-F(5)	1.35(2)	C(16)-F(4)	1.36(2)
N(1)-S(1)-S(2)	94.9(4)	N(2)-S(2)-S(1)	94.3(4)
C(1)-N(1)-S(1)	113.4(9)	C(1)-N(2)-S(2)	115.1(9)
N(2)-C(1)-N(1)	122.2(11)	N(2)-C(1)-C(2)	121.1(11)
N(1)-C(1)-C(2)	116.6(12)	C(3)-C(2)-C(7)	120.5(12)
C(3)-C(2)-C(1)	121.6(11)	C(7)-C(2)-C(1)	117.9(12)
C(2)-C(3)-C(4)	119.3(11)	C(5)-C(4)-C(3)	119.5(12)
C(6)-C(5)-C(4)	122.0(11)	C(6)-C(5)-C(8)	120.9(11)
C(4)-C(5)-C(8)	117.0(11)	C(5)-C(6)-C(7)	118.8(12)
C(2)-C(7)-C(6)	119.7(12)	F(1)-C(8)-F(2)	105.9(11)
F(1)-C(8)-F(3)	105.4(11)	F(2)-C(8)-F(3)	106.9(11)
F(1)-C(8)-C(5)	112.0(12)	F(2)-C(8)-C(5)	113.3(11)
F(3)-C(8)-C(5)	112.8(11)	N(3)-S(3)-S(4)	94.8(4)
N(4)-S(4)-S(3)	94.5(4)	C(9)-N(3)-S(3)	113.8(9)
C(9)-N(4)-S(4)	114.2(8)	N(3)-C(9)-N(4)	122.6(11)
N(3)-C(9)-C(10)	119.7(11)	N(4)-C(9)-C(10)	117.8(11)
C(15)-C(10)-C(11)	118.5(12)	C(15)-C(10)-C(9)	120.8(12)
C(11)-C(10)-C(9)	120.6(12)	C(12)-C(11)-C(10)	121.6(13)
C(13)-C(12)-C(11)	119.5(13)	C(12)-C(13)-C(14)	121.2(12)
C(12)-C(13)-C(16)	121.0(13)	C(14)-C(13)-C(16)	117.8(12)
C(13)-C(14)-C(15)	118.2(12)	C(10)-C(15)-C(14)	120.8(12)
F(6)-C(16)-F(5)	109.1(12)	F(6)-C(16)-F(4)	106.3(11)
F(5)-C(16)-F(4)	104.7(11)	F(6)-C(16)-C(13)	114.2(12)
F(5)-C(16)-C(13)	112.1(12)	F(4)-C(16)-C(13)	109.7(12)

Table 3d. **Anisotropic displacement parameters ($Å^2$ x 10^3) for ajb40.**

The anisotropic displacement factor exponent takes the form: $-2\pi^2(h^2a^{*2}U_{11} + \ldots + 2hka^*b^*U_{12})$.

	U(11)	U(22)	U(33)	U(23)	U(13)	U(12)
S(1)	10(2)	46(3)	27(2)	4(2)	4(2)	-6(2)
S(2)	11(2)	45(3)	19(2)	-4(2)	3(2)	-3(2)
N(1)	16(6)	37(8)	22(7)	11(6)	-2(5)	-6(6)
N(2)	0(5)	55(9)	22(7)	-2(7)	-1(5)	2(6)
C(1)	4(7)	47(11)	26(9)	-7(8)	4(6)	2(7)
C(2)	16(7)	26(9)	14(7)	10(7)	8(6)	5(7)
C(3)	13(6)	8(7)	19(6)	2(5)	11(5)	-1(5)
C(4)	18(8)	37(10)	17(7)	5(7)	3(6)	2(7)
C(5)	11(6)	16(8)	13(7)	1(6)	4(6)	-1(6)
C(6)	8(7)	18(8)	23(8)	8(7)	7(6)	1(6)
C(7)	34(9)	6(8)	21(8)	4(7)	6(7)	-2(7)
C(8)	12(7)	20(9)	26(9)	10(7)	2(6)	6(7)
F(1)	13(4)	54(7)	43(5)	8(5)	-3(4)	2(4)
F(2)	12(4)	53(6)	36(5)	8(4)	9(4)	0(4)
F(3)	19(4)	61(6)	26(5)	-15(5)	-6(4)	1(4)
S(3)	11(2)	42(3)	25(2)	2(2)	7(2)	-1(2)
S(4)	13(2)	39(3)	27(2)	10(2)	1(2)	-6(2)
N(3)	10(6)	52(9)	20(6)	6(6)	3(5)	7(6)
N(4)	2(5)	39(7)	29(6)	2(5)	6(5)	3(5)
C(9)	12(7)	33(10)	16(8)	8(7)	6(6)	4(7)
C(10)	15(7)	26(10)	21(8)	3(7)	13(6)	-2(6)
C(11)	26(8)	45(11)	16(8)	9(7)	13(7)	9(8)
C(12)	19(8)	21(9)	32(9)	5(7)	10(7)	1(7)
C(13)	12(7)	32(10)	17(8)	-12(7)	-1(6)	-2(6)
C(14)	17(7)	33(10)	25(8)	9(7)	13(6)	-2(7)
C(15)	15(7)	44(11)	9(7)	1(7)	2(6)	3(7)
C(16)	24(9)	28(10)	28(9)	-2(7)	10(7)	7(8)
F(4)	17(4)	50(6)	43(5)	-14(5)	5(4)	1(4)
F(5)	13(4)	63(7)	34(5)	8(5)	2(4)	-8(4)
F(6)	17(4)	42(6)	47(5)	-1(4)	3(4)	-15(4)

Table 3e. **Hydrogen atom coordinates (x 10^4) and isotropic displacement parameters ($Å^2$ x 10^3) for ajb40.**

	x	y	z	U
H(3)	-628(10)	2150(5)	-1588(21)	19
H(4)	-2667(11)	2192(5)	-3421(23)	36
H(6)	-3648(11)	1552(5)	2252(22)	24
H(7)	-1611(12)	1517(5)	4143(23)	30
H(11)	-336(11)	916(6)	-2633(22)	42
H(12)	-2353(11)	835(5)	-4276(25)	35
H(14)	-2926(11)	167(5)	1666(23)	35
H(15)	-873(10)	263(5)	3341(22)	35

3B.1.4 pNO_2-C_6H_4-CNSSN•

The dimers of this compound pack head to tail forming ribbons, see fig 13a-c. Interesting favourable $S^{\delta+}\cdots O^{\delta-}$ contacts, ranging from 3.052(5) to 3.146(5)Å, are observed which obviously influence this packing arrangement. The average intra dimer S···S interaction is at 3.066(3)Å. The skew and clam angle for the dimer molecules is 4.1(7)° and 4.8(7)° respectively.

These ribbons pack adjacent and anti-parallel to one another such that the sulphur and nitrogen atoms of neighbouring dithiadiazolyl rings are within the sum of the van der Waals radii of each other, see 13c. Hence chains of S···N contacts, typically of the order of 3.205(5) to 3.405(5)Å, run perpendicular to these ribbons.

The ribbons are all slightly tilted to approximately the same angle as each other such that three 4-centred S···N interactions are observed along the z axis, see fig 13d-e. Looking at these interactions between A and B, in fig 13d-e, it is found that the two external S···N contacts (3.205(5) and 3.231(5)Å) are smaller than the internal S···N contact (3.405(5)Å). If the sizes of these S···N distances are compared with those between B and C the opposite is observed, i.e the external (3.329(5) and 3.325(5)Å) is larger than the internal (3.246(5)Å). This pattern is found to continue between alternate molecules along this plane.

A dihedral angle of 6.7(6)° and 8.4(6)° is observed between the benzene and dithiadiazolyl ring for each pair of dimer molecules. This twist accommodates these unusual S··N interactions between adjacent ribbons.

These sheets stack on top of one another with the ribbons almost overlapping each other in an anti-parallel fashion, fig 13b. This leads to tilted vertical stacks of alternate facing dimers, with no interdimer interactions or contacts between them.

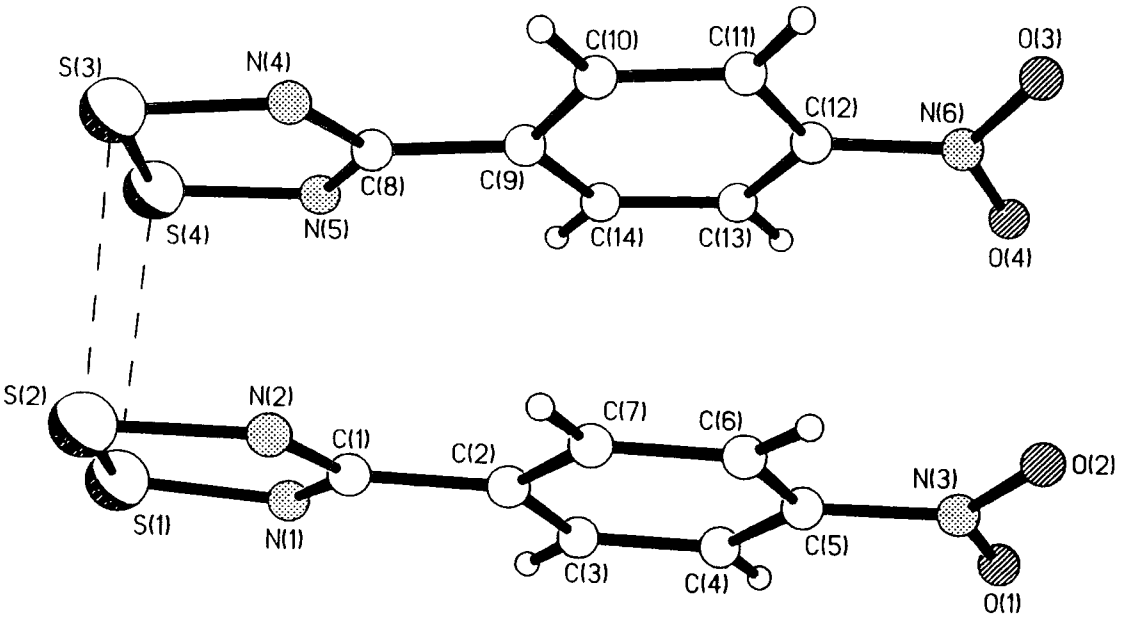

Fig 13a. A dimer

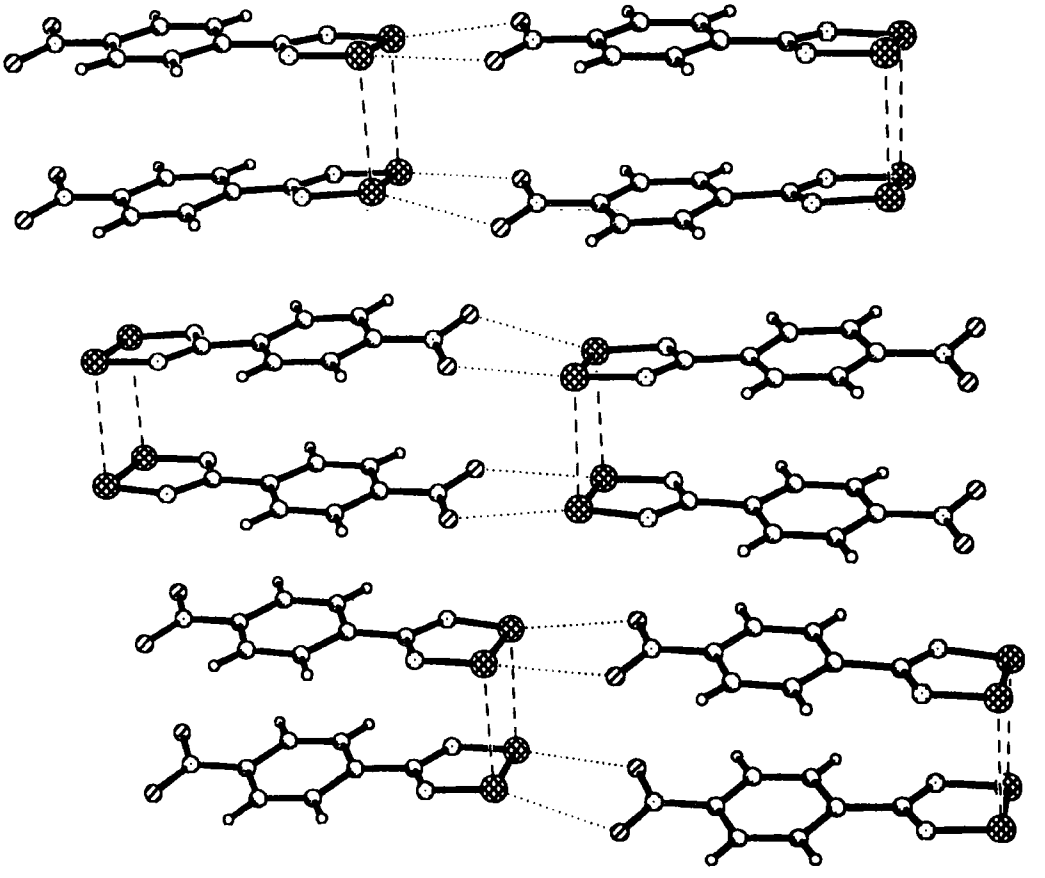

Fig 13b. Vertical stacking of ribbons.

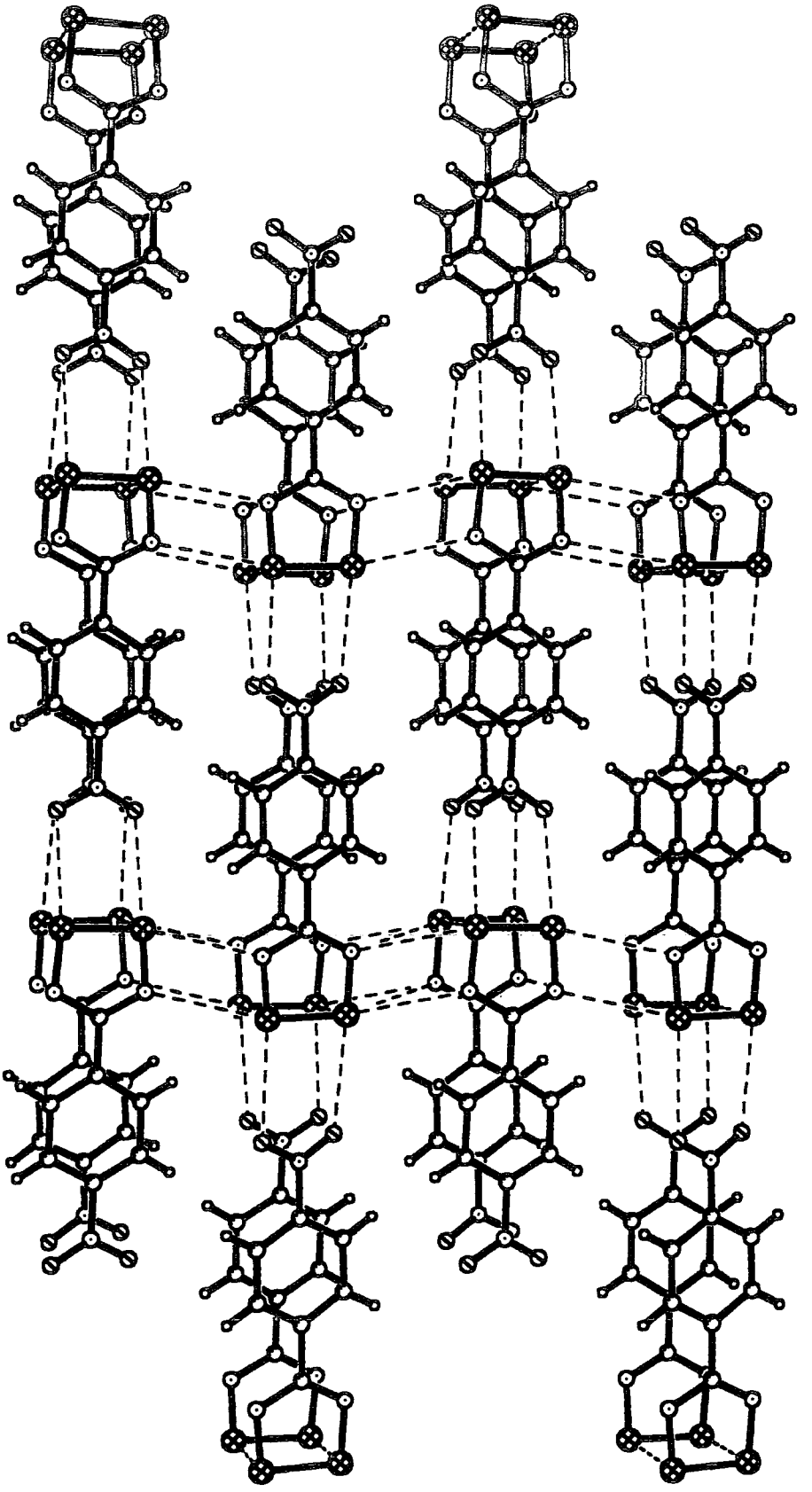

Fig 13c. Packing of adjacent ribbons.

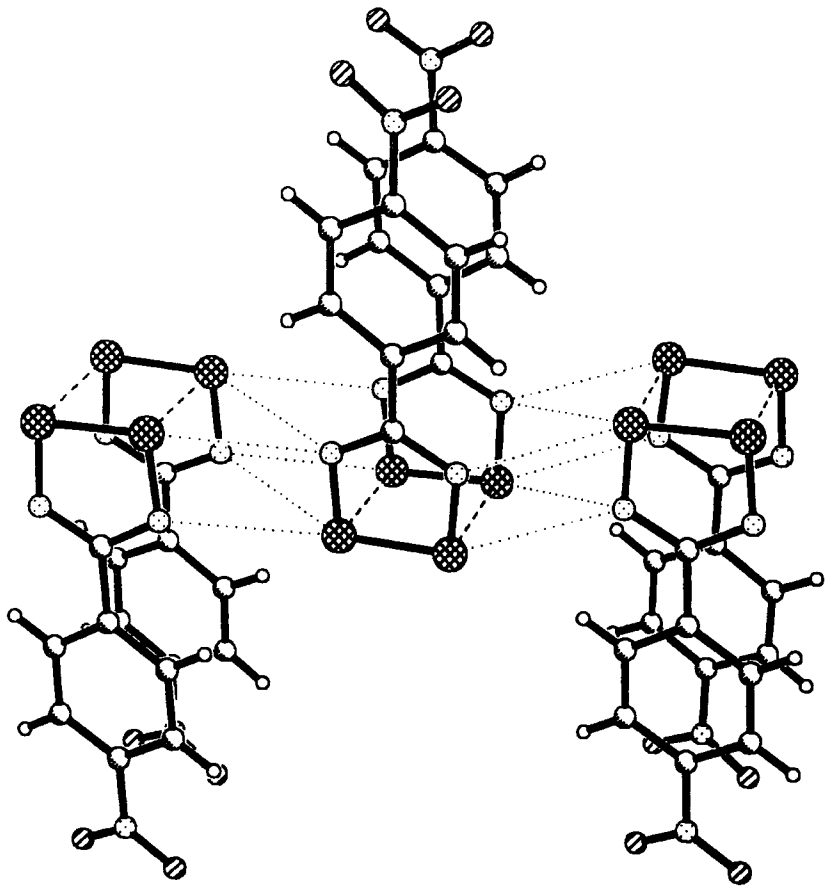

Fig 13d. Diagram demonstrating the S···N inter ribbon contacts

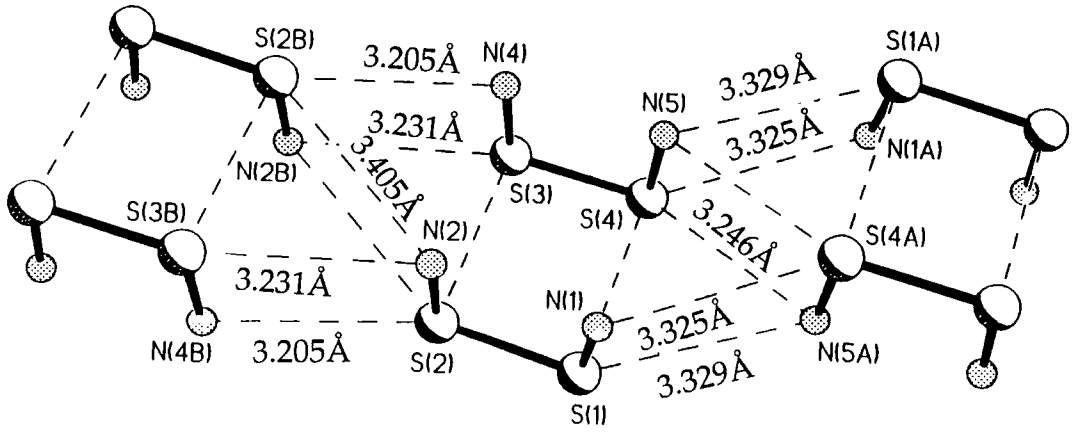

Fig 13e. Molecular fragments of the NO_2 derivatives which demonstate the inter-ribbon S···N interactions

Table 4a. Crystal data, structure solution and refinement for ajb53.

Identification code	ajb53
Chemical formula	$C_7H_4N_3O_2S_2$
Formula weight	226.25
Temperature	160(2) K
Radiation and wavelength	MoKα, 0.71073 Å
Crystal system, space group	triclinic, $P\bar{1}$
Unit cell dimensions	a = 9.054(9) Å α = 96.68(8)°
	b = 10.416(10) Å β = 108.04(4)°
	c = 10.547(12) Å γ = 115.26(3)°
Volume	819(2) $Å^3$
Z	4
Density (calculated)	1.835 g/cm^3
Absorption coefficient μ	0.621 mm^{-1}
F(000)	460
Reflections for cell refinement	26 (θ range 10.66 to 12.39°)
Crystal colour	very dark red
Crystal size	0.62 × 0.08 × 0.08 mm
Data collection method	Stoe-Siemens diffractometer, ω/θ scans
θ range for data collection	2.54 to 25.06°
Index ranges	$-10 \le h \le 10$, $-12 \le k \le 12$, $-9 \le l \le 12$
Standard reflections	3 every 60 minutes
Intensity decay of standards	1.5%
Reflections collected	3030
Independent reflections	2895 (R_{int} = 0.1195)
Reflections with I>2σ(I)	1676
Absorption correction	semi-empirical from ψ-scans
Max. and min. transmission	0.883 and 0.823
Structure solution	direct methods
Refinement method	full-matrix least-squares on F^2
Weighting parameters a, b	0.0362, 0.0000
Data / restraints / parameters	2895 / 0 / 254
Goodness-of-fit on F^2	1.029
Final R indices [I>2σ(I)]	R1 = 0.0539, wR2 = 0.0919
R indices (all data)	R1 = 0.1200, wR2 = 0.1140
Extinction coefficient	0.0004(5)
Largest and mean shift/esd	0.000 and 0.000
Largest diff. peak and hole	0.375 and -0.370 $eÅ^{-3}$

Table 4b. Atomic coordinates (x 10^4) and equivalent isotropic displacement parameters ($Å^2$ x 10^3) for ajb53. U(eq) is defined as one third of the trace of the orthogonalized U_{ij} tensor.

	x	y	z	U(eq)
S(1)	230(2)	8031(2)	10069.9(14)	19.6(4)
S(2)	2499(2)	9585(2)	9755.2(14)	18.9(4)
N(1)	1552(6)	7957(5)	11537(4)	17.8(10)
N(2)	3990(6)	9661(5)	11160(4)	16.4(10)
C(1)	3312(7)	8814(6)	11911(5)	14.1(12)
C(2)	4536(7)	8792(6)	13205(5)	16.0(12)
C(3)	3888(7)	8049(6)	14092(5)	15.4(12)
C(4)	5041(7)	8023(6)	15305(6)	19.9(13)
C(5)	6856(7)	8784(6)	15615(5)	18.5(12)
C(6)	7541(7)	9564(6)	14766(5)	19.2(13)
C(7)	6383(7)	9560(6)	13570(5)	17.5(12)
N(3)	8081(7)	8737(6)	16872(5)	26.8(13)
O(1)	7487(6)	8132(5)	17666(4)	35.0(11)
O(2)	9654(5)	9285(5)	17066(4)	39.7(12)
S(3)	2598(2)	7095(2)	7992.3(14)	18.3(4)
S(4)	517(2)	5531(2)	8392.1(14)	17.7(3)
N(4)	4176(5)	7142(5)	9305(4)	17.4(10)
N(5)	1857(6)	5411(5)	9775(4)	16.7(10)
C(8)	3573(7)	6242(6)	10060(5)	16.4(12)
C(9)	4906(7)	6195(6)	11255(5)	13.0(12)
C(10)	6717(7)	6921(6)	11486(5)	17.3(12)
C(11)	7965(7)	6889(6)	12613(5)	17.7(13)
C(12)	7414(7)	6171(6)	13539(5)	17.0(12)
C(13)	5628(7)	5426(6)	13321(5)	18.2(12)
C(14)	4377(7)	5422(6)	12172(5)	16.6(12)
N(6)	8707(6)	6197(5)	14784(5)	22.7(11)
O(3)	10271(5)	6723(5)	14915(4)	36.1(11)
O(4)	8211(6)	5708(5)	15672(4)	35.3(11)

Table 4c. Bond lengths (Å) and angles (°) for ajb53.

S(1)-N(1)	1.632(5)	S(1)-S(2)	2.099(3)
S(2)-N(2)	1.633(5)	N(1)-C(1)	1.344(7)
N(2)-C(1)	1.336(7)	C(1)-C(2)	1.478(7)
C(2)-C(3)	1.393(7)	C(2)-C(7)	1.405(7)
C(3)-C(4)	1.390(7)	C(4)-C(5)	1.390(8)
C(5)-C(6)	1.390(8)	C(5)-N(3)	1.463(7)
C(6)-C(7)	1.367(7)	N(3)-O(2)	1.223(6)
N(3)-O(1)	1.225(6)	S(3)-N(4)	1.630(5)
S(3)-S(4)	2.101(3)	S(4)-N(5)	1.640(5)
N(4)-C(8)	1.348(7)	N(5)-C(8)	1.325(7)
C(8)-C(9)	1.474(7)	C(9)-C(14)	1.397(7)
C(9)-C(10)	1.404(7)	C(10)-C(11)	1.378(7)
C(11)-C(12)	1.384(8)	C(12)-C(13)	1.388(7)
C(12)-N(6)	1.452(7)	C(13)-C(14)	1.376(7)
N(6)-O(4)	1.231(6)	N(6)-O(3)	1.234(6)
N(1)-S(1)-S(2)	94.8(2)	N(2)-S(2)-S(1)	94.2(2)
C(1)-N(1)-S(1)	113.6(4)	C(1)-N(2)-S(2)	114.3(4)
N(2)-C(1)-N(1)	123.0(5)	N(2)-C(1)-C(2)	119.2(5)
N(1)-C(1)-C(2)	117.8(5)	C(3)-C(2)-C(7)	119.2(5)
C(3)-C(2)-C(1)	121.0(5)	C(7)-C(2)-C(1)	119.8(5)
C(4)-C(3)-C(2)	120.9(5)	C(3)-C(4)-C(5)	117.9(5)
C(6)-C(5)-C(4)	122.4(5)	C(6)-C(5)-N(3)	119.1(5)
C(4)-C(5)-N(3)	118.5(5)	C(7)-C(6)-C(5)	118.7(5)
C(6)-C(7)-C(2)	120.9(5)	O(2)-N(3)-O(1)	123.0(5)
O(2)-N(3)-C(5)	118.1(5)	O(1)-N(3)-C(5)	118.9(5)
N(4)-S(3)-S(4)	94.6(2)	N(5)-S(4)-S(3)	94.1(2)
C(8)-N(4)-S(3)	113.8(4)	C(8)-N(5)-S(4)	114.3(4)
N(5)-C(8)-N(4)	123.2(5)	N(5)-C(8)-C(9)	119.3(5)
N(4)-C(8)-C(9)	117.6(5)	C(14)-C(9)-C(10)	119.2(5)
C(14)-C(9)-C(8)	120.2(5)	C(10)-C(9)-C(8)	120.6(5)
C(11)-C(10)-C(9)	120.6(5)	C(10)-C(11)-C(12)	119.0(5)
C(11)-C(12)-C(13)	121.5(5)	C(11)-C(12)-N(6)	120.4(5)
C(13)-C(12)-N(6)	118.1(5)	C(14)-C(13)-C(12)	119.4(5)
C(13)-C(14)-C(9)	120.3(5)	O(4)-N(6)-O(3)	122.5(5)
O(4)-N(6)-C(12)	119.0(5)	O(3)-N(6)-C(12)	118.5(5)

Table 4d. **Anisotropic displacement parameters ($Å^2$ x 10^3) for ajb53.**

The anisotropic displacement factor exponent takes the form:
$-2\pi^2(h^2a^{*2}U_{11} + \ldots + 2hka^*b^*U_{12})$.

	U(11)	U(22)	U(33)	U(23)	U(13)	U(12)
S(1)	13.9(7)	28.0(9)	15.6(8)	6.3(7)	4.6(6)	10.1(7)
S(2)	16.9(8)	19.5(9)	15.6(8)	6.6(6)	3.3(6)	6.7(7)
N(1)	16(2)	21(3)	14(2)	4(2)	6(2)	7(2)
N(2)	15(2)	19(3)	16(2)	10(2)	5(2)	8(2)
C(1)	12(3)	14(3)	12(3)	-3(2)	1(2)	7(2)
C(2)	18(3)	19(3)	8(3)	-2(2)	0(2)	12(3)
C(3)	17(3)	15(3)	10(3)	-2(2)	5(2)	6(2)
C(4)	27(3)	19(3)	17(3)	3(2)	12(3)	12(3)
C(5)	26(3)	21(3)	10(3)	2(2)	2(2)	17(3)
C(6)	15(3)	23(3)	20(3)	1(2)	7(2)	10(3)
C(7)	19(3)	18(3)	17(3)	5(2)	6(2)	10(3)
N(3)	30(3)	32(3)	14(3)	2(2)	-3(2)	21(3)
O(1)	44(3)	47(3)	18(2)	16(2)	9(2)	26(2)
O(2)	22(2)	55(3)	34(3)	15(2)	2(2)	18(2)
S(3)	17.1(8)	23.5(9)	15.0(7)	7.8(6)	6.7(6)	9.7(7)
S(4)	14.0(7)	18.4(8)	16.1(7)	4.3(6)	3.8(6)	5.9(6)
N(4)	13(2)	21(3)	17(2)	6(2)	5(2)	8(2)
N(5)	15(2)	19(3)	15(2)	5(2)	4(2)	8(2)
C(8)	19(3)	13(3)	15(3)	3(2)	6(2)	7(3)
C(9)	14(3)	13(3)	13(3)	2(2)	7(2)	7(2)
C(10)	22(3)	15(3)	17(3)	3(2)	9(2)	11(3)
C(11)	15(3)	16(3)	18(3)	0(2)	5(2)	7(2)
C(12)	16(3)	22(3)	8(3)	0(2)	-2(2)	11(3)
C(13)	22(3)	19(3)	14(3)	5(2)	5(2)	12(3)
C(14)	17(3)	18(3)	20(3)	6(2)	10(2)	11(2)
N(6)	21(3)	21(3)	21(3)	4(2)	5(2)	8(2)
O(3)	16(2)	56(3)	26(2)	15(2)	3(2)	12(2)
O(4)	37(3)	52(3)	21(2)	21(2)	11(2)	23(2)

Table 4e. **Hydrogen atom coordinates (x 10^4) and isotropic displacement parameters ($Å^2$ x 10^3) for ajb53.**

	x	y	z	U
H(3)	2643(7)	7553(6)	13866(5)	18
H(4)	4601(7)	7501(6)	15904(6)	24
H(6)	8790(7)	10089(6)	15012(5)	23
H(7)	6833(7)	10084(6)	12977(5)	21
H(10)	7086(7)	7439(6)	10861(5)	21
H(11)	9184(7)	7353(6)	12752(5)	21
H(13)	5272(7)	4924(6)	13959(5)	22
H(14)	3150(7)	4891(6)	12002(5)	20

3B.1.5 $mBr\text{-}C_6H_4\text{-}CNSSN^\bullet$

Only one structure of a meta derivative was obtained, this being the meta bromo. Structural analysis revealed that this compound exists as a dimer whose molecules are cis to each other, see Fig 14a. The S···S intradimer interactions are 3.188(1) and 2.985(1)Å.

The eclipse angle of the dimer molecules is 7.4(3)° and the "clam" angle is 7.3(3)°. The angle between the mean planes of the dithiadiazolyl and aryl ring are 9.9(3)° and 3.9(3)° for C(11)-N(12) vs C(12)-C(17) and C(21)-N(22) vs C(22)-C(27) respectively. The angle between the two dithiadiazolyl rings in a dimer unit, [C(11)-N(12) vs C(21)-N(22)], is 7.3(3)° and between the aryl rings, [C(12)-C(17) vs C(22)-C(27)] is 5.7(3)°. Br(1) lies 0.076(4)Å above the mean plane of the benzene ring while and Br(2) is essentially planar as the deviation is a mere 0.001(4)Å. The torsion angles for N(11)-C(11)-C(12)-C(13), N(12)-C(11)-C(12)-C(17), N(21)-C(21)-C(22)-C(23) and N(22)-C(21)-C(22)-C(27) are 9.4(3)°, 7.7(3)°, 4.3(3)° and 2.4(3)° respectively.

So far it has been shown that the S···S intradimer interactions are uneven, one Br atom of a dimer pair is out of plane from the benzene ring it is bonded to and that both aryl rings of a dimer are furthest apart at the site of the bromine atoms. These deviations from planarity are not solely due to steric repulsions between the large bromine atoms. When the bulk packing arrangement is further studied it can be shown that interesting but complicated Br···S attractions and Br···N repulsive contacts also contribute to the twisting of these molecules.

The dimers pack down the x axis forming a zig-zag pattern, as shown in Fig 14c. This picture, along with 14b, shows that this packing gives rise to step like Br···S and S···S attractions which run vertically down the page. Fig 14d shows more clearly the extent of the Br···S interactions. The bromine atom of each molecule in a dimer interacts with one sulphur atom from each of two dimer units of a parallel neighbouring array and with one sulphur of a dimer unit perpendicular to it. The Br···S interactions are 3.639(1) and 3.746(1)Å respectively. Also between the adjacent dimers exist S···N contacts (3.597(3)Å and 3.547(3)Å) of the type observed for $p\text{-}MeS\text{-}C_6H_4\text{-}CNSSN^\bullet$.

Also observed in Figs 14b-c are unfavourable Br···N contacts of 3.533(2)Å, for which only one is observed per Br atom. This interaction can be seen between C&E, D&F, G&A, H&B.

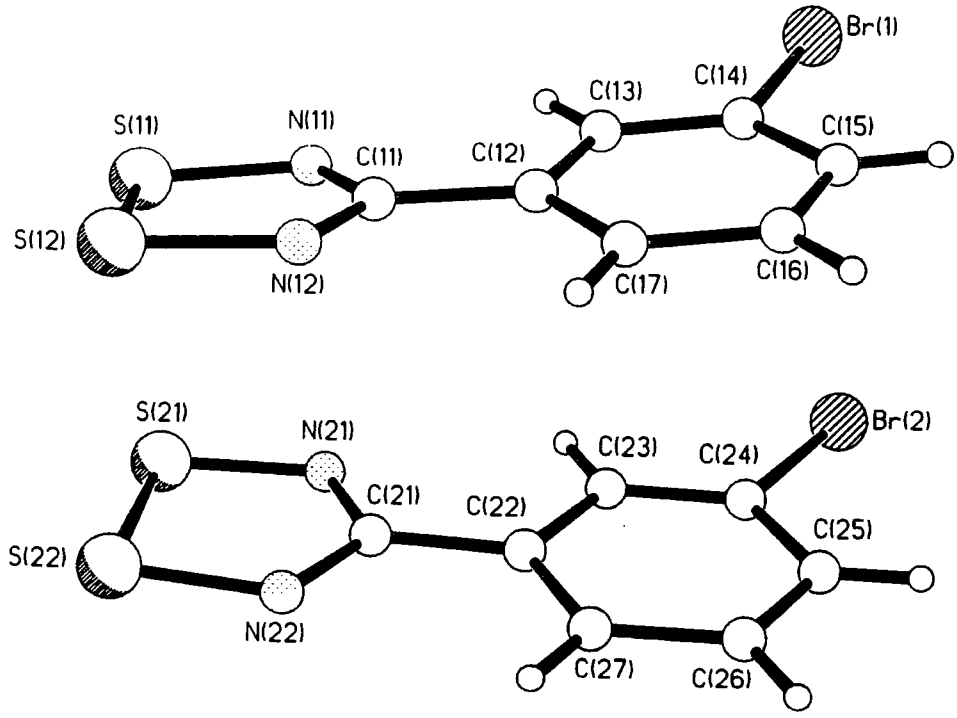

Fig 14a. A dimer

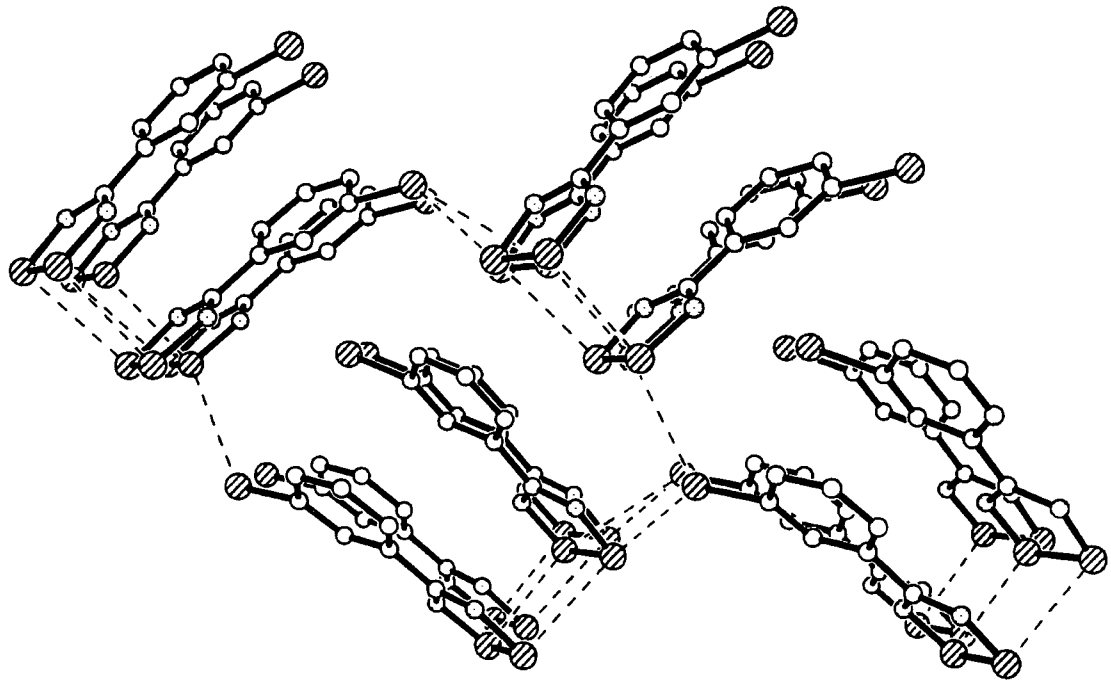

Fig 14b. Perpendicular packing of the dimers.

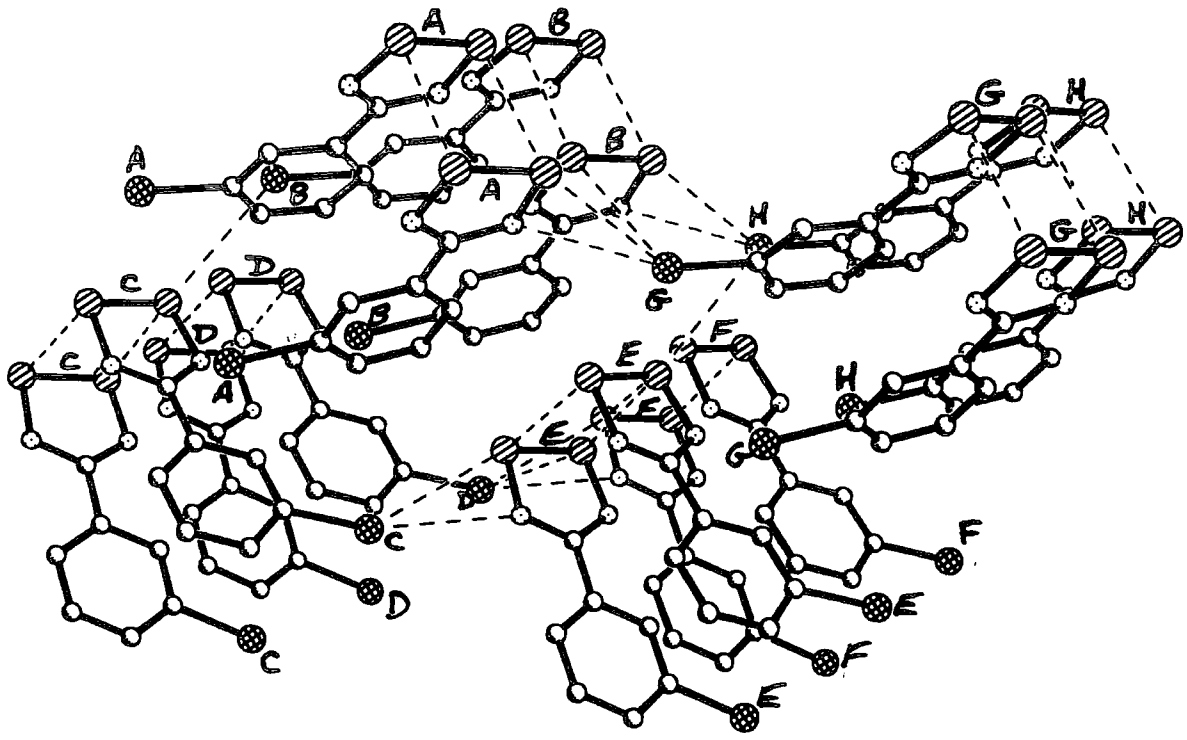

Fig 14c. Diagram showing the Br···S interactions along the zig-zag arrays.

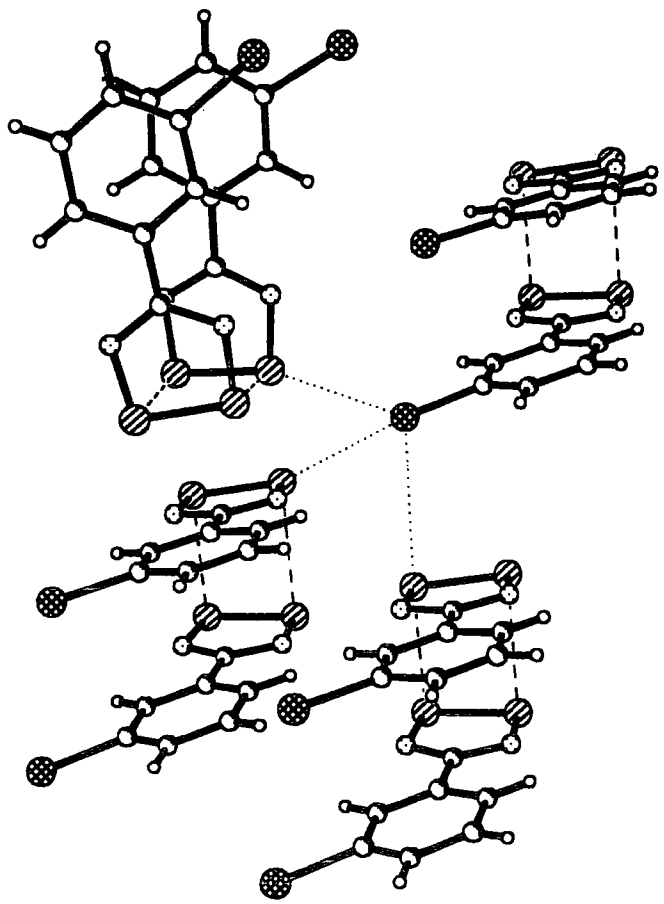

Fig 14d A simplified diagram to show Br···S contacts involving just one of the bromine substituents.

Table 5a. Crystal data, structure solution and refinement for ajb48.

Identification code	ajb48
Chemical formula	$C_7H_4BrN_2S_2$
Formula weight	260.15
Temperature	160(2) K
Radiation and wavelength	MoKα, 0.71073 Å
Crystal system, space group	monoclinic, $P2_1$
Unit cell dimensions	a = 5.879(2) Å $\alpha = 90^\circ$
	b = 13.561(4) Å $\beta = 105.56(3)^\circ$
	c = 10.957(3) Å $\gamma = 90^\circ$
Volume	841.6(4) $Å^3$
Z	4
Density (calculated)	2.053 g/cm^3
Absorption coefficient	5.317 mm^{-1}
F(000)	508
Reflections for cell refinement	33 (θ range 11.18 to 12.50°)
Crystal colour	dark red
Crystal size	0.39 × 0.29 × 0.23 mm
Data collection method	Stoe-Siemens diffractometer,
	ω/θ scans with on-line profile fitting
θ range for data collection	3.00 to 24.99°
Index ranges	$-6 \le h \le 6$, $-16 \le k \le 16$, $-13 \le \ell \le 13$
Standard reflections	3 every 60 minutes
Intensity decay of standards	1%
Reflections collected	5369
Independent reflections	2929 (R_{int} = 0.0209)
Reflections with $I>2\sigma(I)$	2862
Absorption correction	semi-empirical from ψ-scans
Max. and min. transmission	0.952 and 0.550
Structure solution	direct methods
Refinement method	full-matrix least-squares on F^2
Weighting parameters a, b	0.0187, 0.2574
Data / restraints / parameters	2929 / 1 / 219
Goodness-of-fit on F^2	1.081
Final R indices [$I>2\sigma(I)$]	R1 = 0.0160, wR2 = 0.0392
R indices (all data)	R1 = 0.0170, wR2 = 0.0396
Absolute structure parameter	0.425(5)
Extinction coefficient	0.0042(4)
Largest and mean shift esd	0.002 and 0.000
Largest diff. peak and hole	.298 and -.270 $eÅ^{-3}$

Table 5b. **Atomic coordinates (x 10^4) and equivalent isotropic displacement parameters ($Å^2$ x 10^3) for ajb48. U(eq) is defined as one third of the trace of the orthogonalized U_{ij} tensor.**

	x	y	z	U(eq)
Br(1)	8152.3(4)	2109.8(2)	12097.8(2)	27.12(8)
S(11)	4483.7(12)	-769.2(5)	6653.3(7)	25.7(2)
S(12)	7349.7(12)	-775.3(5)	5853.7(7)	26.2(2)
N(11)	5691(4)	7(2)	7768(2)	21.7(5)
N(12)	8861(4)	45(2)	6852(2)	23.0(5)
C(11)	7813(5)	339(2)	7718(3)	19.1(5)
C(12)	9033(4)	1062(2)	8696(2)	17.1(5)
C(13)	8122(4)	1259(2)	9727(3)	18.3(5)
C(14)	9317(5)	1892(2)	10658(2)	19.8(5)
C(15)	11388(5)	2357(2)	10600(3)	22.7(6)
C(16)	12262(4)	2170(2)	9569(3)	22.8(5)
C(17)	11118(5)	1518(2)	8617(3)	19.6(5)
Br(2)	6430.4(5)	4371.9(2)	9608.7(3)	28.47(8)
S(21)	2125.7(11)	832.9(5)	4898.9(6)	22.02(14)
S(22)	4605.5(12)	804.9(5)	3836.7(6)	25.9(2)
N(21)	3448(4)	1717(2)	5838(2)	20.3(5)
N(22)	6226(4)	1691(2)	4640(2)	24.0(5)
C(21)	5434(4)	2046(2)	5586(2)	18.6(5)
C(22)	6791(4)	2841(2)	6381(3)	17.9(5)
C(23)	6067(4)	3184(2)	7426(2)	17.4(5)
C(24)	7386(5)	3908(2)	8179(3)	20.9(5)
C(25)	9395(4)	4309(2)	7934(3)	22.9(5)
C(26)	10069(5)	3968(2)	6904(3)	23.4(6)
C(27)	8802(4)	3237(2)	6122(3)	20.5(5)

Table 5c. Bond lengths (Å) and angles (°) for ajb48.

Br(1)-C(14)	1.903(3)	S(11)-N(11)	1.624(2)
S(11)-S(12)	2.0974(11)	S(12)-N(12)	1.644(2)
N(11)-C(11)	1.341(4)	N(12)-C(11)	1.324(4)
C(11)-C(12)	1.487(4)	C(12)-C(17)	1.396(4)
C(12)-C(13)	1.399(4)	C(13)-C(14)	1.374(4)
C(14)-C(15)	1.388(4)	C(15)-C(16)	1.384(4)
C(16)-C(17)	1.394(4)	Br(2)-C(24)	1.907(3)
S(21)-N(21)	1.635(2)	S(21)-S(22)	2.0957(11)
S(22)-N(22)	1.636(2)	N(21)-C(21)	1.346(3)
N(22)-C(21)	1.335(3)	C(21)-C(22)	1.478(4)
C(22)-C(27)	1.395(4)	C(22)-C(23)	1.403(4)
C(23)-C(24)	1.379(4)	C(24)-C(25)	1.390(4)
C(25)-C(26)	1.373(4)	C(26)-C(27)	1.389(4)
N(11)-S(11)-S(12)	94.52(9)	N(12)-S(12)-S(11)	94.05(9)
C(11)-N(11)-S(11)	114.2(2)	C(11)-N(12)-S(12)	114.1(2)
N(12)-C(11)-N(11)	123.0(3)	N(12)-C(11)-C(12)	119.2(2)
N(11)-C(11)-C(12)	117.8(2)	C(17)-C(12)-C(13)	119.8(2)
C(17)-C(12)-C(11)	120.6(2)	C(13)-C(12)-C(11)	119.5(2)
C(14)-C(13)-C(12)	119.3(2)	C(13)-C(14)-C(15)	122.0(3)
C(13)-C(14)-Br(1)	119.1(2)	C(15)-C(14)-Br(1)	118.8(2)
C(16)-C(15)-C(14)	118.4(2)	C(15)-C(16)-C(17)	121.1(2)
C(16)-C(17)-C(12)	119.3(2)	N(21)-S(21)-S(22)	94.51(9)
N(22)-S(22)-S(21)	94.53(9)	C(21)-N(21)-S(21)	114.0(2)
C(21)-N(22)-S(22)	114.1(2)	N(22)-C(21)-N(21)	122.8(3)
N(22)-C(21)-C(22)	118.4(2)	N(21)-C(21)-C(22)	118.8(2)
C(27)-C(22)-C(23)	119.9(2)	C(27)-C(22)-C(21)	120.9(2)
C(23)-C(22)-C(21)	119.3(2)	C(24)-C(23)-C(22)	118.6(2)
C(23)-C(24)-C(25)	122.2(3)	C(23)-C(24)-Br(2)	118.9(2)
C(25)-C(24)-Br(2)	118.8(2)	C(26)-C(25)-C(24)	118.3(3)
C(25)-C(26)-C(27)	121.5(2)	C(26)-C(27)-C(22)	119.5(3)

Table 5d. Anisotropic displacement parameters ($Å^2$ x 10^3) for ajb48.

The anisotropic displacement factor exponent takes the form:
$-2\pi^2(h^2a^{*2}U_{11} + \ldots + 2hka^*b^*U_{12})$.

	U(11)	U(22)	U(33)	U(23)	U(13)	U(12)
Br(1)	27.70(13)	36.9(2)	18.52(13)	-5.83(12)	9.24(10)	0.89(12)
S(11)	29.0(3)	26.6(3)	22.3(3)	-4.0(3)	8.4(3)	-10.6(3)
S(12)	26.9(3)	26.7(3)	25.5(4)	-9.2(3)	7.8(3)	0.8(3)
N(11)	23.4(11)	25.8(11)	15.7(11)	-2.5(9)	5.2(9)	-5.3(9)
N(12)	20.1(11)	25.5(11)	23.6(12)	-6.5(10)	6.2(10)	0.4(9)
C(11)	19.6(13)	18.6(12)	19.0(13)	3.9(11)	5.1(10)	1.6(10)
C(12)	16.6(12)	18.7(12)	15.8(13)	5.2(10)	3.9(11)	3.3(9)
C(13)	14.8(11)	19.3(11)	20.3(14)	3.2(10)	4.1(10)	2.0(10)
C(14)	22.9(13)	20.7(13)	15.9(13)	3.8(11)	5.3(10)	4.9(10)
C(15)	20.2(13)	21.9(14)	23.4(14)	-3.2(11)	1.4(11)	-3.9(10)
C(16)	16.9(11)	24.9(13)	28.0(14)	1.9(13)	8.6(10)	-2.7(12)
C(17)	21.4(12)	22.6(13)	16.3(13)	2.7(10)	7.7(11)	3.5(10)
Br(2)	32.03(14)	25.65(13)	29.6(2)	-11.73(11)	11.57(12)	-4.11(11)
S(21)	17.9(3)	26.8(3)	21.1(3)	-4.5(3)	4.8(2)	-2.9(3)
S(22)	30.6(4)	30.6(3)	18.6(3)	-7.0(3)	10.4(3)	-6.9(3)
N(21)	18.7(11)	21.7(11)	19.7(12)	-3.8(9)	3.7(9)	-1.7(8)
N(22)	28.0(12)	26.2(11)	20.2(13)	-4.3(9)	10.6(10)	-6.5(9)
C(21)	20.1(11)	20.0(12)	16.6(12)	3.3(11)	6.4(10)	2.8(11)
C(22)	19.8(12)	13.8(11)	19.4(13)	2.4(10)	4.1(11)	2.4(10)
C(23)	18.0(11)	16.0(11)	18.9(13)	1.8(10)	6.0(10)	2.4(10)
C(24)	23.5(13)	16.6(11)	21.4(14)	-0.5(11)	3.9(11)	2.9(10)
C(25)	22.4(12)	18.1(12)	25.5(14)	1.2(12)	1.9(11)	-0.3(11)
C(26)	17.6(12)	20.6(12)	31(2)	6.3(11)	5.5(12)	-2.5(10)
C(27)	21.7(13)	20.1(12)	20.0(14)	6.6(11)	5.9(11)	4.6(11)

Table 5e. Hydrogen atom coordinates (x 10^4) and isotropic displacement parameters ($Å^2$ x 10^3) for ajb48.

	x	y	z	U
H(13)	6693(4)	958(2)	9782(3)	22
H(15)	12188(5)	2793(2)	11253(3)	27
H(16)	13664(4)	2490(2)	9509(3)	27
H(17)	11750(5)	1386(2)	7922(3)	24
H(23)	4698(4)	2923(2)	7611(2)	21
H(25)	10280(4)	4806(2)	8467(3)	27
H(26)	11432(5)	4238(2)	6722(3)	28
H(27)	9300(4)	3009(2)	5415(3)	25

3B.1.6 *m*Cl,*p*Me-C_6H_3-CNSSN•

This radical packs as a cisoid dimer, like that previously described for mBr-C_6H_4-CNSSN•, see Fig 15a. The two intradimer S···S interactions were 3.014(5)Å and 3.159(5)Å and a twist angle of 5.9(10)° between the mean planes of the two dithiadiazolyl rings of a dimer unit is observed. The angle between the dithiadiazolyl ring and the benzene ring for each molecule of the dimer is 7.8(12)° and 9.1(12)°. The angle between the mean planes of the molecules of the dimer unit, is found to be 6.4(14)°. The two chlorine atoms of the dimer unit are found to be 3.835(5)Å apart, i.e, well outside the sum of the van der Waals radii, (3.56Å).

These dimer units pack perpendicular to each other in a head to face T arrangement, down the x axis, to form planes as shown in Fig 15c. Interactions between dimer units within these sheets consist of one Cl and the 2-positioned hydrogen of one of the dimer units interacting respectively with 2-positioned hydrogen and a chlorine of different dimer units, Fig 15c.

These sheets of dimers line up with each other such that arrays of dithiadiazolyl molecules link via S···N and Cl···H interactions 3.551(11) &3.570(11)Å and 3.010(6)&3.649(6)Å respectively, as shown in Fig 15b.

Deviations of the molecules from planarity, as confirmed by the differences in S···S intradimer distances and molecular twist angles, are attributed to intradimer dimer $Cl^{\delta-}/Cl^{\delta-}$ repulsions and intermolecular $H^{\delta+}\cdots Cl^{\delta-}$ attractions. A similar trend was observed for the mBr derivative except that deviations were attributed to $Br^{\delta-}/Br^{\delta-}$ repulsive and $S^{\delta+}\cdots Br^{\delta-}$ attractive forces.

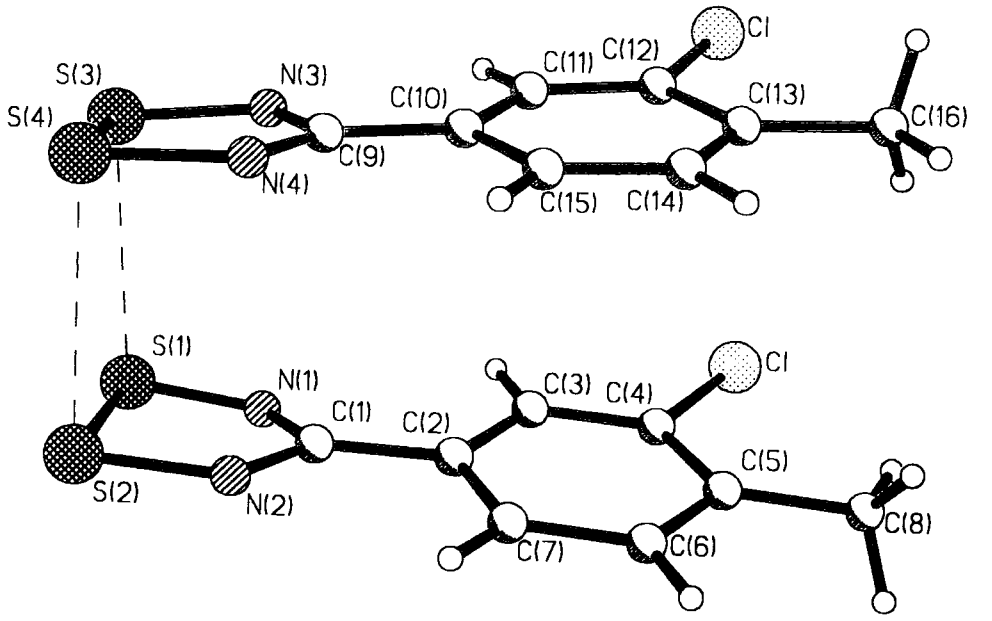

Fig 15a. A dimer

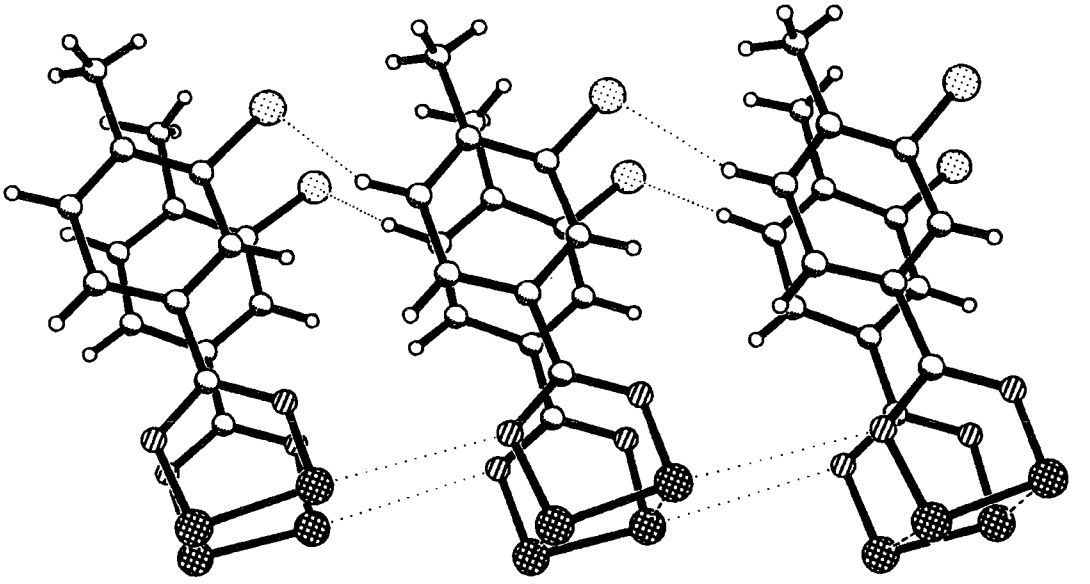

Fig 15b. Packing between adjacent dimers.

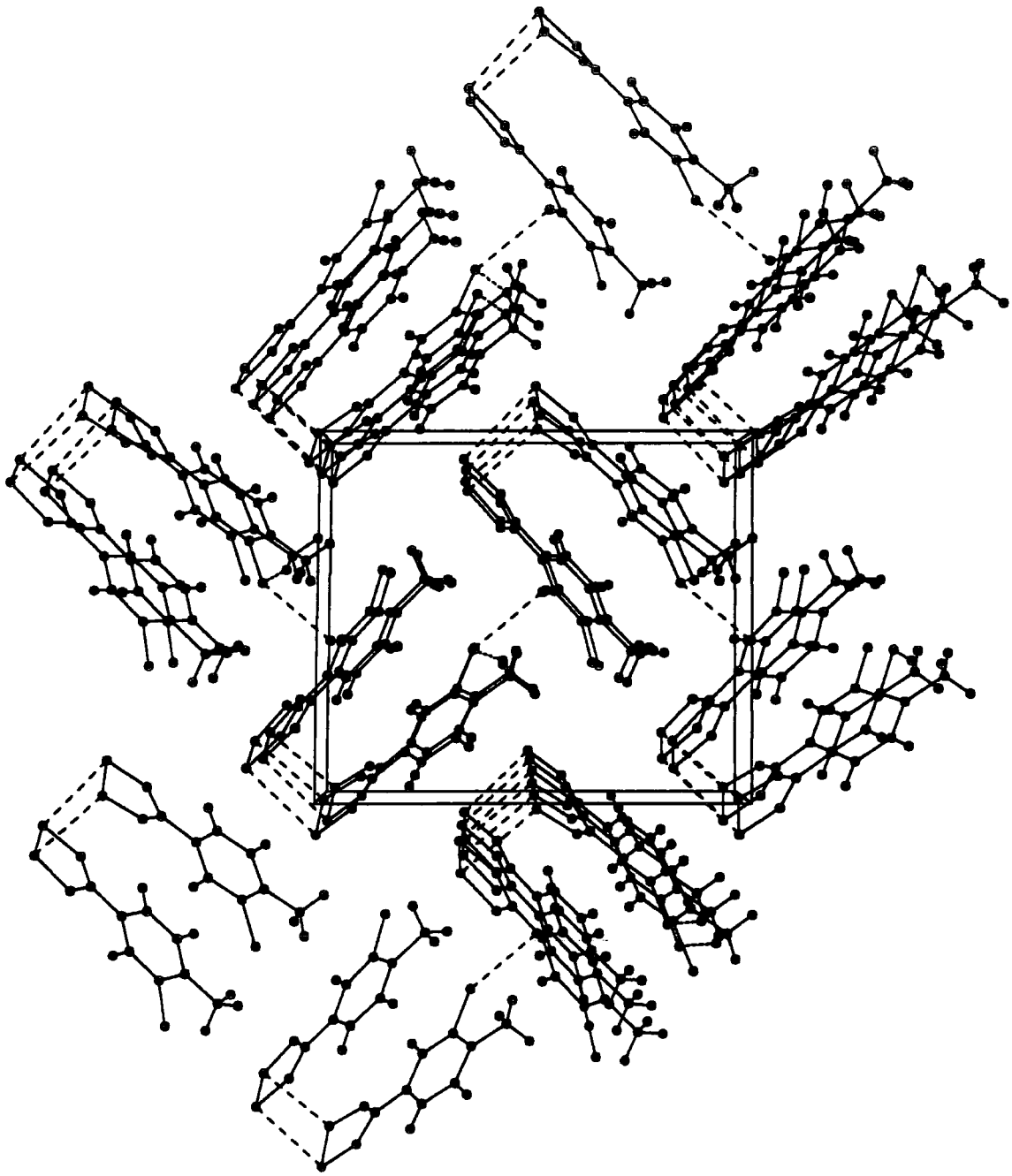

Fig 15c. Perpendicular packing of dimers in a T arrangement.

STRUCTURE DETERMINATION SUMMARY

Table 6a. Crystal Data

Empirical Formula	$C_8 H_6 Cl N_2 S_2$
Color; Habit	red/purple; block
Crystal Size (mm)	0.15 x 0.18 x 0.25
Crystal System	Monoclinic
Space Group	$P2_1$
Unit Cell Dimensions	**a** = 5.937(3) Å
	b = 13.407(3) Å
	c = 11.573(3) Å
	β = 95.87(4)°
Volume	916.3(6) $Å^3$
Z	4
Formula Weight	229.7
Density(calc.)	1.665 Mg/m^3
Absorption Coefficient	0.819 mm^{-1}
F(000)	468

Table 6b. **Solution and Refinement**

System Used	Siemens SHELXTL PLUS (VMS)
Solution	Direct Methods
Refinement Method	Full-Matrix Least-Squares
Quantity Minimized	$\Sigma w(F_o-F_c)^2$
Absolute Structure	N/A
Extinction Correction	N/A
Hydrogen Atoms	Riding model, fixed isotropic U
Weighting Scheme	$w^{-1} = \sigma^2(F) + 0.0005F^2$
Number of Parameters Refined	134
Final R Indices (obs. data)	R = 4.51 %, wR = 5.43 %
R Indices (all data)	R = 8.99 %, wR = 6.92 %
Goodness-of-Fit	1.42
Largest and Mean Δ/σ	0.001, 0.000
Data-to-Parameter Ratio	7.5:1
Largest Difference Peak	0.50 eÅ^{-3}
Largest Difference Hole	-0.41 eÅ^{-3}

Table 6c. **Data Collection**

Diffractometer Used	Rigaku AFC6S
Radiation	MoKα (λ = 0.71073 Å)
Temperature (K)	150
Monochromator	Highly oriented graphite crystal
2θ Range	6.0 to 48.0°
Scan Type	ω/2θ
Scan Speed	Variable; 1.00 to 8.00°/min. in ω
Scan Range (ω)	1.70° + 0.3tanθ
Background Measurement	Stationary crystal and stationary counter at beginning and end of scan, each for 25.0% of total scan time
Standard Reflections	3 measured every 150 reflections
Index Ranges	$0 \leq h \leq 6$, $0 \leq k \leq 15$, $-13 \leq l \leq 13$
Reflections Collected	1668
Independent Reflections	1505 (R_{int} = 5.39%)
Observed Reflections	1107 ($F \geq 6.0\sigma(F)$)
Absorption Correction	N/A

Table 6d. Atomic coordinates ($x10^5$) and equivalent isotropic displacement coefficients ($Å^2x10^4$)

	x	y	z	U(eq)
S(1)	23212(46)	0	98575(25)	249(10)
S(2)	52409(51)	-956(40)	89846(26)	263(10)
Cl(1)	50462(46)	35231(36)	140724(23)	262(10)
N(1)	32997(161)	8934(76)	107213(82)	245(23)
N(2)	65903(166)	7829(79)	97589(82)	236(22)
C(1)	54152(198)	12083(95)	105381(98)	249(28)
C(2)	65047(186)	19974(94)	112897(97)	174(25)
C(3)	53921(177)	23550(92)	122216(90)	213(27)
C(4)	64066(168)	31208(84)	128819(84)	161(25)
C(5)	84116(172)	35681(93)	126837(87)	214(26)
C(6)	94340(173)	31901(85)	117361(81)	176(25)
C(7)	85225(176)	23990(92)	110666(92)	214(26)
C(8)	94163(178)	44134(94)	133931(93)	247(28)
S(3)	39383(54)	-16337(37)	115291(25)	296(10)
S(4)	70826(50)	-16939(36)	108535(25)	287(10)
Cl(2)	56811(49)	13905(35)	162904(24)	260(9)
N(3)	47819(157)	-8548(83)	125420(83)	253(22)
N(4)	82516(145)	-8561(72)	117629(76)	205(22)
C(9)	68929(178)	-5096(86)	125361(91)	183(25)
C(10)	77555(166)	1913(80)	134014(83)	136(23)
C(11)	64817(193)	4679(88)	142987(92)	220(27)
C(12)	72474(167)	11438(80)	151428(84)	130(23)
C(13)	93393(179)	16400(90)	151055(96)	221(28)
C(14)	106008(170)	13842(92)	142068(84)	194(24)
C(15)	98854(183)	6670(91)	133770(95)	240(28)
C(16)	101467(185)	24308(94)	160093(93)	264(29)

* Equivalent isotropic U defined as one third of the trace of the orthogonalized U_{ij} tensor

Table 6e. Bond lengths (Å)

S(1)-S(2)	2.098 (4)	S(1)-N(1)	1.629 (10)
S(2)-N(2)	1.639 (11)	Cl(1)-C(4)	1.752 (11)
N(1)-C(1)	1.362 (16)	N(2)-C(1)	1.324 (16)
C(1)-C(2)	1.476 (17)	C(2)-C(3)	1.405 (16)
C(2)-C(7)	1.362 (16)	C(3)-C(4)	1.381 (15)
C(4)-C(5)	1.373 (15)	C(5)-C(6)	1.401 (15)
C(5)-C(8)	1.488 (16)	C(6)-C(7)	1.390 (16)
S(3)-S(4)	2.098 (5)	S(3)-N(3)	1.611 (11)
S(4)-N(4)	1.644 (10)	Cl(2)-C(12)	1.729 (11)
N(3)-C(9)	1.337 (14)	N(4)-C(9)	1.347 (14)
C(9)-C(10)	1.429 (15)	C(10)-C(11)	1.396 (15)
C(10)-C(15)	1.419 (15)	C(11)-C(12)	1.375 (15)
C(12)-C(13)	1.413 (15)	C(13)-C(14)	1.386 (16)
C(13)-C(16)	1.531 (16)	C(14)-C(15)	1.394 (16)

Table 6f. Bond angles (°)

S(2)-S(1)-N(1)	94.6(4)	S(1)-S(2)-N(2)	94.3(4)
S(1)-N(1)-C(1)	114.1(8)	S(2)-N(2)-C(1)	114.8(8)
N(1)-C(1)-N(2)	122.1(11)	N(1)-C(1)-C(2)	119.1(10)
N(2)-C(1)-C(2)	118.7(11)	C(1)-C(2)-C(3)	119.0(10)
C(1)-C(2)-C(7)	120.8(11)	C(3)-C(2)-C(7)	120.1(11)
C(2)-C(3)-C(4)	117.8(10)	Cl(1)-C(4)-C(3)	117.0(8)
Cl(1)-C(4)-C(5)	118.3(8)	C(3)-C(4)-C(5)	124.7(10)
C(4)-C(5)-C(6)	115.2(10)	C(4)-C(5)-C(8)	123.1(10)
C(6)-C(5)-C(8)	121.7(10)	C(5)-C(6)-C(7)	122.5(10)
C(2)-C(7)-C(6)	119.7(10)	S(4)-S(3)-N(3)	94.2(4)
S(3)-S(4)-N(4)	93.9(4)	S(3)-N(3)-C(9)	116.3(8)
S(4)-N(4)-C(9)	114.8(7)	N(3)-C(9)-N(4)	120.6(10)
N(3)-C(9)-C(10)	119.5(10)	N(4)-C(9)-C(10)	119.7(9)
C(9)-C(10)-C(11)	120.9(10)	C(9)-C(10)-C(15)	122.5(10)
C(11)-C(10)-C(15)	116.6(10)	C(10)-C(11)-C(12)	122.6(10)
Cl(2)-C(12)-C(11)	120.5(8)	Cl(2)-C(12)-C(13)	118.5(8)
C(11)-C(12)-C(13)	121.1(10)	C(12)-C(13)-C(14)	116.8(10)
C(12)-C(13)-C(16)	121.3(10)	C(14)-C(13)-C(16)	121.9(10)
C(13)-C(14)-C(15)	122.5(10)	C(10)-C(15)-C(14)	120.4(10)

Table 6g. Anisotropic displacement coefficients ($Å^2x10^4$)

	U_{11}	U_{22}	U_{33}	U_{12}	U_{13}	U_{23}
S(1)	180(16)	267(17)	290(17)	-1(14)	-20(13)	-93(15)
S(2)	291(19)	271(18)	241(16)	-69(16)	89(14)	-56(14)
Cl(1)	242(15)	261(19)	295(16)	-8(14)	89(12)	-75(15)
S(3)	354(18)	302(20)	237(15)	-107(16)	46(13)	-34(15)
S(4)	305(18)	276(19)	273(16)	50(15)	3(13)	-54(15)
Cl(2)	256(15)	297(18)	240(15)	2(15)	86(12)	-85(15)

The anisotropic displacement factor exponent takes the form:

$-2\pi^2(h^2a^{*2}U_{11} + \ldots + 2hka^*b^*U_{12})$

Table 6h. H-Atom coordinates ($x10^4$) and isotropic displacement coefficients ($Å^2x10^3$)

	x	y	z	U
H(3A)	3978	2077	12399	26
H(6A)	10822	3488	11550	21
H(7A)	9292	2140	10441	26
H(8A)	8481	4569	13998	30
H(8B)	10901	4228	13732	30
H(8C)	9524	4987	12906	30
H(11A)	4991	196	14321	26
H(14A)	12032	1708	14163	23
H(15A)	10832	497	12782	29
H(16A)	11577	2694	15834	32
H(16B)	9055	2960	15989	32
H(16C)	10315	2136	16769	32

3B.1.7 mC_5H_4N-CNSSN•

The molecules pack as cis-oid dimers via characteristic S···S interactions, **(a)**, with an average S···S distance of 3.133(2)Å, see Fig 16a. The clam angle between the mean planes of the molecules of a dimer is found to be 3.6(6)°.

The dimers pack on top of each other forming vertical stacks, see Fig 16b, and the distance between interdimer sulphurs,**(b)**, (4.004(2)/3.987(2)Å) is found to be just within the sum of the van der Waals radii, (4.06Å). Looking at a typical Morse energy curve it can be seen that the energy of interaction between two atoms is very small when the atoms are just within the sum of the van der Waals radii of each other. Thus, it can be assumed that these interdimer S···S contacts will be very small in energy too, i.e very weak. The intradimer interaction will be stronger than the corresponding interdimer contact as the atoms are closer together and can interact more favourably.

However, this combination of alternate interdimer and intradimer S···S interactions, down the stacks is reminiscent of Peierls distortions, see section 3A. This packing feature is also observed for the similar α-meta cyano analogue, see introduction to this chapter.

The dimers in each stack form three centred S···$N_{pyridyl}$ contacts with dimers in two neighbouring stacks, which give rise to pseudo snake like 'wall' of dimers forming, see Fig 16c. Fig 16b shows more clearly that in each 'wall' alternate stacks are out of phase, resulting in a dimer pair, **(III)**, forming S···N bridging contacts **(c)** with two dimer molecules, **(I)** and **(II)**, involved in interdimer S···S interactions with each other. The mean S···N contacts distance, **(c)**, is 2.886(5)Å.

A twist angle of 11.7(5)° and 15.2(5)° is observed for the molecules of each dimer pair and this is attributed to this system's preference for strong S···S interdimer interactions and favourable $S_{intradimer}$···$N_{interdimer}$ contacts.

No significant interactions between adjacent ribbons is observed due to the systems preference for ribbon formation and molecular interactions along the ribbon axis, i.e the energy of the lattice is maximised by this packing arrangement.

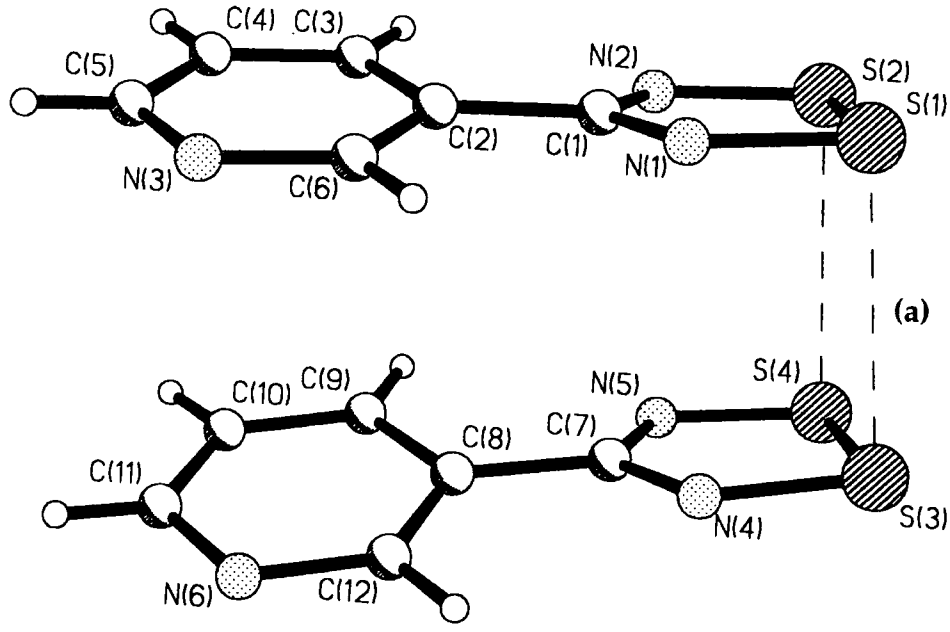

Fig 16a. A dimer

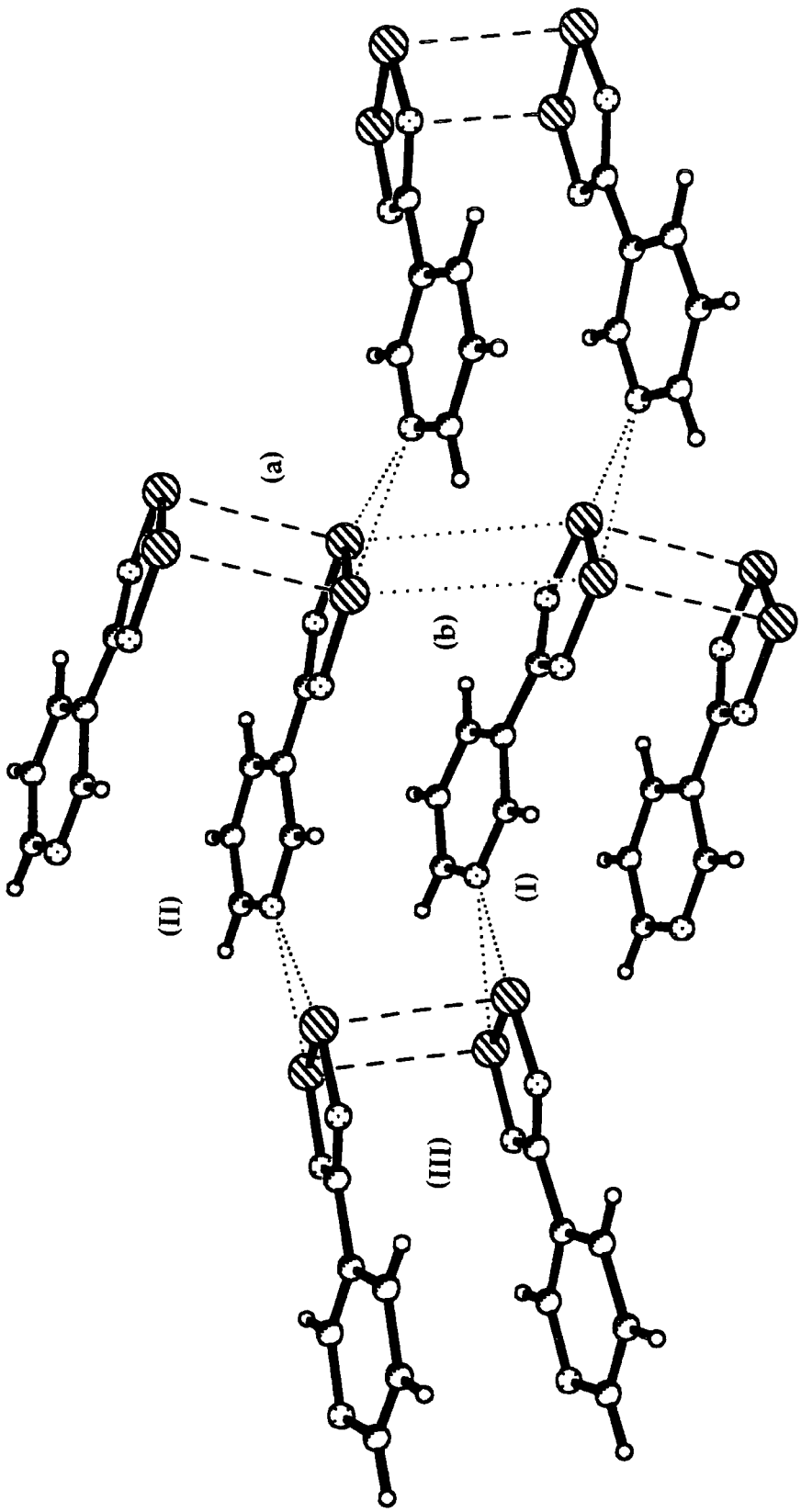

Fig 16b. S···S inter stack interactions

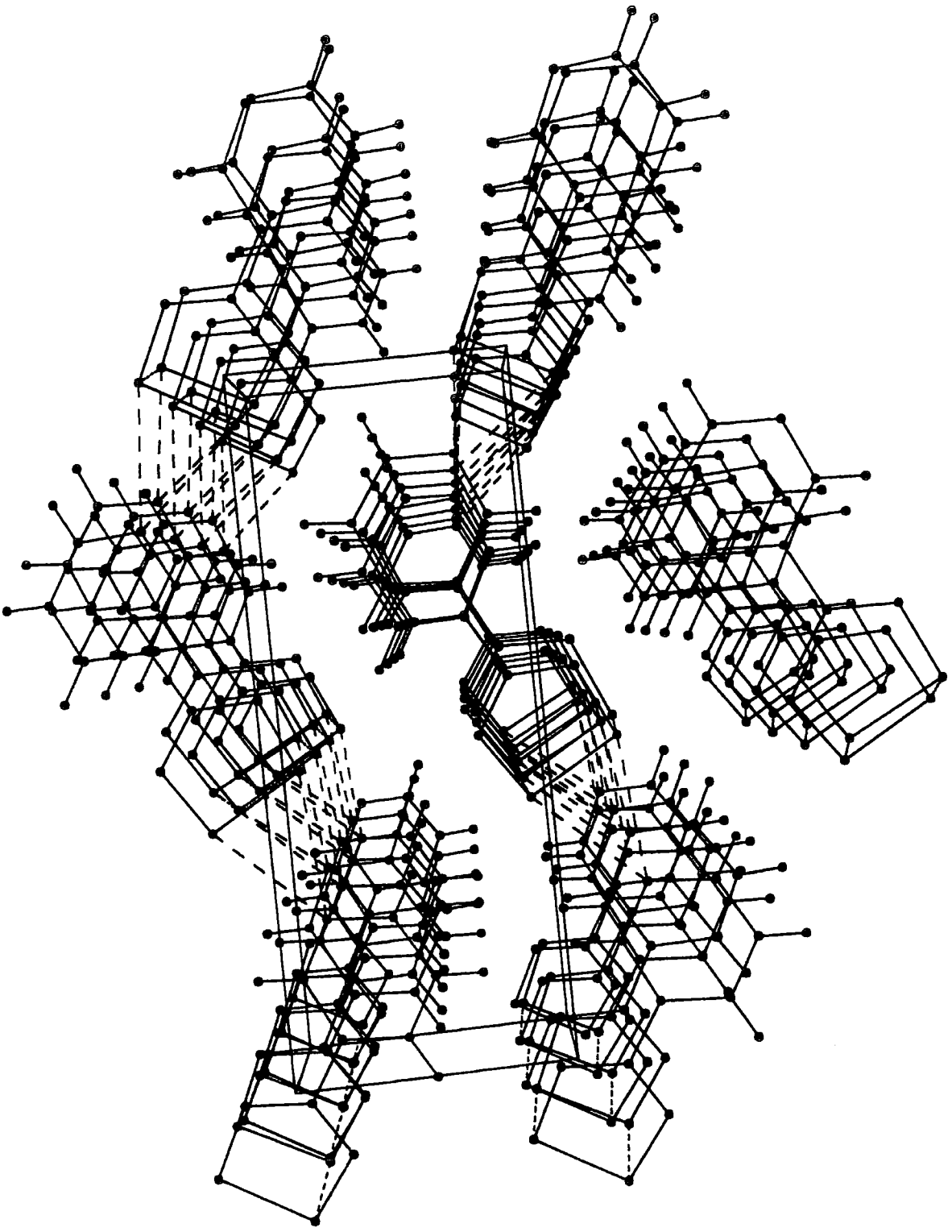

Fig 16c. Ribbon arrays of dimers

Table 7a. Crystal data, structure solution and refinement for ajb52a.

Identification code	ajb52a
Chemical formula	$C_6H_4N_3S_2$
Formula weight	182.24
Temperature	160(2) K
Radiation and wavelength	MoKα, 0.71073 Å
Crystal system, space group	monoclinic, $P2_1$
Unit cell dimensions	a = 6.269(2) Å α = 90° b = 15.834(5) Å β = 95.29(2)° c = 7.024(2) Å γ = 90°
Volume	694.3(4) $Å^3$
Z	4
Density (calculated)	1.743 g/cm^3
Absorption coefficient μ	0.688 mm^{-1}
F(000)	372
Reflections for cell refinement	31 (θ range 9.01 to 12.00°)
Crystal colour	red
Crystal size	0.33 × 0.13 × 0.13 mm
Data collection method	Stoe-Siemens diffractometer, ω/θ scans with on-line profile fitting
θ range for data collection	2.57 to 24.97°
Index ranges	$-7 \le h \le 7$, $-18 \le k \le 18$, $-8 \le \ell \le 8$
Standard reflections	5 every 60 minutes
Intensity decay of standards	0%
Reflections collected	2998
Independent reflections	2454 (R_{int} = 0.0219)
Reflections with I>2σ(I)	2248
Absorption correction	semi-empirical from ψ-scans
Max. and min. transmission	.96239 and .76170
Structure solution	direct methods
Refinement method	full-matrix least-squares on F^2
Weighting parameters a, b	0.0332, 0.5141
Data / restraints / parameters	2452 / 1 / 200
Goodness-of-fit on F^2	1.064
Final R indices [I>2σ(I)]	R1 = 0.0374, wR2 = 0.0787
R indices (all data)	R1 = 0.0440, wR2 = 0.0842
Absolute structure parameter	0.27(10)
Largest and mean shift/esd	0.000 and 0.000
Largest diff. peak and hole	0.326 and −0.337 $eÅ^{-3}$

Table 7b. Atomic coordinates (x 10^4) and equivalent isotropic displacement parameters ($Å^2$ x 10^3) for ajb52a. U(eq) is defined as one third of the trace of the orthogonalized U_{ij} tensor.

	x	y	z	U(eq)
S(1)	1939(2)	4670.2(6)	744(2)	22.3(2)
S(2)	-943(2)	4014.8(6)	550(2)	23.0(2)
N(1)	842(5)	5580(2)	118(5)	20.9(8)
N(2)	-2395(5)	4838(2)	-122(5)	20.8(8)
C(1)	-1284(6)	5544(3)	-286(6)	18.7(9)
C(2)	-2448(7)	6324(3)	-950(6)	18.1(9)
C(3)	-4580(7)	6299(3)	-1689(6)	23.0(10)
C(4)	-5587(7)	7043(3)	-2277(6)	22.5(10)
C(5)	-4464(7)	7794(3)	-2082(6)	22.7(9)
N(3)	-2384(6)	7836(2)	-1357(5)	21.8(8)
C(6)	-1444(6)	7111(3)	-818(6)	20.9(9)
S(3)	1630(2)	4997.3(6)	5073(2)	21.8(2)
S(4)	-1319(2)	4393.6(6)	4918(2)	22.7(2)
N(4)	610(5)	5935(2)	4582(5)	21.2(8)
N(5)	-2721(5)	5246(2)	4359(5)	21.5(8)
C(7)	-1524(7)	5943(3)	4267(6)	17.4(9)
C(8)	-2586(7)	6767(3)	3833(6)	18.5(9)
C(9)	-4720(7)	6815(3)	3088(6)	22.2(11)
C(10)	-5581(7)	7604(3)	2709(6)	23.4(9)
C(11)	-4343(6)	8320(3)	3055(5)	23.1(9)
N(6)	-2290(5)	8284(2)	3812(5)	21.6(8)
C(12)	-1459(7)	7517(3)	4178(6)	21.0(9)

Table 7c. Bond lengths (Å) and angles (°) for ajb52a.

S(1)-N(1)	1.640(3)	S(1)-S(2)	2.077(2)
S(2)-N(2)	1.634(3)	N(1)-C(1)	1.338(5)
N(2)-C(1)	1.328(5)	C(1)-C(2)	1.487(6)
C(2)-C(3)	1.389(6)	C(2)-C(6)	1.395(6)
C(3)-C(4)	1.381(6)	C(4)-C(5)	1.383(6)
C(5)-N(3)	1.357(6)	N(3)-C(6)	1.330(6)
S(3)-N(4)	1.641(3)	S(3)-S(4)	2.076(2)
S(4)-N(5)	1.639(3)	N(4)-C(7)	1.336(5)
N(5)-C(7)	1.339(5)	C(7)-C(8)	1.483(6)
C(8)-C(12)	1.392(6)	C(8)-C(9)	1.393(6)
C(9)-C(10)	1.377(6)	C(10)-C(11)	1.383(6)
C(11)-N(6)	1.347(5)	N(6)-C(12)	1.336(5)
N(1)-S(1)-S(2)	94.62(13)	N(2)-S(2)-S(1)	94.50(13)
C(1)-N(1)-S(1)	113.8(3)	C(1)-N(2)-S(2)	114.5(3)
N(2)-C(1)-N(1)	122.5(4)	N(2)-C(1)-C(2)	118.7(3)
N(1)-C(1)-C(2)	118.8(4)	C(3)-C(2)-C(6)	117.5(4)
C(3)-C(2)-C(1)	121.4(4)	C(6)-C(2)-C(1)	121.0(4)
C(4)-C(3)-C(2)	119.0(4)	C(3)-C(4)-C(5)	119.3(4)
N(3)-C(5)-C(4)	122.9(4)	C(6)-N(3)-C(5)	116.7(4)
N(3)-C(6)-C(2)	124.6(4)	N(4)-S(3)-S(4)	94.45(13)
N(5)-S(4)-S(3)	95.08(13)	C(7)-N(4)-S(3)	114.1(3)
C(7)-N(5)-S(4)	113.6(3)	N(4)-C(7)-N(5)	122.8(4)
N(4)-C(7)-C(8)	117.8(4)	N(5)-C(7)-C(8)	119.5(4)
C(12)-C(8)-C(9)	118.2(4)	C(12)-C(8)-C(7)	120.3(4)
C(9)-C(8)-C(7)	121.5(4)	C(10)-C(9)-C(8)	117.9(4)
C(9)-C(10)-C(11)	120.4(4)	N(6)-C(11)-C(10)	122.3(4)
C(12)-N(6)-C(11)	117.1(4)	N(6)-C(12)-C(8)	124.0(4)

Table 7d. Anisotropic displacement parameters (Å^2 x 10^3) for ajb52a.

The anisotropic displacement factor exponent takes the form:
$-2\pi^2(h^2a^{*2}U_{11} + \ldots + 2hka^*b^*U_{12})$.

	U(11)	U(22)	U(33)	U(23)	U(13)	U(12)
S(1)	19.2(5)	19.3(5)	29.1(6)	0.5(4)	5.8(4)	0.0(4)
S(2)	24.9(6)	16.2(5)	27.4(6)	-2.9(5)	0.5(4)	-3.9(5)
N(1)	21(2)	18(2)	24(2)	5.6(14)	4.9(14)	-2(2)
N(2)	23(2)	17(2)	22(2)	-0.7(13)	-1.0(13)	-1.4(14)
C(1)	20(2)	19(2)	18(2)	-3(2)	5(2)	-4(2)
C(2)	18(2)	20(2)	18(2)	0(2)	6(2)	-2(2)
C(3)	26(2)	26(2)	18(2)	-2(2)	2(2)	-6(2)
C(4)	12(2)	35(3)	20(2)	-1(2)	1(2)	5(2)
C(5)	26(2)	25(2)	17(2)	1(2)	3(2)	8(2)
N(3)	25(2)	18(2)	23(2)	3(2)	4(2)	0(2)
C(6)	18(2)	24(2)	20(2)	0(2)	1(2)	0(2)
S(3)	20.8(5)	15.8(5)	28.0(6)	-1.1(5)	-2.0(4)	-1.0(4)
S(4)	25.3(6)	16.1(5)	27.4(6)	1.3(4)	6.3(4)	-2.2(4)
N(4)	22(2)	12(2)	29(2)	-0.5(14)	-0.9(14)	1.3(14)
N(5)	22(2)	16(2)	26(2)	1.1(14)	6.3(14)	-1.5(14)
C(7)	17(2)	17(2)	19(2)	-3(2)	4(2)	-3(2)
C(8)	23(2)	18(2)	15(2)	-3(2)	4(2)	0(2)
C(9)	23(2)	22(3)	22(2)	-2(2)	6(2)	-1(2)
C(10)	17(2)	31(2)	22(2)	-1(2)	1(2)	2(2)
C(11)	28(2)	22(2)	19(2)	3(2)	3(2)	7(2)
N(6)	22(2)	18(2)	25(2)	1(2)	0.3(14)	2(2)
C(12)	19(2)	22(2)	22(2)	0(2)	3(2)	2(2)

Table 7e. Hydrogen atom coordinates (x 10^4) and isotropic displacement parameters (Å^2 x 10^3) for ajb52a.

	x	y	z	U
H(3)	-5334(7)	5778(3)	-1790(6)	28
H(4)	-7036(7)	7038(3)	-2810(6)	27
H(5)	-5179(7)	8303(3)	-2473(6)	27
H(6)	12(6)	7129(3)	-308(6)	25
H(9)	-5555(7)	6319(3)	2849(6)	27
H(10)	-7035(7)	7657(3)	2208(6)	28
H(11)	-4961(6)	8856(3)	2748(5)	28
H(12)	-11(7)	7482(3)	4705(6)	25

3B.1.8 pC_5F_4N-CNSSN•

The S···S intradimer distance for this compound is 3.111(1)Å. The "clam angle" between the molecules is 7.9(3)°. The torsion angles for N(1)-C(1)-C(2)-C(3) and N(2)-C(1)-C(2)-C(7) are 33.0(2)° and 31.5(2)° respectively.

The dimers pack head to tail in plane with each other, thus forming rows of dimers. Fig 17a shows this packing arrangement for a plane one molecule thick. Looking along these rows it can been seen that each pyridyl nitrogen forms contacts with two sulphurs, (3.309(2) & 3.266(2)), and that one meta fluorine forms a contact (3.148(1)Å) with one of the sulphurs of an in-plane molecule of a neighbouring dimer.

The ribbons of dimers pack adjacent to each other with dimers of alternate rows pointing in opposite directions, such that the neighbouring dithiadiazolyl rings eclipse but are not within the sum of the van der Waals radii of each other. Also, contacts exists between one ortho fluorine of a molecule with a sulphur (attractive) or meta fluorine (repulsive) of another molecule in an adjacent row and these are found to be typically 3.247(1)Å and 2.986(1)Å respectively. No S···N inter-ribbon contacts are observed as the ribbons are not packed closely enough together due to fluorine-fluorine repulsions.

Viewing down the y axis, Fig 17b, it can be seen that a large twist angle of 31.9(2)° exists between the dithiadiazolyl and pyridyl ring . This orientation is influenced mainly by $N^{\delta-}{}_{dithiadiazolyl}$/ortho $F^{\delta-}$ and ortho $F^{\delta-}$/meta $F^{\delta-}$ repulsions being present. This phenomenon is also responsible for the large twists detected in molecules of other perfluoro dithiadiazolyls studied, see 3A.1.1.

The dimers of these ribbons stack on top of one another in an anti-parallel fashion as shown in Fig 17c. There are no significant interactions down these stacks of dimers.

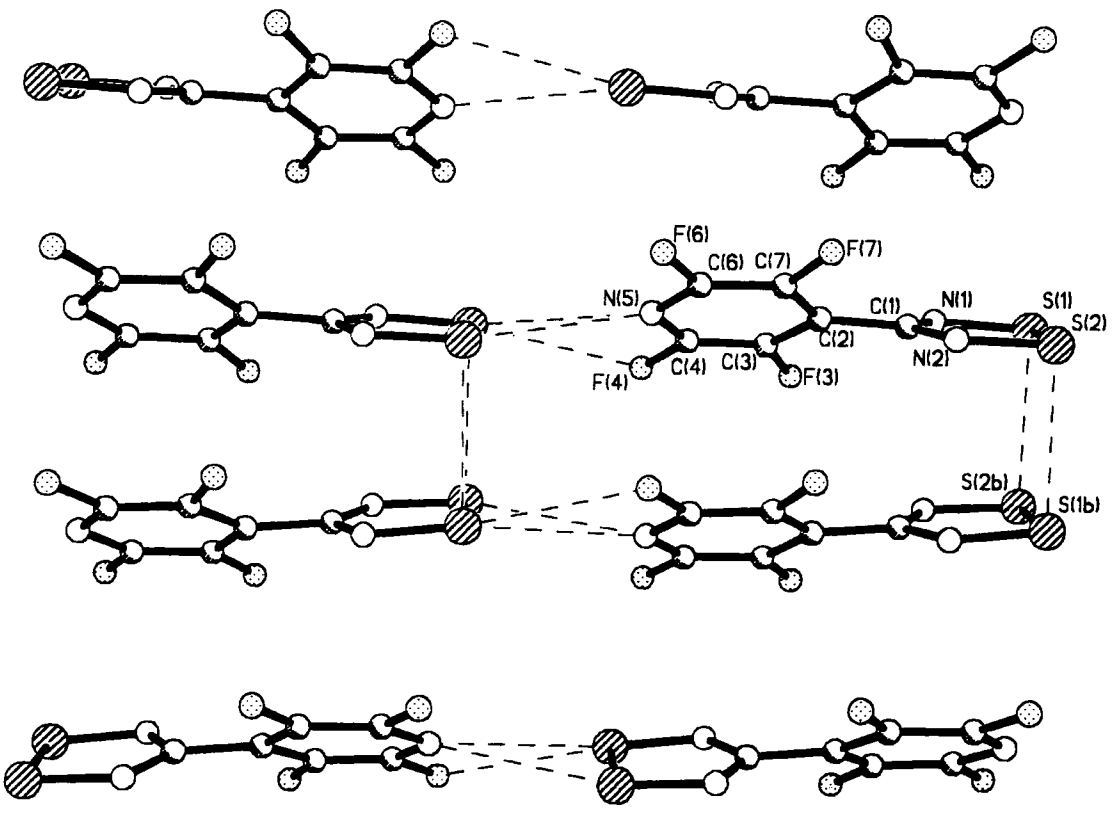

Fig 17a. A close up of the intra ribbon contacts between dimers.

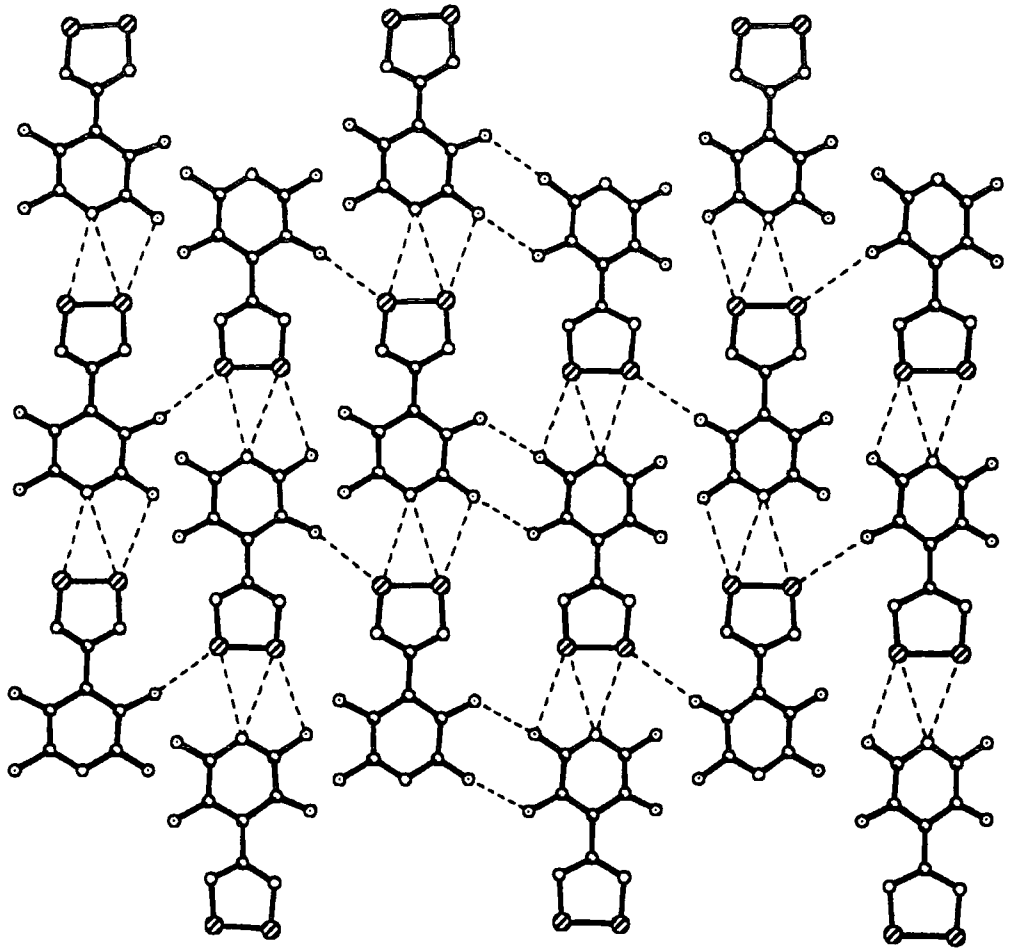

Fig 17b. Packing between adjacent dimers (only one molecule thick).

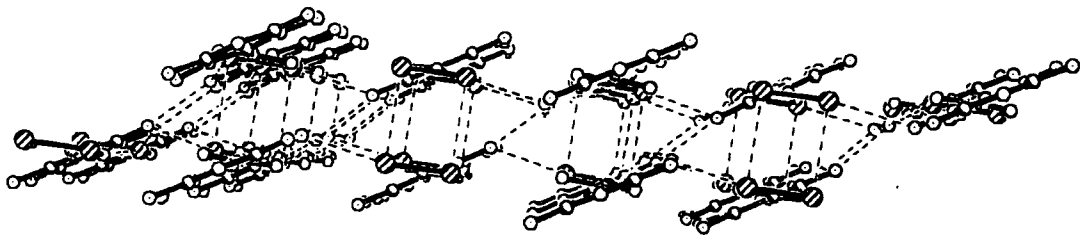

Fig 17c. A view looking down the axis of the ribbons to demonstrate the large twist angle these molecules possess.

Table 8a. Crystal data and structure refinement for $[C_5NF_4.CNSSN]_2$.

Empirical formula	$C_6F_4N_3S_2$
Formula weight	254.21
Temperature, K	150
Mean Wavelength, $\bar{\lambda}$, Å	0.71073
Crystal system	Monoclinic
Space group	I2/a
Unit cell dimensions, Å and °	a = 11.420(4) α = 90 b = 9.654(4) β = 94.06(1) c = 14.563(4) γ = 90
Volume, $Å^3$	1602(1)
Z	8
Density (calc), gcm^{-3}	2.109
Absorption coefficient, mm^{-1} ($\bar{\lambda}$)	0.698
F(000)	1000
Crystal size, mm	0.65 x 0.60 x 0.55
2θ range for data collection, °	5.0 to 50.0
Index ranges	-13<h<11 -11<k<1 -17<l<11
Reflections collected	1768
Independent reflections	1416, R_{int} = 0.0236
Absorption correction	Semi-empirical from psi-scans
Max. and min. transmission	1.0000 and 0.9593
Refinement method	Full-matrix least-squares on F^2
Data, restraints, parameters	1414, 0, 136
Goodness-of-fit on F^2	1.072
Final R indices, I>2σ(I)	R1 = 0.0261 wR2 = 0.0704
R indices, all data	R1 = 0.0340 wR2 = 0.0791
Largest diff. peak and hole, $eÅ^{-3}$	0.409 and -0.373

Table 8b. Selected bond lengths, Å, and angles, °, for $[C_5NF_4.CNSSN]_2$.

N(1)-C(1)	1.335(2)	C(1)-N(1)-S(1)	113.4(1)
N(1)-S(1)	1.640(2)	N(1)-S(1)-S(2)	94.55(6)
S(1)-S(2)	2.100(1)	N(2)-S(2)-S(1)	94.51(6)
S(2)-N(2)	1.636(2)	C(1)-N(2)-S(2)	113.5(1)
N(2)-C(1)	1.337(2)	N(1)-C(1)-N(2)	124.0(2)
C(1)-C(2)	1.484(2)	N(1)-C(1)-C(2)	118.2(2)
		N(2)-C(1)-C(2)	117.8(2)

Table 8c. **Full structural data for $[C_5NF_4.CNSSN]_2$.**

Atomic coordinates and equivalent isotropic displacement parameters for $[C_5NF_4.CNSSN]_2$. U(eq) is defined as one third of the trace of the orthogonalised Uij tensor.

	x	y	z	U(eq)
N(1)	0.3316(1)	-0.0518(2)	0.3773(1)	0.021(1)
S(1)	0.3198(1)	0.1168(1)	0.3869(1)	0.023(1)
S(2)	0.1379(1)	0.1133(1)	0.3997(1)	0.023(1)
N(2)	0.1277(1)	-0.0556(2)	0.3940(1)	0.021(1)
C(1)	0.2298(1)	-0.1185(2)	0.3821(1)	0.017(1)
C(2)	0.2298(1)	-0.2717(2)	0.3744(1)	0.017(1)
C(3)	0.3253(1)	-0.3530(2)	0.4077(1)	0.017(1)
F(3)	0.4220(1)	-0.2954(1)	0.4482(1)	0.023(1)
C(4)	0.3176(1)	-0.4952(2)	0.4033(1)	0.018(1)
F(4)	0.4079(1)	-0.5714(1)	0.4390(1)	0.026(1)
N(5)	0.2255(1)	-0.5643(2)	0.3691(1)	0.020(1)
C(6)	0.1360(2)	-0.4892(2)	0.3356(1)	0.019(1)
F(6)	0.0425(1)	-0.5580(1)	0.3001(1)	0.025(1)
C(7)	0.1338(1)	-0.3462(2)	0.3359(1)	0.018(1)
F(7)	0.0386(1)	-0.2822(1)	0.2981(1)	0.026(1)

Table 8d. Bond lengths, Å, and angles, °, in $[C_5NF_4.CNSSN]_2$.

N(1)-C(1)	1.335(2)	N(1)-S(1)	1.640(2)
S(1)-S(2)	2.010(1)	S(2)-N(2)	1.636(2)
N(2)-C(1)	1.337(2)	C(1)-C(2)	1.484(2)
C(2)-C(7)	1.395(2)	C(2)-C(3)	1.403(2)
C(3)-F(3)	1.335(2)	C(3)-C(4)	1.377(3)
C(4)-N(5)	1.313(2)	C(4)-F(4)	1.341(2)
N(5)-C(6)	1.319(2)	C(6)-F(6)	1.331(2)
C(6)-C(7)	1.381(3)	C(7)-F(7)	1.334(2)

Table 8e.

C(1)-N(1)-S(1)	113.4(1)	N(1)-S(1)-S(2)	94.55(6)
N(2)-S(2)-S(1)	94.51(6)	C(1)-N(2)-S(2)	113.5(1)
N(1)-C(1)-N(2)	124.0(2)	N(1)-C(1)-C(2)	118.2(2)
N(2)-C(1)-C(2)	117.8(2)	C(7)-C(2)-C(3)	114.9(2)
C(7)-C(2)-C(1)	122.7(2)	C(3)-C(2)-C(1)	122.4(2)
F(3)-C(3)-C(4)	118.9(2)	F(3)-C(3)-C(2)	121.2(2)
C(4)-C(3)-C(2)	119.7(2)	N(5)-C(4)-F(4)	116.2(2)
N(5)-C(4)-C(3)	124.8(2)	F(4)-C(4)-C(3)	119.0(2)
C(4)-N(5)-C(6)	116.1(2)	N(5)-C(6)-F(6)	116.7(2)
N(5)-C(6)-C(7)	124.2(2)	F(6)-C(6)-C(7)	119.1(2)
F(7)-C(7)-C(6)	118.4(2)	F(7)-C(7)-C(2)	121.4(2)
C(6)-C(7)-C(2)	120.1(2)		

Table 8f. Anisotropic displacement parameters for $[C_5NF_4.CNSSN]_2$; taking the form :$-2\pi^2[h^2a^{*2}U11+...+2hka^*b^*U12]$

	U11	U22	U33	U23	U13	U12
N(1)	0.025(1)	0.013(1)	0.026(1)	-0.01(1)	0.06(1)	-0.01(1)
S(1)	0.030(1)	0.013(1)	0.026(1)	-0.01(1)	0.07(1)	-0.03(1)
S(2)	0.025(1)	0.014(1)	0.029(1)	-0.01(1)	-0.04(1)	0.04(1)
N(2)	0.021(1)	0.016(1)	0.027(1)	-0.01(1)	-0.05(1)	0.01(1)
C(1)	0.021(1)	0.016(1)	0.014(1)	0.01(1)	-0.02(1)	0.01(1)
C(2)	0.019(1)	0.017(1)	0.015(1)	0.00(1)	0.01(1)	-0.01(1)
C(3)	0.016(1)	0.018(1)	0.018(1)	-0.02(1)	0.01(1)	-0.01(1)
F(3)	0.018(1)	0.020(1)	0.031(1)	-0.02(1)	-0.06(1)	-0.02(1)
C(4)	0.018(1)	0.018(1)	0.019(1)	0.01(1)	0.01(1)	0.04(1)
F(4)	0.023(1)	0.018(1)	0.037(1)	0.02(1)	-0.05(1)	0.06(1)
N(5)	0.023(1)	0.015(1)	0.022(1)	-0.02(1)	0.03(1)	0.00(1)
C(6)	0.019(1)	0.019(1)	0.018(1)	-0.04(1)	0.01(1)	-0.04(1)
F(6)	0.022(1)	0.022(1)	0.031(1)	-0.06(1)	-0.04(1)	-0.07(1)
C(7)	0.017(1)	0.019(1)	0.017(1)	0.01(1)	-0.02(1)	0.02(1)
F(7)	0.021(1)	0.022(1)	0.032(1)	0.01(1)	-0.010(1)	0.03(1)

Table 8g. Torsion angles, °, in $[C_5NF_4.CNSSN]_2$.

C(1)-N(1)-S(1)-S(2)	-0.6(1)	N(1)-S(1)-S(2)-N(2)	1.13(8)
S(1)-S(2)-N(2)-C(1)	-1.5(1)	S(1)-N(1)-C(1)-N(2)	-0.3(2)
S(1)-N(1)-C(1)-C(2)	-180.0(1)	S(2)-N(2)-C(1)-N(1)	1.4(2)
S(2)-N(2)-C(1)-C(2)	-179.0(1)	N(1)-C(1)-C(2)-C(7)	-148.9(2)
N(2)-C(1)-C(2)-C(7)	31.5(2)	N(1)-C(1)-C(2)-C(3)	33.0(2)
N(2)-C(1)-C(2)-C(3)	-146.7(2)	C(7)-C(2)-C(3)-F(3)	-178.4(1)
C(1)-C(2)-C(3)-F(3)	-0.1(2)	C(7)-C(2)-C(3)-C(4)	-2.0(2)
C(1)-C(2)-C(3)-C(4)	176.3(2)	F(3)-C(3)-C(4)-N(5)	176.8(2)
C(2)-C(3)-C(4)-N(5)	0.4(3)	F(3)-C(3)-C(4)-F(4)	-0.7(2)
C(2)-C(3)-C(4)-F(4)	-177.2(1)	F(4)-C(4)-N(5)-C(6)	178.8(1)
C(3)-C(4)-N(5)-C(6)	1.2(3)	C(4)-N(5)-C(6)-F(6)	179.5(1)
C(4)-N(5)-C(6)-C(7)	-0.9(3)	N(5)-C(6)-C(7)-F(7)	178.7(2)
F(6)-C(6)-C(7)-F(7)	-1.7(2)	N(5)-C(6)-C(7)-C(2)	-0.9(3)
F(6)-C(6)-C(7)-C(2)	178.7(1)	C(3)-C(2)-C(7)-F(7)	-177.3(2)
C(1)-C(2)-C(7)-F(7)	4.4(2)	C(3)-C(2)-C(7)-C(6)	2.3(2)
C(1)-C(2)-C(7)-C(6)	-176.0(2)		

Table 8h. Secondary contacts, Å, in $[C_5NF_4.CNSSN]_2$.

S'(1)...S(2)	3.111(1)	S''(1)...N(5)	3.266(2)
S''(2)...N(5)	3.309(2)	S''(1)...F(7)	3.304(1)
S'''(2)...F(3)	3.148(1)		

S(1)' is related to S(1) by 0.5-x, y, 1-z
S(1)'' is related to S(1) by x, y-1, z
S(1)''' is related to S(1) by x-0.5, -y, z

Angle between planes of the two rings = 31.93 (4)

3C Conclusion

3C.1.1 General

All of the eight derivatives studied were found to exist as overlapping dimers with four centred S···S intradimer interactions with mean values ranging from 3.053(5) to 3.133(3)Å. Seven out of the eight compounds form cisoid dimers. By cisoid, I mean the molecules of the dimer are essentially on top of one another and are orientated in the same direction, i.e. mirror images of each other. However the pMeS derivative deviates from being strictly cisoid as the two methyl groups are trans to each other. Structures of other dithiadiazolyls in the literature reveal that they too generally exist as cisoid dimers in the solid state. Again there are reported exceptions, these include pCN-C_6F_4-CNSSN$^\bullet$ which exists as monomers and β-mCN-C_6H_4-CNSSN$^\bullet$ which forms trans-facial dimers via four centred S···S interactions[12,18].

Table 9 shows averaged selected bond lengths, N-C-N angle and S···S intradimer contact distances for the dithiadiazolyl ring in substituted aryl derivatives studied in this survey and also reported in the literature. Since many of the bond lengths are within experimental error of each other no trends with respect to acceptor strength of the R group can be deduced; e.g. the second smallest and largest S-N value is 1.629(11) and 1.640(3). Therefore, these two values have to be 3(0.011+0.003) or 0.042 angstroms apart for them to be independent of each other, which is clearly not the case here. Even if the errors were ignored no relationship between these bond lengths with the acceptor strength of the R group is evident.

When the S-S, S-N and S···S distances listed in Table 9 were compared with the acceptor/donor strength of the functional group(s) no correlation was found, i.e. there seems to be no correlation between the above ring parameters and electron withdrawing strength of the substituent group attached.

At first glance the N-C-N bond angles of compounds with electron donating groups, e.g. pMeS and mCl, pMe, seem to possess a smaller angle, typically ~122°, than the compounds with many or strong acceptor groups, typically ~124°. These values are not found to be independent of each other as determined by the relative size of their ESD's. Therefore no accurate comparison between them can be made.

From the above observations, no relationship between electron withdrawing ability of the substituent and the size of these bond lengths or N-C-N angle exists. A trend of this type would be expected if the electronic effects of the substituent group(s) were the major contributor to the charge

distribution in the dithiadiazolyl ring. However, this is obviously not the case here and additional solid state factors (such as repulsive and attractive intermolecular interactions) which differ for all of the derivatives, are responsible for no trend being observed.

These structural findings differ from results obtained on some of these derivatives from solution ESR and CV investigations which show clear relationships between either $E_{pc/2}$ or spin density with acceptor strength of the substituent group[15] (see Chapter 2). ESR solution results on a selection of fluorinated radicals have shown that spin density is dispersed away from the ring nitrogen by electron withdrawing substituent groups. This results in some of the spin density going on the $\delta+$ sulphur atoms, leading to stronger dimerization, i.e. smaller S···S distance. Electrochemical measurements showed that electron withdrawing groups help stabilise the 7π dithiadiazolyl ring (i.e. make the ring more aromatic or 6π in nature), to a greater extent than donor groups.

The major difference between crystallography and the above two physical techniques is that the first is more sensitive to intermolecular interactions whilst the other techniques are more sensitive to electronic effects within the unassociated monomer, (especially as the measurements are conducted at low concentrations hence making intermolecular interactions negligible).

Therefore, no trend in ring parameters with acceptor strength of the substituent group is observed due to the superimposed effects of a variety of secondary interactions, which affect the electronic environment of the ring and ultimately the bond and angle sizes.

Comparisons of solid state packing patterns and intermolecular interactions, of the eight compounds studied and several analogous literature compounds, will now follow.

R	Space group	C-N / Å	N-S / Å	S-S / Å	S···S / Å	N-C-N / °	Ref.
para							
pMeS	$P2_1$ § Monoclinic	1.346(9)	1.630(6)	2.097(3)	3.061(2)	121.7(6)	(*)
H	$P2_12_12_1$ § Orthorhombic	1.33(2)	1.63(1)	2.089(11)	3.109(5)	121(4)	(1)
pF	$P2_1/n$ Monoclinic	1.343(18)	1.629(11)	2.101(6)	3.053(4)	122.3(11)	(*)
pCl	$P2_1/n$ Monoclinic	1.336(7)	1.635(4)	2.089(3)	3.099(9)	123.4(4)	(8)
pCF_3	$P2_1/n$ Monoclinic	1.35(3)	1.630(16)	2.093(7)	3.089(5)	122.4(15)	(*)
pCN	P_1^- Triclinic	–	–	2.081(1)	3.10(2)	–	(12)
pNO_2	P_1^- Triclinic	1.338(10)	1.634(7)	2.100(4)	3.133(3)	123.1(7)	(*)
meta							
mCl,pMe	$P2_1$ § Monoclinic	1.343(20)	1.631(16)	2.098(7)	3.087(7)	121.4(14)	(*)
mBr	$P2_1$ § Monoclinic	1.337(6)	1.635(3)	2.0966(16)	3.087(1)	122.9(4)	(*)
α-mCN	$P2_1/n$ Monoclinic	–	–	2.080(3)	3.13(2)	–	(12)
β-mCN	$P2_1/n$ Monoclinic	–	–	–	3.121(1)	–	(12)
mpy^H	$P2_1$ § Monoclinic	1.335(7)	1.639(4)	2.077(3)	3.133(2)	122.7(6)	(*)
perfluoro							
ppy^F	I2/a Monoclinic	1.336(3)	1.638(3)	2.100(1)	3.111(1)	124.0(2)	(*)
C_6F_5	C2/c Monoclinic	1.338(6)	1.640(3)	2.097(1)	3.067(2)	124.1(1)	(16)
α-pCN^F	P_1^- Triclinic	1.327(2)	1.638(2)	2.0897(14)	Monomer†	123.9(2)	(18)
β-pCN^F	Fdd_2 § Orthorhombic	1.325(3)	1.638(3)	2.0816(14)	Monomer†	124.0(3)	(18)
bis							
1,4 C_6F_4	P_1^- Triclinic	1.333(8)	1.634(6)	2.096(3)	3.154(3)	123.9(6)	(17)
1,4 C_6H_4	$P2_1/n$ Monoclinic	1.333(14)	1.638(22)	2.099(9)	3.121(6)	123.4(8)	(10)
1,3 C_6H_4	$I4_1/a$ Tetragonal	1.34	1.627	2.084	3.140	122	(10)

Table 9. Mean bondlengths, N-C-N angle and S···S intradimer contact distances of the dithiadiazolyl ring of selected substituted aryl 1,2,3,5 derivatives.
† S···S distance greater than 4.06Å (inc. esds), * This work, § asymmetric packing

3C.1.2 *Para* Derivatives

Perpendicular packing dimers

Of the *para* derivatives investigated the pMeS and pF were both found to pack in herringbone type arrays, (see 3B.1.1 and 3B.1.2). The molecules in these arrays line up with adjacent molecules, such that they are almost in phase with each other. This results in the sulphurs on one side of a dimer unit being within the van der Waals radii of the nitrogens on one side of a neighbouring dimer unit. Thus lines of Type A S···N interactions run between adjacent molecules, as shown in Fig 18a. The typical S···N value is 3.473(13)Å and 3.398(6)Å for the pF and pMeS compounds respectively, see Table 10.

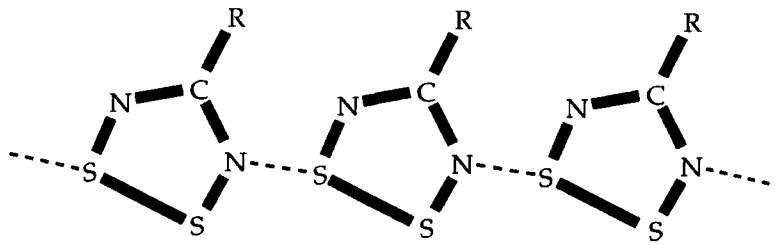

Fig 18a. Type A S···N interactions

X substituent	S···N range	mean S···N
pMeS	3.268/3.527(4)	3.398(6)
mCl, pMe	3.551/3.570(11)	3.561(16)
pF	3.468/3.478(9)	3.473(13)
mBr	3.597/3.547(2)	3.572(3)
pCF_3	3.429(11)	3.429(11)
pNO_2[a]	3.246/3.405(5)	3.326(7)

Table 10. Type A S···N contact distances of some X substituted aryl 1,2,3,5 dithiadiazolyls, ([a] internal S···N contact)

The 1,4 bis dithiadiazolyl and pCl compounds also pack in herringbone arrays, 3A.1.1. For the first compound the alignment of the molecules is almost identical to that described for the pMeS and pF compounds, with the

exception that the adjacent molecules are more in phase with each other in this compound such that S···S rather than S···N interactions are observed.

For the latter pCl compound, the molecules of alternate herringbone arrays pack anti parallel to each other such that the dithiadiazolyl rings of adjacent rings overlap each other which results in four perpendicular Type B S···N contacts (3.060Å) are observed, see Table 11a and Fig 18b.

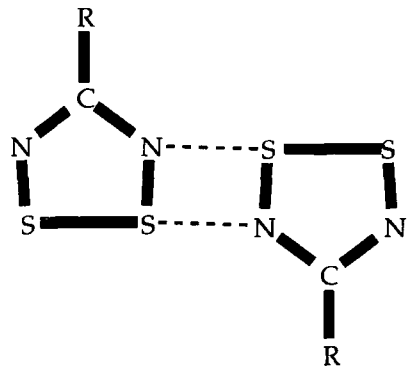

Fig 18b. Type B S···N interactions

Parrallel packing

The remaining three *para* derivatives, pNO_2, pCF_3 and ppy^F, were all found to possess a common packing feature different to those of Fig 18a and 18b. In each case their molecules packed head to tail, thus forming linear rows of dimers. The interactions between each end of the molecule were observed along these rows and they are now described.

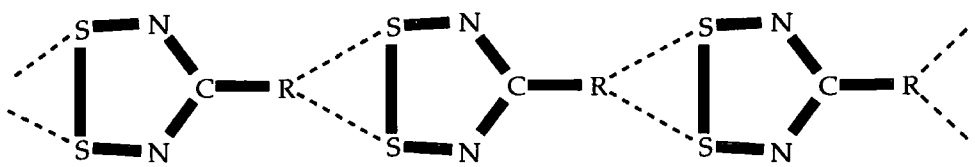

Fig 18c Ribbons of dimer. Type C S···N interactions occur when R=pyridyl, cyanophenyl and other related compounds.

For the pNO_2 derivative each oxygen interacts with one sulphur atom such that four S···O interactions occur between each pair of dimers in the row or ribbon, see sections 3B.1.4.

For the pCF_3 derivative, two fluorines of one dimer half are each involved in one $S^{\delta+}\cdots F^{\delta-}$ interaction of an identical half of a neighbouring dimer unit. It is important to note these two $S^{\delta+}\cdots F^{\delta-}$ contacts involve different fluorines and sulphurs, see 3B.1.3.

Finally, for the fluorinated pyridyl derivative, each pyridyl nitrogen interacts with both sulphurs of a neighbouring dithiadiazolyl ring involved in interdimer contacts with each other, such that molecules interacting are in plane with each other, see Fig 18c for Type C S···N contacts. There are also secondary interactions involving one *ortho* fluoro per molecule with a neighbouring sulphur in the row, see Fig 3B.1.8. However, orientation of these rows of these three compounds was found to differ for each of the three derivatives. The environment between the rows of these compounds will now be considered.

Starting with the pNO_2 derivative again, the rows of these dimers pack adjacent and slightly tilted to each other with dimers of alternate rows pointing in the opposite direction. Adjacent to these rows the dithiadiazolyl rings overlap with each other allowing chains of S···N interactions to exist. These S···N interactions are unusual; between dimers there are four "external" interactions similar to those observed for the pCl compound, Type B, and two diagonal "internal" S···N interactions as observed for pMeS and pF derivatives, Type A. The relative size of these "internal" and "external" S···N interactions, (i.e. which one is the bigger of the two) alternates between layers. The ribbons stack on top of one another to form slanted stacks of alternate facing dimers, see Fig 13.

R	S···N	mean S···N
Cl	3.060	3.060
C_6F_5	3.23 & 3.24(02)	3.235(03)
NO_2[b]	**3.329/3.325(5)** **3.205/3.231(5)**	**3.273(8)**

Table 11a Type B S···N contact distances, ([a] internal S···N contact)

For the pCF_3 derivative the ribbons align adjacent to each other to form planar arrays, see Fig 12. The molecules of each array all face the same direction with neighbouring dimers being out of phase slightly, such that S···N interactions Type A as observed for pMeS and pF exist. These sheets stack on top of each other to form ABCD stacking with dimer molecules orientated in four different directions. This packing arrangement is described in more detail in section 3B.1.3. There are $F^{\delta-}\cdots F^{\delta-}$ repulsive contacts between every second and third layer.

Last but not least the perfluoro pyridyl derivative is considered. The molecules of the ribbon pack adjacent and anti parallel to each other to the same degree as seen already for the pNO_2 derivative. But unlike the pNO_2 compound no Type A or B S···N interactions are observed due to o-$F^{\delta-}$···m-$F^{\delta-}$ repulsions preventing the ribbons getting close enough, for the S and N atoms to be within the sum of the van der Waals radii. However, favourable o-$F^{\delta-}$···$S^{\delta+}$ inter ribbon contacts are observed, see Table 11b. The large twist angle of 31.9(2)°, (relative to the other non-fluorinated *para* compounds discussed so far), reduce F···F and $N_{dithiadiazolyl}$···F repulsions and allows S···F attractions.

Another common feature for these three *para* derivatives studied is that negligible interactions occur between stacking ribbons. There is a definite preference for interactions to be in the plane of the dimer molecules and not perpendicular as observed with the earlier compounds in this section.

Other compounds whose molecules pack as ribbons include pCN, pCN^F and the perfluoro phenyl dithiadiazolyl derivatives, see 3A1.1.

The pCN and pCN^F compounds forms three centred CN···S (Type C) interactions of the type observed for the ppy^F derivative, see 3A.1.1.

No trend between the type of substituent and the distance between the S and N atoms, of cyano and pyridyl derivatives, involved in inter-ribbon contacts, was found. This is not too surprising as they are not all dimers, (pCN^F is a monomer).

R	S···N	*o*F···S (inter rib)	*m*F···S (intra rib)	Av S···N
α-mCN	3.075	-	-	
β-mCN	-	-	-	
pCN	3.04	-	-	
α-pCN^F	3.088/3.105(2)	None	None	3.097(2)
β-pCN^F	2.986(3)	None	None	
mpy^H	**(2.945/2.817)**(4) **(2.844/2.938)**(4)	-	-	**2.886(5)**
ppy^F	**3.309(2)-3.266(2)**	**3.247(1)**	**3.148(1)**	**3.288(3)**
C_6F_5	-	3.27, 3.29(03)	None	

Table 11b Type C S···N contact distances.

The C_6F_5 derivative packs in a similar style to the pNO_2 derivative with chains of 4 centred "external" S···N Type B interactions between dimers but no internal S···N interactions Type A. These S···N interactions are reminiscent of those observed for the pCl structure as well. Looking at Table 11a, the S···N Type B distance for the C_6F_5 and pNO_2 compounds agree within experimental error but for the pCl derivative it is definitely smaller. This is an unusual trend as one would expect the C_6F_5 derivative to possess the largest S···N distance due to additional inter-ribbon F-F repulsions compared to the other derivatives. Therefore, the S···N Type B interactions of these three examples are influenced by other packing considerations such as favourable S···F, S···O, S···Cl attractions and unfavourable δ- δ- repulsions amongst them. It is these factors which are responsible for a large twist angle being present in the C_6F_5 derivative, thus allowing the ribbons of this derivative to get closer than those of the pNO_2 and pCl derivatives and hence a smaller S···N contact distance is observed.

Also observed for the C_6F_5 are *o*F···S contacts (3.28(03)Å) between the ribbons which are slightly smaller than those observed for the ppy^F compound (3.247(1)Å), see Table 11b. This difference in size is probably due to a larger twist angle in the former case (38.2(4)°) relative to the latter (31.9(2)°) which is responsible for these atoms being further apart.

3C.1.3 *Meta* Derivatives

The *meta* derivatives were investigated mainly to determine whether these compounds crystallised as cis or trans dimers. A structure determination on the mCN-C_6H_4-CNSSN$^\bullet$ showed that this dimer existed as cisoid dimer, see 3A.1.1. When structures of mpy^H, mBr and mCl,pMe were examined it was found that they too all existed as co-facial dimers with the *meta* substituents group cis to each other, see Fig 16, 14 and 15 respectively.

The mBr derivative packs in zig zag arrays which are dominated by Br-S interactions, which are described in more detail in section, 3B.1.5.

For the mCl,pMe compound, the dimer molecules pack in linear arrays, with the molecules within these arrays packing perpendicular to each other in an end to face arrangement. Cl···H contacts exist between dimers as well as standard S···S intradimer interactions. The molecules of these arrays are almost superimposed over each other such that Type A S···N inter dimer interactions as observed like those for pMeS and pF analogues, see Table 10. Also in this plane additional m-H···Cl contacts are observed, section 3B.1.6.

The final compound for discussion is the *meta* pyridyl derivative, see 3B.1.7. The dimers of these molecules form stacks, such that alternating inter (3.996(3)Å) and intra dimer (3.133(2)Å) S···S interactions run down the stacks. The interdimer interactions are very close to the sum of the van der Waals radii of two sulphur atoms (4.06Å) and hence is a very weak contact. This type of columnar packing is reminiscent of Peierls distortions[11]. These stacks in turn pack to form snake like shaped 'walls' where Type C $S\cdots N_{pyridyl}$ interactions run along the back bone of the wall. Closer investigation of these walls reveals that molecules of each component stack of the wall are completely out of phase with their neighbours. Thus the sulphurs involved in inter dimer interactions interact with pyridyl nitrogens from a neighbouring dimer. The α–mCN derivative packs similarly to this except that cyano N rather then pyridyl N secondary interactions are observed. Also, the stacks are in phase with each other, see 3A.1.

Looking at Table 11b again, the S···N inter-ribbon contact distances for the *meta* and *para* cyano and pyridyl derivatives show no relationship between electron withdrawing ability or type of substituent and these distances.

3C.1.4 Conclusions

These results, in conjunction with the literature structures, show that there is a strong preference for substituted aryl derivatives to form co-facial dimers with cis configurations.

From the evidence collected the mBr and mCl, pMe have many packing features in common with the *para* halogen derivatives, i.e. they pack perpendicular to each other giving similar zig zag arrays. Therefore, these results strongly suggest that all *meta* and *para* mono halogen and RS derivatives (where R=alkyl group) are likely to pack perpendicular to each other in some form of zig zag array and that there is a high probability that S···N interactions will occur.

To date in the literature no S···O interactions have been observed for dithiadiazolyl species. Structures on furanyl derivatives have been examined but oxygen interactions were not observed due to oxygens being sterically hindered by *ortho* side groups. However, significant S···O contacts play an important role in the molecular packing of the pNO_2 derivative, where preference for ribbon formation of dimers is observed.

The results showed that the ppy^F derivatives pack very similarly to analogous cyano derivatives. This is not at all too surprising as both have

substituent nitrogens with two unpaired electrons and the electron withdrawing ability of pyridyl and cyano nitrogen are found to be extremely close as deduced by cyclic voltammetry. However subtle differences in packing between analogous derivatives is due to the nitrile nitrogen projecting out of the aryl ring while the pyridyl nitrogen is enclosed in the aryl ring, i.e. the molecules cover a different spatial area.

For all the perfluoro compounds studied to date, including the ppy^F compound, the twist angle between the aryl and dithiadiazolyl ring is typically 30° to 55°. These large twist angles are probably present in the solid state in order to minimise $N_{dithiadiazolyl}/oF$ intramolecular and F···F inter ribbons repulsions. It is because of these repulsions that a large twist angle of 53° is observed for pCN-C_6F_4-CNSSN$^\bullet$, see 3A.1. More importantly F···F repulsions between the molecules of this particular compound are responsible for it existing as a monomer as the molecules are prevented from getting close enough together to form S····S interdimer interactions. For the unfluorinated compounds discussed already, the twist angles are far smaller (in the range of 0-18°) where these types of repulsions are absent.

Ribbon formation also occurred in pNO_2, multifluoro and CN derivatives. However, it was noticed that alternate adjacent rows or stacks packed in opposite directions, i.e. anti-parallel to each other, see section 3B.1.4.

Linking all these results with the electrochemical data discussed in chapter 2, it can be seen that the molecules that pack in ribbons have larger $E_{pc/2}$ values compared with the compounds which tend to pack in perpendicular arrays. Therefore, the preference of packing could be related to the dipoles of the molecules and how these dipoles align. However, more detailed studies on a larger variety of substituted dithiadiazolyls containing different shaped R groups will have to be conducted before this can be confirmed.

The *para* derivatives have a slight bias towards packing centrosymmetrically while the reverse is true for derivatives possessing *meta* substituents. Therefore, if a compound was required to pack asymmetrically for an application, (e.g. second order NLO) the best bet would be to make a derivative possessing a *meta* group in order to raise the odds of achieving a compound with the right packing symmetry. However, this procedure is very hit and miss.

The compounds so far discussed have either packed perpendicular to each other or formed ribbon like arrays. In order to achieve dithiadiazolyls with interesting physical properties, i.e. highly conducting or possessing

interesting magnetic features, the key lies in producing derivatives whose molecules pack in ribbon like arrays. Ribbon formation is important for conductivity as the molecules in the ribbons have the ability to stack on top of one another, with the possibility to form conduction bands. (This can't be achieved in herring bone style packing). Even if the molecules do stack on top of each other, these types of compounds have a preference towards dimer formation which considerably reduces the conductivity. But this problem can be overcome by making charge transfer materials, (see chapter 5). To obtain dithiadiazolyls possessing interesting magnetic properties it has been shown that it is crucial that the material exists as a monomer in the solid state. Also another much under estimated packing feature is that the molecules should pack asymmetrically, i.e. point in one direction, so that the dipoles of all the molecules are aligned.

These crystallographic results do strongly indicate that it is possible to make dithiadiazolyl derivatives possessing the above physical responses through molecular design. Our results suggest that ribbon formation is preferred by derivatives possessing strong electron withdrawing groups and whose substituents are not too sterically bulky. Further there is a bias to achieving asymmetric packing by the addition of a *meta* substituent. Derivatives with substituent groups possessing nitrogen or oxygen have always been seen to pack in ribbon arrays and these types of substituents are probably a good place to start further investigations. In order to achieve monomer formation the best method is to add substituents groups which will preferably repel each other and thus prevent dimer formation. However, great care must be taken when following this pathway as the groups should not be so bulky as to lower the melting point of the compound such that it is a liquid at room temperature. In summary, the above ideas could lead to some very fruitful research avenues.

References:

1. A.Vegas, A.Pérez-Salazar, A.J.Banister & R.G.Hey; *J.Chem.Soc., Dalton Trans.*, 1980, 1812-5.
2. H.U.Höfs, J.W.Bats, R.Gleiter, G.Hartmann, R.Mews, M,Eckert-Macksic´, H.Oberhammer & G.M.Sheldrick; *Chem. Ber.*, 118, 1985, 3781-3804.
3. A.J.Banister, M.I.Hansford, Z.V.Hauptman, S.T.Wait & W.Clegg; *J.Chem.Soc., Dalton Trans.*, 1989, 1705-13.
4. A.W.Cordes, J.D.Goddard R.T.Oakley and N.P.C.Westwood; *J.Am.Chem.Soc.*, 1989, 111, 6147-54.
5. R. C. Haddon, *Nature*, 1975, 256, 394
6. T. S. Cameron, R. C. Haddon, S. M. Mattar, S. Parson, J. Passmore and A. P. Ramirez, *Inorg. Chem.*, 1992, 31, 2274.
7. C.D.Bryan, A.W.Cordes, R.M.Fleming, N.A.George, S.H.Glarum, R.C.Haddon, R.T.Oakley, T.T.M.PTS.alstra, A.S.Perel, L.F.Schneemeyer & J.V.Waszczak; *Nature*, 1993, 365, 821.
   A. J. Banister, M. I. Hansford, Z. V. Hauptman, A. W. Luke, S. T. Wait, W. Clegg and K. A Jørgensen, *J. Chem. Soc., Dalton Trans.*, 1990, 2793.
8. I.Lavender, Ph.D Thesis, University of Durham, England, 1992.
   R. T. Boere, K. H. Moock and M. Parvez, *Z. anorg. allg. Chem.*, 1994, 620, 1589
9. P.Del Bel Belluz, A.W.Cordes, E.M.Kristof, P.V.Kristof, S.W.Liblong & R.T.Oakley; *J.Am.Chem.Soc.*, 1989, 111, 9276.
   W. M. Davis, R. G. Hicks, R. T. Oakley, B. Zhao and N. J. Taylor, *Can. J. Chem.*, 1993, 71, 180
10. A.W.Cordes, R.C.Haddon, R.T.Oakley, L.F.Schneemeyer, J.V.Waszczak, K.M.Young & N.M.Zimmerman; *J.Am.Chem.Soc.*, 1991, 113, 582-88.
    M.PTS..Andrews, A.W.Cordes, D.C.Douglass, R.M.Fleming, S.H.Glarum, R.C.Haddon, P.Marsh, R.T.Oakley, T.T.M.PTS.alstra, L.F.Schneemeyer, G.W.Trucks, R.Tycko, J.V.Waszczak, K.M.Young & N.M.Zimmerman; *J.Am.Chem.Soc.*, 1991, 113, 3559-68.
11 R. T. Oakley, *Can. J. Chem.*, 1993, 71, 1775.
12 A.W.Cordes, R.C.Haddon, R.G.Hicks, R.T.Oakley & T.T.M.PTS.alstra; *Inorg Chem.*, 1992, 31, 1802-08.
13 S. A. Fairhurst, K. M. Johnson, L. H. Sutcliffe, K. F. Preston, A. J. Banister, Z. V. Hauptman and J. Passmore, *J. Chem. Soc., Dalton Trans.*, 1986, 1465.
14 A. W. Cordes, R. C. Haddon, R. G. Hicks, D. K. Kennepohl, R. T. Oakley, L. F. Schneemeyer and J. V. Waszczak, *Inorg. Chem.*, 1993, 32, 1554.
   A. W. Cordes, R. C. Haddon, C. M. Chamchoumis, R. G. Hicks, R. T. Oakley and K. M. Young, *Can. J. Chem.*, 1992, 919.
15. S.A.Fairhurst, L.H.Sutcliffe, K.F.Preston, A.J.Banister, A.S.Partington, J.M.Rawson, J.Passmore and M.J.Schriver; *Magn.Reson.Chem.*, 1993, 31, 1027-30.
16. Andrew Partington, Final year undergraduate research project report, University of Durham, England, 1993.
17. A. J. Banister and I. Lavender, unpublished results
18. A. J. Banister, W. Clegg, M. Elsegood, C. I. Gregory, I. Lavender, J. M. Rawson and B. Tanner, to be submitted for publication.
19. S.C.Nyburg & C.H.Faerman; *Acta Cryst.*, 1985, B41, 274-79.

Chapter 4

V DISTILLATION OF SULPHUR
From M. Mercati, *Metallotheca*, Rome, 1719, p. 78

4. Experimental

4A.1 Introduction:

All the sulphur nitrogen species synthesised and investigated in this thesis were air and moisture sensitive. Many of the reagents used to make these materials were sensitive to the atmosphere too. Hence special apparatus had to be used in order to avoid degradation during synthesis, isolation and characterisation of these compounds. The types of equipment, solvents, experimental procedures and observations during synthesis and characterisation of these compounds are now discussed.

4A.2 Apparatus

4A.2.1 Closed extractor

This piece of apparatus was designed by Dr Z.V. Hauptman[1]. It is essentially a more advanced form of a soxhlet extractor, see Fig 1. The beauty of this equipment is that it allows extractions to be completed in a closed or sealed environment. During the extraction process the bulb is warmed (vapour pressure of the solvent not to exceed 5atm) so that enough solvent can condense in the condensor section of the vessel in order to wash soluble material through the frit.

This method was generally used for the purification of substituted phenyl 1,2,3,5 dithiadiazolylium salts using liquid SO_2 (at 20°-25°C) as a solvent.

4A.2.2 The "dog"

This is a two limbed vessel with a J. Young taps in each compartment, see Fig 2, which permits small scale reactions involving liquefied gases to be conducted within, e.g. SO_2. The apparatus has a glass sinter incorporated into it to allow filtration of material present in one portion of the vessel. The vessel also has a 1/4 inch glass tubing outlet which can be connected to a Swagelok Teflon compression fitting attached to a vac line.

4A.2.3 Sublimation apparatus

Three types of sublimation vessels were used, (1) cold finger, (2) tube and (3) a variable temperature devices.

(1) Cold finger.

As the name suggests the apparatus has a condenser or 'cold finger' incorporated into it, on to which material that has been heated above its sublimation temperature can condense onto, see Fig 3. Purification of the starting materials such as solid nitriles or Ph_3Sb were undertaken using this method. However bulk scale sublimation of radicals was less common as sulphur contamination of the product often occurred at the surface of the cold finger.

(2) Tube

This was the most common method employed to obtain pure and crystalline samples of the 1,2,3,5 dithiadiazolyl radicals studied in this project, see Fig 4a. This process involved heating the sample, in a tube under a dynamic vacuum, with an oil bath or heating tape to sublimation temperature. Crystalline material naturally formed on the surface of the air cooled region of the tube. Conditions such as temperature and vacuum pressure were often fine tuned in order to produce suitable crystals for x-ray structure determination.

(3)Variable temperature device.

The experimental procedure is very similar to (2) except for the method of heating. For this method a tube containing the sample is loaded into a machine which can generate an even temperature gradient and not a harsh change in temperature as observed with (1) or (2), see Fig 4b. This method was conducted for samples, of large scale quantities (5g), which failed to give crystalline samples via the other two methods.

4A.2.4 Electrochemistry

The cell

Electrochemistry was conducted in a three-limbed vessel designed by Dr. Z. V. Hauptman[1]. The reference, counter and working electrodes were each held in place by Swagelok fittings at these limbs. The cell also had an additional side arm fitted with a greaseless J. Young taps. These fittings enabled the contents of the cell to be isolated from the outside world, i.e. CV on air sensitive compounds or pressured liquid solvents could be conducted, see Fig 5.

Electrodes

The working electrode was a 1mm diameter platinum disc which was sealed into a P.T.F.E casing.

The counter electrode was a standard platinum coil.

The reference electrode used was an Ag/Ag^+ system, see Fig 6. After every experiment this was referenced to the S.S.C.E via a 0.1mol dm^{-3} $[NBu_4][BF_4]$ salt bridge.

Supporting Electrolyte

The supporting electrolyte used was tetrabutyl ammonium tetrafluoroborate ($TBABF_4$). This was supplied by Fluka (electrochemical grade) and used without further purification. Electrochemical solutions used for CV measurements were typically made to 0.1 M.

Sample concentration

The concentration of the analyte in solution was typically $1x10^{-3}M$.

CV device

The potential wave generator used was a Bioanalytical Systems Machine, type CV-1B, W. Lafayette, I. N. This was connected to a Linseis x-y chart recorder (type LY 17100).

4A.2.5 Glove box

A Vacuum Atmosphere HE43-2 glove box fitted with an HE493 Dri-Train was used for manipulations of air sensitive materials.

4A.2.6 IR

IR's were conducted on Nujol mulls of these samples between two KBr discs. The IR's were run using a Perkin Elmer 1600 series machine.

4A.2.7 Mass Spectrometry

Samples were run on a VG Analytical 7070E spectrometer using electron-impact (EI^+) or chemical ionisation (CI^+) techniques.

4A.2.8 DSC - Differential scanning calorimetry

All measurements were conducted using a Mettler FP80 control unit linked to a Mettler FP85 thermal analysis cell. These units were in turn interfaced with an Opus PC III computer with a DSC analysis program, written by Dr J.M. Rawson, which produced the DSC traces. The samples were sealed in aluminium pans in the glove box and run under argon in the lab.

4A.2.9 Elemental analysis

Results for carbon, hydrogen and nitrogen analysis were obtained from a Carlo Erba 1106 Elemental Analyser.

The closed extractor

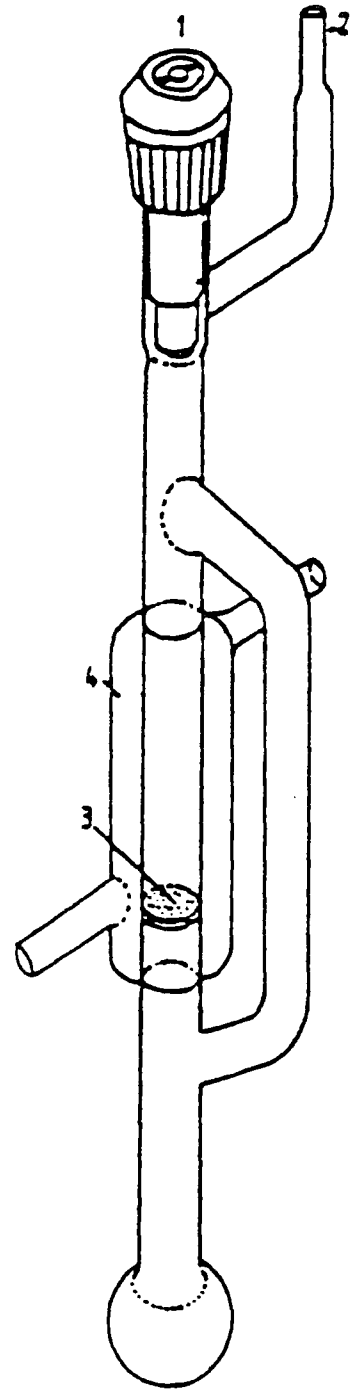

Fig 1

1. J. Young teflon tap.
2. 1" Ground glass.
3. Glass sinter (usually porosity grade 3).
4. Cooling jacket.

The twin-bulbed reaction vessel or 'dog'

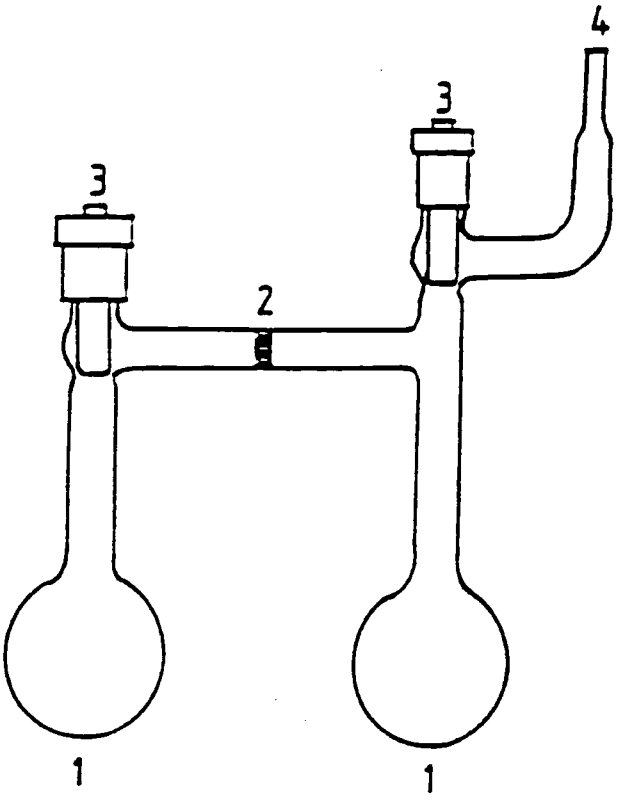

Fig 2

1. Reaction bulb.
2. Glass sinter (usually porosity grade 3).
3. J. Young teflon tap.
4. ¼" ground glass.

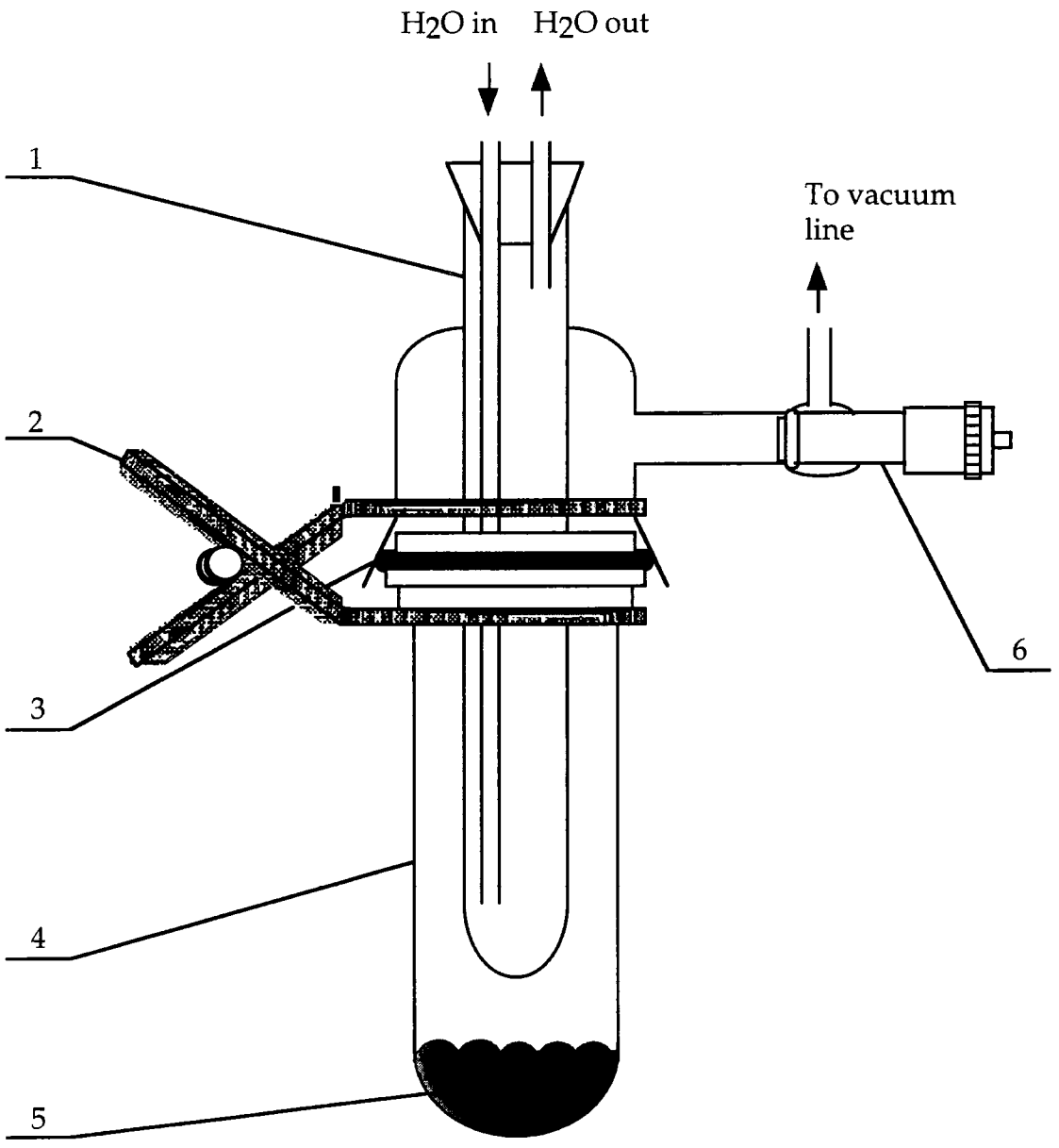

Fig3
1 Cold finger
2 Spring clamp
3 Rubber washer
4 Bottom detachable section
5 Sample
6 J. Young tap

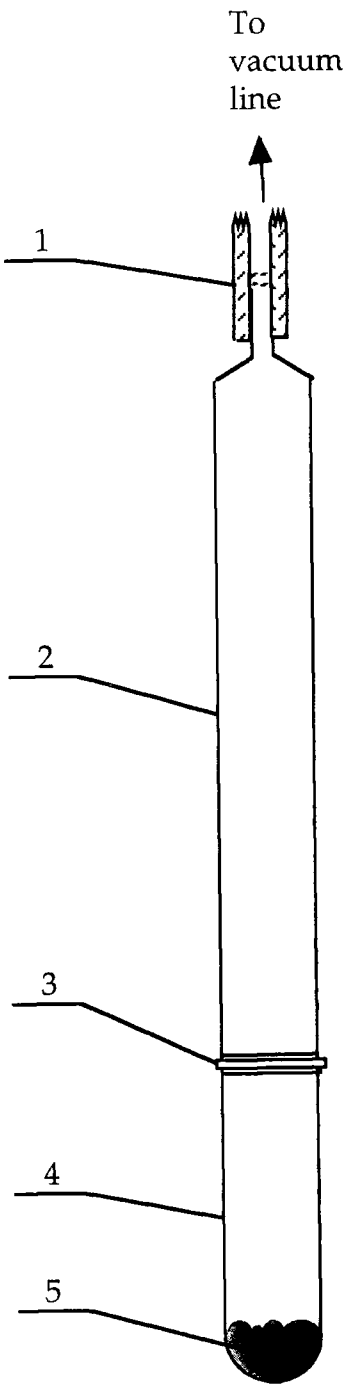

Fig 4a
1 Tubing to connect to a vacuum line
2 Top detachable section
3 Rubber ring holding the two halves together
4 Bottom detachable section
5 Sample

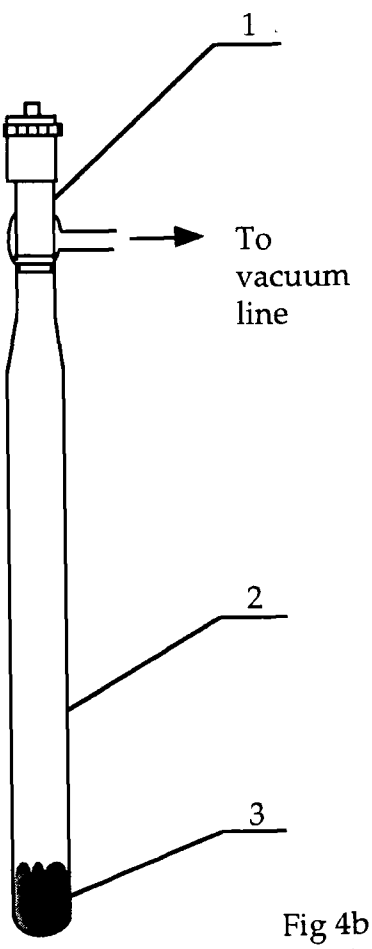

Fig 4b
1 J. Young tap
2 Glass vessel
3 Sample

The cyclic voltammetry cell illustrating the modified Swagelok glass to metal connector (insert).

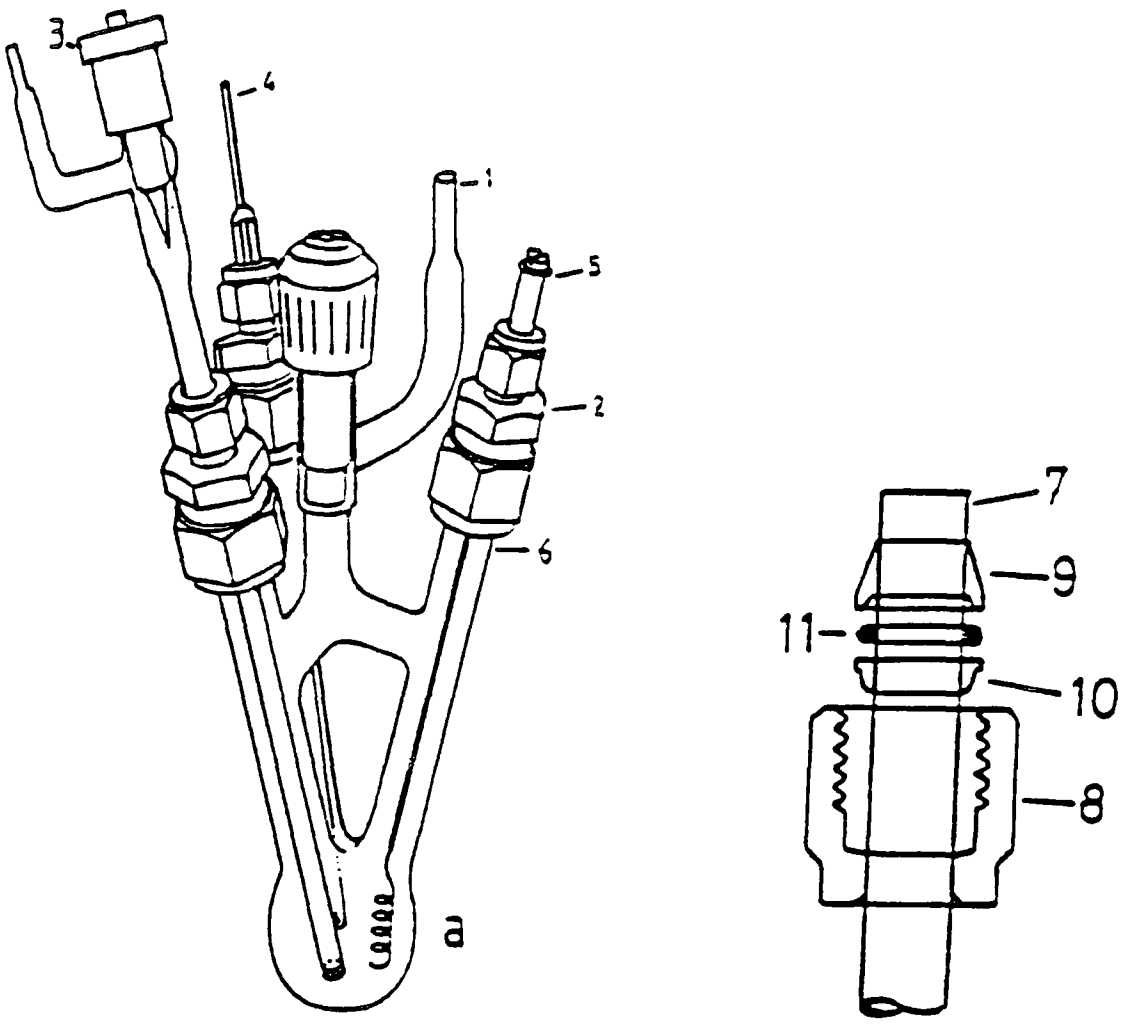

Fig 5

1. ¼" Ground glass.
2. Swagelock ¼" to ¼" reducing union.
3. Reference electrode.
4. Micro electrode (usually platinum).
5. Auxiliary electrode (platinum).
6. ¼" Ground glass.
7. Same as 6.
8. Compression nut.
9. Front ferrule.
10. Back ferrule (reversed).
11. PTFE "O" ring.

The Ag / Ag^+ reference electrode

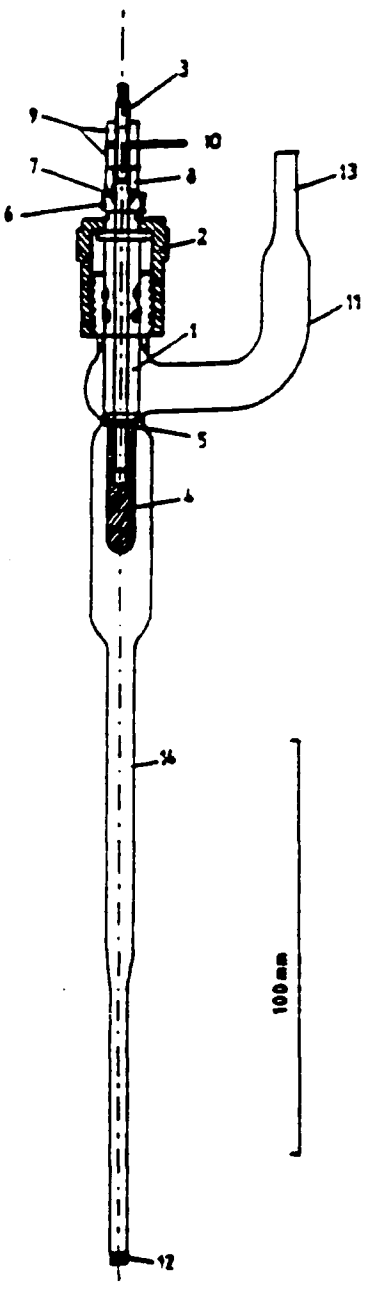

Fig 6.

1. PTFE stem of a J. Young tap.
2. Turning knob of J. Young tap.
3. Stainless steel (or monel) rod, eighth inch diameter, with 5BA thread on both ends tightly fitting into the central bore in the PTFE stem
4. Metal electrode (e.g. silver) screwed onto a central rod.
5. Knife edge machined on the flat end of 4 (to achieve a tight seal).
6. Brass ring around PTFE stem (to prevent yielding through axial compression).
7. "o" ring in conical groove machined in the top of the PTFE stem.
8. Washer.
9. 5BA nuts.
10. Soldering eyelet.
11. Side arm of J. Young tap ended with a 1/4in O.D. tube for swagelock connection.
12. Pyrex sinter porosity grade 4.
13. See 11.
14. 1/4in O.D. section for air tight mounting (using the swagelock connector).

4A.3 Solvents

All solvents used were typically from Aldrich and at least H.P.L.C grade.

4A.3.1 Diethyl ether (Et_2O)

This was stored over Na wire and under nitrogen prior to use.

4A.3.2 n-Hexane (n-C_6H_{14})

This was distilled over P_2O_5 and then stored under N_2 before being used.

4A.3.3 Dichloromethane (CH_2Cl_2)

This was distilled over CaH_2 and then stored under N_2

4A.3.4 Acetonitrile (MeCN)

This was distilled over CaH_2, passed through an alumina column and finally stored under N_2.

4A.3.5 Sulphur dioxide (SO_2)

50g of SO_2 (BDH canister) were vac transferred, using a Monel metal vac line, to a suitable high pressure cylinder containing P_2O_5 and stored for a week. Then the solvent was transferred into another similar cylinder containing CaH_2 and left for a few days before use in order to ensure the SO_2 was completely dry.

4A.3.6 Tetrahydrofuran (THF)

This was stored over Na wire and nitrogen prior to use.

4A.3.7 1,2-Dichlorobenzene (1,2 Cl_2-C_6H_4)

This was stored over $CaCl_2$ and nitrogen prior to use.

4A.4 Electrochemical procedures

4A.4.1 Setting up a cell for a CV experiment.

The correct amount of sample and supporting electrolyte were placed into the cell, complete with the auxiliary and working electrode, in a glove box. The Swagelok fittings and Youngs tap were tightened to ensure an air tight seal and the vessel transferred to the cyclic voltammetry machine.

During this research only two kinds of solvent were used, SO_2 and MeCN. If the solvent to be used in the measurements was the former, the cell would be attached to a metal vac line in one of the fume hoods and liquid SO_2 condensed into it. The temperature of the liquid was not allowed to exceed -15°C in order to keep the vapour pressure to a minimum. If the solvent was the latter then this was syringed into the cell under a counterflow of nitrogen from a vessel containing the dry solvent.

Next, the Ag/Ag^+ reference electrode was transferred to the cell under a counterflow of nitrogen and the solution cooled to the desired temperature. The electrodes were then connected to the CV machine and scans conducted until the right settings were found for which the CV trace fitted on the paper attached to the chart recorder. During each scan the solution was not stirred, but between scans it was.

Once the CV traces were run the reference electrode was transferred to a salt bridge attached to a S.S.C.E (standard saturated calomel electrode). The potential of this system was then recorded and hence the cell could now be referenced to a well known standard. The reference electrode was then transferred to a silver salt solution identical to its own for storage. Finally, the rest of the cell was dismantled and cleaned for the next experiment.

4B Synthesis of the Sulphur Nitrogen Heterocycles

4B.1 Starting Materials

The solid nitriles (Aldrich, Lancaster) used were generally purified further by sublimation prior to use. SCl_2 (BDH), Ph_3Sb (Aldrich), Zn/Cu (Alpha) couple, $AgAsF_6$ (Fluka), $LiN(SiMe_3)_2$ (Aldrich) and $S_2N^+AsF_6^-$ (J. M. Rawson and I. Lavender) were used without further purification. The last two compounds were kept in sealed containers or in the box as they are air sensitive.

4B.2 Reference materials

The following compounds were made according to the literature routes,

C_6H_5-CNSSN$^+AsF_6^-$	(2)	Cl-C_6H_4-CNSSN$^+AsF_6^-$	(2)
NC-C_6H_4-CNSSN$^+AsF_6^-$	(3)	C_6H_5-CNSSN$^\bullet$	(4)
C_6H_5-CNSNS$^+AsF_6^-$	(5)	pNO_2-C_6H_4-CNSNS$^+AsF_6^-$	(6)

4C Preparation and characterisation of substituted phenyl and pyridyl 1,2,3,5 dithiadiazolylium chlorides.

Standard experimental procedure

These compounds were made by an amended version of the literature method, see references (3,7).

Stage 1 A one to one mole ratio of $LiN(SiMe_3)_2$ and RCN were placed into a round bottomed flask under an atmosphere of nitrogen. Dry diethyl ether was added (30mls per $1x10^{-2}$mols of starting material) to the reaction mixture under a counter-flow of nitrogen. The reaction mixture generally formed a coloured solution which was stirred for a minimum of 4hrs.

Stage 2 A slight excess of two equivalents of SCl_2 was then carefully added to this solution cooled to 0°C, as the reaction is very exothermic. Immediately on addition of the reactant a highly coloured precipitate forms. This mixture was stirred for a further 3hrs or overnight during which time no colour change was observed.

Stage 3 The solvent was then removed by cannula transfer and the isolated solid washed twice with the same volume of fresh Et_2O. The wet solid was pumped to dryness and transferred to a closed extractor. A third of a bulb of SO_2 was condensed in and then allowed to cycle until the process was complete. Where upon the side product (LiCl) and other insoluble impurities

remain behind on the frit and the soluble product washes through. The SO_2 was then bled off to reveal a crystalline solid.

Individual experimental details of each chloride salt made by the above method now follows.

ortho R-C_6H_4-CNSSN$^+Cl^-$

o-R	Mass of $LiN(X)_2$ X=$SiMe_3$	Colour of solution at stage 1	Colour of precipitate after stage 2	Elemental analysis	Yield %	Final product (Stage 3)
Br	1.67g	Dark green	Dark orange brown precipitate, stir for a day	Obs C 30.90; H 2.00; N 7.20 Req C 28.44; H 1.36; N 9.48	-	Brown solid
Cl	2.5g	Straw	Bright orange solid visibly contaminated with nitrile	Obs C 34.80; H 1.90; N 12.90 Req C 33.48; H 1.61; N 11.16	42%	Orange solid
F	1.67g	Red	Luminous yellow solid	Obs C 36.10; H 1.98; N 12.01 Req C 35.82; H 1.72; N 11.94	61%	Crystalline yellow solid

IR(Br): 2222m, 1680w, 1619w, 1594w, 1566w, 1485m, 1463s, 1377s, 1261w, 1228w, 1156w, 1091w, 1046w, 959m, 843w, 759vs, 740m, 722w, 602w, 556m and 516s.
IR(Br-C_6H_4-CN): 2222w, 1583m, 1564w, 1465s, 1436m, 1377m, 1263w, 1200w, 1166w, 1123w, 1044s, 1028m, 952m, 756vs, 704m, 658s, 569vw, 556s, 486w and 450s.
IR(Cl): 1671vw, 1590m, 1464s(br), 1432m, 1385s(br), 1266w, 1203w, 1154m, 1134w, 1057m, 1042w, 1001w, 926w, 890s, 866vw, 844s, 773s, 757s, 732vs, 720s, 686m, 640w, 554s, 518w, 469m and 460m
IR(F): 1677w, 1610s, 1600m(sh), 1493m, 1457s, 1394s, 1383m, 1306s, 1274m(sh), 1234s, 1162m, 1141m, 1102m, 1032w, 934w, 900s, 846s, 813s, 773vs, 755m, 741s, 674m, 684m, 640w, 562s and 530s

meta R-C_6H_4-CNSSN$^+Cl^-$

m-R	Mass of $LiN(X)_2$ X=$SiMe_3$	Colour of solution at stage 1	Colour of precipitate after stage 2	Elemental analysis	Yield %	Final product (Stage 3)
NO_2	3.34g	Deep red	Orange	Obs C 33.67; H 1.40; N 16.54 Req C 32.12; H 1.54; N 16.06	80%	Orange solid
CF_3	5g	Golden	Bright yellow	Obs C 34.20; H 1.56; N 10.12 Req C 33.75; H 1.42; N 9.84	87%	Bright yellow crystalline solid

meta R-C_6H_4-CNSSN$^+Cl^-$ cont'd

m-R	Mass of $LiN(X)_2$ X=$SiMe_3$	Colour of solution at stage 1	Colour of precipitate after stage 2	Elemental analysis	Yield %	Final product (Stage 3)
Br	3.34g	Straw	Yellow	Obs C 27.87; H 1.35; N 9.66 Req C 28.44; H 1.36; N 9.48	82%	Yellow crystalline solid
Cl	3.34g	Olive oil	Yellowy orange	Obs C 32.88; H 1.46; N 11.00 Req C 33.48; H 1.61; N 11.16	83%	Yellowy orange solid
F	3.34g	Dark orange	Orange	Obs C 35.65; H 1.93; N 11.01 Req C 35.82; H 1.72; N 11.94	82%	Orange crystalline solid
Me	1.67g	Straw	Yellow	Obs C 42.03; H 3.50; N 12.56 Req C 41.64; H 3.06; N 12.14	88%	Bright yellow crystalline solid
MeO	2.00g	Straw	Bright orangey red	Obs C 37.98; H 2.43; N 11.01 Req C 38.94; H 2.86; N 11.36	95%	Red crystalline solid

IR(NO_2): 1680w, 1615w, 1536s, 1486m, 1463s, 1393m, 1377m, 1351s, 1305s, 1288w, 1163w, 1138w, 1095vw, 1076vw, 963w, 919vw, 896s, 860m, 844m, 817m, 788w, 748vw, 734m, 718m, 705vs, 671w, 557vw, 536w, 470vw and 429vw.
IR(CF_3): 1610m, 1594vw, 1461s, 1397s, 1377m, 1324s, 1312s, 1294s, 1190s, 1172s, 1123s, 1096m, 1075s, 1000vw, 953s, 924w, 913m, 893s, 850s, 814s, 786vw, 722s, 696s, 690m, 647w, 620w, 547s and 528m.
IR(Br): 1564m, 1464s, 1428m, 1379s, 1295w, 1275w, 1212w, 1156m, 1086w, 1068m, 994m, 938s, 896s, 890s, 847s, 806s, 715vs, 672m, 644vw, 547s, 518m and 434w.
IR(Cl): 1573m, 1464s, 1436m, 1380s, 1313w, 1298w, 1275w, 1212w, 1160m, 1138w, 1092m, 1072m, 997w, 948s, 896s, 848s, 804s, 742s, 717vs, 674m, 548s and 526m.
IR(F): 1676m, 1587s, 1493m, 1453s, 1387s, 1312m, 1300m, 1281w, 1227m, 1138m, 1124m, 1076w, 1002w, 976s, 900s, 856m, 822s, 801s, 772w, 723vs, 674m, 549m, 526m and 464w.
IR(Me): 1584w, 1459s, 1379vs, 1307m, 1221m, 1168vw, 1136m, 1090w, 1048vw, 999vw, 956w, 926w, 892s, 851s, 806m, 717vs, 684w, 617vw, 546s and 526m.
IR(MeO): 1600m, 1579m, 1490m, 1461vs, 1375s, 1347s, 1288m, 1265w, 1252m, 1238m, 1200w, 1181w, 1156w, 1110s, 1085w, 1040m, 954m, 940m, 886w, 858w, 810w, 800w, 755vs, 732s, 704s, 682m, 545vw, 519w and 443s.

para R-C_6H_4-CNSSN$^+Cl^-$

p-R	Mass of $LiN(X)_2$ X=$SiMe_3$	Colour of solution at stage 1	Colour of precipitate after stage 2	Elemental analysis	Yield %	Final product (Stage 3)
NO_2	1.67g	Dark brown	Orangey-yellow	Obs C 33.19; H 1.33; N 16.90 Req C 32.12; H 1.54; N 16.06	70%	Orangey yellow solid
CF_3	1.67g	Golden /straw	Bright yellow	Obs C 33.50; H 1.45; N 9.80 Req C 33.75; H 1.42; N 9.84	58%	Lemon yellow solid
Br	1.67g	Golden /straw	Orange	Obs C 28.92; H 1.35; N 9.43 Req C 28.44; H 1.36; N 9.48	60%	Orange solid
Cl	1.67g	Golden	Orange	Obs C 33.58; H 1.66; N 11.56 Req C 33.48; H 1.61; N 11.16	71%	Orange solid
F	1.67g	Straw coloured solution	Bright orange	Obs C 35.80; H 1.70; N 11.35 Req C 35.82; H 1.72; N 11.94	63%	Orange crystalline solid
Me	1.67g	Straw	Orange	Obs C 40.90; H 3.00; N 12.00 Req C 41.64; H 3.06; N 12.14	55%	Orange solid
MeS	1.67g	Straw	Burgundy red	Obs C 36.90; H 2.70; N 10.60 Req C 36.56; H 2.69; N 10.66	60%	Black / dark red solid
MeO	1.67g	Straw	Burgundy red	Obs C 38.65; H 2.70; N 11.45 Req C 38.94; H 2.86; N 11.36	67%	Dark red solid
CF_3O	1g	Straw	Orange	Obs C 30.91; H 1.32; N 8.85 Req C 31.95; H 1.34; N 9.32	75%	Orange
$MeCO_2$	1g	Lemon yellow	Bright yellow	Obs C 39.97; H 2.22; N 9.68 Req C 39.34; H 2.57; N 10.20	68%	Bright yellow

IR(CF_3): 1520w, 1417w, 1405m, 1322s, 1250w(br), 1222w, 1170m, 1157m, 1140m, 1122s, 1110m, 1065s, 1012s, 985w, 920w, 890s, 860s, 845s, 770w, 755m, 750m, 698m, 690m, 680(sh), 595m, 550m and 515w.

IR(Br): 1680w(br), 1592m, 1390s, 1290w, 1180m, 1160m, 1070m, 1010s, 960w, 920w, 890s, 843s, 770w, 730s, 700m, 680s, 625w, 545s and 495m.

IR(F): 1600s, 1515m(br), 1395s, 1300m, 1270w, 1240m, 1225m, 1165s, 1105vw, 1090w, 1040w, 1010w, 930m, 900s, 890s, 845s, 810m, 735s, 680m, 588m and 515m.

IR(Me): 1605m, 1400s, 1300vw, 1215w, 1200m, 1185w, 1160m, 1040m, 1024m, 925s, 900s, 845s, 825m, 724s, 685m, 548m, 525w and 490m

IR(MeS): 1590s, 1438s, 1395s, 1180m, 1140m, 1117w, 1090m, 1005w, 970w, 930m, 882s, 832s, 728s, 680m, 550s and 500w

IR(MeO): 1605m, 1400s, 1300vw, 1215w, 1200m, 1185w, 1160m, 1040m, 1024m, 925s, 900s, 845s, 825m, 724s, 685m, 548m, 525w and 490m.

IR(CF_3O): 1605w, 1512w, 1462vs, 1402s, 1377s, 1258s(br), 1213s, 1165s(sh), 1152s, 1015m, 926w, 892m, 858m, 848m, 808w, 722w, 696m, 655w, 613w.

IR($MeCO_2$): 1706s, 1609vw, 1576vw, 1511m, 1459s, 1436m, 1424w, 1410m, 1400s, 1386s, 1307s, 1289s, 1190m, 1155m, 1138m, 1112m, 1017m, 966w, 952w, 923w, 896s, 876m, 849m, 826m, 782m, 776w, 713vs, 680vw, 548m, 530m.

F_2-C_6H_3-CNSSN$^+Cl^-$

F,F	Mass of $LiN(X)_2$ X=$SiMe_3$	Colour of solution at stage 1	Colour of precipitate after stage 2	Elemental analysis Req C 33.27; H 1.20; N 11.09	Yield %	Final product (Stage 3)
2,3	1.20g 2.66g	Orange	Orange	Obs C 33.28; H 1.01; N 11.05	70%	Marigold yellow solid
2,4	4.2g 2.08g	Deep red	Orange / yellow coloured precipitate which forms a sticky intractable oil in SO_2	-	N/A	N/A
2,5	3g 4.90g	Red solution which darkens overnight to a brown	Bright yellow	Obs C 33.04; H 1.22; N 11.14	52%	Crystalline yellow precipitate
2,6	3g	Red solution which darkens to brown after three hours	Instant yellow	Obs C 32.99; H 1.50; N 11.68	58%	Yellow solid
3,4	4.75g	Red	Bright orange	Obs C 33.90; H 1.40; N 11.98	63%	Orange solid
3,5	2.5g	Red coloured solution which darkens gradually to brown after 4 hours	Bright orange	Obs C 32.89; H 1.39; N 11.90	75%	Bright orange crystalline material

IR(2,3F_2): 1684m, 1624w, 1594w, 1540vw, 1489s, 1464vs, 1398vs, 1389s, 1377s, 1317w, 1269s, 1212vw, 1164w, 1139w, 1063w, 1016s, 952w, 905m, 840s. 810m, 793s, 733vs, 696vw and 608m.
IR(2,5F_2): 1681m, 1623s, 1595s, 1496s, 1452s, 1375s, 1310m, 1264m, 1225s, 1215m, 1190s, 1139m, 1096m, 1007vw, 982m, 905m, 884s, 865vw, 846m, 835s, 766vs, 739m, 690vw, 663vw, 567w, 528s and 466w
IR(2,6F_2): 1626s, 1590m, 1564m, 1466s, 1378s, 1310m, 1300m, 1248s, 1203m, 1149m, 1140m, 1062m, 1009vs, 926w, 887s, 843s, 791vs, 745m, 719w, 696m and 654m.
IR(3,4F_2): 1696w, 1609m, 1522m, 1461s, 1443s, 1378s, 1282s, 1213m, 1127m, 1112m, 977s, 896m, 881s, 860m, 838m, 827m, 774s, 723s, 698w, 622s, 535s, 483vw and 454vw
IR(3,5F_2): 1733vw, 1682vw, 1618m, 1596m, 1559w, 1537m, 1463s, 1444s, 1404s, 1377s, 1340m, 1248vw, 1125vs, 1060vw, 1008m, 984s, 892m, 863s, 852m, 787m, 740w, 721s, 702w, 666m, 606vw, 577m, 537m, 524m and 506m

mixed X,Y-C_6H_3-CNSSN$^+Cl^-$

X,Y	Mass of $LiN(X)_2$ X=$SiMe_3$	Colour of solution at stage 1	Colour of precipitate after stage 2	Elemental analysis	Yield %	Final product (Stage 3)
3,5Cl_2	4.75g	Red orange	Orange / yellow	Obs C 30.20; H 1.05; N 9.61 Req C 29.44; H 1.06; N 9.81	72%	Orange solid
2F, 4CF_3	0.97g	Red	Orange	Obs C 30.75; H 1.10; N 9.33 Req C 31.74; H 1.00; N 9.26	80%	Marigold orange solid
3Cl, 4Me	1.67g	Straw	Orangey red	Obs C 36.01; H 1.25; N 10.20 Req C 36.23; H 2.28; N 10.57	87%	Orange solid
3Cl, 4F	1.67g	Red	Bright orange	Obs C 31.03; H 1.25; N 10.10 Req C 31.24; H 1.12; N 10.41	85%	Orange solid

IR(3,5Cl_2): 1678w, 1593vw, 1569s, 1462m, 1452s, 1430m, 1368s, 1296vw, 1209vw, 1113w, 1101m, 970s, 898m, 888m, 864s, 854s, 805vs, 731m, 722s, 663m, 556m, 524w and 430w.
IR(2F, 4CF_3): 1641vw, 1631vw, 1582w, 1518m, 1463vs, 1429s, 1377s, 1333vs, 1267m, 1210m, 1179s, 1162m, 1134vs, 1067m, 937w, 919vw, 888s, 878s, 838s, 746s, 722m, 705m, 668m, 558m, 537m, 509vw and 470vw
IR(3Cl, 4Me): 1611w, 1561w, 1500vw, 1463s, 1402s, 1384s, 1307s, 1273m, 1212w, 1166m, 1139m, 1052s, 997m, 952s, 902m, 895s, 852s, 831s, 808m, 722vs, 701s, 685m, 570vw, 560m, 540s and 530m
IR(3Cl, 4F): 1594m, 1590m, 1558vw, 1540vw, 1511m, 1464s, 1412s, 1390s, 1305s, 1289w(sh), 1279w(sh), 1267s, 1252m, 1212vw, 1168m, 1139m, 1127m, 1061m, 954s, 916w, 906m, 893vs, 855s, 834s, 729s, 709s, 692m, 612m, 573w, 545m, 529w, 516s and 445m

pyridyl x-NC_6Y_4-$CNSSN^+Cl^-$

x-py^Y	Mass of $LiN(X)_2$ X=$SiMe_3$	Colour of solution at stage 1	Colour of precipitate after stage 2	Elemental analysis	Yield %	Final product (Stage 3)
p-py^F	2.9	Red	Mandarin	Obs C 24.92; H 0.00; N 14.64 Req C 24.88; H 0.00; N 14.51	89%	Orangey yellow crystalline material
m-py^H	5g	Straw	Orangey yellow	Obs C 33.14; H 1.90; N 19.26 Req C 33.10; H 1.85; N 19.31	89%	Orange solid
p-py^H	4.18g	Straw coloured solution and white precipitate	Mustard	Obs C 32.63; H 1.94; N 19.02 Req C 33.10; H 1.85; N 19.31	87%	Yellow crystalline solid

IR(p-py^F): 1649m, 1594w, 1467s(br), 1421s, 1373s, 1334m(sh), 1279w, 1258m, 1236m, 1150w, 1055w, 1035s, 971s, 883vs, 852m, 789m, 760w, 735m, 690s, 572w and 534s.
IR(m-py^H): 1631w, 1585m, 1536w, 1462s, 1425w, 1377s, 1154m, 1115w, 1039m, 1022m, 915m, 883s, 848s, 832s, 713vs, 699s(br), 622s, 585w and 547vs.
IR(p-py^H): 1620w, 1581w, 1460s(br), 1232w, 1150m, 1044w, 987w, 921m, 886s, 846s, 837s, 815m, 779w, 738m, 720w, 688s, 674m, 661m, 639w, 541s, 509m, 400w(br), 372w, 312s and 276m.
IR(p-py^H): 2241m, 1973w, 1718w, 1594s, 1543s, 1500m, 1460s(br), 1417s, 1380m, 1338m, 1241m, 1208m, 1194m, 1112w, 1082s, 1075m, 990vs, 982w, 980w, 970w, 938w, 827vs(br), 778s, 749w, 725w, 662w, 615w, 561vs.

4D Preparation and characterisation of substituted phenyl and pyridyl 1,2,3,5 dithiadiazolyl radicals

4D.1.1 Preparation

All preparations of 1,2,3,5 radicals involved reduction of the chloride salt. Two different types of reducing agents were used for these reductions, these were triphenyl antimony and zinc/copper couple.

Stage 1

Method 1 Zn/Cu

A 1·2:1 mole ratio of Zn/Cu and R-CNSSN$^+$Cl$^-$ was placed in a schlenk under an inert atmosphere. Dry THF was then syringed in against a counterflow of nitrogen (~20mls of THF per 1.5g of compound). After 5 minutes the solution had turned purple or red depending on the sample. After 30 minutes all the chloride salt had visibly disappeared and a purple or red solution and precipitate had formed. The reaction mixture was left to stir for a further 5 hours and pumped to dryness. The material was then scraped out of the vessel and transferred to a sublimation vessel where it was purified (stage 2).

Method 2 Ph_3Sb

In an inert atmosphere, a 1:2 molar ratio of Ph_3Sb and R-CNSSN$^+$Cl$^-$ was placed into a schlenk. Against a counterflow of nitrogen, dry CH_2Cl_2 was then syringed in and the reaction allowed to stir (~10mls per 1g). A purple solution and precipitate started to form within minutes. After 15 minutes the reaction had almost gone to completion. It was left to stir for 5 hours in total. The solution was then canulared off and the remaining solid washed with an equivalent portion of fresh dry CH_2Cl_2 as before. The vessel was then evacuated to reveal a solid material that could be further purified by sublimation (stage 2).

4D.1.2 Crystal growths of 1,2,3,5 radicals

Producing crystals suitable for x-ray structure determination for many of these compounds was attempted in order to reveal more information about packing criteria of these compounds and better understanding of their physical properties. The crystal growth techniques used included sublimation and solution methods.

Sublimation was the preferred technique for producing crystals of the radical species as it could be conducted in conjunction with the purification of these materials. However using this method many radicals failed to yield suitable crystals, for structure determination, (i.e. crystals were too small or twinned). This technique could not be used to purify the cationic analogues as heating these compounds often resulted in their degradation, usually to yield S_4N_4. On the other hand crystal growths involving solution techniques could readily be used to obtain crystals of both dithiadiazolylium and associated radical derivatives.

Details of crystallisation.

To produce crystals of these types of compounds suitable for x-ray structure determination the best sublimation conditions were achieved when the vacuum was low, (10^{-2} torr), and the temperature regulated such that crystals were seen to form slowly. This technique proved to be a very successful method for me in achieving crystals whose structures were determined. Even though the majority of the radicals sublimed to give crystalline material, producing crystals large enough, especially for the di-fluoro derivatives, was elusive. Many of the derivatives, e.g. pCF_3O and pMeO produced dendritic fluffy crystals and changing sublimation conditions did little to alter this too.

The fluoro derivatives were found to be readily soluble in 1,2dichlorobenzene. As this solvent has such a high boiling point, the idea was to make saturated solutions of the radicals and remove the solvent slowly which should aid crystal formation. This was achieved by applying a constant vacuum, resulting in the solvent slowly being removed. Of the fluoro compounds investigated by this method only the *ortho* fluoro gave good looking crystals. However these crystals were found to be heavily twinned when examined by diffraction methods and hence no structure was attempted.

Unfortunately none of the above techniques for crystal growth could be used for the *para* pyridyl radical as it didn't readily sublime and was highly insoluble in practically every solvent. Other crystal growth techniques were not attempted.

4D.1.3 DSC

Many factors influence the temperature at which a compound melts. One of these is the direct relationship that exists between molecular mass and melting point of a compound, i.e. the heavier the molecule the more energy is needed for it to break free of the crystal lattice, i.e. melt, assuming inter and intra molecular interactions are constant. The strength of inter- and intra-molecular attractions, and also of repulsions, between the molecules, will influence the melting point. Naturally, the shape and type of substituents of a molecule will determine the most favourable packing arrangements and influence the types of interactions present. Generally, repulsions will assist in decreasing the melting point and attractions will have the opposite effect. Therefore among a series of substituted derivatives all the above factors will vary, hence a range of melting points for a series of compounds will be observed.

DSC was conducted on samples of several *para, meta* and di-substituted phenyl dithiadiazolyl derivatives (30-400°C temperature range). Also, pyridyl analogues were studied. Using this technique the melting points of these compounds were detected.

From the above opening paragraph it has been stated that m.pt. is related to the structure. Many of the structures of the above compounds examined by DSC are not known. However, structures of analogous compounds are, which can be used to speculate on the type of packing in the compounds of unknown structure. Therefore, a very crude rationalisation of how the relative sizes of the melting points for these compounds is related to their individual molecular mass, structure and type of substituent was attempted. (Further details on structural and ESR data can be found readily in Chapter 3).

The crystallographic data available on dithiadiazolyls suggest that all these compounds will predominantly exist as dimers in the solid state via four centred S···S interactions. From these results there appears to be no trend between the S···S distance (i.e. strength of interaction), and the donor or acceptor nature of a substituent. Simultaneous ESR studies indicate that the electron density of the dithiadiazolyl sulphur will increase (while the neighbouring nitrogen decreases) as the electron withdrawing ability of the substituent group increases. From these data stronger S···S interactions and shorter intradimer S···S distances as the substituent group becomes more electron withdrawing are predicted. Combining these two pieces of data it can

be deduced that the donor acceptor strength of the substituents of these derivatives has a very small effect on the strength of the S···S interactions as the S···S distances are within experimental error of each other. Hence the force required to break the S···S bond among these derivatives will be approximately the same among these derivatives. Therefore the deviations in m.pts. among these derivatives are not attributed to varying S···S strengths.

If no trend between m.pt. and m.w. is observed among a series of compounds there is good reason to suspect that differing strengths and types of solid state molecular interactions or steric forces are present.

Para

The discussion begins with an analysis of the melting points of the *para* substituted dithiadiazolyl derivatives, as shown in Table 1.

X substituent	m.pts. for *para* X/ C°	m.pts. for *meta* X/ C°
NO_2	252.0	-
CF_3	123.8	81.9
Br	153.3	128.8
Cl	140.8	117.4
CF_3O	97.4	-
F	120.1	128.0
MeS	149.6	-
MeO	124.7	94.5

Table 1. Melting points (m.pts.) of some *para* and *meta* substituted phenyl 1,2,3,5 dithiadiazolyl.

It is evident from these results that the size of the m.pts. of *para* derivatives are not related to an increase in molecular mass, as the compounds with the highest and lowest molecular mass have the lowest two m.pts. of this group. Therefore, varying types of interactions between the molecules of these derivatives must be contributing significantly to the observed variations in melting point. Hence a closer examination of the crystal structures of these *para* compounds is required in order to assess this situation. Of this group of compounds only the structures of the pNO_2, pCF_3, pCl, pF and pMeS derivatives were known.

Starting with the *para* halogen substituted derivatives (F, Cl, Br), the melting point trends of these particular *para* dithiadiazolyl analogues

contradict those of the group as their m.pts. are seen to increase with molecular weight. Crystallographic details are required in order clarify the reason for this trend.

The crystal structures of the *para* substituted F and Cl phenyl dithiadiazolyl derivatives show that they pack in herring bone arrays via S···S and S···Cl contacts respectively, see chapter 3. Between these arrays similar types of S···N interactions exist. Hence, the strength of molecular interactions between molecules of these two derivatives are anticipated as being very similar. Therefore this evidence suggests that the pCl derivative has a larger m.pt. than the pF because it has a higher molecular weight.

The structure of the *para* substituted Br analogue is unknown but it is anticipated that the pBr will pack similarly to the other two derivatives for the following two reasons. The fact that the pBr substituent is larger than and more electropositive than the other two halogen substituents (i.e. greater steric forces and weaker interactions) would not prevent the pBr packing in an analogous way. Also, analysis of the crystal structure of (mCl, pMe) and mBr analogues reveals that the dimers of these similar halogen compounds pack in a manner analogous to the pF and pCl compounds (herring bone style packing).

Therefore in the proposed structure of p-Br interdimer, either Br···S or S···S contacts would run between the molecules in a herring bone array. If $Br^{\delta-}$ ···$S^{\delta+}$ contacts exist, it is assumed that they would be weaker than $Cl^{\delta-}$···$S^{\delta+}$ contacts of the pCl, due to weaker electrostatic attraction because Br is less electronegative than Cl. Therefore, this suggests that the molecules would be more tightly bound together in pCl than pBr derivative with this type of structure. If inter dimer S···S interactions exist instead, then they are assumed to be about equal in size to those observed in the pF derivative.

Using all the above evidence, it certainly appears that the increase in melting point is due to increasing molecular weights of these halogen compounds.

If the CF_3 derivative is now compared, its melting point is approximately the same as that observed for the fluoro derivative even though the former has the lower m.w. The reason why this occurs is not due to both derivatives packing differently in the solid state. (The CF_3 derivative does not pack in herring bone arrays like the F derivative but in ribbons with S···F contacts linking the dimers the axis of the ribbons). Neither is it due to differences in the interactions between the planar arrays of these molecules, as similar S···N contacts are observed for both derivatives. It is attributed to the

CF_3 group being sterically more bulky and possessing more fluorines per molecule than the F group, i.e. a greater chance of F···F repulsions.

This reason also readily explains why the other halogen derivatives, pCl and pBr, have even larger m.pts. than the pCF_3 analogue even though the molecular weights of all these derivatives are similar. Now on to the remaining derivatives, pMeS, pMeO and pCF_3O.

The m.w. and m.pts. of pMeS are comparable to those of the pBr derivative. Analysis of the appropriate structures was required in order to assess this situation. Of these two derivatives only the structure of the pMeS derivative is known. The molecules of the pMeS compound are found to exist as cis-oid dimers with the MeS groups trans to each other. This assists in minimising the steric repulsions between the two methyl groups per dimer. These dimers pack in herring bone arrays via (thioether)S···S(dithiadiazolyl) contacts. Between these arrays S···N contacts similar to those observed for the pF derivative are present. A style of packing similar to the above is also predicted for the *para* bromo derivative. Therefore if the sum of the attractive and repulsive forces of the molecules of pBr and pMeS in the herring bone arrays are similar as are their m.w's, then their m.pts. would be expected to be similar as observed. The same reasoning used to explain why pBr m.pt. is higher than the pCF_3 can be used to explain why pMeS has a higher melting point than this derivative too.

Now glancing at the melting points for the pMeO and pMeS derivatives it would appear that their m.pts. are related to their m.w., as observed among the halogen derivatives. This can't be confirmed by comparing their molecular interactions in the solid state as the structure of the pMeO derivative is unknown. As both derivatives have similar shapes it is possible that the pMeO could pack like the pMeS for which a structure is known. If this were the case then O···S rather than S···S interactions could occur along the herring bone arrays. To assess the relative strengths of S···O contacts versus S···S contacts requires a more detailed examination of bond lengths, van der Waals radii and steric nature of the substituent groups.

Looking more closely at the relative bond lengths, the aryl C-O bond and Me-O (typically 1.37Å and 1.43Å respectively) will be shorter than the corresponding aryl C-S and Me-S (typically 1.76Å and 1.80Å respectively) bond and therefore the MeO substituent is bonded more closely to the aryl ring than the MeS group. The aryl C-X-Me bond angle (where X=O or S) will be typically 118° for p-MeO and is 104° for pMeS. This clearly shows that the Me group can sterically interfere more in the pMeO analogue.

Also sulphur has a larger van der Waals radius than oxygen, thus the orbitals of the dithiadiazolyl sulphurs of neighbouring molecules may be able to overlap more with the orbitals of the sulphur of the MeS group rather than those of the oxygen of the MeO group. S···O attractions are higher in energy, i.e. stronger, than S···S. Therefore, these interdimer interactions of these two derivatives could be similar in strength due to a trade off between greater orbital overlap of the sulphurs versus the stronger interactions involving the oxygen atom. Hence, this evidence suggests that for these two derivatives their m.pts. are related to their molecular weight rather than differences in the energies of molecular interactions and contacts.

The pCF_3O analogue has the lowest m.pt. of the *para* compounds studied even though it has the largest m.w. of all the *para* derivatives studied. This is attributed to the large steric bulk of OCF_3 group preventing the molecules from packing closely together, which is further hindered by $F^{\delta-}\cdots F^{\delta-}$ and additional $F^{\delta-}\cdots O^{\delta-}$ repulsions, thus considerably lowering the melting point of this compound relative to the other substituents of the *para* derivatives, *cf* pCF_3.

Finally, the pNO_2 compound has by far the highest melting point but has an average m.w. among the *para* derivatives. Analysis of this compound's crystal structure readily shows that this is due to the type and multitude of interactions present between its dimers. These dimers pack as ribbons via very favourable S···O contacts. Between these ribbons the molecules overlap such that there are six S···N contacts between each pair of adjacent dimers. For the other derivatives this is anticipated as being no higher than four. As the pNO_2 molecule is essentially planar then intradimer steric repulsions are at a minimum too. The combination of all these factors results in this compound possessing a high m.pt. relative to the other *para* derivatives. This clearly shows the influence strong interactions and minimum steric forces can have on inducing higher m.pts.

Meta

Starting off with the three *meta* halogen derivatives studied, it can be seen that, in contrast to the *para* halogen analogues, the m.pt. doesn't increase with m.w. This suggests that the packing arrangements and resulting interactions for the *meta* derivatives must be sufficiently different among them to cause these differences in m.pts. This can't be confirmed from available crystallographic data as only the structure of mBr has been determined. However, structures of other related halogen compounds are

found to pack similarly to the mBr, i.e. zig-zag style packing of dimers. Therefore, this idea will be extended to the *meta* halogen compounds too.

The mBr molecules pack as cisoid dimers, such that the two Br groups in each dimer overlap each other. This arrangement results in the molecules twisting with the largest distance existing between the two Br groups, i.e. to minimise Br-Br repulsions. More importantly, this arrangement also allows the dimers to pack in zig-zag arrays via S···Br interactions. The packing for this derivative is reminiscent of that seen for the analogous *para* fluoro and *para* chloro derivatives.

The structure of the mCl derivative is not known but the structure of the mCl, pMe analogue is. Therefore investigation of this structure may give clues to the type of packing in the former compound. The molecules of this disubstituted derivative exist as cisoid dimers which pack perpendicular to each other in the solid state. Between these dimer units, only H···Cl contacts are observed. This packing arrangement is slightly different from that observed for the mBr derivatives. However, the structures of all the analogous halogen derivatives discussed so far, including *para* samples, do show that perpendicular packing of dimers is definitely preferred for halogen dithiadiazolyl compounds.

The above evidence suggests that the mCl derivative could possibly pack like the mCl, pMe analogue. However, the steric bulk of the Me group rather than mCl interactions could be influencing the packing arrangement of mCl, pMe making the above assumption seriously open to question.

Alternatively, the mCl might pack like the mBr. If X=Cl or Br stronger S···X attractive forces and weaker X···X repulsions would exist for the Cl derivative. Therefore, one would expect these forces to contribute to the mCl having a higher m.pt. than mBr. However the reverse trend in m.pts. is observed.

So, all the evidence so far collected suggests that the m-Cl derivative has a lower m.pt. than the mBr simply because it has a lower molecular weight assuming their structures are both similar, *cf para* analogues.

At this stage it is important to note that the m.pts. of the mBr and mCl derivatives are smaller than there associated *para* isomers. This is mainly attributed to an increase in intradimer steric repulsive forces between the halogens substituents as they move from the *para* position to the *meta*, i.e closer to the intramolecular S···S `hinge' of the dithiadiazolyl dimer unit, cf pCF_3.

The above trend in m.pts. of *meta* halogen compounds increasing with molecular weight is not observed when the mF is allowed into the discussion. The m.pt. for this derivative is approximately the same as that of the mBr derivative even though their molecular weights differ. Therefore, the sum of the energies of the intermolecular forces of these derivatives must be stronger in the mF than mBr. As only the structure of the mBr is known, the possible differences in the type of interactions between the two derivatives can only be speculated upon.

So, if the mF derivative packs like the mBr derivative, as they are similar in shape and distribution of dipole charges, the electrostatic $S^{\delta+}\cdots F^{\delta-}$ attractive interactions along the herringbone arrays would be anticipated as being stronger than for $S^{\delta+}\cdots Br^{\delta-}$ as fluorine is more electronegative than bromine. The presence of these stronger interactions would contribute to the m.pt. of the F derivative being higher than predicted from m.pts. and mw of other halogen derivatives.

Alternatively, the mF derivative could pack very differently to the other halogen derivatives, such that resulting attractive molecular forces are considerably stronger than those in mBr. It is envisaged that the molecules of this derivative will exist as dimers in the solid state.

A comparison of the melting points of mF and pF derivatives shows that the latter has the lower m.pt. This is the opposite trend to that observed for Cl and Br substituted analogues, clearly increasing steric repulsions between groups going from *para* to *meta* can't be used to explain the situation for the fluoro derivatives. This result strongly indicates that the packing arrangement in the mF is very different from that of the *para* F analogue.

These *meta* derivatives would be an interesting set of compounds to study crystallographically in order to confirm which mode of packing and interactions are contributing to the observed trends in m.pts.

The mCF_3 derivative has a lower m.pt. and similar molecular weight to the analogous mCl and mBr derivatives. This can be rationalised from available structural evidence of mBr and related compounds. Even though the structures of the mCl and mCF_3 derivatives are unknown but that of the mBr is, it is anticipated that the preferred orientation of the dimers of all three derivatives will be completely *cis*. Evidence from the structure for the mBr derivative indicates that steric repulsive forces between the two Br groups of a dimer do exist. As the CF_3 group is larger than the Br substituent, larger unfavourable intradimer steric forces between mCF_3 substituents will be present due to larger steric hindrance and $F^{\delta-}\cdots F^{\delta-}$ repulsions between the

substituent groups, ie the dimer will fall apart more easily thus decreasing the melting point of the compound.

The mCF_3 derivative is observed to have a lower m.pt. than the pCF_3 analogue. This is because the intradimer repulsive forces between CF_3 substituents groups of these derivatives increases from going from the *para* position to the *meta*, *cf* mBr discussion.

The only other *meta* derivative studied was the mMeO derivative which was found to melt at a slightly higher temperature than the mCF_3 analogue but lower than the halogens. This trend is mainly attributed to the connection between decreasing steric bulk of the substituent group with increasing m.pts. among these groups of *meta* derivatives.

Difluoro

These disubstituted phenyl dithiadiazolyl derivatives possess only two fluoro substituents, i.e. their molecular masses are the same. Also, at least one of the fluorines is at the *meta* position. Despite these similarities, only three of these four compounds were found to have similar m.pts., i.e. 2,3; 3,4; 3,5 derivatives. This difference in m.pts. of the 2,5 derivative relative to the others must be due to differences in packing arrangements among these difluoro substituted derivatives. The most obvious scenario is that the 2,5 packs differently to the others. As the positions of the fluorines are different for each derivatives it is more likely that the packing is different for all the derivatives. Therefore, the m.pts. of three derivatives are the same because the difference between the sum of the repulsive forces (e.g. F···F and F···N) and attractive forces (S···S and S···F) between the molecules is approximately the same. A more detailed explanation would naturally be able to be given if structural data were available. Again, a very interesting crystallographic muse.

$F_2C_6H_3$-CNSSN	**m.pts./ C°**	XYC_6H_3-CNSSN	**m.pts./ C°**	p-py^X-CNSSN	**m.pts./ C°**
2,3	**125.5**	**2F, 4CF_3**	**99.7**	**ppy^F**	**84.5**
2,5	**109.6**	**3Cl, 4Me**	**123.9**	**py^H**	**178.0**
3,4	**131.6**	**3Cl, 4F**	**139.2**		
3,5	**132.9**	**3Cl, 5Cl**	**127.7**		

Table 2 Melting points of some substituted 1,2,3,5 dithiadiazolyl derivatives

The m.pts. among these difluoro compounds are found to be the same or lower than those of the lighter mono substituted *meta* or *para* F analogues.

Obviously, the sum of the energies of differing molecular forces, among these two groups of derivatives, must be smallest for the heavier difluoro analogues as a larger mw isn't seen to give rise to larger m.pts. relative to the mono fluoro substituted derivatives. These possible differences between the molecular forces that could exist between these mono and di substituted derivatives are connected with the number of fluorine atoms present.

The presence of twice as many fluorines, (i.e. mono to disubstituted derivatives), increases the chances of S···F attractive forces which would contribute to increasing the m.pts. However with more fluorines comes the problem of the higher probability of F···F and F···N repulsions which will depress m.pts. Also, larger spatial area of the difluoro derivatives may make favourable packing harder to achieve. Therefore, the latter two causes are assumed to be responsible for the relative magnitude of m.pts. of these compounds.

Mixed.

Four compounds were studied. Their m.pts. were not observed to increase with molecular weight. As discussed in previous sections, this is presumably due to varying molecular interactions of varying strength and type. Of these four derivatives only the structure of the 3Cl,4Me is known. Therefore, speculations of possible structures of the others, using information from similar derivatives, will be made in order to assist in explaining trends in the relative magnitude in m.pts. among these compounds.

Starting off with the 3Cl,4Me substituted compound, the structure of this material reveals that its dimers pack perpendicular to each other with intermolecular H···Cl contacts existing, see mCl discussion chapter 3.

When the *para* Me group of this derivative is replaced by a fluorine, i.e. 3Cl,4F, the m.pt. is seen to increase even though the m.w. decreases. This is probably due to the presence of favourable F interactions and/or reduction in the steric bulk or hindrance of the *para* group assisting in elevating the m.pt. Results from *meta* and *para* derivatives have clearly shown that steric repulsions due to the addition or moving bulky substituents closer together can be responsible for lowering melting points.

The 3Cl, 5Cl has a m.pt. which is in between the previous two. This is attributed to a differing molecular packing arrangement due to differing distribution of the substituent groups. Speculation on the type of packing this derivative might possess was not attempted as there are no similar dithiadiazolyl structures upon which to base a sensible structural proposal.

The remaining compound, the 2F,4CF_3 substituted derivative, has the lowest m.pt. relative to the others. This is attributed to the steric repulsive forces, involving the two substituents, being larger than those of the other three derivatives. The type of repulsive forces present include F···F and F···N(dithiadiazolyl) intradimer and interdimer repulsions due to the bulky nature of the CF_3 group and the *ortho* position of the F substituent. These types of steric repulsive forces are discussed in more detail in the forthcoming pyridyl section.

Pyridyl

The ppy^H has a larger melting point than the analogous ppy^F even though it has a lower molecular weight. Structural evidence readily explains why this is so. The structure of the ppyF shows that its molecules pack in rows via $_{(pyridyl)}N\cdots S_{(dithiadiazolyl)}$ contacts. Unfortunately the structure of py^H is unknown. However the packing of pCN-C_6H_4-CNSSN$^\bullet$ and pCN-C_6F_4-CNSSN$^\bullet$ derivatives is shown to be analogous to ppy^F, but $_{(cyano)}N\cdots S_{(dithiadiazolyl)}$ interactions being observed instead. Therefore due to the structural similarities among these four compounds it is not unreasonable to assume that py^H would duplicate this type of packing too.

So, the discussion will now continue with the assumption that both pyridyl derivatives studied have similar packing arrangements. The structures of ppyF and pCN^F show a twist angle twice the size of that observed for pCN and other structures with two *ortho* hydrogens. This is attributed to steric repulsions (ortho$F^{\delta-}\cdots N^{\delta-}$) compared with attractive forces (ortho$H^{\delta+}\cdots N^{\delta-}$). This trend is also observed for the *para* C_6F_5-CNSSN$^\bullet$ derivative; $F^{\delta-}\cdots F^{\delta-}$ repulsions between the molecules of perfluoro derivatives do also occur. These repulsions and the large twist angle hindering packing readily assist in the pCN^F derivative existing as a monomer in the solid state. For the ppyF and C_6F_5 dithiadiazolyl derivatives this effect is not as great as their molecules are seen to exist as dimers.

Therefore the differences in melting points between the two pyridyl derivatives are attributed to greater steric repulsion between the molecules in ppyF due to $F^{\delta-}\cdots F^{\delta-}$ and $F^{\delta-}\cdots N^{\delta-}$ repulsions which are absent in py^H. In the perfluoro derivatives S···F inter ribbon interactions are also observed. However, these are not sufficiently numerous or strong enough to mask the effect the $F^{\delta-}\cdots F^{\delta-}$ repulsions have on depressing the m.pts. of perfluoro dithiadiazolyl compounds.

The anticipated packing of the py^H is similar to that observed for the *para* nitro phenyl 1,2,3,5 dithiadiazolyl, however the pNO_2 compound has a larger m.pt. than py^H. This is attributed to stronger molecular attractions existing between the pNO_2 molecules than between py^H. It is anticipated that the S···O contacts are stronger than respective N···S ribbon interactions due to the greater electrostatic attraction between atoms of higher and opposite polarity. In addition to this, S···N inter ribbon interactions of pNO_2 are assumed to be more numerous than for py^H, *cf* pNO_2 discussion.

It would be very interesting to determine the structure of py^H to see if it is similar to the predicted structure. However obtaining crystals to prove this will be difficult from standard crystal growth techniques as the material readily forms powders on sublimation and is very insoluble all the solvents tried.

Conclusion

The above discussion clearly outlines how the m.pts. of analogous compounds, in conjunction with the structures of some of these compounds and related materials, can be used to make a reasonable assessment of an unknown structure by comparing relative strengths of interactions. Also, these results tend to suggest that the strength of the S···S intra dimer interaction is not an important factor in determining m.pt. but other molecular interactions, steric forces and position of substituent are. This discussion has certainly outlined some compounds which would be of crystallographic interest, in particular mF and py^H derivatives.

4D.1.4 Mass spectra of 1,2,3,5 radicals

The 1,2,3,5 dithiadiazolylium chloride salts and associated radicals made in this thesis generally gave very good mass spectral breakdown patterns using EI^+ technique. A typical example of a complete fragmentation pattern of the heterocyclic ring of these derivatives due to EI^+ is shown below. Notice that the ring readily breaks up with the loss of small sulphur nitrogen species.

For the compounds examined R was either a phenyl or pyridyl group which was substituted or unsubstituted. Loss of a substituent(s) from the R group of particular derivatives together with ring fragmentation was also observed in the mass spectra of these analogues. More detail on this can be found by examining the individual fragmentation patterns of many of the synthesised radical derivatives given at the end of this section.

CI^+ was also conducted on these derivatives. Typical fragments identified were $[R\text{-}CN]H^+$, $[R\text{-}CN]NH_4^+$, $[R\text{-}CNSSN]H^+$, $[R\text{-}CNSSN]2H^+$ and $[R\text{-}CNSSN]NH_4^+$, where the substituent R is generally observed to be intact.

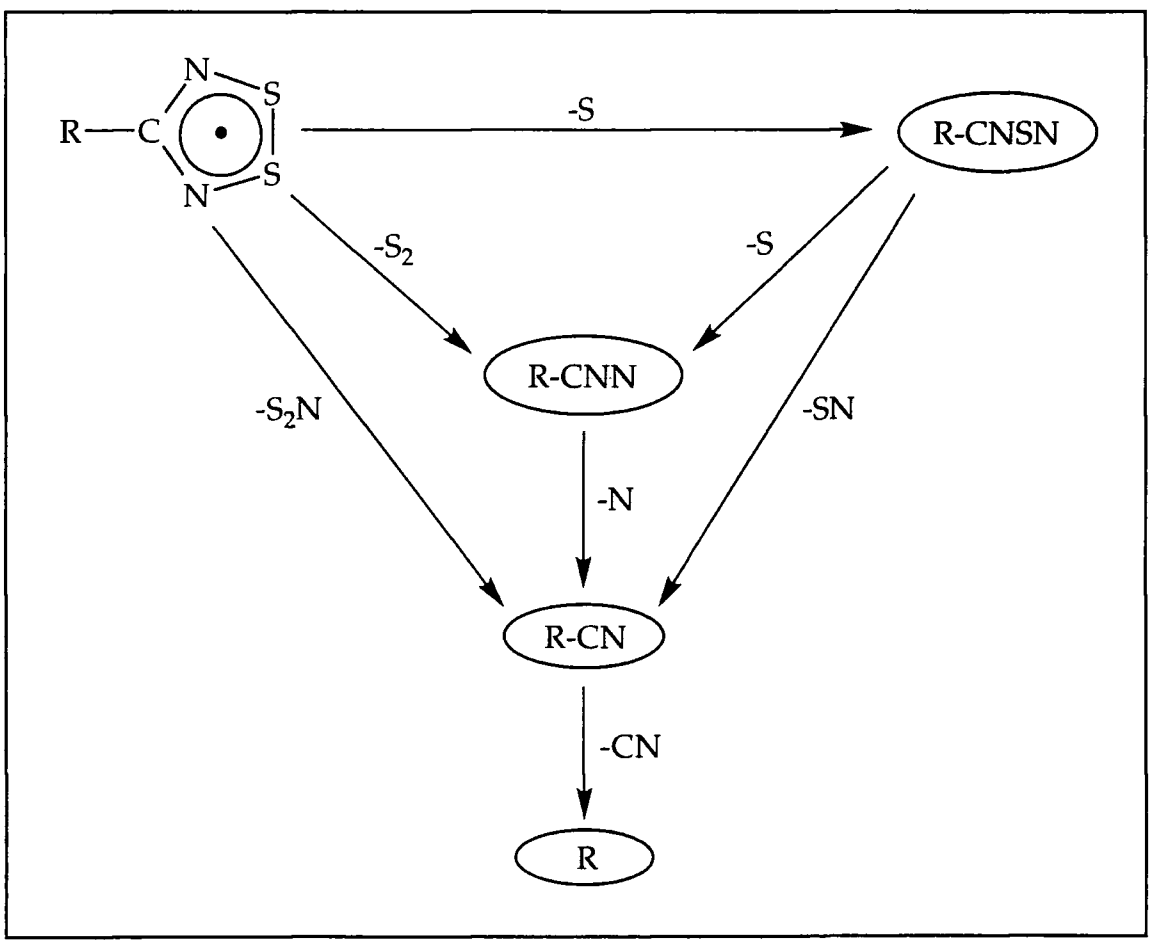

Mass spec fragmentation diagram

The hexafluoroarsenate dithiadiazolylium salt derivatives synthesised in this thesis generally gave very poor and unclear mass spectra. Hence they were not investigated in any depth and will not be reported here.

Below are the mass spectrometry data obtained for the substituted pyridyl and phenyl 1,2,3,5 dithiadiazolyls synthesised for structural and electrochemical analysis.

Para

p-NO_2 **EI**$^+$: O_2N-C_6H_4-CNSSN 226 (100.00), ON-C_6H_4-CNSSN 210 (27.35), O_2N-C_6H_4-CNS or C_6H_4-CNSSN 180 (57.42), C_6H_4-CNS 134 (15.55), ON-C_6H_4-C 118 (12.58), C_6H_4-CN 102 (10.47), S_2N 78 (64.79), SN 46 (15.24). **CI**$^+$: [C_6H_4-CNS]2H$^+$ or [ON-C_6H_4-C]NH_4^+ 136 (53.94)

p-$MeCO_2$ **EI**$^+$: MeO_2C-C_6H_4-CNSSN 239 (100.00), OC-C_6H_4-CNSSN 208 (10.99), MeO_2C-C_6H_4-CNS 193 (11.81), C_6H_4-CNSSN 180 (13.22), OC-C_6H_4-CNS 162 (17.02), OC-C_6H_4-CN 130 (29.26), C_6H_4-CN 102 (20.01), S_2N 78 (58.50), SN 46 (15.90). **CI**$^+$: [MeO_2C-C_6H_4-CNSSN]2H$^+$ 241 (41.25)

p-Br **EI**$^+$: Br^{79}-C_6H_4-CNSSN 259 (22.02), Br^{81}-C_6H_4-CNSSN 261 (21.25), Br^{79}-C_6H_4-CNS 213 (18.68), Br^{81}-C_6H_4-CNS 215 (15.64), Br^{79}-C_6H_4-CN 181 (23.05), Br^{81}-C_6H_4-CN 183 (21.94), C_6H_4-CNS 134 (12.68), C_6H_4-CNSSN 102 (57.46), S_2N 78 (100.00), S_2 64 (17.40), SN 46 (34.15). **CI**$^+$: [Br^{79}-C_6H_4-CNSSN]2H$^+$ 261 (24.13), [Br^{81}-C_6H_4-CNSSN]2H$^+$ 263 (20.51), [Br^{79}-C_6H_4-CN]NH_4^+ 199 (100.00), [Br^{81}-C_6H_4-CNSSN]NH_4^+ 201 (97.08).

p-CF_3O **EI**$^+$: CF_3O-C_6H_4-CNSSN 265 (52.96), CF_3O-C_6H_4-CNS 219 (57.29), CF_3O-C_6H_4-CN 187 (44.25), CFO-C_6H_4-CN 149 (19.37), S_2N 78 (100.00). **CI**$^+$: [CF_3O-C_6H_4-CN]NH_4^+ 205 (100.00), [CF_3O-C_6H_4-CNSSN]2H$^+$ 267 (17.05).

p-F **EI**$^+$: F-C_6H_4-CNSSN 199 (53.70), F-C_6H_4-CNS 153 (31.11), F-C_6H_4-CNN 135 (40.47), F-C_6H_4-CN 121 (27.04), F-C_6H_4 95 (15.73), S_2N 78 (100.00), S_2 64 (15.47), SN 46 (12.45). **CI**$^+$: [F-C_6H_4-CNSSN]2H$^+$ 201 (2.97), [F-C_6H_4-CN]NH_4^+ 139 (100.00).

p-Me **EI**$^+$: Me-C_6H_4-CNSSN 195 (55.41), Me-C_6H_4-CNS 149 (33.11), Me-C_6H_4-CN 117 (58.33), Me-C_6H_4 89 (43.24), S_2N 78 (100.00), S_2 64 (30.56), SN 46 (62.84). **CI**$^+$: [Me-C_6H_4-CNSSN]H$^+$ 196 (44.94).

p-MeS **EI**$^+$: MeS-C_6H_4-CNSSN 227 (100.00), MeS-C_6H_4-CNS 181 (25.34), MeS-C_6H_4-CNN 163 (23.21), MeS-C_6H_4-CN 149 (48.93), S-C_6H_4-CN or C_6H_4-CNS 134 (16.20), S-C_6H_4-CNN or C_6H_4-CNSN 116 (11.59), S_2N 78 (56.92), SN 46

(17.99). **CI**$^+$: [MeS-C_6H_4-CNSSN]H^+ 228 (46.55), [MeS-C_6H_4-CN]NH_4^+ 167 (39.84).

p-MeO **EI**$^+$: MeO-C_6H_4-CNSSN 211 (29.28), MeO-C_6H_4-CNS 165 (12.52), O-C_6H_4-CNS 150 (17.57), MeO-C_6H_4-CN 133 (100.00), O-C_6H_4-CN 118 (11.71), S_2N 78 (32.71), S_2 64 (89.20). **CI**$^+$: [MeO-C_6H_4-CN]NH_4^+ or [O-C_6H_4-CNS] 151 (61.25), [MeO-C_6H_4-CNSSN]H^+ 212 (78.25).

metas

m-CF_3 **EI**$^+$: CF_3-C_6H_4-CNSSN 249 (61.60), CF_3-C_6H_4-CNS 203 (29.69), CF_3-C_6H_4-CN 171 (11.89), CF_2-C_6H_4-CN 152 (14.03), CF_3-C_6H_4 145 (13.48), C_6H_4F-CN 121 (13.49), S_2N 78 (100.00), SN 46 (22.98). **CI**$^+$: [CF_3-C_6H_4-CNSSN]$2H^+$ 251 (1.79), [CF_3-C_6H_4-CN]NH_4^+ 189 (16.09).

m-Br **EI**$^+$: Br^{79}-C_6H_4-CNSSN 259 (34.93), Br^{81}-C_6H_4-CNSSN 261 (33.00), Br^{79}-C_6H_4-CNS 213 (11.68), Br^{81}-C_6H_4-CNS 215 (11.56), Br^{79}-C_6H_4-CN 181 (14.93), Br^{81}-C_6H_4-CN 183 (14.45), C_6H_4-CNS 134 (14.46), C_6H_4-CNSSN 102 (38.39), S_2N 78 (100.00), S_2 64 (31.20), SN 46 (29.31). **CI**$^+$: [Br^{79}-C_6H_4-CNSSN]$2H^+$ 261 (20.36), [Br^{81}-C_6H_4-CNSSN]$2H^+$ 263 (15.20), [Br^{79}-C_6H_4-CN]NH_4^+ 199 (46.98), [Br^{81}-C_6H_4-CNSSN]NH_4^+ 201 (43.51).

m-Cl **EI**$^+$: Cl^{35}-C_6H_4-CNSSN 215 (30.53), Cl^{37}-C_6H_4-CNSSN 217 (11.51), Cl^{35}-C_6H_4-CNS 169 (21.14), Cl^{37}-C_6H_4-CNS 171 (7.00), Cl^{35}-C_6H_4-CN 137 (31.07), Cl^{37}-C_6H_4-CN 139 (10.08), C_6H_4-CN 102 (22.38), S_2N 78 (100.00), S_2 64 (2.65), SN 46 (30.36). **CI**$^+$: [Cl^{35}-C_6H_4-CNSSN]$2H^+$ 217 (1.25), [Cl^{37}-C_6H_4-CNSSN]$2H^+$ 219 (0.44), [Cl^{35}-C_6H_4-CN]NH_4^+ 155 (11.47), [Cl^{37}-C_6H_4-CN]NH_4^+ 157 (3.38).

m-F **EI**$^+$: F-C_6H_4-CNSSN 199 (55.06), F-C_6H_4-CNS 153 (38.28), F-C_6H_4-CN 121 (48.75), F-C_6H_4 95 (18.47), S_2N 78 (100.00), S_2 64 (32.63), SN 46 (7.97). **CI**$^+$: [F-C_6H_4-CNSSN]$2H^+$ 201 (1.89), [F-C_6H_4-CN]NH_4^+ 139 (10.99).

m-OMe **EI**$^+$: MeO-C_6H_4-CNSSN 211 (21.15), MeO-C_6H_4-CNS 165 (6.22), O-C_6H_4-CNS 150 (1.57), MeO-C_6H_4-CN 133 (100.00), S_2N 78 (49.82), S_2 64 (7.62), SN 46 (11.32). **CI**$^+$: [MeO-C_6H_4-CN]NH_4^+ or [O-C_6H_4-CNS]H^+ 151 (18.52), [MeO-C_6H_4-CNSSN]H^+ 212 (10.16).

difluoro

2,3 **EI**$^+$: F_2-C_6H_3-CNSSN 217 (16.81), F_2-C_6H_3-CNS 171 (15.66), F_2-C_6H_3-CN 139 (100.00), S_2N 78 (34.98), S_2 64 (18.07), SN 46 (18.26). **CI**$^+$: [F_2-C_6H_3-CNSSN]H^+ 218 (10.54), [F_2-C_6H_3-CN]NH_4^+ 157 (40.67).

2,5 **EI**$^+$: F_2-C_6H_3-CNSSN 217 (78.90), F_2-C_6H_3-CNS 171 (16.93), F_2-C_6H_3-CN 139 (45.63), F_2-C_6H_3 113 (10.97), S_2N 78 (64.54), S_2 64 (10.05), SN 46 (21.36). **CI**$^+$: [F_2-C_6H_3-CN]NH_4^+ 157 (60.69).

3,5 **EI**$^+$: F_2-C_6H_3-CNSSN 217 (31.44), F_2-C_6H_3-CNS 171 (18.90), F_2-C_6H_3-CN 139 (37.27), F_2-C_6H_3 113 (10.90), S_2N 78 (100.00), S_2 64 (6.07), SN 46 (29.06). **CI**$^+$: [F_2-C_6H_3-CNSSN]$2H^+$ 219 (2.05), [F_2-C_6H_3-CN]NH_4^+ 157 (19.40).

3,4 **EI**$^+$: S_8 256 (10.27), S_7 224 (4.14), S_6 192 (12.06), F_2-C_6H_3-CNS 171 (5.05), S_5 160 (20.99), F_2-C_6H_3-CN 139 (41.27), S_4 128 (15.06), F_2-C_6H_3 113 (10.90), S_3 96 (3.73), S_2 64 (87.09). **CI**$^+$: [F_2-C_6H_3-CN]NH_4^+ 157 (99.40).

mixed

3,5 Cl_2 **EI**$^+$: $Cl^{35}Cl^{35}$-C_6H_3-CNSSN 249 (12.29), $Cl^{35}Cl^{37}$-C_6H_3-CNSSN 251 (7.41), $Cl^{37}Cl^{37}$-C_6H_3-CNSSN 253 (1.94), $Cl^{35}Cl^{35}$-C_6H_3-CN 171 (100.00), $Cl^{35}Cl^{37}$-C_6H_3-CN 173 (69.00), $Cl^{37}Cl^{37}$-C_6H_3-CN 175 (14.36), $Cl^{35}Cl^{35}$-C_6H_2-CN 172 (52.59), $Cl^{35}Cl^{37}$-C_6H_2-CN 174 (35.12), $Cl^{37}Cl^{37}$-C_6H_2-CN 176 (4.56), Cl^{35}-C_6H_3-CN 136 (26.41), Cl^{37}-C_6H_3-CN (8.16), S_2N 78 (34.84), SN 46 (17.26). **CI**$^+$: [$Cl^{35}Cl^{35}$-C_6H_3-CNSSN]H^+ 250 (10.38), [$Cl^{35}Cl^{37}$-C_6H_3-CNSSN]H^+ 252 (7.42), [$Cl^{37}Cl^{37}$-C_6H_3-CNSSN]H^+ 254 (1.98), [$Cl^{35}Cl^{35}$-C_6H_3-CNSSN]$2H^+$ 251 (61.09), [$Cl^{35}Cl^{37}$-C_6H_3-CNSSN]$2H^+$ 253 (14.57), [$Cl^{37}Cl^{37}$-C_6H_3-CNSSN]$2H^+$ 255 (1.23), [$Cl^{35}Cl^{35}$-C_6H_3-CN]NH_4^+ 189 (32.02), [$Cl^{35}Cl^{37}$-C_6H_3-CN]NH_4^+ 191 (19.75), [$Cl^{37}Cl^{37}$-C_6H_3-CN]NH_4^+ 193 (3.53).

mCl,pMe **EI**$^+$: Cl^{35}Me-C_6H_3-CNSSN 229 (25.06), Cl^{37}Me-C_6H_3-CNSSN 231 (11.89), Cl^{35}Me-C_6H_3-CNS 183 (14.68), Cl^{37}Me-C_6H_3-CNS 185 (6.54), Cl^{35}Me-C_6H_3-CN 151 (19.19), Cl^{37}Me-C_6H_3-CNSSN 153 (7.85), Me-C_6H_3-CN 116 (37.43), S_2N 78 (100.00), S_2 64 (33.12), SN 46 (15.23). **CI**$^+$: [Cl^{35}Me-C_6H_3-CN]NH_4^+ 169 (100.00), [Cl^{37}Me-C_6H_3-CN]NH_4^+ 171 (31.23), [Cl^{35}Me-C_6H_3-CNSSN]H^+ 230 (50.65), [Cl^{37}Me-C_6H_3-CNSSN]H^+ 232 (17.11)

pyridyl

py^f **EI**$^+$: NC_5F_4-CNSSN 254 (52.24), NC_5F_4-CNS 208 (14.95), NC_5F_4-CN 176 (55.45), S_2N 78 (100.00), S_2 64 (11.91), SN 46 (50.24). **CI**$^+$: [NC_5F_4-CN]NH_4^+ 194 (16.48)

py^h **EI**$^+$: NC_5H_4-CNSSN 182 (100.00), NC_5H_4-CNS 136 (26.56), NC_5H_4-CN or CNSSN 104 (42.07), S_2N 78 (67.47), S_2 64 (7.41). **CI**$^+$: [NC_5H_4-CNSSN]H^+ 183 (64.98), [NC_5H_4-CN]NH_4^+ or [CNSSN]NH_4^+ 122 (33.26), [NC_5H_4-CN]H^+ or [CNSSN]H^+ 105 (27.82).

the 1,2,3,5 radicals)

ortho- R-C_6H_4-CNSSN•

o-R	Mass of R^+Cl^-	Type of reducing agent	Colour of solution and precipitate at stage 1	Purification of product, stage 2	Elemental analysis	Yield %	Colour of final purified product	DSC
Br	1g	Zn/Cu	No reduction process observed	The solid isolated after the reaction was shown to be starting material from IR spectroscopy investigations.	N/A	N/A	N/A	N/A
Cl	1g	Ph_3Sb Zn/Cu	Dark red	Both routes resulted in the isolation of an intractable oily red coloured material which proved difficult to analyse.	N/A	N/A	N/A	N/A
F	0.95g	Zn/Cu	Purple	The isolated sticky purple solid readily sublimed at 100°C to give red green dichroic crystals which were too small for structural determination. Repeated sublimations failed to produce larger crystals. These crystals readily dissolved in 1,2 dichlorobenzene. When this solvent was pumped off over 2 days large hexagon (2x2x0.5mm) and toblerone (1x2x2mm) shaped crystals formed. A structure was achieved using these crystals but it was found to be highly disordered and unsuitable for publication.	Obs C 42.90; H 2.05; N 14.50 Req C 42.19; H 2.02; N 14.06	45%	Red green dichroic crystals	-

IR(Br crude material): 2216m, 1652w(br), 1594w, 1566w, 1463s(br), 1377s, 1260w, 1228vw, 1156w(br), 1087vw, 1046w, 858m, 758vs, 740m, 722m, 602w, 556m and 516s.
IR(F): 1608m, 1579w, 1491m, 1458s, 1369s, 1274m, 1223m, 1160w, 1141m, 1095m, 1034m, 949vw, 908w, 864vw, 838m, 804s, 777vs, 763vs, 731m, 652m, 640m(sh), 550m, 511m, 488vw and 416w.

meta- R-C_6H_4-CNSSN•

m-R	Mass of R^+Cl^-	Type of reducing agent	Colour of solution and precipitate at stage 1	Purification of product, stage 2	Elemental analysis	Yield %	Colour of final purified product	DSC
NO_2	3g	Ph_3Sb	purple	The vessel was then evacuated to reveal a sticky intractable purple oily substance.	N/A	N/A	N/A	N/A
CF_3	4.04g	Zn/Cu	Deep red	The isolated deep red coloured material readily sublimed at 80°C to produce bronze crystalline material. These crystals were just too small for x-ray structure determination. Altering the experimental conditions had little affect on crystal size.	Obs C 39.01; H 1.70; N 11.28 Req C 38.55; H 1.62; N 11.24	68%	Bronze crystalline material	82
Br	2.39g	Zn/Cu	Deep red solution and a purple precipitate	The purple/red coloured solid sublimed at 120° to yield metallic green crystals that were very suitable for crystallographic x-ray structure determinations.	Obs C 32.00; H 1.47; N 10.57 Req C 32.32; H 1.55; N 10.77	42%	Metallic green crystals	129
Cl	3.00g	Zn/Cu	purple	The solvent was pumped off to reveal a purple solid. This material sublimed at 105°C to give extremely small red green dichroic crystals. Changing the experimental conditions had little affect on crystal size.	Obs C 39.45; H 1.90; N 12.59 Req C 38.98; H 1.87; N 12.99	64%	Red green dichroic crystals	117.5
F	3.83g	Zn/Cu	Deep red	Removal of the solvent by applying a vacuum yielded a deep blue grey solid. This material under a dynamic vacuum and 100°C slowly sublimed to yield numerous green red dichroic crystals. The crystals were too small for x-ray structure determination and altering the sublimation conditions did not improve this. This compound readily dissolved in 1,2-dichlorobenzene. When the solvent was pumped off slowly over several days bronze needles formed which were heavily twinned and hence unsuitable for structure determinations.	Obs C 41.76; H 2.00; N 13.94 Req C 42.19; H 2.02; N 14.06	68%	Red green dichroic crystals	128
MeO	2.9g	Zn/Cu	dark red	Removal of the solvent by evacuation yielded a slightly sticky dark coloured material. When this was sublimed at 100°C a few black crystals and parent nitrile were isolated. These crystals didn't diffract.	Obs C 45.80; H 3.70; N 13.70 Req C 45.48; H 3.34; N 13.26	<1%	Black crystals	94.5

IR(CF_3): 1612vw, 1463s, 1376s, 1320s, 1287s, 1164m, 1137s, 1115s, 1091m, 1071m, 930m, 920m, 835w, 814m, 788m, 776m, 722vw, 694m, 685s, 664vw, 648w, 600vw, 518m, 448vw and 420vw
IR(Br): 1700w, 1561w, 1467m, 1427m, 1365m, 1280w, 1242w, 1160w, 1142m, 1081w, 1070m, 994w, 915m, 898m, 837m, 801s, 790s, 777s, 710s, 691s, 648w, 512s, 502m, 426w and 400w.
IR(Cl): 1594vw, 1573w, 1463s, 1433m, 1366s(br), 1297vw, 1275w, 1230w, 1163w, 1143m, 1088w, 1074w, 998vw, 928m, 884m, 833m, 803m(sh), 788s, 777vs, 740s, 689vs, 519m, 502m, 469vw, 449w and 429w.
IR(F): 1610w, 1587m, 1488m, 1450s, 1366s, 1277m, 1235w, 1211m, 1158m, 1107s, 1077m, 961s, 876m, 837m, 820s, 793vs, 692s, 660w, 542m, 526m, 512s, 459w and 426w
IR(MeO): 1609.2m, 1582m, 1490m, 1460s, 1437m, 1367s, 1314vw, 1294s, 1242s, 1186vw, 1170vw, 1120m, 1086m, 1047s, 939w, 886vw, 870m, 830m, 806s, 783s, 773s, 723w, 698s, 656vw, 575w, 556w, 515m, 479vw and 436vw.

para- R-C_6H_4-CNSSN•

p-R	Mass of R^+Cl^-	Type of reducing agent	Colour of solution and precipitate at stage 1	Purification of product, stage 2	Elemental analysis	Yield %	Colour of final purified product	DSC
NO_2	2g	Ph_3Sb	Purple	The purple solid sublimed at 220°C to yield black / green crystals suitable for x-ray structure determination.	Obs C 37.30; H 1.75; N 18.70 Req C 37.16; H 1.78; N 18.58	54%	Black green crystals	252
CF_3	3g	Zn/Cu	Purple	The purple solid readily sublimed at 110°C to give bronze coloured crystals from which an x-ray structure was obtained.	Obs C 38.56; H 1.70; N 11.42 Req C 38.55; H 1.62; N 11.24	44%	Black green crystals	124
Br	3g	Zn/Cu	Dark red	This purple/red solid sublimed at 135°C to give crystalline material which was heavily twinned and unsuitable for structural determinations. Altering the sublimation conditions had a very small effect on crystal quality.	Obs C 32.66; H 1.56; N 10.74 Req C 32.32; H 1.55; N 10.77	60%	Red green dichroic crystals	153.5
Cl	2g	Zn/Cu	Purple	This purple solid readily sublimed at 120°C to give crystalline material.	Obs C 38.78; H 1.90; N 13.20 Req C 38.98; H 1.87; N 12.99	74%	Dark green crystals	141

para- R-C_6H_4-CNSSN$^\bullet$ cont'd

p-R	Mass of R^+Cl^-	Type of reducing agent	Colour of solution and precipitate at stage 1	Purification of product, stage 2	Elemental analysis	Yield %	Colour of final purified product	DSC
F	2g	Zn/Cu	Red	This purple solid sublimed at 100°C onto a cold finger resulting in isolation of bronze coloured plates from which a structure was obtained.	Obs C 41.46; H 2.11; N 13.84 Req C 42.19; H 2.02; N 14.06	63%	Bronze coloured plates	120
Me	4.41g	Zn/Cu	Dark red	The isolated burgundy solid sublimed at 70°C to give bronze dendritic crystals which were too fine to obtain a structure on.	Obs C 49.70; H 3.67; N 14.56 Req C 49.20; H 3.61; N 14.34	64%	Dark red crystals	–
MeS	0.5g	Ph_3Sb	Red	This deep red solid readily sublimed at 120°C to give block like red crystals from which a structure was obtained.	Obs C 41.77; H 3.07; N 12.33 Req C 42.68; H 3.15; N 12.15	45%	Red crystals	149.5
MeO	3g	Zn/Cu SO_2	Red	This red solid sublimed at 100°C to give dendritic crystals which were unsuitable for x-ray structure determinations. Altering sublimation conditions did not result in any change in crystallinity.	Obs C 45.80; H 3.41; N 13.56 Req C 45.48; H 3.34; N 13.26	66%	Dark red crystals	124.5
CF_3O	1g	Zn/Cu	Purple	The isolated purple solid sublimed at 70°C to give tiny bronze crystals. Attempts to increase crystal size by altering sublimation conditions were unsuccessful and hence no structure could be obtained.	Obs C 36.15; H 1.47; N 10.43 Req C 36.22; H 1.52; N 10.56	54%	Dark green crystals	97.5
$MeCO_2$	0.3g	Ph_3Sb	Purple	The solvent was removed to reveal a purple solid which readily sublimed at 100°C to give crystals that were far too small for x-ray structure determination to be conducted.	Obs C 45.36; H 3.02; N 11.90 Req C 45.17; H 2.95; N 11.71	48%	Red green dichroic crystals	x

IR(NO_2): 1600w, 1510m, 1460vs(br), 1418w, 1378s, 1344s, 1321m, 1303w, 1141m, 1101m, 1010w, 856s, 849m, 832m, 811m, 777s, 752m, 719w, 690s, 639m and 506s.
IR(CF_3): 1616m, 1463s, 1415s, 1376s, 1324vs, 1220m, 1168s, 1138s, 1107s, 1067s, 1018m, 906w, 849s, 834s, 807m, 779s, 710w, 684m, 655vs, 589m, 509s and 441m
IR(Br): 1586m, 1463vs, 1398m, 1376s, 1239w, 1174w, 1166w, 1137m, 1100m, 1069m, 1010s, 903w, 828s, 807m, 777s, 723w, 714m, 700w, 664vw, 647m, 626w, 508s, 479m and 432vw.

IR(F): 1598s, 1513s, 1464m, 1418m, 1376s, 1355s, 1301w, 1233s, 1159m, 1134s, 1098m, 1015w, 905w, 841vs, 812s, 805m, 774vs, 724m, 650s, 588s, 520vw, 503s and 426vw.
IR(Me): 1602w, 1513w, 1463s, 1401w, 1310m, 1238m, 1181m, 1132m, 1110w, 1022m, 902m, 820s, 806s, 775s, 714m, 652s, 588w, 509s, 482s and 425m.
IR(MeS): 1591w, 1460s(br), 1406m, 1380s, 1241m, 1191m, 1183m, 1139m, 1114w, 1091m, 1016m, 966w, 902w, 844m, 838m, 820s, 803s, 777vs, 719s, 651s, 513m, 490m and 424w.
IR(MeO): 1604w, 1517w, 1302w, 1266m, 1200w, 1175m, 1140w, 1105w, 1030w, 820m, 794m, 766w, 656w, 588m and 505w.
IR($MeCO_2$): 1720s, 1696m, 1609w, 1462vs(br), 1414m, 1377s, 1284s, 1196w, 1139w, 1116m, 1019m, 963w, 863w, 836w, 805w, 776s, 722m, 701m and 650w.

di-fluoro- F_2-C_6H_3-CNSSN•

F,F	Mass of R^+Cl^-	Type of reducing agent	Colour of solution and precipitate at stage 1	Purification of product, stage 2	Elemental analysis Req C 38.70; H 1.39; N 12.90	Yield %	Colour of final purified product	DSC
2,3	1g	Zn/Cu	Purple / red	The purple solid sublimed at 120^0 to give green/bronze crystalline material, which was heavily twinned.	Obs C 38.90; H 1.49; N 12.95	45%	Green / bronze coloured crystals	125.5
2,5	1.5g	Zn/Cu	Purple	The isolated grey black solid sublimed at 95^0C to yielded purple / green coloured crystals. Unfortunately these were too small for structure determination.	Obs C 39.10; H 1.35; N 12.94	67%	Purple / green coloured crystals	109.5
2,6	1g	Zn/Cu	Purple	A purple oily substance was isolated when the vessel was evacuated. Sublimation of this material to isolate crystalline material was unsuccessful.	-	N/A		x
3,4	3.88g	Zn/Cu	Deep red solution and a purple solid	The solvent was removed by vacuum to reveal a purple red coloured solid from which dark red crystals readily sublime out at 120^0C. Unfortunately these were too small for structure determination.	Obs C 30.30; H 1.49; N 12.57	57%		131.5
3,5	1.5g	Zn/Cu	Purple	When the vessel was evacuated a purple solid was isolated. This material readily sublimes at 100^0C	Obs C 39.30; H 1.50; N 12.67	35%		133

IR(2,3F_2): 1592vw, 1484s, 1464vs, 1377s, 1276s, 1240w(sh), 1210vw, 1190w, 1154m, 1077m, 997s, 840m, 835m, 799m, 788s, 774s, 723s, 662m, 605m, 577m, 521w, 477vw and 428w.
IR(2,5F_2): 1596vw, 1496s, 1465m, 1440s, 1377w, 1357m, 1298w, 1263m, 1236w, 1191s, 1129m, 1084m, 969m, 878m, 823s, 801m, 776s, 760vs, 720m, 668w, 657vw, 554m, 531w, 498w, 459vw, 421vw and 384m.
IR(3,4F_2): 1614m, 1546vw, 1516s, 1464s, 1437vs, 1376vs, 1280m, 1261w, 1230m, 1204w, 1193m, 1117w, 1102w, 968s, 882s, 837m, 823s, 812m, 784s, 772vs, 705m, 672m, 619m, 578vw, 511vs, 447vw and 429vw.
IR(3,5F_2): 1616w, 1603m, 1461vs, 1377vs, 1312w, 1267m, 1129m, 1102m, 1006w, 988s, 877w, 866m, 849m, 840m, 808m, 786s, 762m, 723m, 694m, 651w, 559m, 524w, 496m and 420w.

mixed- X,Y-C_6H_3-CNSSN•

X,Y	Mass of R^+Cl^-	Type of reducing agent	Colour of solution and precipitate at stage 1	Purification of product, stage 2	Elemental analysis	Yield %	Colour of final purified product	DSC
2F, 4CF_3	1.08g	Zn/Cu	Purple red	Purple solid isolated readily sublimed to give bluish black crystals, which were too small for x-ray crystallography to be conducted on them.	Obs C 35.45; H 1.23; N 10.58 Req C 35.95; H 1.13; N 10.48	60%		99.5
3Cl, 4Me	2.4g	Zn/Cu	Deep red	Red/purple solid isolated sublimed at 100°C to produce green red dichroic crystals. A structure was obtained from these crystals	Obs C 42.12; H 2.43; N 12.45 Req C 41.83; H 2.63; N 12.20	75%	Red green dichroic crystals	124
3Cl, 4F	2.3g	Zn/Cu	Purple	Purple solid isolated readily sublimed at 130°C to give tiny crystals.	Obs C 35.78; H 1.34; N 12.34 Req C 35.96; H 1.29; N 11.99	69%	Red green crystals	139
3,5Cl_2	1.59g	Zn/Cu	Red purple	The purple solid isolated sublimed at 110°C to give dark blue / pink dichroic crystals.	Obs C 33.89; H 1.50; N 11.12 Req C 33.61; H 1.21; N 11.20	54%	Dark blue / pink dichroic crystals	127.5

IR(2F, 4CF_3): 1579w, 1511m, 1463s, 1440s(sh), 1377s, 1331vs, 1218m, 1177s, 1153s, 1143s, 1117vs, 1067m, 932m, 879m, 810w, 824m, 801w, 774m, 746m, 725w(sh), 675m, 555m and 498w
IR(3Cl, 4Me): 1558w, 1463vs, 1376vs, 1386m(sh), 1272w, 1238w, 1205vw, 1133m, 1050m, 996w, 934m, 893w, 829m, 804m, 777s, 722w, 703m, 668m, 616w, 511m and 434m
IR(3Cl, 4F): 1588w, 1496m, 1463s, 1401w, 1376s, 1252m, 1227m, 1153w, 1125m, 1056m, 938w, 897w, 891w, 832m, 825m, 806m, 781s, 706m, 664m, 615m, 531w and 500s

IR(3,5Cl_2): 1591vw, 1567m, 1463s, 1428m, 1377m, 1352s, 1248vw, 1228vw, 1160w, 1102w, 959m, 892m, 865s, 834w, 806vs, 779s, 730m, 692s, 653vw, 528m, 502w, 471vw and 432vw.

py- x-NC_6Y_4-CNSSN•

x-py^Y	Mass of R^+Cl^-	Type of reducing agent	Colour of solution and precipitate at stage 1	Purification of product, stage 2	Elemental analysis	Yield %	Colour of final purified product	DSC
p-py^F	1.22g	Ph_3Sb	Purple	All the products of this reaction were very soluble in CH_2Cl_2. The solvent was removed by applying a vacuum and replaced with toluene. This material was also found to be very soluble in this solvent too. The solvent was removed. Dry material was isolated and placed into a sublimer. When the temperature reached 65°C lovely blue metallic crystals sublimed away from the other products. Crystallography x-ray structure determination on one of these crystals revealed that they were of the desired compound	Obs C 28.56; H 0.00; N 16.99 Req C 28.35; H 0.00; N 16.53	63%	Blue metallic crystals	84.5
m-py^H	2g	Zn/Cu	Purple	When the solvent is removed a purple solid is isolated. This readily sublimes at 80°C to give small red green dichroic crystals suitable for x-ray structure determination.	Obs C 39.50; H 2.30; N 23.60 Req C 39.54; H 2.21; N 23.06	70%	Red green dichroic crystals	
p-py^H	4g	Ph_3Sb	Highly insoluble precipitate forms above a very pale purple solution	The precipitate was washed three times with solvent by back condensation method and pumped to dryness to reveal a purple coloured powder	Obs C 38.22; H 2.16; N 22.02 Req C 39.54; H 2.21; N 23.06	57%	purple powder	178

IR(p-py^F): 1644m, 1503m, 1460vs(br), 1412m, 1400m, 1377m, 1354m, 1286w, 1255w, 1242m, 1054vw, 1014s, 973s, 831m, 808s, 791m, 771s, 830m, 701m, 663m, 522w and 503m.
IR(m-py^H): 1588m, 1463s, 1430m, 1375s, 1324w, 1243w, 1188w, 1147m, 1117m, 1091m, 1040m, 1025s, 930vw, 904vw, 833m, 808s, 783s, 722w, 700s, 666m, 628m, 512m and 460m.

4E Preparation and characterisation of substituted phenyl and pyridyl 1,2,3,5 dithiadiazolylium hexafluoroarsenate salts

0.297g (0.100 mols) of $AgAsF_6$ and a stoichiometric amount of R-CNSSN$^+$Cl$^-$ were placed into one limb of a 'dog'. A third of a bulb of SO_2 was condensed into the other limb of the vessel. On addition of the solvent to the reactants, a coloured solution above a white precipitate immediately formed. During the first 2-5 minutes of the reaction the solution usually intensified in colour. The reaction was stirred for a further 24 hours to ensure the reaction had gone to completion. During this period no change in colour was observed.

After this time the coloured solution was decanted off. The solvent was then back condensed into the reaction limb in order to wash any remaining soluble product across. This process was repeated once more and the solvent removed by evacuation to reveal the solid product.

meta R-C_6H_4-CNSSN$^+AsF_6^-$

m-R	Colour of solution above white precipitate	Elemental analysis		Yield %	Colour of final purified product
CF_3	Yellow .	Obs C 22.01; H 1.01; N 6.90	Req C 21.93; H 0.92; N 6.39		Off white powder
Br	Orangey red	Obs C 18.89; H 1.01; N 6.20	Req C 18.72; H 0.90; N 6.24	95%	Bright orange red solid
Me	Orange	Obs C 25.20; H 1.90; N 7.39	Req C 25.01; H 1.84; N 7.29	80%	Bright orange solid
MeO	Red	Obs C 24.30; H 1.57; N 6.83	Req C 24.01; H 1.76; N 7.00	89%	Burgundy powder

IR(CF_3):

IR(Br): 1684m, 1595w, 1570m, 1478m(sh), 1464s, 1433s, 1384vs, 1303w, 1278m, 1168m, 1090w, 1073m, 996w, 957w, 930m, 914m, 894m, 850m, 799s, 704vs(br), 673s, 557m and 516vw.
IR(Me): 1665w(br), 1604w, 1587m, 1462vs(br), 1378vs(br), 1290m, 1228w, 1143w, 1092w, 933m, 922s, 858vw, 800s, 703vs(br), 560m and 517vw
IR(MeO): 1670w(br), 1602m, 1578s, 1510w, 1493m, 1460vs(br), 1378vs, 1297s, 1256s, 1175vw, 1136m, 1092w, 1036vs, 992vw, 965w, 921m, 898w, 883m, 856w, 805s, 788m, 706vs(br), 673vs, 554s and 478vw.

para R-C_6H_4-CNSSN$^+AsF_6^-$

p-R	Colour of solution above white precipitate	Elemental analysis		Yield %	Colour of final purified product
NO_2	Red	Obs C 20.35; H 1.01; N 10.01	Req C 20.25; H 0.97; N 10.12	85%	Yellow
CF_3	Yellow	Obs C 22.45; H 1.05; N 6.45	Req C 21.93; H 0.92; N 6.39	83%	Lemon yellow
Br	Orange	Obs C 18.50; H 1.00; N 6.10	Req C 18.72; H 0.90; N 6.24	80%	Orange
F	Orange .	Obs C 21.55; H 1.05; N 7.15	Req C 21.66; H 1.04; N 7.22	84%	Orange
Cl	Orange	Obs C 21.55; H 1.05; N 7.15	Req C 21.66; H 1.04; N 7.22	89%	Yellow

para R-C_6H_4-CNSSN$^+AsF_6^-$ cont'd

p-R	Colour of solution above white precipitate	Elemental analysis		Yield %	Colour of final purified product
Me	Orange	Obs C 24.85; H 1.90; N 7.15	Req C 25.01; H 1.84; N 7.29	87%	Red-Orange
MeS	Deep purple/blue	Obs C 22.80; H 1.60; N 6.55	Req C 23.08; H 1.70; N 6.73	86%	Malachite green
MeO	Purple	Obs C 23.80; H 1.75; N 6.80	Req C 24.01; H 1.76; N 7.00	70%	Purple
$MeCO_2$	Yellow solution above a white precipitate	Obs C 24.34; H 1.72; N 6.27	Req C 25.24; H 1.65; N 6.54	81%	Yellow solid
CF_3O	Yellow	Obs C 21.20; H 0.95; N 6.54	Req C 21.15; H 0.88; N 6.16	85%	Yellow solid

IR(CF_3): 1515w, 1447m, 1410m, 1320s, 1187s, 1122s, 1070s, 1020m, 986m, 970w, 917m, 852s, 804m, 695s(br), 670m, 634m, 590w, 443m and 400s
IR(Br): 1680w(br), 1590s, 1400s, 1310vw, 1290w, 1200w, 1182m, 1160m, 1114w, 1075m, 1012m, 962w, 940w, 922s, 840s, 835s, 730s, 700vs(br), 675(sh), 560m, 498m and 397vs.
IR(F): 1670m(br), 1602s, 1520w, 1402s, 1304m, 1260m, 1247s, 1197w, 1168s, 1165w, 1160s, 1112w, 1015w, 970vw, 960vw, 945vw, 927s, 849s, 825w, 810m, 740s, 730s, 695s(br), 675s, 592m, 560m, 519m, 400s(br) and 375m
IR(Me): 1735w(br), 1680m(br), 1606s, 1395s, 1300w(br), 1190s, 1163m, 1020w, 925s, 845m, 840m, 825s, 790w, 730(sh), 703vs(br), 671s, 560m, 498w and 396vs.
IR(MeS): 1590s, 1415m, 1390(br), 1198s, 1190(sh), 1168m, 1094s, 1015m, 980w, 970w, 965w, 925m, 844s, 840m, 830m, 730s, 725m, 700s(br), 685(sh), 675m, 560m, 502w, 495w, 400s and 390(sh).
IR(MeO): 1680m, 1605s(br), 1582m, 1570m, 1520w, 1430m, 1400vs, 1370(sh), 1335w, 1320m, 1309s, 1300w, 1278s, 1267m, 1177s, 1120m, 1020s, 952w, 930s, 840s, 818m, 810m, 790m, 742m, 700vs(br), 672s, 630w, 591m, 550m, 510m and 390vs(br).
IR($MeCO_2$): 1714vs, 1581vw, 1510w, 1462s, 1413m, 1404m, 1378s, 1292s, 1251m, 1193w, 1162m, 1111s, 1019m, 944vw, 926m, 870m, 849w, 828m, 782m, 702vs(br), 583vw, 560m, 506vw.
IR(CF_3O): 1681m(br), 1602w(br), 1461vs(br), 1403s, 1380s, 1288s(br), 1220s(br), 1183m, 1167m, 1110w, 1040w, 1021m, 928m, 867m, 850m, 811w, 703vs(br), 676m.

difluoro F_2-C_6H_3-CNSSN$^+AsF_6^-$

F,F	Colour of solution above white precipitate	Elemental analysis		Yield %	Colour of final purified product
2,6	Deep orange red	Obs C 20.82; H 0.83; N 6.70	Req C 20.70; H 0.74; N 6.90	95%	Dark yellow solid

IR(2,6): 1687m, 1630m, 1593m, 1569w, 1466vs(br), 1392m, 1377s, 1297vw, 1247m, 1198w, 1156w, 1089vw(br), 1064vw(br), 1017vs, 910m, 846w, 800s, 700vs(br), 590vw, 566m, 542w and 517w

mixed XY-C_6H_3-CNSSN$^+AsF_6^-$

X,Y	Colour of solution above white precipitate	Elemental analysis		Yield %	Colour of final purified product
3,5Cl_2	Orange	Obs C 19.25; H 0.71; N 6.45	Req C 19.15; H 0.69; N 6.38	86%	Pale orange solid

IR(3,5Cl_2): 1772vw(br), 1687s, 1654m, 1571s, 1518m, 1455s, 1373s, 1333m, 1301w, 1247w, 1203vw, 1188m, 1147w, 1107m, 998w, 982m, 929m, 873s, 854m, 841vw, 809s, 704vs(br), 561m, 522w and 482vw.

pyridyl X-NC_5Y_4-CNSSN$^+AsF_6^-$

x-py^Y	Colour of solution above white precipitate	Elemental analysis		Yield %	Colour of final purified product
p-py^F	orange	Obs C 16.59; H 0.00; N 9.70	Req C 16.25; H 0.00; N 9.48	79%	orange

4F Preparation and characterisation of substituted phenyl 1,3,2,4 dithiadiazolylium hexafluoroarsenate salts

4F.1.1 Preparation

Stage 1 0.267g (0.100mols) of $S_2N^+AsF_6^-$ and 0.100mols of the appropriate nitrile was placed into one limb of a 'dog'. A third of a bulb of SO_2 was condensed in where upon an instant coloured solution formed. The reaction mixture was then left to stir for 24 hours. During the first few minutes the solution usually intensified in colour and didn't change for the remaining stirring time.

Stage 2 The next step was to isolate the product and this was done using either route A,B or C depending on the compound formed.

A Most of the SO_2 was then removed to reveal a wet solid. 5mls of dry CH_2Cl_2 was then added and the solid washed with the solvent mixture three times by decanting the washings across and back condensing the solvents onto the product. The vessel was then pumped to dryness to reveal a pure powdery product.

B Most of the SO_2 was then removed to reveal a wet solid. 5mls of dry hexane was then added and the solid washed with the solvent mixture three times by decanting the washings across and back condensing the solvents. The vessel was then pumped to dryness to reveal a pure powdery product.

C Most of the SO_2 was then removed to reveal a wet solid. 5mls of CH_2Cl_2 was added in order to wash impurities away from the insoluble product. However if after the first wash it was evident that these solvents were rendering the material to be very sticky hence another solvent needed to be used. In this case addition of 1ml of MeCN removed this problem and after two more washes a powder could now be isolated as in the previous two stages.

4F.1.2 Discussion on the synthesis of ortho substituted phenyl 1,2,3,5 and 1,3,2,4 dithiadiazolylium compounds

The synthesis of *ortho* substituted aryl 1,3,2,4 dithiadiazolylium salts was seen to be very straight forward. However, the same could not be said for the attempted synthesis of *ortho* halogen substituted 1,2,3,5 dithiadiazolylium salts and associated radical. In the later case it was noticed that the bigger the steric bulk of the *ortho* substituent the less favourable the reaction became, i.e. *ortho* fluoro derivatives could be made but *ortho* bromo derivatives couldn't. This result definitely tends to indicate that the *ortho* substituent is sterically interfering with the synthesis reaction for these 1,2,3,5 salts but not for the corresponding 1,3,2,4 analogues.

The reaction schemes of the synthesis processes for these two types of isomeric derivatives are given in Fig 7 and 8. Straight away it can be seen from these diagrams that the 1,2,3,5 derivative forms an intermediate which possesses very bulk $SiMe_3$ groups which can sterically interfere with the *ortho* side group. For the 1,3,2,4 isomer this is not the case. Therefore this evidence does suggest that larger steric forces in the 1,2,3,5 synthesis reaction compared to 1,3,2,4 isomer are responsible for the observed trend among these two isomeric groups of compounds.

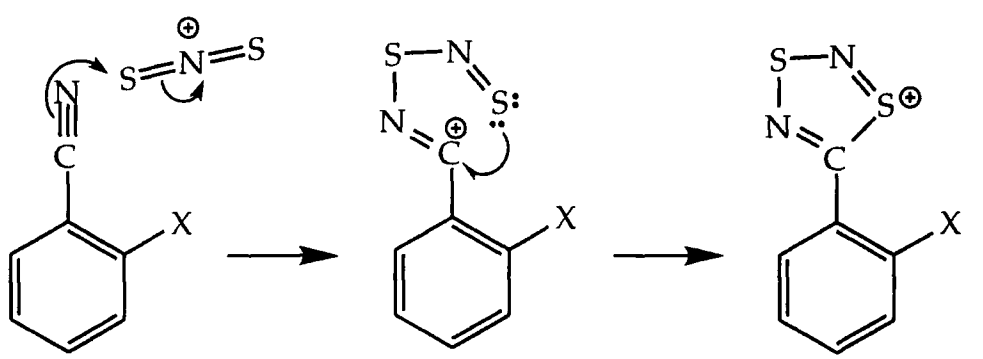

Fig 7. Scheme of the reaction between $S_2N^+AsF_6^-$ with an aryl nitrile.

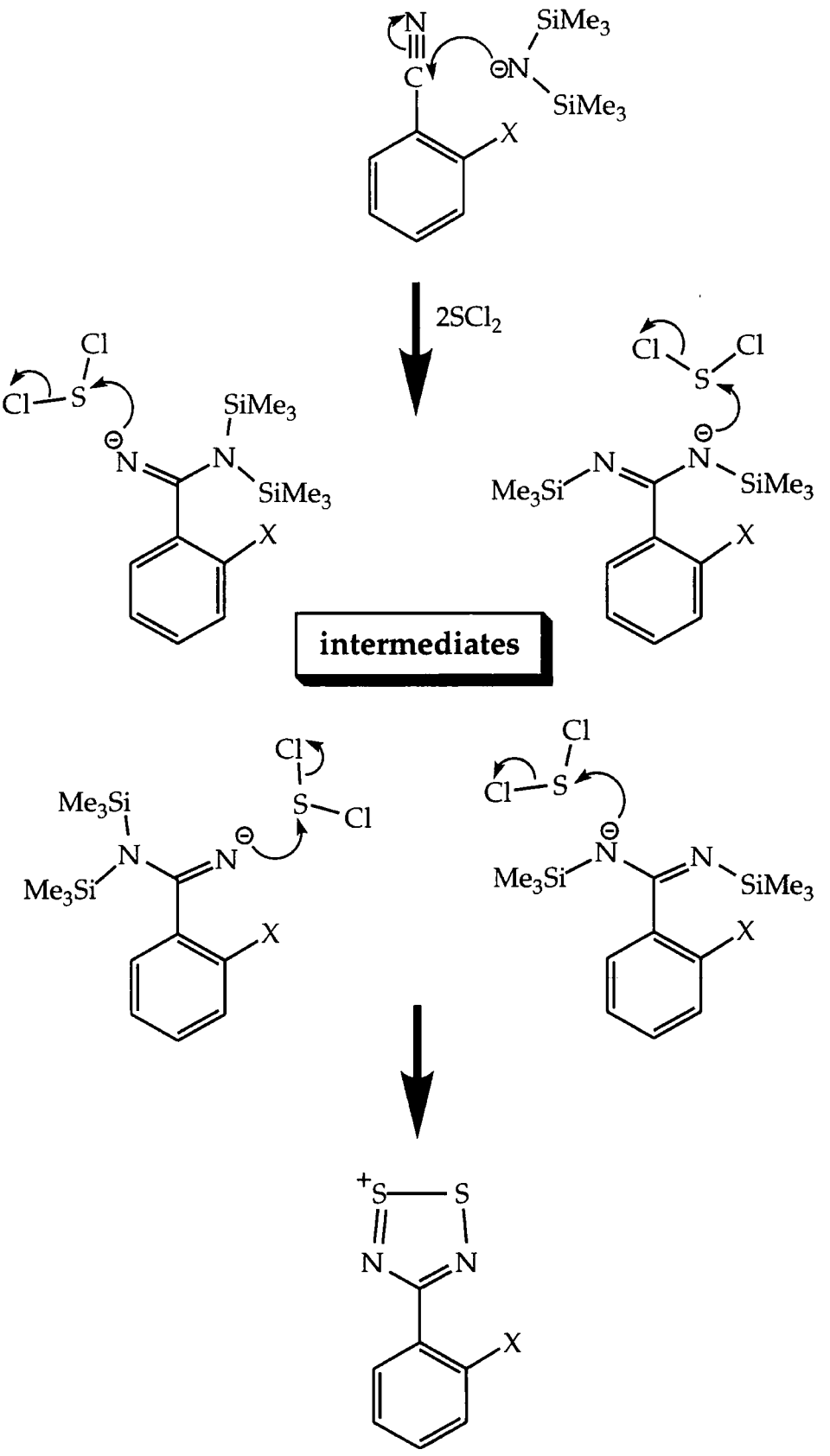

Fig 8. Scheme of the reaction between $Li^+[N(SiMe_3)_2]^-$ with an aryl nitrile.

ortho R-C_6H_4-CNSNS$^+AsF_6^-$

o-R	Colour of solution, Stage 1	Purification, stage 2	Elemental analysis		Yield %	Colour of final purified product
NO_2	Dark red	C	Obs C 20.68; H 1.04; N 10.50	Req C 20.25; H 0.97; N 10.12	82	white precipitate
CF_3	Dark red	B	Obs C 21.50; H 1.01; N 6.90	Req C 21.93; H 0.92; N 6.39	77	Off white
Br	Dark red	B	Obs C 18.90; H 0.70; N 6.70	Req C 18.72; H 0.90; N 6.24	76	Yellow solid
Cl	Dark red	B	Obs C 20.90; H 0.80; N 6.76	Req C 20.78; H 1.00; N 6.93	75	Yellow solid
F	Dark red	B	Obs C 21.55; H 1.01; N 7.01	Req C 21.66; H 1.04; N 7.22	71	Yellow solid
Me	Dark red	A	Obs C 25.34; H 1.90; N 7.56	Req C 25.01; H 1.84; N 7.29	70	Bright yellow solid
MeO	Dark yellow	A	Obs C 23.78; H 1.87; N 7.20	Req C 24.01; H 1.76; N 7.00	83	Bright orange solid
EtO	Red	A	Obs C 26.34; H 2.34; N 6.92	Req C 26.09; H 2.19; N 6.76	91	Mandarin orange solid

IR(CF_3): 1676vw, 1597m, 1580m, 1419m(sh), 1318m, 1302m(sh), 1160w, 1121s(br), 1067m, 1041m, 985m, 908w, 879w, 803s, 784s, 704vs(br), 662m(sh), 639m(sh), 596m(sh), 589m, 570m and 452s.
IR(Br): 1734w, 1646vw(br), 1584vw(br), 1559s, 1308w, 1292w, 1276m, 1213vw, 1170w, 1126vw(sh), 1082vw, 1059w, 1029s, 983s, 915m, 903w, 794s, 780m, 771s, 755vw, 701vs(br), 669w(sh), 577m, 484vw, 451vw(sh), 440w and 428vw(sh).
IR(Cl): 1660s, 1592w(sh), 1133m, 1059s, 1035w, 984m(br), 717w, 756w, 721vs(br), 630m(sh), 575m, 556s and 490w.
IR(F): 1648w, 1612s(br), 1514vw(sh), 1486m, 1403s, 1318w, 1287m, 1270w, 1237m, 1224w, 1200w, 1162m, 1157w, 1109m, 1100w(sh), 1028vw(br), 990s, 968w, 923m, 917w, 898m, 875w, 860vw(br), 815m, 792s, 779s, 770m(sh), 758vw, 737w(sh), 700vs(br), 670m(sh), 630w, 585w, 540w, 524vw(br), 456vw(br), 438m and 400vs.
IR(Me): 1600w, 1402s, 1294m, 1212w, 1172w, 1116vw, 980w, 911vw, 806m, 772s, 760w(sh), 692vs(br), 636m, 588vw and 444m(sh).

IR(EtO): 1599m, 1576m, 1463s(br), 1397m(sh), 1312m, 1293m, 1253m, 1168m, 1124m, 1093w, 1052w(sh), 984m, 923m, 896w, 882w, 865w, 788s, 789s, 692vs(br), 633m, 604w, 581w, 528w, 496w, 458w and 432m
IR(MeO): 1560w, 1560vw, 1462vs, 1405m, 1377s, 1293w, 1213w(br), 1130w(br), 1084w, 980w, 916w, 806m, 774m, 758m, 698vs(br), 636w, 584w, 460w and 443w.

meta R-C_6H_4-CNSNS$^+AsF_6^-$

m-R	Colour of solution, Stage 1	Purification, stage 2	Elemental analysis		Yield %	Colour of final purified product
NO_2	Red	A	Obs C 20.68; H 0.87; N 10.34	Req C 20.25; H 0.97; N 10.12	89%	Off white powder
CF_3	Dark yellow	A	Obs C 21.58; H 0.98; N 6.43	Req C 21.93; H 0.92; N 6.39	78%	Off white solid
Me	Yellow	A	Obs C 25.35; H 1.90; N 7.12	Req C 25.01; H 1.84; N 7.29	75%	Yellow solid
MeO	Cherry red	A	Obs C 24.13; H 1.64; N 7.20	Req C 24.01; H 1.76; N 7.00	83%	Tangerine coloured solid

IR(MeO): 1604m, 1580s, 1495m, 1457vs, 1441s, 1405s, 1377m, 1342vw, 1304m, 1266s, 1195vw, 1172vw, 1094vw, 1055w, 1005m, 904w, 88vw, 872m, 812m, 776s, 697vs(br), 677vs, 647w, 590vw, 564w, 548vw, 471vw, 449w, 428m, 395vs and 374m.

para R-C_6H_4-CNSNS$^+AsF_6^-$

m-R	Colour of solution, Stage 1	Purification, stage 2	Elemental analysis		Yield %	Colour of final purified product
NO_2	Red	A	Obs C xx.xx; H xx.xx; N xx.xx	Req C 20.25; H 0.97; N 10.12	85%	Off white
CF_3	Red	A	Obs C 21.55; H 0.95; N 6.40	Req C 21.93; H 0.92; N 6.39	92%	Peach
Br	Red	A	Obs C 18.90; H 0.90; N 6.30	Req C 18.72; H 0.90; N 6.24	80%	Yellow
Cl	Red	A	Obs C 20.45; H 1.00; N 6.95	Req C 20.78; H 1.00; N 6.93	95%	Yellow

F	Red	A	Obs C 21.30; H 0.95; N 7.15	Req C 21.66; H 1.04; N 7.22	96%	Yellow
Me	Dark red	A	Obs C 24.75; H 1.80; N 7.20	Req C 25.01; H 1.84; N 7.29	72%	Lemon yellow
MeS	Dark red	A	Obs C 23.40; H 1.90; N 6.75	Req C 23.08; H 1.70; N 6.73	83%	Red-Black
MeO	Red	A	Obs C 23.90; H 1.75; N 6.85	Req C 24.01; H 1.76; N 7.00	65%	Red

IR(CF_3): 1517m, 1432m, 1410m, 1320s(br), 1180s(br), 1120s(br), 1070s, 1020m, 985s, 965w, 915m, 890w, 880w, 850s, 835w, 830w, 800s, 770w, 695vs(br), 670m, 632m, 588m, 570w, 442m and 388vs.
IR(Br): 1587s, 1418s, 1395m, 1312w, 1287w, 1212w, 1195vw, 1187m, 1180w, 1125w, 1075s, 1014m, 986s, 914m, 890w, 842s, 835s, 830m, 820m, 800s, 715s(br), 690vs(br), 670s, 628m, 590w, 580w, 490m, 440m and 398vs
IR(Cl): 1592s, 1420s, 1400s, 1315w(br), 1288m, 1212m, 1185m, 1127vw, 1110vw, 1095s, 1017m, 987s, 912m, 890m, 880w, 840s, 833w, 820m, 815w, 800s, 710s, 690vs(br), 672s, 629m, 620m, 593w, 580w, 500m, 492m, 443s and 400vs.
IR(F): 1605s, 1600(sh), 1518w(br), 1430s, 1410s, 1315m, 1305m, 1253s, 1215w, 1165(sh), 1150s, 1110m, 988s, 980(sh), 950w, 914m, 898m, 890w, 845s, 840w, 820m, 815w, 783s, 715s, 690s(br), 675s, 632m, 620m, 570m, 515m, 447m, 438m and 400s
IR(Me): 1605s, 1515w, 1400s, 1320w, 1212m, 1185s, 995w, 980w, 915w, 890w, 835w, 810s, 800m, 780w, 690vs(br), 630m, 600w, 565w, 485w, 440m and 397s
IR(MeS): 1586m, 1579(sh), 1420m, 1390s, 1198m, 1092s, 975m(br), 910w(br), 890w, 827m, 790m, 695vs(br), 625w, 548w(br), 494vw, 480vw, 440m and 397vs
IR(MeO): 1610m, 1435m, 1392s, 1335w, 1320m, 1310m, 1285m, 1270m, 1178s, 1125w, 1018w, 1005vw, 985m, 920w, 890w, 832s, 805m, 785m, 715s, 690s(br), 672m, 630w, 620w, 575w, 520vw, 440m and 397s

difluoro F_2-C_6H_3-CNSNS$^+AsF_6^-$

F,F	Colour of solution, Stage 1	Purification, stage 2	Elemental analysis Req C 20.70; H 0.74; N 6.90	Yield %	Colour of final purified product
2,4	Red	A	Obs C 20.75; H 0.80; N 6.99	80%	Pale yellow powder
2,5	Orange red	A	Obs C 20.34; H 0.87; N 6.94	92%	Pale yellow powder
2,6	Orange	A	Obs C 20.22; H 0.69; N 6.76	77%	Peach coloured solid
3,4	Orange red	A	Obs C 20.90; H 0.65; N 6.86	85%	Orangey yellow powder

3,5	Red	A	Obs C 20.63; H 0.87; N 6.93	79%	Peach coloured solid

IR(2,4F_2): 1611s, 1594m, 1461vs(br), 1402s, 1377s, 1281s, 1262m, 1198w, 1150m, 1107m, 993m, 970m, 918w, 887w, 870m, 830m, 802m, 699vs(br), 634m, 564m, 549w, 509w and 438m.
IR(2,5F_2): 1624m, 1596w, 1495s, 1454vs(br), 1392s, 1377vs, 1312w, 1264m, 1197m, 1162w, 1110w, 1019m, 953m, 906m, 886m, 836s, 797s, 760s, 694vs(br), 592m and 542s.
IR(2,6F_2): 1627s, 1591m, 1565w, 1463vs(br), 1405s, 1377s, 1311vw, 1278w, 1251m, 1130w(br), 1027s, 977m, 907w, 890w, 803vs, 732s, 700vs(br), 669s and 626m.
IR(3,4F_2): 1610s, 1520s, 1495m, 1449vs, 1381s, 1377s, 1314w, 1293s, 1216w(br), 1165m, 1126m, 1091vw, 1004m, 964w, 947s, 912m, 873m, 836s, 809w, 796s, 778m, 696vs(br), 656m, 618w, 586m, 574m, 451w and 440m.
IR(3,5F_2): 1602s, 1576w, 1483m(sh), 1454vs, 1422s, 1409s, 1377m, 1327w, 1312m, 1235w, 1160w, 1134s, 997s, 977w, 947m, 907m, 888w, 873m, 858m, 812s and 694vs(br).

References:

1 A. J. Banister, Z. V. Hauptman, A. G. Kendrick and R. W. H. Small, *J. Chem. Soc., Dalton Trans.*, 1987, 915.

2 A. J. Banister, M. I. Hansford, Z. V. Hansford, S. T. Wait and W. Clegg, *J. Chem. Soc., Dalton Trans.*, 1989, 1705.

3 A. J. Banister, I. Lavender, J. M. Rawson and R. J. Whitehead, *J. Chem. Soc., Dalton Trans.*, 1992, 1449.

4 A. J. Banister, N. R. M. Smith and R. G. Hey, *J. Chem. Soc., Dalton Trans.*, 1983, 1181.

5 B. Ayres, A. J. Banister, P. D. Coates, M. I. Hansford, J. M. Rawson, C. E. F. Rickard, M. B. Hursthouse, K. M. Malik and M. Motevalli, *J. Chem. Soc., Dalton Trans.*, 1992, 3097.

6 S. Parsons, J. Passmore, M. J. Schriver and X. Sun, *Inorg. Chem.*, 1991, 30, 3342.

7 P. D. B. Belluz, A. W. Cordes, E. M. Kristof, P. V. Kristof, S. W. Liblong and R. T, Oakley, *J. Am. Chem Soc.*, 1989, 111, 9276.

Chapter 5

5A Conclusion

This thesis has been mainly concerned with the electrochemical and structural properties of a wide selection of substituted 1,2,3,5 and 1,3,2,4 dithiadiazolylium/zolyl moieties. The compounds of interest included (i) mono substituted phenyl 1,2,3,5 and 1,3,2,4 dithiadiazolylium salts and their related 1,2,3,5 dithiadiazolyls, (ii) di-substituted phenyl 1,3,2,4 dithiadiazolylium salts and related 1,2,3,5 dithiadiazolyls and (iii) perfluoro and unsubstituted pyridyl 1,2,3,5 dithiadiazolylium salts and related radicals.

The electrochemical investigations on these compounds involved a study of the reduction process from the 6π cationic dithiadiazolylium ring to the 7π radical analogue, using CV techniques. These CV studies showed that all these derivatives were quasi-reversible in MeCN to the same degree, which indicates a similar electrochemical charge transfer mechanism occurs for all of them (under these experimental conditions).

The redox potentials of 1,2,3,5 derivatives were seen to be higher then their associated 1,3,2,4 analogues. Using MO's diagrams and the fact that $\Delta G=-nE°F$, this trend occurs because the reduction process for a 1,2,3,5 derivative is energetically more favourable relative to an analogous 1,3,2,4 derivative.

For the *meta* and *para* substituted phenyl dithiadiazolylium/zolyl derivatives the $E_{pc/2}$ potentials were seen to increase with electron-withdrawing ability of the substituent group attached. When $E_{pc/2}$ (cathodic half peak potential) values of these *meta* and *para* derivatives were plotted against corresponding Hammett σ_p values excellent linear free energy plots were found to exist. The gradients of all these linear free energy plots were positive and within experimental error of each other. This confirmed the suspicion that the electronic influence (resonance and inductive) substituent groups, of these phenyl dithiadiazolylium/zolyl species, have on the reaction centre is comparable to that observed among associated benzoic acid derivatives. Also, this clearly indicated that the stronger the electron withdrawing ability of the substituent group the more favourable the reduction process is.

For the *ortho* derivatives no Hammett trend was observed. This is attributed to the steric effects the *ortho* substituents of analogous benzoic acid and dithiadiazolylium/zolyl derivatives have on the electronic environment of the ring are not comparable. The steric repulsive and attractive forces differ because these reaction centres have different component atoms.

For difluoro substituted compounds no Hammett relationship was seen to exist. This is partly due to steric effects of *ortho* substituents, as previously

mentioned. In addition to this effect, there is further evidence to suggest that differing solvent effects and competing resonance contributions may be responsible for deviations for these difluoro derivatives too.

For the other disubstituted compounds, too few derivatives were studied to say conclusively if a linear free energy plot existed. However if more derivatives were studied, observed deviations from linearity could be readily explained using similar arguments as in the difluoro case, but steric effects would be between *meta* and *para* groups this time.

For the small selection of pyridyl derivatives studied no Hammett plot was attempted as there would only be a small number of points. However unlike the other measurements, CV of these samples was also conducted in liquid SO_2. These results showed that these materials are more quasi-reversible in this medium then in MeCN as deduced by the larger peak separation observed with the former solvent. This suggests that the diffusion coefficient or viscosity of liquid SO_2 is larger than that of MeCN and hence responsible for slowing down the charge transfer process.

These results clearly show what a useful technique CV can be in assessing relative charge transfer properties, steric effects and solvent effects between samples.

The structures of eight 1,2,3,5 dithiadiazolyl radical derivatives were obtained, pMeS, pF, pCF_3, NO_2, mClpMe, mBr, ppy^F and mpy^H

All these derivatives existed as cisoid dimers via four centred two electron S···S interactions. No universal trend between the S···S distance and donor acceptor property of the substituent group was observed. This tends to indicate that the electronic influence which a substituent places on the electron density of the ring has little effect on the energy of the S···S interaction. A greater effect in the geometry of these molecules is observed from other intra and inter molecular interactions. These can affect the electronic influence a substituent places on the environment of the ring and hence mask the effect of the substituent.

For these eight compounds and associated literature derivatives larger twist angles are observed for compounds possessing two *ortho* fluorines (~30°) compared to the hydrogen analogues (~10°). This is due to the presence of repulsive forces, eg $F^{\delta-}\cdots N^{\delta-}$.

The derivatives possessing strong *para* or *meta* withdrawing groups were found to pack in ribbons. The same was observed for perfluoro systems too. However, derivatives possessing electron donating or weak electron withdrawing

groups packed in herring-bone arrays. Therefore this suggests that derivatives with larger dipoles may favour ribbon formation.

The influence that molecular weight and solid state interactions have on the melting point of these compounds was analysed. For compounds whose structure was unknown, feasible structures were drawn up using the available data of similar compounds. So, examination of the mps of the para radicals indicated that for groups of similar compounds e.g. halogens or RO, the mp is related to mw. The pCF_3 derivative was found to have a lower mp then lighter para derivatives due to the larger steric bulk of the CF_3 substituent group. When meta analogues were compared, most of their mps were seen to be smaller than those of the corresponding para analogues. This is attributed to an increase in intradimer sterics repulsions between the substituent groups as they get nearer the dithiadiazolyl S···S hinge. This trend was not observed for the mF derivative whose mp is larger than the pF analogue. Therefore, this result tends to indicate that the packing between these two compounds is very different, i.e. different molecular forces present. Hence this is a useful method in assessing different packing modes between derivatives. More crystallographic data would be required to prove this.

Linking both sets of data together in conjunction with synthesis and characterisation results, it is evident that *ortho* substituents will sterically interfere with the reaction centre, be it repulsive or attractive forces. These will result in the electronic environment of the ring being affected. Also steric hindrance is held responsible for problems encountered in the synthesis of 1,2,3,5 dithiadiazolylium salts as intermediates can't form due to steric bulk. This is not the case for the 1,3,2,4 salts where no problem was encountered as the intermediate is less sterically bulky.

So, to briefly summarise these results: (1) the crystallography results indicate these types of compounds predominantly exist as dimers and that the substituents have little effect on the S···S distance, i.e. strength. This effect is masked by competing inter and intra molecular forces in the lattice playing a more important role. (2) Contrary to this, these electrochemical studies, especially the *meta* and *para* derivatives, show that substituents do effect the electronic environment of the ring. (3) Comparisons between m.pt. and structures of many of the radical derivatives strongly indicate that these other forces and mw have more influence on m.pt. than S···S interaction.

These results will greatly assist molecular design of dithiadiazolylium /zolyls with the desired physical properties. Therefore an improved set of guidelines to achieve the following physical responses are now given.

Magnetics

The dithiadiazolyl molecules must exist as monomers if they are to have interesting or unusual χ properties. For aryl derivatives they should possess a *meta* or *para* electron withdrawing substituent that can strongly interact with the sulphurs of a neighbouring monomer, e.g. O or N. The other substituents should possess atoms which will readily repel similar atoms of a neighbouring monomer. However to ensure the material is a solid at room temperature it is important these substituents are not so big as to prevent interactions between the ordered arrays of molecules.

Conductivity

The theory is that if dithiadiazolyl derivatives packed in stacks such that S···S interactions ran down these stacks that they would act as conduction bands. However evidence suggests that inter and intra molecular interactions strongly disfavour this type of packing formation. The molecules can not get sufficiently close enough together for this to occur, even when the substituent is simply hydrogen. Evidence also suggests that dimer formation is preferred over the above type of packing. Therefore, the best method of achieving these types of materials is if the molecules are attached to a template, i.e. a polymer backbone or complexed to a transition metal. Alternatively conducting materials with radicals involved in charge transfer salts can be made to be conducting.

Charge transfer salts

These radicals have the ability to form half filled bands and therefore are excellent candidates for charge transfer (donor acceptor) salts. To alter or fine tune the donor acceptor property, details about the electronic influence substituents have on the reaction centres are vital. These electrochemical results enable the electronic influence of substituents to be gauged.

NLO

For second order NLO activity molecule must have a large dipole, i.e. strong donor and acceptor at either end of the molecule and a polarisable system. The electrochemistry results can be used to assess the relative resonance contributions and donor acceptor properties of materials. This can be used to

finely tune molecules. Also, dimer formation is favoured for these molecules therefore it is important to test these materials by EFISH in order to examine their NLO activity as a monomer.

In closing, creating a dithiadiazolylium/zolyl material for 21st Century applications is one step near to being achieved!

Appendix A

substituent group X	Distance between N···X in Å	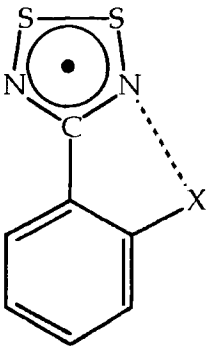	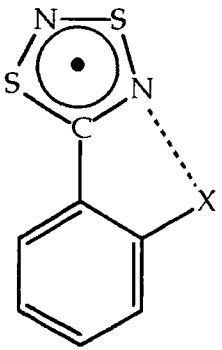		Distance between S···X in Å	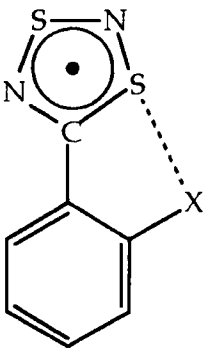		Distance between O···X in Å	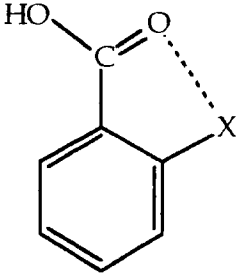
			Major	Minor		Major	Minor		
H	N···H	2.52	2.64	2.34	S···H	2.91	2.62	O···H	2.53
F	N···F	2.50	2.63	2.32	S···F	2.88	2.56	O···F	2.52
Cl	N···Cl	2.53	2.67	2.35	S···Cl	2.86	2.53	O···Cl	2.56
Br	N···Br	2.56	2.69	2.36	S···Br	2.86	2.53	O···Br	2.59
NO_2	N···N	2.50	2.63	2.32	S···N	2.87	2.54	O···N	2.53
	N···O	1.58	1.71	1.40	S···O	1.82	1.47	O···O	1.64
$^*CH_3O$ / $CH_3{}^*CH_2O$	N···O	2.50	2.63	2.32	S···O	2.87	2.56	O···O	2.52
	N···*C	1.40	1.54	1.21	S···*C	1.63	1.29	O···*C	1.46
CF_3	N···C	2.50	2.64	2.33	S···C	2.86	2.54	O···C	2.53
	N···F	1.43	1.55	1.24	S···F	1.66	1.32	O···F	1.48
CH_3	N···C	2.50	2.64	2.33	S···C	2.86	2.54	O···C	2.53
	N···H	1.56	1.69	1.37	S···H	1.84	1.49	O···H	1.61

Fig 1. Distances between selected atoms of ortho substituted phenyl 1,2,3,5 dithiadiazolyls, 1,3,2,4 dithiadiazolyls or carboxylic acids, when the molecules are planar.

substituent group X	Distance between N···X in Å	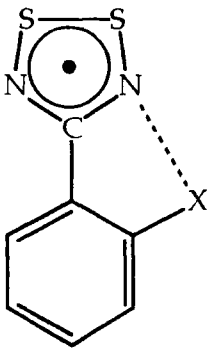	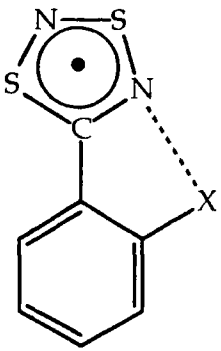		Distance between S···X in Å	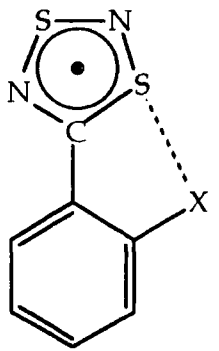		Distance between O···X in Å	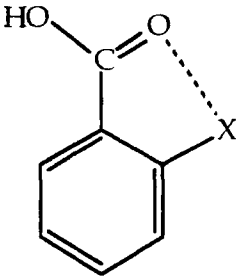
			Major	Minor		Major	Minor		
H	N···H	3.37	3.42	3.23	S···H	3.81	3.66	O···H	3.32
F	N···F	3.44	3.48	3.30	S···F	3.88	3.72	O···F	3.39
Cl	N···Cl	3.57	3.61	3.43	S···Cl	3.99	3.83	O···Cl	3.53
Br	N···Br	3.63	3.67	3.49	S···Br	4.04	3.89	O···Br	3.60
NO_2	N···N	3.47	3.51	3.33	S···N	3.91	3.74	O···N	3.43
	N···O	2.88	2.88	2.72	S···O	3.25	3.12	O···O	2.84
$^*CH_3O$ / $CH_3{}^*CH_2O$	N···O	3.44	3.48	3.31	S···O	3.88	3.72	O···O	3.40
	N···*C	2.73	2.75	2.58	S···*C	3.09	2.98	O···*C	2.69
CF_3	N···C	3.49	3.53	3.35	S···C	3.92	3.75	O···C	3.45
	N···F	2.74	2.75	2.59	S···F	3.10	2.99	O···F	2.71
CH_3	N···C	3.49	3.53	3.35	S···C	3.92	3.75	O···C	3.45
	N···H	2.81	2.82	2.66	S···H	3.20	3.06	O···H	2.77

Fig 2. Distances between selected atoms of ortho substituted phenyl 1,2,3,5 dithiadiazolyls, 1,3,2,4 dithiadiazolyls or carboxylic acids, when the heterocycle or acid is 90° out of the plane of the rest of the molecule.

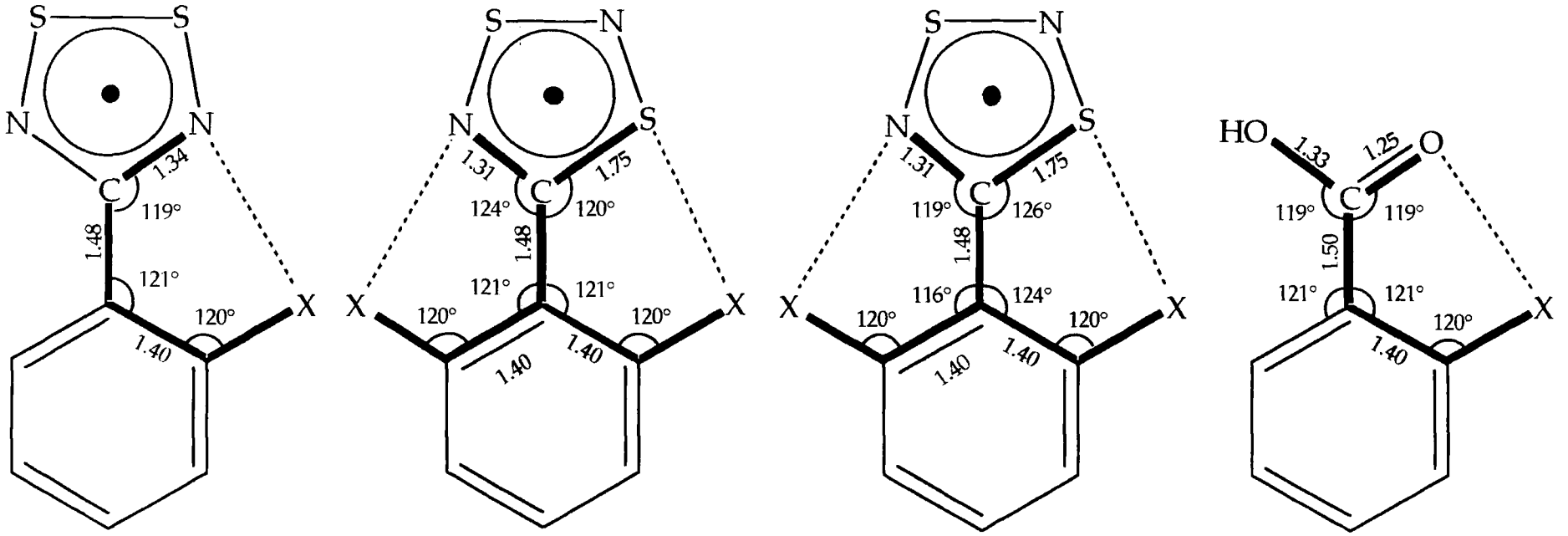

3a.

Bond distances (Å) and angles of Ar-X											
Ar-H	Ar-F	Ar-Cl	Ar-Br	Ar-NO_2	ArN-O_2	Ar-CF_3	ArC-F_3	Ar-OR	ArO-R	Ar-CH_3	ArC-H_3
1.08	1.34	1.74	1.89	1.46	1.23	1.51	1.33	1.37	1.433	1.51	1.10
-	-	-	-	-	C-N-O	-	C-C-F	-	C-O-R	-	C-C-H
					119°		112°		118°		110°

3b

Fig 3a and 3b **Bond lengths and angles used to determine distances in fig 1 and 2.**

	S···H	S···F	S···Cl	S···Br	S···N	S···O
Pauling	3.05	3.20	3.65	3.80	3.35	3.25
Bondi	2.94	3.21	3.50	3.59	3.44	3.24
F&N Major	3.23	3.41	3.81	3.87	3.63	3.57
F&N minor	2.80	2.90	3.18	3.14	3.20	3.14
ΔEN	0.4	1.5	0.5	0.3	0.5	1.0

Fig 4a **Sum of the Van der Waals radii and differences in electronegativity between S and X atoms of differing substituent groups**

	N···H	N···F	N···Cl	N···Br	N···N	N···O
Pauling	2.70	2.85	3.30	3.45	3.00	2.90
Bondi	2.90	3.17	3.46	3.55	3.40	3.20
F&N Major	2.80	2.98	3.38	3.44	3.20	3.14
F&N minor	2.80	2.90	3.18	3.14	3.20	3.14
ΔEN	0.9	1.0	0.0	0.2	0.0	0.5

Fig 4b **Sum of the Van der Waals radii and differences in electronegativity between N and X atoms of differing substituent groups**

	O···H	O···F	O···Cl	O···Br	O···N	O···O
Pauling	2.60	2.75	3.20	3.35	2.90	2.80
Bondi	2.70	2.97	3.26	3.35	3.20	3.00
F&N Major	2.74	2.92	3.32	3.38	3.14	3.08
F&N minor	2.74	2.84	3.12	3.08	3.14	3.08
ΔEN	1.4	0.5	0.5	0.7	0.5	0.0

Fig 4c **Sum of the Van der Waals radii and differences in electronegativity between O and X atoms of differing substituent groups**

$C_6F_5.CNSSN^{\bullet}$

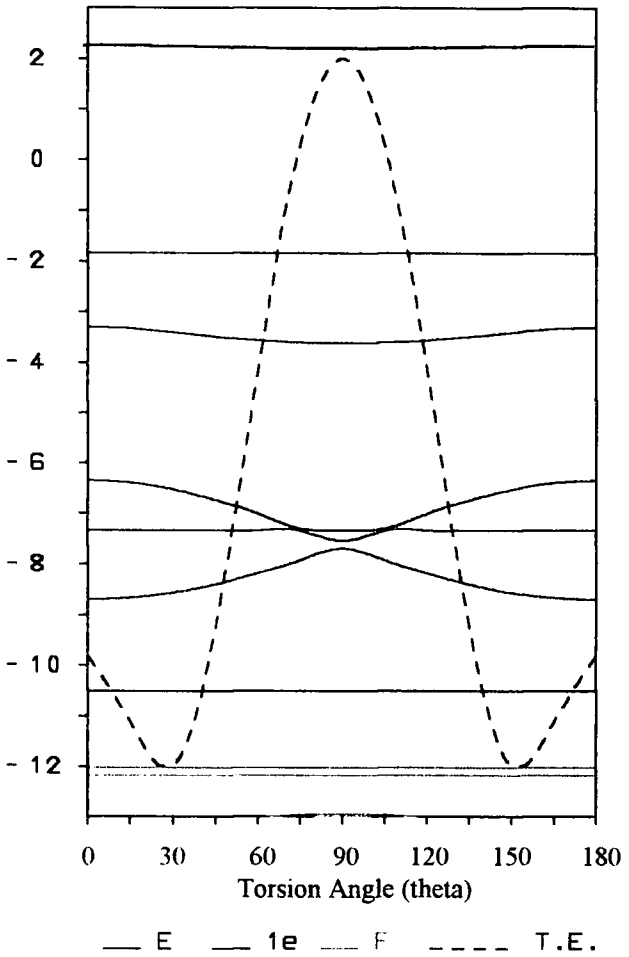

$C_6H_5.CNSSN^{\bullet}$

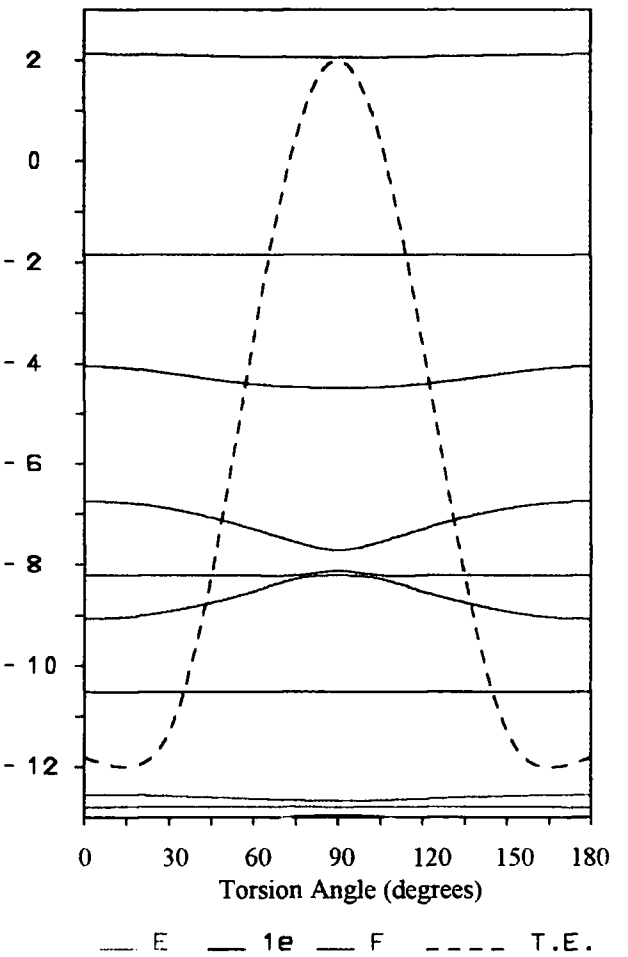

The End